REPURPOSING OF SLUDGE GENERATED FROM THE TREATMENT OF ACID MINE DRAINAGE

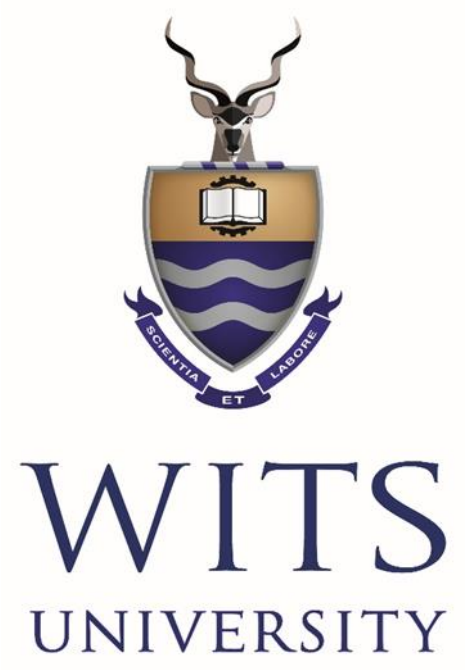

KHATHUTSHELO EMMANUEL NETSHIONGOLWE

A Thesis submitted to the Faculty of Science for the degree of Doctor of Philosophy, University of the Witwatersrand, Johannesburg

MARCH 2022

DECLARATION

I declare that this thesis is my own, unaided work. It is being submitted for the Degree of Doctor of Philosophy at the University of the Witwatersrand, Johannesburg. It has not been submitted before for any degree or examination at any other University.

Signature of Candidate: 

Date: 14th March 2022

ABSTRACT

This study had a two-pronged approach, the first part of which involved assessment of the potential to precipitate different ochres from acid mine drainage (AMD) by using various neutralising agents. This was achieved through computational simulations using the PHREEQC geochemical modelling code. Inferences could then be drawn from the simulations as to which neutralising agents (or a mix thereof) were suitable, taking into account the predicted treated water quality, types of ochres formed and their predicted yields. NaOH and $MgCO_3$ were found to be the most suitable neutralising agents for this purpose, producing ochres with colours varying from yellow to orange and red. Other colours such as green and blue could also be produced following addition of ferrous cyanide to the neutralisation reaction. Naturally, such colourations occur at tailings sites as a result of the presence of cyanide that is used as a lixiviant in gold extraction. The ochres were tested in simple artwork and were found to perform as their commercial counterparts. Further testing of their applicability as paint pigments for building purposes remains possible and should be considered in future studies. The second part of the study was based on exploring the potential to repurpose high density sludge (HDS) generated from AMD treatment plants by taking advantage of the ferric hydroxide ($Fe(OH)_3$) and/or goethite (FeOOH) contained in its matrix that can act as an adsorbent for conditioning of AMD. This AMD would mainly be in mine voids and shafts. Another potential use of HDS as an adsorbent was focused on the adsorption of phosphate from agricultural type and sewage type of water with the aim of applying the phosphate-laden sludge as an amendment for mine tailings on which woodlots are planted for phytoremediation.

BACKGROUND

Acid mine drainage (AMD) continues to pose a threat to water quality in active and abandoned mining areas globally. Stages of mining development (e.g. active and abandoned) result in exposure of sulphide minerals (pyrite, chalcopyrite, arsenopyrite, etc.) to atmospheric oxygen and moisture, resulting in the oxidation of these minerals (mainly pyrite) and subsequent release of sulphuric and potentially toxic trace elements e.g. Pb, Cu, Zn, Ni and As among others. These Fe sulphides may be complexed with covellite (CuS), galena (PbS), sphalerite (ZnS), etc. The effects of AMD are deleterious to plants, humans, wildlife and aquatic life. Due to this complex problem, several researchers are looking for the development of cost-effective and sustainable environmental remediation solutions for dealing with AMD. Several treatment methods have been used, including reverse osmosis, electrodialysis, ultrafiltration, chemical precipitation, ion exchange, and adsorption. Chemical precipitation (neutralisation) is the commonly used technique in large-scale AMD treatment plants such as the high density sludge (HDS) treatment plants where polymeric components are added for flocculation and to densify the sludge. While the treated water, which is usually discharged into streams, contains elevated SO_4^{2-} concentrations, most of the potentially toxic trace elements are removed through precipitation onto the sludge. The HDS process results in the generation of large volumes of sludge, which poses an environmental challenge in its disposal as it tends to act as a secondary source of pollution. The HDS is mostly disposed of at landfill sites or on old mine tailings. Not much has been done in AMD treatment plants (in the Witwatersrand Basin and elsewhere in the world) to explore alternative precipitation approaches that can be used to derive value from AMD treatment and the potential to repurpose HDS.

AIMS

The main aim of the study was to explore the possibility of repurposing sludge produced from AMD treatment. This was achieved by pursuing the following objectives:

(1) To explore the possibility of selectively precipitating ochres from AMD that can be used in artwork and as paint pigments;
(2) To repurpose the high density sludge (HDS) currently produced in AMD treatment plants by using it for *in situ* conditioning and pretreatment of mine void and shaft water;

(3) To explore the possibility of use of the HDS for phosphate removal from agricultural type and sewage type water with the goal of using the sludge further as an amendment in woodlots on mine tailings.

METHODOLOGY

As indicated earlier, this study was predicated around two approaches, viz: selective precipitation of ochres from AMD as a way to recover value; and sorption studies to assess the potential of HDS for use in conditioning/pretreatment of AMD and removal of phosphate from contaminated water.

Precipitation of ochres

The reasoning behind this part of the study has been informed by the need to explore a different neutralisation pathway that will avoid production of a bulky and less useful HDS as is the case currently at the AMD treatment plants. Production of potentially useful ochres (as well as the resulting treated water) would likely reduce the footprint of HDS, making the treatment process environmentally friendly and economically exploitable.

The study on precipitation of ochres involved conducting computational simulations from which the chemistry of the treated water and precipitates produced could be assessed. This became a virtual experimental design step as optimised parameters from it were later used in actual experimental studies.

Geochemical simulations: Simulations of the neutralisation (base dosage) and precipitation of ochres were conducted for different pH regimes and using different neutralising agents. For instance, sodium hydroxide, sodium carbonate, magnesium carbonate, lime, and limestone. Mine drainage in gold commodities was used as the input solution and stepwise reactions (titrations) with the neutralising agents simulated. The effect of other parameters such as temperature, dissolved oxygen content, and presence of other components was also assessed. The PHREEQC geochemical modelling code was used for simulations.

Experimental work: The geochemical simulations provided a framework for designing the relevant and appropriate experiments. Stepwise precipitation reactions were conducted in benchtop experiments (e.g. using burettes and beakers) with filtrations conducted at appropriate intervals to separate the precipitates. The precipitates were dried and analysed using powder X-ray diffraction (PXRD) for mineral identification.

Sorption studies

This work involved characterisation of the HDS collected at an AMD treatment plant in the Central Rand goldfield. This was conducted using X-ray fluorescence spectroscopy (XRF), PXRD for mineral identification, sequential extractions (for phase partitioning), inductively coupled plasma optical emission spectroscopy (ICP-OES) for elemental analysis, and ion chromatography for anion (including phosphates) analysis. Assessment of the potential of HDS as an adsorbent for potentially toxic trace metals (including Pb, Cu, Zn, Ni, Co, Cd, etc) in mine drainage and phosphate ($P\text{-}PO_4^{3-}$) in sewage water was conducted in batch and column studies. Desorption studies were also conducted to assess the leachability of metals from the HDS as well as the possibility of slow release of the adsorbed $P\text{-}PO_4^{3-}$.

Computational simulations were conducted to understand the solution chemistry, adsorbent-solution interaction as well as to establish some parameters that were useful for column adsorption studies. These are explained further later.

Batch adsorption studies: these were conducted to determine some important parameters such as adsorbent dosage; effect of pH; effect of ion concentration; effect of contact time; effect of anions and other competing ions; and the effect of temperature on the adsorption of cations and anions (especially $P\text{-}PO_4^{3-}$ ion). Sorption isotherms that are influential on the adsorption process were determined including Langmuir, Freundlich, Dubinin-Radushkevich, and Temkin isotherms. Time studies were determined to evaluate the reaction kinetics.

Thermodynamic effects (activation energies, enthalpy, entropy, etc.) were determined to understand the adsorption process. Desorption studies were also conducted to assess the potential release of the adsorbed cations (metals) and anions ($P\text{-}PO_4^{3-}$).

Column adsorption studies: these were conducted to assess the properties that are essential in a large-scale application of the HDS as an adsorbent. The provisional column dimensions were 30 cm in length and 2 cm in diameter. These were varied to assess the best configurations. The columns were assessed in the upward and downward flow modes. Parameters obtained from batch studies (including reaction kinetics and adsorption isotherms) were useful in establishing parameters for column studies that include adsorbent packing height and flow rates. Column adsorption studies are intended to test whether flow-through exposure of the sludge would be more effective than static in-container exposure.

Computational simulations: these included hydrochemical modelling and reactive transport modelling. In the former, speciation of cations and anions in solution (in both synthetic and real AMD) was assessed. Also, adsorption processes at the solution-adsorbent interface could be elaborated from these simulations. In reactive transport modelling, simulations of reactions and solute transport through columns were conducted. This was helpful in giving insight into the residence times and breakthrough times. Simulations were conducted using the PHREEQC geochemical modelling code.

RESULTS AND DISCUSSION

Precipitation of ochres

Computational simulations were successfully used to predict optimal and best conditions for selective precipitation of ochres from AMD, with NaOH and $MgCO_3$ identified as the best neutralising agents. Ochres with colours varying from yellow to orange to reddish and turquoise were successfully produced when the optimised conditions were used in the experimental work. These were tested on some simple artwork and were comparable to the commercial versions. The resulting treated water had acceptable industrial discharge quality, save for the elevated sulphate concentrations.

Batch and column studies

Batch studies in which HDS was used to condition/pretreat AMD showed promising results that pointed to uptake of trace elements. The adsorption data best fitted the Langmuir isotherm and followed pseudo second-order kinetics, fitting to both linear and non-linear models. The results corroborated those from computational simulations which had shown that hydrous ferric oxide (Hfo) was the dominant adsorption surface in HDS, more like the pure Hfo that had been used in the simulations.

Results also showed effective uptake of phosphates, a reflection of the interaction between Hfo and phosphate in solution. Simulations showed this interaction to be based on surface complexation, which is a chemisorptive process. Sodium hydroxide was found to perform effectively in the desorption of phosphate adsorbed onto HDS. Further work remains to be done related to the kinetics of the desorption process so as to contextualise the potential use of phosphate laden HDS as an amendment in mine tailings.

Simulations for reactive transport showed the expected trends such as longer breakthrough times for more cells (i.e. longer column length) and low concentrations. These results were observed in actual column studies for both AMD conditioning and phosphate removal and the data best fitted the bed depth service time model (which best describes breakthrough times).

CONCLUSIONS

The study has shown that AMD has potential to produce ochres (in varied colours e.g. yellow, orange and red) that can be used as pigments for paint and art applications. Thus, a separate train within the AMD treatment process can be introduced that will reduce production of HDS and lessen environmental liability. Batch and column studies showed the potential of HDS to be repurposed for conditioning/pretreatment of AMD such as

that in abandoned mine voids and shafts. This way, the AMD pumped out for treatment would not require as much neutralising agents and would produce a smaller footprint of AMD. Adsorption parameters showed favourable adsorption of trace elements and their effective removal from solution. This was apparent in the models that were found to best fit the adsorption process e.g. the Langmuir isotherm and pseudo second order kinetic models. These findings were further corroborated by computational simulations which proved useful as an experimental design step for all the parts of the study. HDS also showed promising results for removal of phosphate from agricultural and sewage type water, indicating a strong interaction between Hfo and phosphate in solution. This implied that there is a possibility to control the release of this phosphate when the loaded HDS is used as an amendment on woodlots in mine tailings.

RECOMMENDATIONS

The promising results and findings discussed above give an opportunity for consideration of NaOH and $MgCO_3$ (e.g. from magnesite) for use in trial train within the AMD treatment flow process to conduct selective precipitation of potentially valuable ochres. This would mean a split in the AMD, with the other portion going through the current treatment that produces bulk HDS.

The HDS can then be tested for *in situ* or in-process (a series of pre-steps) conditioning/pretreatment of AMD. This is currently done as a pre-step, but the volumes are very small resulting in the bulk of the sludge being disposed of in landfill sites. HDS may also be used for phosphate removal as has been indicated, with the intention to use waste to treat waste and deriving further value from the products thereof.

DEDICATION

This thesis and all my academic achievements are dedicated to my late mother Tshisaphungo Netshiongolwe. May her soul rest in peace

ACKNOWLEDGEMENTS

I am very fortunate to have been supervised by Professor Hlanganani Tutu. His supervision is of a high standard and his continuous encouragement, support and advice were so amazing throughout this work. Under his supervision, I gained both academic and real life lessons. You acted like a father to me, thank you once again. I am also very grateful for all the opportunities and knowledge you have given me access to. I know geochemical modelling techniques today because you never gave up on me. May God bless you more. I will never forget you even for my future achievements because you laid a good foundation on my academic journey.

To my co-supervisors Profs, Luke Chimuka and Ewa Cukrowska thank you for all your support. To Prof Chimuka, I would also like to thank you for assisting with all field trips for acid mine drainage (AMD) collection in the Central Rand basin of the Witwatersrand goldfields. Special thanks to Ms Sophia Tlale and Ms Nompumelelo Msezane (Trans-Caledon Tunnel Authority) for granting permission to collect high density sludge, and Mr Francois de Jager (Trans-Caledon Tunnel Authority) for assisting with sampling in the Central Rand AMD treatment plant.

I would also like to thank the following people for their contribution to the study: Dr John Zvimba (Water Research Commission), Prof Craig Sheridan (University of the Witwatersrand), Prof Sabelo Mhlanga (SabiNano (Pty) Ltd), Dr Levi Ochieng (Digby Wells Environmental), Dr Caliphs Zvinowanda (University of Johannesburg), Dr Vhahangwele Masindi (Magalies Water), Ms Carla Hudson (Mine Water Coordinating Body), Mr Nkateko Kubayi (Water Research Commission) and Mr Bennie Mokgonyana (Water Research Commission). The experience of presenting and the advice received from Environmental Analytical Chemistry (EACH) research group meetings and at inaugural meetings held in Pretoria at the Water Research Commission have played a significant role to make this work of good quality and to me personally. I am grateful to the National Research Foundation (Grant no. 112921) and Water Research Commission (Project K5/2582) for funding this study.

The EACH welcomed me with warm hands and has been a second home to me. I appreciate Profs Hlanganani Tutu, Luke Chimuka, and Ewa Cukrowska for welcoming me into their research group. Thanks also to Mokgaetji Monyai (Environmental Technician) for ICP-OES training, Prof Marc Humphries for assisting with XRF analysis, Prof Neil Coville for assisting with BET analysis and Ms Petra Dinham for assisting with SEM analysis. In EACH, I am fortunate to have built friendships with the staff members and fellow postgraduates. I would like to thank Kitondo, Kgomotso, Mahadi, Mbongiseni, Emely, Thato, Alseno, and Yannick for their good spirit, willingness to help and support. Thank you to the School of Chemistry, University of the Witwatersrand.

Thank you to Dr Tammy Hodgskiss (Curator, Wits Origin Centre) for ochre workshops and for allowing me to work as a volunteer in your department. I am thankful for the opportunity the school of chemistry has given me to work as a laboratory demonstrator for several years to assist first- and third-year students. This gave me the opportunity of engaging with fellow postgraduates from different research groups within the School of Chemistry.

I was grateful to co-supervise three students during their research, Sicelo Kubheka, Yongezile Mhlana and Siviwe Qokomisa. I would like to thank the School of Chemistry for allowing me to work with these brilliant individuals together with many of the many undergraduates that I have demonstrated and tutored over the years. It was a good experience to work with these amazing students and learn a lot from ideas shared during their research studies.

Thanks to my family for their kindness, patience, and support from the first day of my PhD journey and without them, I would not have been able to do this without their love and encouragement. Thank you to Patson Mudau, Oritonda Netshiongolwe, Lufuno Netshiongolwe and my late mother Tshisaphungo Netshiongolwe.

To my wife, Lufuno Netshiongolwe, thank you for being a source of endless encouragement throughout my PhD journey. I do not have enough to describe how thankful I am for everything that she has done, thank you for the love that you show me daily.

To the almighty God, thank you for giving me wisdom and power to hold on until the end of this study, you remain my God in all situations

To Him, "GOD ONLY", He deserves honour and glory

CONTENTS

LIST OF FIGURES

LIST OF TABLES

ACRONYMS & ABBREVIATIONS

AMD	Acid mine drainage
BET	Brunauer-Emmett-Teller technique
BMED	Bipolar membrane electrodialysis
CRB	Central Rand Basin in Witwatersrand goldfields
DA	Dosing with alkali
DO	Dissolved oxygen
DWA	Department of Water Affairs
DWS	Department of Water and Sanitation
EC	Electrical conductivity
ECL	Environmental critical level
ED	Electrodialysis
Eh	Redox potential
EIA	Environmental impact assessment
FTIR	Fourier-transform infrared spectroscopy
GARD	Global acid rock drainage
GDP	Gross domestic product
HDS	High-density sludge
Hfo	Hydrous ferric oxide
IC	Ion Chromatography
ICP-OES	Inductively Coupled Plasma Optical Emission Spectroscopy
MF	Microfiltration
MPRDA	Minerals and Petroleum Resources Development Act
NEM:WA	National Environmental Management Waste Act
NF	Nanofiltration
ODAS	O-oxidation, DA-dosing with alkali, and S-sedimentation
PEST	Parameter Estimation
PHREEQC	pH REdox EQuilibrium (in C language)
PRBs	Permeable reactive barriers
PXRD	Powder X-ray diffraction
REEs	Rare earth elements
RO	Reverse osmosis
SEM	Scanning electron microscope
TCTA	Trans Caledon Tunnel Authority
TDS	Total dissolved solids
UF	Ultrafiltration
USEPA	United States Environmental Protection Agency
USGS	United States Geological Survey
XRF	X-ray fluorescence

GLOSSARY

Adsorption. The process by which solids holds molecules of liquid or solute as a thin film

Chemical precipitation. The process of removing dissolved trace metals from AMD into insoluble solids (ochre minerals

Coagulation process. Chemical water treatment process utilised to remove solids from AMD influenced by the electrostatic charge particles suspended on aqueous solution

Economic implication. Actions that affect economy

Geochemical process. Processes of change in the chemical composition of rocks and minerals

Geochemical simulations. Computational models used to optimise experimental parameters using PHREEQC geochemical code

Gold-bearing conglomerate. Economic ore deposit containing sulphide minerals

High density sludge. Sludge with higher density containing 10-30% solids

Hydrous ferric oxide. Adsorbent that shares similar characteristics with high density sludge

Neutralising agent. Alkaline solution or powder used to regulate acid/base balance of the reaction

Ochres. Iron precipitates from acid mine drainage

Repurposing High density sludge. Treatment and reuse of sludge

CHAPTER 1: BACKGROUND

This chapter presents an overview of the work, providing a background to the study, its aims, objectives, scope and limitations.

1.1 INTRODUCTION

The world's greatest gold deposit forms part of the Archean Witwatersrand sedimentary basin, situated at the central part of the Kaapvaal of South Africa (Barnicoat *et al.,* 1997; Agangi *et al.,* 2015; Tucker *et al.,* 2016). The geological setting of this clastic sedimentary deposit has yielded more than one third of gold produced on earth (Tucker *et al.,* 2016). The stratigraphy and structural geology of the Witwatersrand basin was investigated to understand the sedimentology, mineralogy, and geochronology (dating of rocks) of the auriferous conglomerate reefs (Dankert and Hein, 2010). The Witwatersrand basin is divided into the eastern, central, and western basins (Netshiongolwe, 2018). This study was based on the Central Rand goldfield where most of the gold mineralisation occurs. The detrital gold largely within the sulphides and uraninite were concentrated along with the place minerals including chromite and zircon (Tucker *et al.,* 2016). The Central Rand goldfield is dominated by the arenaceous sequence consisting of quartz pebble conglomerates, quartzite, quartzwacke, and minor shales (Fuchs *et al.,* 2016).

Pyrite is the dominant Fe containing sulphide in the gold bearing conglomerate and some quartzites are mostly enriched in gold (Tutu *et al.,* 2008; Netshiongolwe, 2018). The pyrite is found in allogenic (rounded compact pyrite associated with detrital zircon and chromite), syngenetic (rounded porous pyrite associated with the colloidal precipitation of Fe sulphide gels), diagenetic (originated in the sediment before lithification and metamorphism), and epigenetic (euhedral to subhedral pyrite originated during the metamorphic or hydrothermal process) forms (Dankert and Hein, 2010; Tucker *et al.,* 2016).

The sector of mining in the South African economy contributes 20% of gross domestic product (GDP) due to availability of economic ore resources (Akinwekomi, 2017). The challenge phased on the environment in mining activities is the formation of large volumes acid mine drainage (AMD) from mine voids as well as in tailing dumps and this threatens the biodiversity, groundwater, infrastructures (especially foundations) and health of communities around the area (Akinwekomi, 2017; Brindha *et al.,* 2017). AMD continues to be a challenging water pollution problem in mining impacted areas worldwide (Akcil and Koldas, 2006; Brahaita *et al.,* 2017). To solve this problem South African government has allocated billions of Rands for short term solution while still looking for long term solution (Akinwekomi, 2017). Acidic mine water is commonly experienced in coal and gold mine activities (Netshiongolwe, 2018). In both active and abandoned mines, once AMD is formed, it becomes more difficult to control the geochemical process and the remediation (treatment procedures) requires high capital (Brahaita *et al.,* 2017; Brindha *et al.,* 2017).

The sources of AMD include the flooded mine voids, as well as other sources including tailings and waste rocks generated by mining (Netshiongolwe *et al.,* 2020; Ojonimi *et al.,* 2021). Humphries et al. (2017) reported that in the Witwatersrand basin, the major source of AMD has been seepage from tailings storage facilities, although the discharge of water from flooded mine voids in abandoned gold mines as well as effluent (from partially treated water) pumped from active mines also contributed to the problem in the recent years. This can be from active mines, abandoned mines, ore processing, and as well as coal washing facilities based on the commodities mined in different geological settings. Factors that determine the rate of acid generation is the hydrogen ion activity, temperature, oxygen content of the gas phase (if saturation is less than 100%), the oxygen concentration in the liquid (water) phase, degree of saturation of water, chemical activity of ferric ion, the surface area of exposed Fe sulphide, the chemical activation energy required to kick start acid generation as well as bacterial activity (John *et al.,* 2017; Ojonimi *et al.,* 2021). Although there is a need to understand the flow monitoring network for quantification of these impacts, this will assist to minimise the impacts of sources of AMD.

The characteristics of AMD differ from site to site due to differences in terms of geological setting, chemical composition, rate of oxidation, and presence of Fe sulphide ores (John *et al.,* 2017). AMD is characterised by low pH, the concentration of dissolved trace metals, high electrical conductivity, and a load of sulphates (Shirin *et al.,* 2021). Gitari et al. (2008) reported the chemical composition of AMD in coal mining and found a significant concentration of Al, Na, Mg, Mn, Ca, Ni, Pb, Cu, and trace metals, the hydrogen ion activity value of 2-3, as well as Fe concentration greater than 6000 mg ℓ^{-1} and higher than 24000 mg ℓ^{-1} sulphate levels. The acidity, Fe, and SO_4^{2-} levels exceeded the standard limit (unfit) for use in agricultural, industry as well as commercial activities. The gold ore contains an elevated concentration of Mg, Al, Ca, Mn, Co, Ni, Cu, Zn, Pb, Cd, As and U, among others (Tucker *et al.,* 2016). The AMD also has low pH (ranging from 2-4) which enhances the mobilisation of above mentioned trace metals as well as the highest concentration of Fe greater than 835 mg ℓ^{-1} (regarded as a suitable source of Fe) and sulphate concentration (as a predominant anion) greater than 2831 mg ℓ^{-1} from gold ores (Humphries *et al.,* 2017).

The environmental impacts of AMD particularly on soil, water and aquatic environments change the biodiversity of which some species may extinct (WHO, 2016; Andersson *et al.,* 2016; Atangana, 2019). The sulphide mineral ores including pyrite, chalcopyrite, and others, are the main source of AMD when they undergo oxidation (Johnson and Hallberg, 2005; Kefeni *et al.,* 2017; Moodley *et al.,* 2018). These minerals are initially exposed to the environment at different stages of mining from mine development to its full operation (Netshiongolwe, 2018). Among the metal sulphides, pyrite (FeS_2) is the common mineral that was found to be more influential in the generation of AMD, as it can easily undergo oxidation when exposed to atmospheric oxygen, water, and microorganisms (Simate and Ndlovu, 2014; Beucher *et al.,* 2017; Dold, 2017). The challenge of AMD discharges is the salinity and metal content in surface and groundwater increasing daily.

AMD causes a severe environmental pollution and health problem to current and future generations, especially due to low hydrogen ion activity, high concentrations of potentially toxic trace metals dissolved in acidic mine water, and sulphates (Ochieng *et al.,* 2017; Dutta *et al.,* 2020). The high metal concentrations pose a health risk where water users are exposed to acidic mine water in streams and tailings ponds (Netshiongolwe, 2018). In particular, among the dissolved metals, ferrous ion (Fe^{2+}) is the dominant ion in most of AMD (Park *et al.,* 2019). Fe^{2+} in the chemistry of AMD reacts with dissolved oxygen to produce iron oxide (Fe_2O_3) and hydroxide ($Fe(OH)_3$) precipitates (Park *et al.,* 2019). The formation of $Fe(OH)_3$ precipitates makes the pollution problem worse by lowering the pH and damage majority of microorganism existing in it (Bejan and Bunce, 2015; Han *et al.,* 2015; Siebert *et al.,* 2019). AMD is corrosive and interacts with waste rocks containing different types of minerals from the ore deposit and this influences the solubility of toxic metals (Siebert *et al.,* 2019).

The generated AMD raises the concentration of dissolved metals in the receiving water medium (particularly surface water) and negatively affects the plants and animal life in general (Li *et al.,* 2014; Camden-Smith *et al.,* 2015; Skousen *et al.,* 2019). The degree of pollution caused by AMD depends on its chemical composition and hydrogen ion activity, of which the main driving force depends on the geology of the area (Dwiki *et al.,* 2015). For example, in South Africa, Fe^{2+} is very high; however, source depends on variations in concentration based on where the data was collected. Kefeni *et al.,* (2015) detected the Fe^{2+} concentrations in coal and gold mines and the average values were found to be 2135 mg ℓ^{-1} and 835 mg ℓ^{-1}, respectively. Other Fe^{2+} concentrations of AMD reported in Spain were found to be 2040 mg ℓ^{-1} in average (Valente *et al.,* 2013; Carrero *et al.,* 2015). These results reported in both South Africa and Spain clearly showed considerable variation of mineral composition and dissolved metal ions in AMD based on the stratigraphy of the geology of where mining activities is taking place (Kefeni *et al.,* 2017). The high concentration of iron in AMD can lead to recovery of potential Fe precipitates that can be used as art pigments.

Therefore, the long-term solution for AMD remediation requires effective and efficient technology that can reduce its negative impacts on the environment (Bussiere, 2009; Akinwekomi, 2017). Remediation of AMD with more dissolved toxic metals is complex and very expensive (Anawar, 2015). If there is no proper environmental management plan for AMD, it may result in environmental degradation, water, and soil pollution (Albanese *et al.,* 2014; Ngure *et al.,* 2014; Anawar, 2015; Mulopo, 2015a; Netshiongolwe, 2018; Khazaal *et al.,* 2019). Therefore, to preserve and protect the natural environment and enhance environmental sustainability, AMD generation should be prevented. However, once AMD is generated, urgent remediation

becomes essential. The challenge with most remediation methods developed for AMD is that they are prohibitively expensive (Martí-Calatayud *et al.,* 2014; Anawar, 2015; Carolin *et al.,* 2017; Li *et al.,* 2019). Some of the developed remediation options for AMD mainly focus on neutralising, stabilising, and removing contaminants through various physical, chemical, and biological processes (Macingova and Luptakova, 2012; Ali *et al.,* 2019). Other methods that have been reported in the literature include biological passive treatment using sulphate-reducing bacteria, environmentally friendly materials available (e.g. bentonite, lignite, and zeolite), magnetic nanoparticles, membrane technology etc. However, AMD neutralisation (which results in chemical precipitation) is still preferred widely and results in the production of high density sludge (Masukume *et al.,* 2014; Qureshi *et al.,* 2016; Kefeni *et al.,* 2017; Akinwekomi, 2017). Precipitation of metals in water has been practiced as a prime method of treatment in industrial waters for many years (Kaur *et al.,* 2018). The process involves the transformation of dissolved contaminants into insoluble solids, thereby facilitating the contaminant's subsequent removal from the liquid phase by physical methods, such as filtration (Ascott *et al.,* 2016; Atibu *et al.,* 2016; Kaur *et al.,* 2018).

The conceptual mechanism of metal removal by chemical precipitation is:

$$M^{2+} + 2OH^{-} \rightleftharpoons M(OH)_2\downarrow$$

The coagulation process involves destabilisation of colloidal particles by adding a coagulant, resulting in sedimentation (Beuche *et al.,* 2017). To increase the particle size, coagulation is followed by flocculation of unstable particles into bulky floccules (Gautam *et al.,* 2014). The general approach of this technique includes pH adjustment and involves addition of ferric/alum salts as a coagulant to overcome repulsive forces between particles (Creed *et al.,* 2017). This type of flocculation is usually used in conventional potable water treatment plants. In HDS plants, a polymer is added as a flocculant and acts as a densifying agent for the produced sludge (Akinwekomi, 2017). While the treated water discharged into streams usually contains elevated concentrations of sulphates, most trace elements are co-precipitated with Fe and contained in the resulting hydrous ferric oxides (Hfo) that constitute the bulk of the HDS.

For AMD treatment plants on the Witwatersrand Basin, environmental impact assessments (EIAs) on selected sites where construction of the plants was to take place were done. The main purpose was to pump acidic mine water from abandoned mine shafts to meet the environmental critical levels (ECL). For instance, there is a risk of AMD seeping into groundwater and this mine water threatens heritage sites like Cradle of the Humankind in the western basin of the Witwatersrand (Maree *et al.,* 2010; Aubertin *et al.,* 2016; Nieva *et al.,* 2018). With a total volume 200 Mℓ d^{-1} of AMD produced, its neutralisation was a matter of urgency. The central and western basins AMD is characterised by elevated Fe concentrations of up to 1000 mg ℓ^{-1} and up to 4000 mg ℓ^{-1} of sulphates. Owing to this, treatment plants in these basins produce large volumes of HDS and gypsum as its major constituents.

Disposal of this HDS poses an environmental challenge as it tends to act as a secondary source of pollution. The sludge is sometimes disposed of at landfill sites or on old mine tailings. Not much has been done (at least in AMD treatment plants in Witwatersrand Basin) to assess alternative uses of this sludge nor in modifying the treatment flow path so as to generate valuable products.

1.2 AIMS AND OBJECTIVES

The main aim of this study was to explore ways of repurposing the sludge generated from AMD treatment and to innovate around the neutralisation process so as to yield valuable products from it. This was achieved by pursuing the following objectives:

1. To conduct computational simulations that would provide insights into the neutralisation process (using various neutralisation agents) and interactions between solutions and the adsorbent high density sludge.

2. To use optimal simulations in #1 to design experiments for selective precipitation of ochres from AMD and assess the potential of these for use in artwork and as paint pigments.
3. To characterise HDS from an AMD treatment plant and use it, based on predictions from optimal simulations in #1, to conduct adsorption studies (batch and column) to assess its capability to remove contaminants in mine water.
4. To conduct adsorption studies (batch and column) to assess the capability of sludge to remove phosphate in agricultural- and sewage-type of water.
5. To assess release of the adsorbed phosphate and potential use of phosphate-laden sludge as an amendment in woodlots on mine tailings.

1.3 SCOPE AND LIMITATIONS

The scope of this study covered: the potential of conducting selective precipitation of ochres from AMD and assessing the potential use of such ochres in artwork and as paint pigments; potential use of the conventional high density sludge formed from the current neutralisation of AMD as an adsorbent for trace metals for *in situ* treatment of mine void and shaft water; and potential use of the sludge as an adsorbent for phosphate, with the intention to apply the phosphate-laden sludge as an amendment and source of phosphate for plants used for phytoremediation on mine tailings. To achieve this, geochemical simulations were used to optimise experimental parameters in both batch and column studies using the PHREEQC geochemical modelling code. The computational studies assisted to understand the geochemical processes and speciation of trace metals and phosphates.

The limitations included: the use of HDS as an adsorbent for mine water treatment in pilot scale, the challenge is that the design of the treatment plant need the assistance of chemical engineers' opinions and space of building pilot scale is needed as space in the lab is small. The idea of the pilot scale was to test the performance of HDS before it is implemented in the AMD treatment plant by pumping HDS underground in the flooded mine tunnels to improve the quality of water pumped in the surface. The test of using adsorbed phosphates in HDS (as fertilizers) as supplements of phosphorous to plants used for phytoremediation. The HDS with phosphate was supposed to be used as fertilizers to plants growing in the greenhouse before doing the real applications to plants growing in the tailings. This involves the effect of the phytoremediation of different plants on the pH value and organic matter of HDS.

1.4 STRUCTURE OF THESIS

The thesis is structured as follows:

Chapter 1 – focuses on the background, aims, objectives, scope and limitations of the study.

Chapter 2 – describes: gold mining overview; AMD generation; techniques implemented to prevent AMD generation; methods used for AMD remediation including both passive and active methods; innovative methods to derive value from AMD, including those suggested and pursued by this study.

Chapter 3 – focuses on the simulation studies for ochres (Fe precipitates) prediction; batch and reactive transport models using geochemical modelling; the characterisation of high density sludge (HDS); repurposing of this HDS for further treatment of AMD and adsorption of phosphates from contaminated water (e.g. sewage and agricultural-type water).

Chapter 4 – describes the findings of the study based on the protocols followed from the methodology. Results were discussed following the findings and seconded by relevant literature where appropriate. Brief conclusions have been included at the end of each section whose findings are reported.

Chapter 5 – focuses on the outcome of the study that came up with general conclusions and recommendations.

PUBLICATIONS AND OUTPUTS

The following are the publications and outputs emanating from the thesis:

1. Netshiongolwe K, Mhlana Y, Mosai A, Richards H, Chimuka L, Cukrowska E, and Tutu H (2020). Recovery of ochers from acid mine drainage treatment: a geochemical modelling and experimental approach, Chapter 6. In: Elvis Fosso-Kankeu, Christian Wolkersdorfer and Jo Burgess (editors). *Recovery of Byproducts from Acid Mine Drainage Treatment*. Scrivener Publishing LCC. ISBN:9781119620075; Online ISBN:9781119620204. 159-185. DOI:10.1002/9781119620204.

   Role of candidate: conducted experimental work, conducted data modelling, wrote the draft chapter and final chapter.

   This publication relates to Chapter 4.1 and 4.2

2. Netshiongolwe K, Chimuka L, Cukrowska E, Tutu H. *Computer simulations for sludge-mine water interaction and batch sorption studies of sludge for mine water treatment: geochemical modelling and experimental approach* (draft manuscript to be submitted to Journal of Environmental Pollution).

   Role of candidate: conducted experimental work, conducted data modelling, wrote the draft manuscript and final article.

   This manuscript relates to Chapter 4.4 and 4.5

3. Netshiongolwe K, Qokomisa S, Mosai A, Chimuka L, Ewa Cukrowska E, Tutu H. *Computational and batch adsorption studies for phosphate recovery in wastewaters on High-Density Sludge: geochemical modelling and experimental approach* (draft manuscript to be submitted to Journal of Science of the Total Environment).

   Role of candidate: conducted experimental work, conducted data modelling, wrote the draft manuscript and final article.

   This manuscript relates to Chapter 4.8 and 4.9

4. Netshiongolwe K, Mosai A, Chimuka L, Ewa Cukrowska E, Tutu H. *Computer simulations and batch sorption studies of High-Density sludge for high removal of sulphates in acid mine drainage: geochemical modelling and experimental approach* (draft manuscript to be submitted to Journal Environmental Management).

   Role of candidate: conducted experimental work, conducted data modelling, wrote the draft manuscript and final article.

   This manuscript relates to Chapter 4.4 and 4.5

5. Netshiongolwe K, Chimuka L, Ewa Cukrowska E, Tutu H. *Computational and Column adsorption studies for phosphate recovery in wastewaters on High-Density Sludge: geochemical modelling and experimental approach* (draft manuscript to be submitted to Journal of water, air and soil pollution).

   Role of candidate: conducted experimental work, conducted data modelling, wrote the draft manuscript and final article.

   This manuscript relates to Chapter 4.10 and 4.11

6. Netshiongolwe K, Chimuka L, Ewa Cukrowska E, Tutu H. *Computational and column sorption studies using High Density Sludge for mine water treatment: geochemical modelling and experimental approach* (draft manuscript to be submitted to Journal of Environmental Protection).

   Role of candidate: conducted experimental work, conducted data modelling, wrote the draft manuscript and final article.

   This manuscript relates to Chapter 4.6 and 4.7

7. Poster presentation for SUSTREM 2021. Network for industrial contaminated land in Africa (NICOLA). *Empowering Sustainable Land Management for the future*. 4-5 November 2021, Virtual Conference.

   Khathutshelo Netshiongolwe and Hlanganani Tutu. *Precipitation of ochres from acid mine drainage treatment: a computational and experimental approach.*

   Role of candidate: conducted experimental work, conducted data modelling and wrote the draft of the poster presentation.

   This poster relates to Chapter 4.1 and 4.2

CHAPTER 2: LITERATURE REVIEW

2.1 LITERATURE REVIEW

This chapter gives an overview of gold mining on the Witwatersrand Basin and generation of AMD; methods that are used to prevent AMD generation; passive and active methods for remediation of AMD; and methods for the recovery of value from AMD, including those suggested and pursued by this study.

2.1.1 Gold mining in the Witwatersrand goldfields

Gold was mined in different gold bearing conglomerates in seven goldfields of the Witwatersrand Basin (Feather and Koen, 1975; Li *et al.,* 2022). Almost 70 minerals in the gold bearing ore deposits, including a variety of silicates, cobaltite (CoAsS), pyrite (FeS_2), sphalerite (ZnS), arsenopyrite (FeAsS), chalcopyrite ($CuFeS_2$), brannerite ($UO_3Ti_2O_4$) and uraninite (U_3O_8) among others were found (Viljoen and Viljoen, 2004; Tutu *et al.,* 2008). The basin (Figure 2.1) is replete with mine tailings (slimes dams and sand dumps) that are currently being reprocessed.

Figure 2.1. Google Earth image showing the scatter of mine tailings from the West, through the Central to the East Rand Goldfields and the associated drainage systems e.g. streams, rivers, wetlands and dams. Most of these systems are impacted by acid mine drainage.

Reprocessing activities are quite evident, characterised by tailings ponds and weathered tailings (Figure 2.2). The process involves pumping tailings slurry to plants where a mixture of NaCN, KCN and $Ca(CN)_2$ in a high pH and aerated solution (to keep cyanide in solution) are applied in vat tanks (Figure 2.3). High stability complexes of gold (Au) and silver (Ag) are formed as illustrated by the Elsener reaction (Equation 2.1) (Adamson, 1972).

$$4Au(s) + 8CaCN(aq) + O_2(g) + 2H_2O(l) \rightarrow 4CaAu(CN)_2(aq) + 4CaOH(aq) \quad (2.1)$$

(a)  (b)  (c) 

Figure 2.2. Gold recovery from tailings (a) AMD generated in the Central Rand basin (b) and (c) ferrocyanide containing water at pH 9 that mixed with AMD in the stream at pH 2.5, resulting in the formation of Prussian blue (Bakatula *et al.,* 2012).

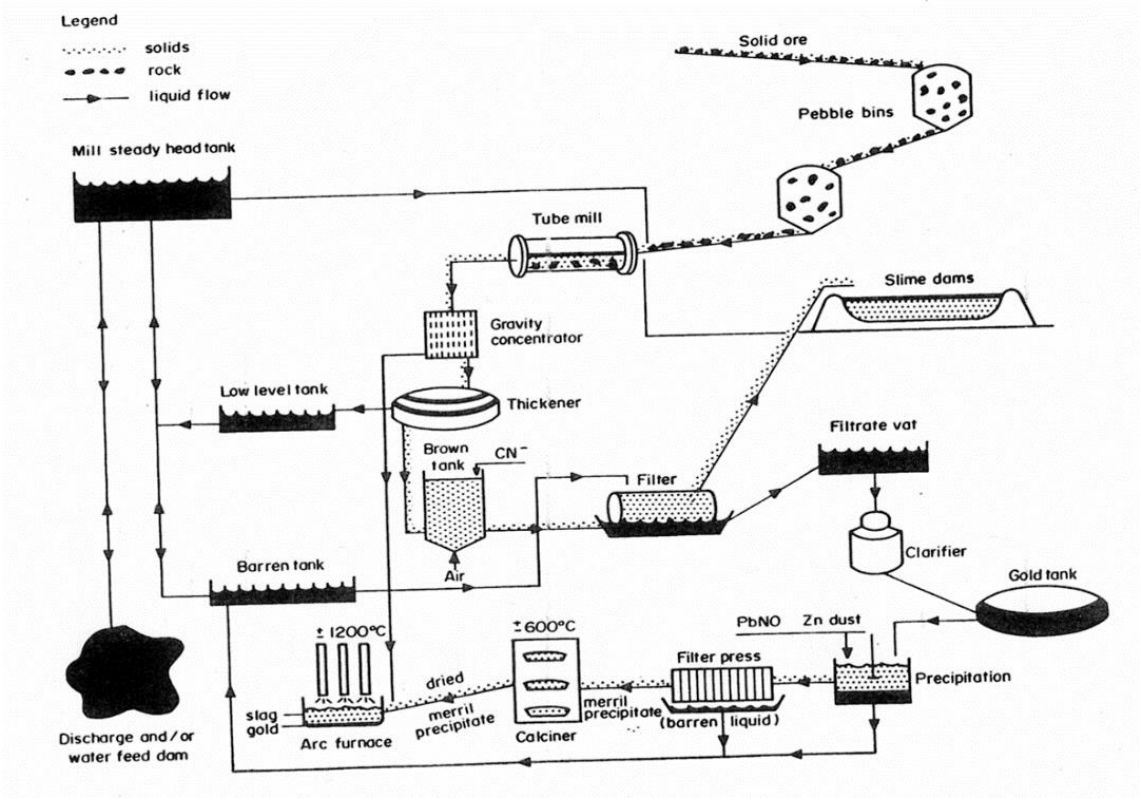

Figure 2.3. Recovery techniques of gold using cyanide (Crown Gold Recovery, 2003).

2.1.2 Summary of the chemistry of acid mine drainage

The formation of AMD results when sulphur containing minerals in the ores and mine tailings are exposed to water and atmospheric oxygen during coal and gold mining (Cheng *et al.,* 2009; Bálintová and Singovszká, 2011; Chopard *et al.,* 2017; Cozzolino *et al.,* 2018; Hansen, 2020). The AMD solutions formed sometimes display the apparent constituents in them, usually a red colouration that is typical of high Fe^{3+} concentrations (Figure 2.4).

(a)  (b) 

Figure 2.4. AMD formed on the tailing dumps in the (a) Central Rand basin (b) West Rand basin of the Witwatersrand goldfields. The deep red colouration shows the presence of high Fe^{3+} concentration (Coetzee, 2010; Netshiongolwe, 2018; Naidu *et al.,* 2019).

The chemistry of AMD involves the oxidation of FeS_2 to Fe^{2+} and then further oxidation to form Fe^{3+} (Equations 2.2 and 2.3) (Singer and Stumm, 1970; Garland, 2012; Li *et al.,* 2013; Masindi *et al.,* 2018):

$$2FeS_2(s) + 7O_2(g) + 2H_2O(l) \rightarrow 2Fe^{2+}(aq) + 4SO_4^{2+}(aq) + 4H^+(aq) \quad (2.2)$$

$$4Fe^{2+}(aq) + O_2(g) + 4H^+(aq) \rightarrow 4Fe^{3+}(aq) + 2H_2O(l) \quad (2.3)$$

The Fe^{3+} reacts with water and to form a precipitate, $(Fe(OH)_3)(s)$, and this insoluble precipitate releases more acidity (Equation 2.4):

$$Fe^{3+}(aq) + 3H_2O(l) \rightarrow Fe(OH)_3(s) + 3H^+(aq) \quad (2.4)$$

The production of Fe^{3+} in abundance by reactions at the latter stage may also influence further oxidation of FeS_2 to oxidize into Fe^{2+} and this becomes a self-perpetuating reaction (Equation 2.5):

$$FeS_2(s) + 14Fe^{3+}(aq) + 8H_2O(l) \rightarrow 15Fe^{2+}(aq) + 2SO_4^{2+}(aq) + 16H^+(aq) \quad (2.5)$$

As a result of the last reaction and also the large volumes of acidity formed, AMD is known to continue for hundreds of years after active mining has stopped (Akcil and Koldas, 2006; Naidu *et al.,* 2019). This also implies a continual release of toxic elements within the host ores (Gautama and Kusuma, 2016) . The above reactions have been simplified, but other factors such as microbial activity (*Thiobacillus ferroxidans*), the types of sulphur-containing minerals and temperature are very important (Singer and Stumm, 1970; Boukhalfa and Chaguer, 2012; Bonnelye, 2015; Park *et al.,* 2018). Further, AMD is propagated by the dissolution of secondary sources of contamination in the form of mineral crusts such as gypsum ($CaSO_4.2H_2O$), melanterite ($FeSO_4.7H_2O$), copiapite ($Fe^{2+}Fe^{3+}{}_4(SO_4)_6(OH).20(H_2O)$) and jarosite ($KFe^{3+}{}_3(OH)_6(SO_4)_2$) (Akcil and Koldas, 2006; Tutu *et al.,* 2008; McCarthy, 2011; Grover, 2016). These minerals are formed during the evaporation of AMD solutions and are quite common on the fringes of receptor water systems (Lecomte *et al.,* 2017; Hansen, 2018). Even though gypsum ($CaSO_4.2H_2O$) is usually the predominant mineral and slightly increases the water pH on dissolution, its impact is overridden by that of the other acid-generating salts (Grover *et al*., 2015; Grover, 2016).

2.1.3 Prevention of acid mine drainage (AMD) generation

Prevention of AMD generation should start with the protection of sulphide minerals from air, water, and bacteria, as this influences the chemical reactions (Bunce *et al.,* 2018; Igarashi *et al.,* 2020). This can be achieved by several environmental management methods that can be implemented in tailings and waste rocks. In active mines, among other management methods, backfilling by using a mixture of mine waste materials including mixtures mine tailings and soil, quarried and crushed aggregate, sand, and Portland cement are used

as binders to reduce acid generation (Kefeni *et al.,* 2017; Tabelin *et al.,* 2018). The mine wastes used as backfills are placed into underground mine tunnels and mine voids to improve the underground conditions (including the stability of the ground), and this improves alkalinity to neutralise the acidic mine water (Johnson and Hallberg, 2005; Nejeschlebova *et al.,* 2015; Kefeni *et al.,* 2017). Mine wastes used in backfilling can be dry, cemented, hydraulic, and paste backfills. In Canada, paste backfill is the common method implemented (Villain *et al.,* 2013; DIIS, 2016). The main purpose of filling mined voids with mine wastes is to prevent atmospheric oxygen to interact with rocks to limit the oxidation of iron sulphides (Villain *et al.,* 2013; Dold, 2014; Lebre *et al.,* 2017).

On the surface, several AMD generation prevention alternatives could be used like dry, cover, and oxygen consuming cover; and tailings disposal can be useful to act as oxygen barriers to prevent AMD generation (Blowes *et al.,* 2014; Demers *et al.,* 2015; Kefeni *et al.,* 2017). Prevention of AMD generation is an essential task to prevent environmental risks in the future (Lu *et al.,* 2014; Neamtiu *et al.,* 2017). In other countries like Sweden, dry and water cover are the most common methods used to prevent the oxidation of sulphides (Ljungberg and Öhlander, 2001; Benner *et al.,* 2002). In a dry cover, tailings with low-sulphide content, clay soils, alkaline materials, organic wastes, and other neutralising agents are used to prevent AMD generation (Smart *et al.,* 2010; Olds *et al.,* 2013; Demers *et al.,* 2013; Demers *et al.,* 2017; Kefeni *et al.,* 2017).

Recently, alkaline industrial by-products have also used to cover waste rocks and tailings to prevent AMD generation (Lottermoser, 2010; Mulopo, 2015a; Grande *et al.,* 2018; Igarashi *et al.,* 2020). At Stockton mine (New Zealand), a small-scale trial was conducted, and high alkalinity generation was observed from a mixture composed of cement kiln dust to granite in a 1:4 ratio by volume (Allison and Margaret, 2015). The alkalinity generation stabilised after 31 weeks at approximately 500 mg $CaCO_3$ eq. ℓ^{-1} (Olds *et al.,* 2013). Abreu *et al.,* (2012) conducted a study where seven waste cover options including waste rock; red mud-waste; limestone-waste rock; lime-waste rock; red mud; limestone, and lime were assessed for 100 days to prevent the generation of AMD. The mixture of red mud waste rock was found to be the best option to prevent AMD generation. A subaqueous tailing disposal was also used to restrict oxygen interaction with reactive materials in tailings to prevent the oxidation of iron sulphide (Blowes *et al.,* 2014; Wei *et al.,* 2014; Wei *et al.,* 2018).

2.1.4 Options for AMD Remediation

AMD can present environmental risks that may lead to unaffordable costs if it is not identified and its generation prevented at an earlier stage. To succeed in achieving sustainable mine rehabilitation, proper environmental management during active mining operations is important. In Canada, they have introduced various initiatives to address the pollution problem experienced in abandoned mines and AMD like National Orphaned and Abandoned Mine Initiative (Kojo *et al.,* 2013; Sangiorgi *et al.,* 2016). AMD treatment is classified as active and passive treatment methods. In active treatment methods, a variety of neutralising agents (alkaline) is used to ensure the water discharged after treatment meets the required discharge standard (Chen *et al.,* 2015; Chopard *et al.,* 2017; Pyrbot *et al.,* 2019).

The primary chemical and physical processes of active treatment *in situ* and in a fixed treatment plant such as precipitation (chemical neutralisation is generally adopted) which is influenced by pH control and electrochemical process; sulphate reduction through microbial intervention, flocculation, adsorption, and ion exchangers, filtration, and crystallization (Golder Associates, 2009; Bai *et al.,* 2013; Zhang *et al.,* 2021). In large scale AMD remediation, commonly used neutralising agents include caustic soda (NaOH), lime ($Ca(OH)_2$) and limestone ($CaCO_3$), magnesium oxide (MgO), and magnesium hydroxide ($Mg(OH)_2$ (Akinwekomi, 2017). Due to $CaCO_3$ low cost among these neutralising agents, it is commonly used in acid neutralisation (Kefeni *et al.,* 2017). However, the neutralisation and chemical precipitation through hydrogen ion activity change alone are not enough, particularly when trace metals including arsenic (As), molybdenum (Mo), mercury (Hg), selenium (Se), and chromium (Cr) form part of AMD matrix. Secondary treatment of effluent may be therefore necessary. Another environmental challenge of the neutralisation method is aqueous sludge produced with more than 90% water and containing trace metals (Xu *et al.,* 2020).

In terms of cost analysis for AMD treatment, active treatments are considered expensive compared to passive treatment, especially in abandoned mines (Santos Jallath *et al.,* 2018). Passive treatment methods mostly achieve precipitation of metal sulphide by creating reducing conditions and utilising organic substances as buffers or alkaline agents (Filipek *et al.,* 2003; Clyde *et al.,* 2016). Passive treatment methods include aerobic wetlands, compost reactors, anoxic and open limestone drains and channels, bioreactors, and permeable reactive barriers. Active treatment methods on the other hand involve use of powered equipment such as pumps and include membrane technologies and neutralisation in tanks (Figure 2.5).

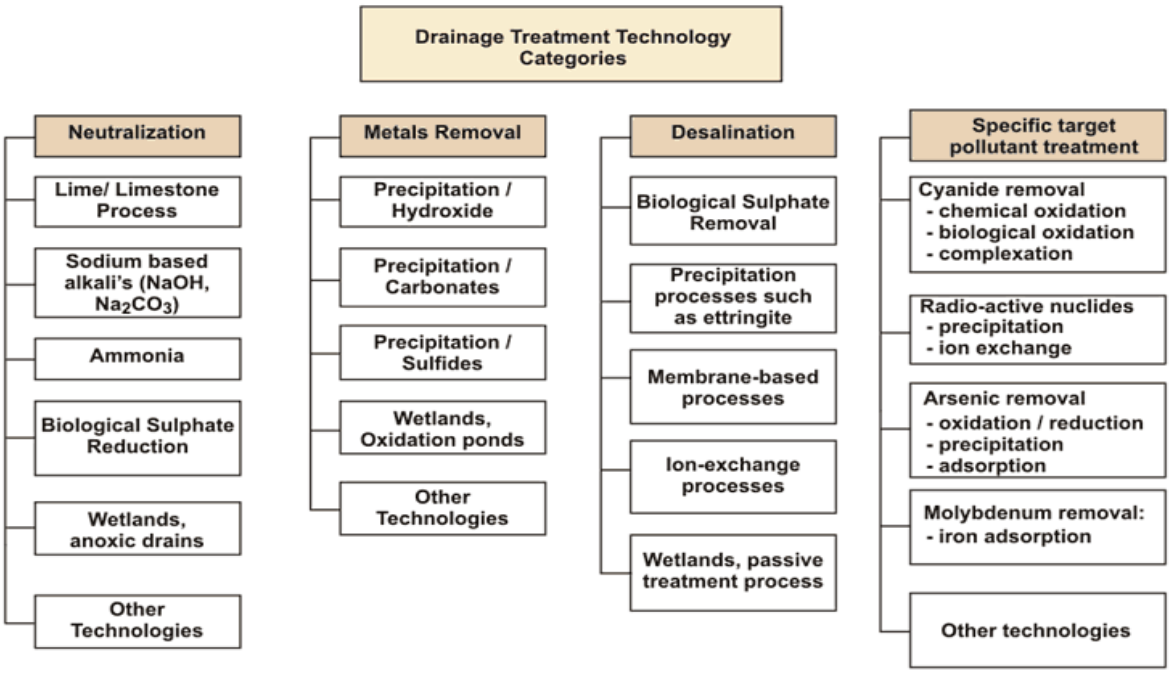

Figure 2.5. AMD treatment technology categories (GARD Guide).

Some of the methods are discussed below.

Ion exchange

Ion exchange is one of the most common technique used to treat wastewaters. In this method, water (aqueous phase) flows through a bed (solid phase) which is an ion exchange material (Hou *et al.,* 2020). The cations and anions in the wastewater are attracted to the surface of the material and make an exchange with those on the material surface (Hernandez-Santin *et al.,* 2020). This technique has proved to be effective in treating water, especially at low trace metal concentrations. The exchange material has water-insoluble ion exchangers which are usually synthetic organic ion exchange resins (Shah and Daverey, 2021). Sodium (Na^+) and hydrogen (H^+) are ions in the exchangers which are replaced by trace metals from wastewater (Igalavithana *et al.,* 2017; Rodríguez-Galán *et al.,* 2019).

Membrane filtration

The membrane filtration technique is one of the most widely utilised for the treatment of water and wastewaters (Ferreira *et al.,* 2018; Ryu *et al.,* 2019). Several membrane filtration types including ultrafiltration and reverse osmosis are used and this is dependent on the size of the molecules (trace metal) that can be retained (Aguiar *et al.,* 2016; Kirkelund *et al.,* 2019). Permeable membranes that can separate trace metals from wastewaters are utilised in this method. The lower driving force and small space required are some of the benefits that led to the high usage of membrane filtration (Vital *et al.,* 2018; Song *et al.,* 2019). The widely used ultrafiltration technique is the polymer-supported ultrafiltration method which uses polymeric ligands which are soluble in water. These ligands can bind trace metals from wastewaters and form complexes (Ahamed and Lichtfouse,

2020). This technique needs low energy and it has high selectivity of the trace metal. In reverse osmosis, pressure is utilised to apply force on water through a semipermeable membrane that retains the trace metals and allows treated water to pass through to the receiver (Ahmed *et al.,* 2021). The separation occurs at the dense barrier layer in the polymer matrix of the semipermeable membranes (Ahmed *et al.,* 2021). This method is effective but has high operation costs (due to the expensive membranes) (Chen *et al.,* 2018).

Solvent extraction

The solvent extraction technique is widely applied in hydrometallurgical processing to remove trace metals from wastewaters (Hoang *et al.,* 2019). The significant three steps in this method include the extraction, scrubbing, and stripping step (Ahmed *et al.,* 2021; Elizabeth Rani *et al.,* 2021). In the extraction step, the wastewater interacts with the solvent extractant in a mixer-settler. In the mixer-settler, the trace metals are transferred to the water immiscible phase which is moved to another mixer-settler containing the stripping aqueous solution (Khan *et al.,* 2015). The remaining solution is then submitted for recovery of other trace metals, discharged, or re-treated. The water-immiscible phase goes to the scrubbing step if the selectivity in the extraction step was lower (Li *et al.,* 2019). Other metals in the matrix of the sample (impurities) are removed in this step. In the final step, the stripping step, the trace metals are stripped out of the water-immiscible phase to another solution, and this results in a concentrated aqueous solution of the trace metals (Mosa *et al.,* 2019). The trace metals are then purified to obtain metal oxides or pure metals (Ok *et al.,* 2020).

Electrochemical treatment

Electrochemical treatment techniques can be utilised to remove trace metals from wastewaters. In this technique, power (electricity) is applied to pass current through the wastewater solution which has a cathode plate and an insoluble anode (Dutta *et al.,* 2020). As electrons move from metal to metal, the current is generated (Jadhav *et al.,* 2017). In the electrochemical process, the trace metals must be precipitated in a weak acid. Many chemicals ($CaCO_3$, NaOH etc.) are used to reduce trace metals so that they can be discharged (Deng and Lin, 2013).

Phytoremediation

Several studies focused on other advanced techniques (to find alternative solutions) for the recovery of trace metals (Bhargava *et al.,* 2012; Alloway, 2013; Hazotte *et al.,* 2017). Phytoremediation is one of those methods and it refers to the usage of plants for environmental remediation (Liu *et al.,* 2018; Mirzaei *et al.,* 2021). Its focus is on phytodegradation, phytoextraction, phytostimulation, phytovolatilization, phytostabilisation, and rhizofiltration (Mirzaei *et al.,* 2021). In phytodegradation, plants uptake contaminants, store and degrade them within their tissues (Mandzhieva *et al.,* 2016; Moameri and Abbasi-Khalaki, 2019). Phytoextraction is a process whereby plants adsorb contaminants from the soil matrix, translocate and store them into their root and shoot tissue (Mirzaei *et al.,* 2021). This process can occur naturally through plants (hyperaccumulators) or can be induced by adding chelators which increase bioavailability (Nsanganwimana *et al.,* 2021). Hyperaccumulators can absorb large amounts of trace metals than other plant species (Rossini-Oliva *et al.,* 2018; Rusinowski et al., 2019). Phytostimulation uses rhizosphere associations between plants and symbiotic soil microbes to degrade contaminants (Antwi-Agyei *et al.,* 2009; Sheoran *et al.,* 2016). Phytovolatilisation is a process whereby plants uptake contaminants and transform them to other forms after which can be volatilised into the atmosphere (Zeng *et al.,* 2019). This process occurs as plants uptake water and other organic contaminants (Nsanganwimana *et al.,* 2021). In phytostabilisation, plant roots are used to reduce the movement of contaminants through adsorption and therefore reducing their bioavailability (Zehra *et al.,* 2020). These contaminants can also be precipitated in the rhizosphere (Sheoran *et al.,* 2016). The reduction in mobility of contaminants prevents their migration to surface and groundwater (Hazotte *et al.,* 2017). Rhizofiltration is one of the phytoremediation methods whereby contaminants are adsorbed or precipitated onto plant roots or even absorption into the roots (Mandzhieva *et al.,* 2016). This process is like phytoextraction. Trace metals including Cu, Cd, Pb, and Ni have been removed from wastewaters using rhizofiltration with great success (Nsanganwimana *et al.,* 2021).

Bioremediation

Bioremediation using microbes to remove contaminants from wastewaters has received much attention lately due to high efficiency and less costs (Sheoran *et al.,* 2016; Skousen *et al.,* 2017; Amann *et al.,* 2018). Bioremediation known as biosorption is a safe and economic physicochemical process that occurs in biological systems (Masindi *et al.,* 2015; Alam *et al.,* 2018). The trace metals are adsorbed onto the cellular structure of microbes (Chen *et al.,* 2019). Some of the advantages of this technique are that no energy is required, cost effective, less chemical, physical sludge, environmentally friendly, no waste generated, and self-sustaining (Liu *et al.,* 2018). However, it is not easy to obtain microbes that can be used for trace metal remediation, it is time consuming, and it is not always suitable. In biosorption, the biological material (solid phase) and wastewater (liquid phase) containing trace metals come into contact and adsorb onto the cell walls of microbes (Ali and Khan, 2018; Fan *et al.,* 2020). Carbonyl, hydroxyl, ketone, and amino groups in cell walls are responsible for the biosorption of trace metals (Li *et al.,* 2018) . Bacteria, fungi, and algae can be used in this process (Ayangbenro and Babalola, 2017; Dickinson *et al*., 2019; Nsanganwimana *et al.,* 2021). The more attractive processes are reverse osmosis, ion exchange, and adsorption due to low costs and relatively high investment (Lian and Xing, 2017). Moreover, metal values can be easily recovered using these processes (Lian and Xing, 2017; Li *et al.,* 2018). However, adsorption has been given more attention because of the readily available adsorbents which cost less and the design is simple with a sludge free environment.

Adsorption

Adsorption has been proven to be the most efficient and economical alternative technique for removing trace metals in wastewaters (Antelo *et al.,* 2005; Anna *et al.,* 2014; Liang *et al.,* 2017). The adsorption process uses adsorbents such as bentonite, zeolites, bentonite, polymers, chitosan, fly ash, and clay to remove trace metals (Benavente *et al.,* 2011; Lin *et al.,* 2017; Liu *et al.,* 2021). Adsorption of trace metals can occur through chemical and physical processes (Babel and Kurniawan, 2003; Liu *et al.,* 2016; Arroyave *et al.,* 2018). Adsorption is a mass transfer process whereby there is a transfer of trace metal (adsorbate) or substance from the liquid phase to the solid phase surface (adsorbent) and is bound through physical or chemical interactions or even both (Otunola and Ololade, 2020). In adsorption, two forces of interaction can occur between the adsorbent and the adsorbate through physisorption and chemisorption (Aydin *et al.,* 2008; Zou *et al.,* 2016; Bai *et al.,* 2017; Zhang and Ding, 2018). The characteristics of both forces are described in Table 2.1.

Table 2.1. Characteristics of physisorption and chemisorption

Physisorption	Chemisorption
Physical adsorption occurs in physisorption where the forces involved are van der Waals forces.	Chemical bonds form which are based on chemical specificity.
There is a minimal perturbation of the electronic states of the adsorbent and adsorbate.	There are significant changes in the electronic state which can be detected by spectroscopy, electrical conductivity, and magnetic susceptibility.
The adsorption and desorption of the adsorbate do not change the chemical nature of the liquid phase in which the adsorbate is contained.	The adsorption may not be reversible thus desorption is impossible.
Adsorption energy between the adsorbent and adsorbate is the same. Always exothermic.	The chemical reactions can be exothermic or endothermic
The elementary step does not include activation energy.	The elementary step includes activation energy.
Equilibrium is reached between the adsorbate and the liquid phase.	If the activation energy is large enough, equilibrium may be reached slowly or not reached at all.
Multilayer adsorption occurs	Monolayer adsorption occurs

In physisorption, the adsorbate can move over the surface since the forces involved are weak, not fixed to a particular site (Zinck and Griffith, 2013; Yi *et al.,* 2017). In chemisorption, the adsorbate is fixed on the surface due to the strong forces involved (Wuana and Okieimen, 2011; Wu *et al.,* 2019). Electrostatic or covalent bonds exist between the adsorbent and the adsorbate with sorter bond lengths and higher bond energies (Kasaini *et al.,* 2013; Vhahangwele and Mugera, 2015). Four steps take place during the adsorption process: bulk solution transport, film diffusion transport, pore transport, and adsorption (Uddin, 2017). In the bulk solution, the adsorbate is transported from the bulk solution to the reaction sites on mineral surfaces through advection and dispersion (Wu *et al.,* 2019). In film diffusion transport, the adsorbate is transported by diffusion through the stagnant liquid film to the surface (Sdiri *et al.,* 2016; Ambiado *et al.,* 2017). The pore transport occurs through the pores on the surface of the adsorbent where the adsorbate travels through the pores by a combination of molecular diffusion and by diffusion along the surface (Dzombak and Morel, 1990; Liu *et al.,* 2016). Lastly, the adsorption involves the attachment of the adsorbate to the adsorbent at an available adsorption site.

Chemical precipitation

Chemical precipitation is another commonly used method whereby dissolved trace metals in wastewater are transformed into insoluble solids (Chen *et al.,* 2014; Akinwekomi, 2017; Akinwekomi *et al.,* 2020). In the treatment of mine impacted water, alkaline reagents including sodium hydroxide (NaOH), limestones ($CaCO_3$), or lime (CaO) are used as coagulants or flocculants to enlarge trace metal species (Akinwekomi, 2017). The results obtained from this method, however, are not satisfactory; other treatment methods such as ion exchange are used for high efficiency (Kefeni *et al.,* 2017). There are several disadvantages associated with the chemical precipitation method; some of the disadvantages are the high cost of waste disposal, hydroxides used are not always the proper chemicals and each of the dissolved trace metals have their particular pH for hydroxide precipitation (Cheong *et al.,* 2016; Abel-Denee *et al.,* 2018; Akinwekomi *et al.,* 2020). At certain pH regimes (it can be above or below) trace metals precipitates become soluble (Akinwekomi *et al.,* 2020). Thus, even a slight change of pH can dissolve precipitated trace metals back into the aqueous solution (Hansen, 2015; Mulopo, 2015b; Bonnail *et al.,* 2018; Akinwekomi *et al.,* 2020).

As indicated earlier, active treatment methods tend to be quite expensive and this is more pronounced in large scale applications. For instance, the estimated capital expenditure and operating costs for the AMD treatment plants operated by the Trans Caledon Tunnel Authority on the East, Central and West Rand of the Witwatersrand Basin and have an average treatment volume of 80 Mℓ/day (TCTA, 2011) were given by the Department of Water and Sanitation (Figure 2.6).

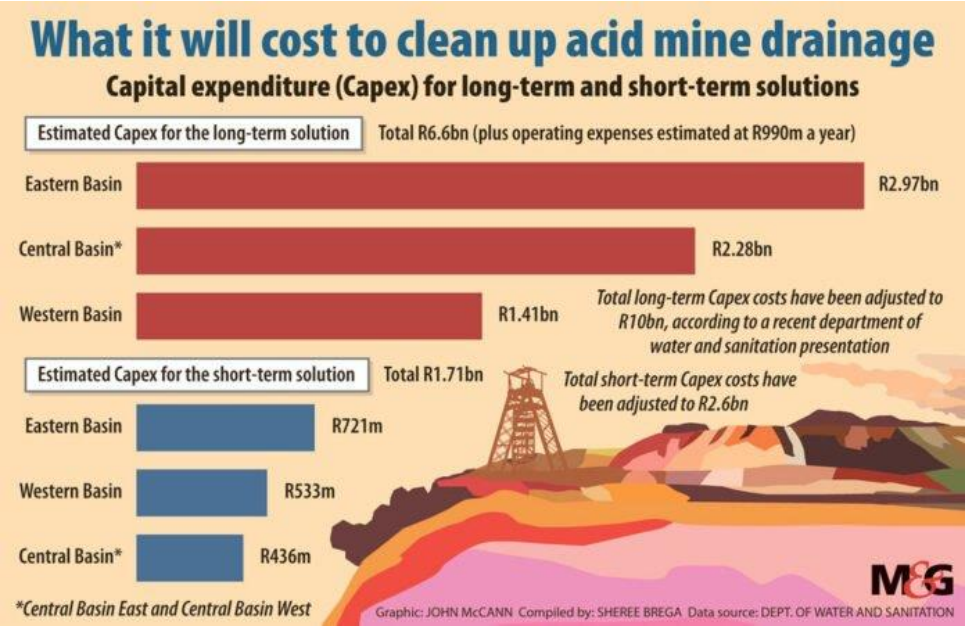

Figure 2.6. Cost analysis of AMD treatment in the Eastern Rand, Central Rand, and West Rand basin for short- and long-term solutions (Department of Water and Sanitation).

2.1.5 Reuse and resource recovery from AMD

2.1.5.1 Reuse of treated acidic mine water

Membrane technologies including reverse osmosis (RO) and nanofiltration (NF) have so far proved to be promising in the treatment of AMD for minimising discharge while achieving the water good quality for reuse (Chesters *et al.,* 2016; Wadekar *et al.,* 2017; Andalaf *et al.,* 2018). These two methods are currently implemented at actual mining sites and in research conducted for AMD treatment (Crini and Lichtfouse, 2018). For example, Chesters *et al.* (2016) discovered that about 363 mines of which RO and NF membranes can be applicable in the treatment of contaminated mine water. In Peru and Chile, approximately 67 mining site RO was adopted to treat acidic mine water (Naidu *et al.,* 2019). The RO and NF membranes has advantage as it easy in operation, with high treatment efficiency and the discharge effluent can meet the environmental discharge standards (Crini and Lichtfouse, 2018). The challenge that may be experienced during the AMD treatment it might be membrane fouling and pre-treatment might be necessary (Name and Sheridan, 2014; Gu *et al.,* 2018). High concentration of Fe in AMD may affect the performance of membrane, pre-treatment is necessary to remove Fe in AMD to reduce membrane fouling (Meschke *et al.,* 2015; Aguiar *et al.,* 2018). Other previous studies utilised sand filtration, microfiltration (MF) and ultrafiltration (UF) membranes as well as several adsorbents for AMD pre-treatment before NF and RO implemented to increase hydrogen ion activity and removes major ions including Fe, SO_4^{2-} and Mn (Aguiar *et al.,* 2018; Wadekar *et al.,* 2017; Wadekar and Vidic, 2018).

Electrodialysis (ED) is an electrochemical and membrane based treatment process (Luiz *et al.,* 2018). The separation of ions occurs across cation and anion exchange semi-permeable selective membranes from non-ionic analytes in AMD (Xu and Huang, 2008; Luiz *et al.,* 2018). The cations and anions move towards the electrodes on application of a direct current (Buzzi *et al.,* 2013). Cations move towards cathodes across a cation-exchange membrane. ED is a promising approach with limited chemical needed and this applied for water reuse and value recovery from seawater (Sadrzadeh and Mohammadi, 2008; Buzzi *et al.,* 2013; Naidu *et al.,* 2019), industrial effluents (Luiz *et al.,* 2018; Naidu *et al.,* 2016) and the acid industry (Cifuentes *et al.,* 2006). Buzzi *et al.* (2013) pointed out that ED has potential for treatment of AMD, and it was also observed that it can achieve 97% contamination rejection to produce good water quality that fit for reuse. ED was also used in the treatment of AMD with the aim of recovering pure sulphuric acid (H_2SO_4) (Martí-Calatayud *et al.,* 2014; Naidu *et al.,* 2019).

2.1.5.2 Resource recovery from AMD

Acidic nature of AMD may assist in unlocking wealth by the recovery of H_2SO_4 from chemistry of AMD (Naidu *et al.,* 2019). This may assist in the supply of acid to the chemical and metal industries that used acids in their various treatment processes (Naidu *et al.,* 2016). The demand of H_2SO_4 is increasing due to its application as leaching agent in Cu, Co, Ni, and U industries (Simate and Ndlovu, 2014; Nleya *et al.,* 2016; Naidu *et al.,* 2019). The high H_2SO_4 generated in AMD chemistry makes it to be more and corrosive (Gaikward and Gupta, 2008; Davis *et al.,* 2015; Etter and Langill, 2016). Recovery of H_2SO_4 from AMD assist in environmental protection as most trace metals dissolves under acidic medium (Naidu *et al.,* 2019). Several methods were tested in the recovery of acids from industrial waste solutions including electrodialysis, diffusion dialysis, crystallization, acid retardation, solvent extraction etc. (Cifuentes *et al.,* 2006; Regel-Rosocka, 2010; Wei *et al.,* 2010; Sheedy *et al.,* 2012). Electrodialysis has the advantage that it can achieve highly concentrated and purified acid (Simate and Ndlovu, 2014).

The bipolar membrane electrodialysis (BMED) on other electrodialysis (conventional electrodialysis), is the one that is so promising in AMD treatment (López *et al.,* 2019). BMED uses multidisciplinary approach where electric field with bipolar membrane is applied to successfully separate cations (e.g. Pb) and anions (SO_4^{2-})

into divided sections by separating water in a form of protons and hydroxide (Davis *et al.,* 2015; Rozoy *et al.,* 2015). The advantage of BMED is that acid in AMD can be separated from base salts with no chemical dosage and it was also established by Martí- Calatayud *et al.* (2014) that the potential of ED to selectively recover H_2SO_4 from AMD may be due ion exclusion technique. However, the performance of ED may decrease due to precipitation on the membrane (Luiz *et al.,* 2018). Recovery of H_2SO_4 influenced by the transport of SO_4^{2-} ions via anion-exchange membranes and metallic hydroxide precipitate at the surface of cation-exchange membranes (López *et al.,* 2019). The distillation membrane and freeze crystallisation methods are also promising in the recovery of high purity acid and their selectivity in H_2SO_4 recovery still need further clarity (Tomaszewska *et al.,* 2001; Padhiyar and Thakore, 2013; Etter and Langill, 2016; Naidu *et al.,* 2019).

Many methods including chemical, electrochemical, and biological methods were adopted in the recovery of trace metals including Fe, Pb, Cu, Cd, Zn, Ni, and Co from AMD (Gaikward and Gupta, 2008; Michalkova *et al.,* 2013; Kefeni *et al.,* 2015; Nordstrom *et al.,* 2017; Crane and Sapsford, 2018). Chemical precipitation remains the widely adopted method for the recovery of trace metals from AMD (Akinwekomi, 2017). Recovery of rare earth elements (REEs) from AMD has been drawing interest lately owing to the increased use of these elements in low-energy emission fields, renewable energy and in high technology defense-related applications such as in batteries, permanent magnets, and optical glasses (Binnemans *et al.,* 2013; Soltani *et al.,* 2013; Haque *et al.,* 2014; Ayora *et al*., 2016; Ziemkiewicz *et al.,* 2016; Bonnail *et al.*; 2017; Vass *et al.,* 2019; Badhurahman *et al.,* 2020).

To revisit the method of chemical precipitation, its predominant variant is ODAS (O-oxidation, DA-dosing with alkali, and S-sedimentation), which is common in traditional wastewater treatment plants (USEPA 2000; USEPA 2004). Although the most common order of treatment in industrial wastewater treatment systems is ODAS, for treatment of AMD the most common order is DAOS (Younger *et al*. 2002). Dosing with alkali (DA) is typically the first step followed by oxidation (O) and sedimentation (S) (Figure 2.7). The AMD is pumped into a neutralising tank where neutralising agents such as limestone ($CaCO_3$) are added before aeration and flocculation or sedimentation (to precipitate iron) occurs in subsequent tanks. For the AMD treatment plants on the Witwatersrand Basin, after treatment processes, precipitated HDS and treated water are separated. A certain percentage (about 10%) of the HDS is pumped back to the neutralising tank as a conditioner while the rest is discharged to landfills. The neutralised mine water is discharged into natural streams.

There remains some gaps to be exploited in relation with the current process as has been indicated earlier. There is a possibility to reconfigure the neutralisation route by splitting the AMD into another portion that will undergo selective precipitation of ochres (Figure 2.8) while another portion can continue through the current route which produces bulk HDS. However, the amount of HDS produced will be reduced and thus alleviating the environmental burden of its disposal. Further, the current amount of sludge used for conditioning influent AMD is too little and is used only once. This application can be explored further to assess potential use in mine voids and shafts as well as removal of phosphate from contaminated water.

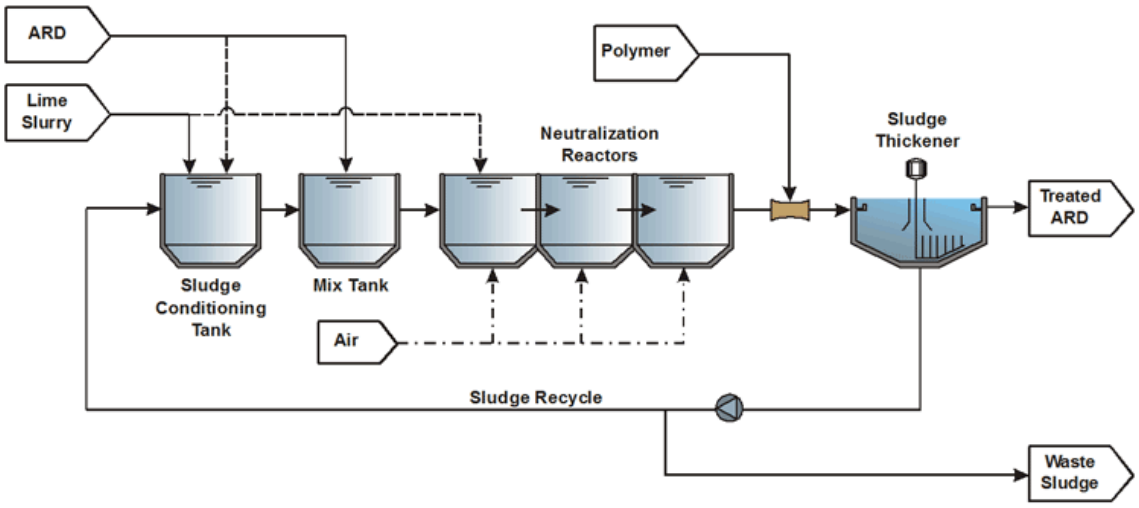

Figure 2.7. Schematic diagram of a typical HDS AMD treatment plant (GARD Guide).

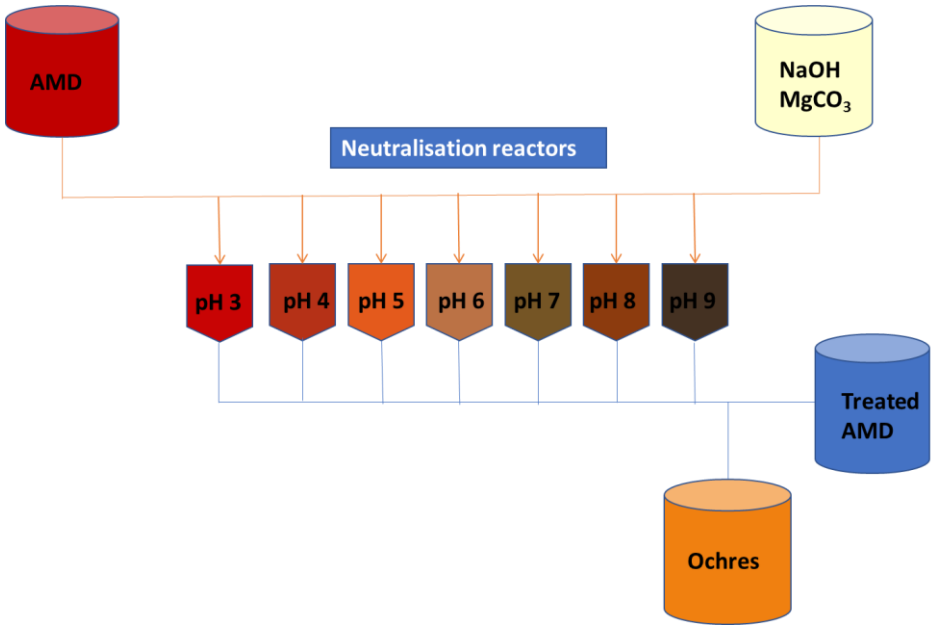

Figure 2.8. Schematic diagram of a proposed new route of AMD treatment (Netshiongolwe *et al.,* 2020).

A study by Akinwekomi *et al*. (2017) showed that it is possible to precipitate magnetite (Fe_3O_4), goethite (FeOOH) and hematite (Fe_2O_3) from synthetic acidic water. This study will introduce an approach involving predictive selective precipitation of Fe ochres using hydrochemical modelling, with a number of neutralising agents and some combinations thereof considered. It also explores solution chemistry in this context to account for any type of AMD as well as assess solution-adsorbent interactions, in this case the adsorbent being HDS.

CHAPTER 3: MATERIALS AND METHODOLOGY

This chapter presents three cases: the first being the simulated precipitation of iron ochres using geochemical modelling and the second being the characterisation of high density sludge (HDS) collected from an acid mine drainage (AMD) treatment plant. In the first case, various neutralising agents and their combinations are used to simulate the neutralisation of AMD with the aim of getting treated water of better quality while precipitating iron ochres that can have potential beneficial use e.g. in paint pigments. In the second case, a sample of HDS is characterised in terms of composition, physical and physical-chemical characteristics. This is intended to shed some light on the HDS currently produced at the AMD treatment plants. In the third case, the focus is on the potential use of this HDS for further treatment of AMD and for adsorption of phosphates from contaminated water (e.g. agricultural- and sewage-type water) as a way of repurposing the sludge.

3.1 COMPUTATIONAL SIMULATIONS OF THE PRECIPITATION OF OCHRES

The approach in this study involved simulating neutralisation of AMD and removal of trace metals from impacted waters, as well as the simulation of the precipitation of useful ochres. Several neutralising agents including $MgCO_3$, MgO, CaO, $CaCO_3$, and Na_2CO_3 among others as well as their combinations (mixtures) were used for the simulations. Other conditions considered in the simulations included varying pH regimes; equilibration with gases such as CO_2 and O_2; and varying temperatures. The simulations were conducted using the PHREEQC geochemical modelling code (US Geological Survey, USA). The PHREEQC model successfully predicted the removal of trace metals such as Mn, Cd, Fe, Al, Mg, and Zn from the mine water as well as the potential precipitation and formation of iron ochres such as goethite, hematite, $Fe(OH)_3$, FeS, mackinawite, pyrite, and siderite. The pH of the resulting water was found to increase notably. It was also possible to fix the pH and assess the potential precipitates and the resulting water chemistry. $MgCO_3$ was found to form the most desirable treated water and precipitates although it is more expensive than other neutralising agents. The findings of the study have revealed that computational simulations are important in designing experimental conditions, thus offering a cost-effective approach.

3.1.1 Model set-up as an experimental design approach

The previous descriptions have shown that the simulated neutralisation of AMD and subsequent precipitation of ochres can be used as an experimental design technique. It helps in gaining insights into the experimental set-up to be used and what can be anticipated. The forward geochemical modelling approach was used in which two or more initial states were used to determine the resulting state. For instance, reacting AMD (initial state 1) with a neutralising agent (initial state 2) while changing the temperature of reaction (initial state 3) will result in treated water (final state 1) and some precipitates (final state 2).

The AMD composition used in the simulations in this study was taken from a previous study by Akinwekomi (2017), where 1 ℓ of the AMD was collected from coal washing and mine processes. The composition details of the initial water solution collected are shown in Figure 3.1. The PHREEQC geochemical model was used for assessing elemental speciation and solubility using the Phreeqc.dat database. The following neutralising agents (NA) were used for the treatment of the AMD contaminated water; $MgCO_3$, MgO, $Mg(OH)_2$, $CaCO_3$, CaO, $CaHCO_3$, $Ca(OH)_2$, Na_2CO_3, Na_2O, NaOH, $NaHCO_3$, NH_3, NH_4OH. Each of the reaction steps represented a different simulation e.g. in the reaction with $CaCO_3$, 4 moles of the neutralising agents were used in 10 steps i.e. at 0.4 moles per step. In a separate reaction step (Figure 3.2), $MgCO_3$ is reacted with the same initial water to obtain a different output. In another step, a mixture of $MgCO_3$ and NaOH was reacted with the initial water, giving another outcome. In yet another reaction step, $MgCO_3$ was reacted with the same initial water at a fixed pH of 9.0 (shown as “Fix H+ -9.0 $MgCO_3$ 10”) to reach a different output. The output scripts (not shown here) would show the original AMD with the initial conditions, followed by the treated AMD and possible precipitated minerals (based on the saturation indices calculated for the system). Notable changes in

treated water were in pH, pe (redox potential), and total alkalinity as the species change. Up to 1130 simulations were conducted with about 200 proving to be satisfactory with respect to the desired predicted treated water quality and ochres precipitated. Figure 3.3 shows the solution that was equilibrated with carbon dioxide (CO_2) while Figure 3.4 shows equilibration with atmospheric oxygen (O_2).

```
TITLE RAW AMD WATER
SOLUTION 1
Temp      25
pH        2.8
pe        4
redox     pe
units     mg/l
density   1
Al        472.5
Ca        470
Cd        0.01
Fe        6051.3
K         1
Mg        0.03
Mn        125.9
S(6)      18000
Si        30
Zn        0.2
-water    1 # kg
```

```
Addition of neutralizing agent
REACTION 1
CaCO3     4
4 moles in 10 steps
END
```

Figure 3.1. PHREEQC script for forward modelling of AMD

```
Addition of neutralizing agent
REACTION 1
MgCO3       4
4 moles in 10 steps
END

Addition of neutralizing agent
REACTION 1
NaOH        4
4 moles in 10 steps
END

Combined neutralizing agent
REACTION 1
MgCO3       4
NaOH        4
4 moles in 10 steps
END
```

```
Fixed pH
PHASES
Fix_H+
H+=H+
log_k       0

EQUILIBRIUM_PHASES 1
Fix_H+      -9.0 MgCO3        10
END
```

Figure 3.2. PHREEQC script for forward modelling of AMD at fixed pH values

```
Equilibration with CO2
REACTION 1
MgO         4
NH4OH       4
2 moles in 10 steps
```

```
EQUILIBRIUM_PHASES 1
CO2(g)      -2.0  8
END
```

Figure 3.3. PHREEQC script for forward modelling of AMD equilibrating with CO_2

```
Equilibration with O2
REACTION 1
MgO          4
NH4OH        4
4 moles in 10 steps
EQUILIBRIUM_PHASES 1
O2(g)        -0.5  8
END
```

Figure 3.4. PHREEQC script for forward modelling of AMD equilibrating with O_2

3.2 PRECIPITATION OF OCHRES - EXPERIMENTAL WORK

3.2.1 Simulation of AMD (Experiment 1)

The aim of the experiments was to produce Fe precipitates using synthetic AMD (Table 3.1) based on that reported by Grover (2016) without heating (energy) throughout the experiments. A stepwise selective precipitation mechanism was applied to assess the effect of parameters such as oxidation, pH adjustment, settlement rates and temperature (experiments conducted at room temperature). All the weighted chemicals were transferred into seven 600 mℓ beakers and dissolved in 500 mℓ of deionised water. A magnetic stirrer was used to homogenize the samples at 2 rpm (Figure 3.5).

Table 3.1. Chemicals (names, formula) and masses, *m*, used to synthesize AMD in Experiments 1 (m_1) and 2 (m_2)

Chemicals	Chemical formula	m_1, g	m_2, g
Aluminium Potassium Sulphate dodecahydrate	$AlK(SO_4)_2 \cdot 12H_2O$	0.50	0.50
Manganous Sulphate monohydrate	$MnSO_4.H_2O$	0.30	0.30
Ferrous Sulphate heptahydrate	$FeSO_4.7H_2O$	1.00	1.00
Copper Sulphate anhydrous	$CuSO_4$	0.20	0.20
Calcium Sulphate dihydrate	$CaSO_4.\ 2H_2O$	15.0	15.0
Ferric Sulphate anhydrous	$Fe_2(SO_4)_3$	1.00	1.00
Nickel nitrate hexahydrate	$Ni(NO_3).6H_2O$	0.20	0.20
Cadmium nitrate tetrahydrate	$Cd(NO_3)_2.4H_2O$	0.20	0.20
Zinc nitrate tetrahydrate	$Zn(NO_3)_2.4H_2O$	0.30	0.30
Ferrocyanide	$[Fe(CN)_6]^{4-}$	–	1.00

(a)  (b) 

Figure 3.5. (a) pH adjustment on each beaker (b) Stirred solutions at 2 rpm without heating for 48 h.

3.2.1.1 Using NaOH as a neutralising agent

The pH values were measured in each beaker (Figure 3.6) after homogenisation through stirring and the recorded pH values (shown in brackets) were as follows: beaker A (2.80), beaker B (2.80), beaker C (2.79), beaker D (2.78), beaker E (2.78), beaker F (2.76) and beaker G (2.76). To precipitate iron oxides from synthesised AMD, different pH values were obtained by a varying adjustment in each beaker. The pH in beaker A was adjusted to 3; beaker B to 4; beaker C to 5; beaker D to 6; beaker E to 7; beaker F to 8 and beaker G to 9. The stock solution of NaOH was calculated to be 18.939 mol ℓ^{-1} based on the density of 1.515 g $m\ell^{-1}$, formula weight of 40 g mol^{-1} and a concentration of 50% w/w were used. Therefore, to make 1 mol ℓ^{-1} solution, 5.281 mℓ of prepared stock solution was slowly added to 25 mℓ deionised and final the volume of solution was adjusted to 100 mℓ with deionised water. To reach the targeted pH, drops of 1 mol ℓ^{-1} NaOH were added to raise the pH depending on the targeted pH in each beaker. The seven beakers were stirred at 2 rpm for 48 h at room temperature. After 48 h, the beakers were removed from the magnetic stirrer to allow the precipitates to settle at the bottom through a vacuum suction using a 0.45 µm Whatman cellulose nitrate filter paper. After filtering the Fe precipitates, some of the filtrates were selected for re-treatment with NaOH for further precipitation to yield more precipitates.

(a)  (b)  (c) 

Figure 3.6. (a) pH adjustment with NaOH in initial solutions (b) precipitates formed in solutions after stirring for 48 h at 25 °C (c) vacuum system used to filter precipitates.

3.2.1.2 Using MgCO3 as a neutralising agent

The experimental setup for neutralisation with $MgCO_3$ was similar to that for NaOH, that is, the various AMD solution beakers were at the same initial pH values as above. Adjustment of pH was conducted using $MgCO_3$, added as a powder followed by stirring. The beakers were stirred to the same temperature (room temperature, 25 ºC) as was done for the experiments using NaOH.

Selected filtrates from the above $MgCO_3$ neutralisation were used for re-treatment with $MgCO_3$ to assess the possibility of precipitating more ochres.

3.2.2 Addition of ferrocyanide to chemicals used to simulate AMD (Experiment 2)

To produce the turquoise Fe precipitates in Experiment 2, ferrocyanide ($[Fe(CN)_6]^{4-}$) was added to the chemicals used to synthesise AMD (Table 3.1). This was just a once-off experiment that was conducted to assess the possibility of obtaining such precipitates. Chemicals were transferred into four 600 mℓ beakers and 500 mℓ of deionised water was used to dissolve them. A magnetic stirrer was used to homogenize the samples at 2 rpm (Figure 3.7). pH values in each beaker after homogenisation ranged between 2.58 and 2.67. To precipitate the cyanide containing iron ochres from the synthesised AMD, different pH values were used by adding NaOH, ranging from pH 3 in beaker A to pH 9 in beaker D. After the pH adjustments, the precipitates were extracted through filtration.

(a)  (b) 

Figure 3.7. (a) chemicals that were weighed out (600 mℓ beakers) in weighing balance and dissolved in deionised water (b) beakers stirred for 48 h to allow oxygen circulation in the reactions.

The pH values were measured in each beaker after homogenisation through stirring and the recorded pH values (shown in brackets) were as follows: beaker A (2.58), beaker B (2.59), beaker C (2.67), beaker D (2.59). To precipitate the iron ochres (in this case, cyanide containing ochres) from the synthesised AMD, different pH values were obtained by varying adjustments in each beaker using NaOH. The pH in beaker A was adjusted to 3; beaker B to 5; beaker C to 7; beaker D to 9. The pH adjustments were conducted as before followed by filtration of the precipitates.

3.2.3 Collected AMD in the Central Rand of the Witwatersrand Basin (Experiment 3)

The aim of the experiments here was to produce Fe precipitates using real AMD (Figure 3.8) using the same optimised parameters from the preliminary setup throughout the experiments. A stepwise selective precipitation mechanism was applied to assess the effect of parameters such as oxidation, pH adjustment, settlement rates and temperature (conducted at room temperature). AMD was transferred into eight 600 mℓ beakers and filled up to 500 mℓ. A magnetic stirrer was used to homogenize the samples at 2 rpm.

(a)  (b)  (c) 

Figure 3.8. (a) eight beakers stirred for 48 h to allow oxygen circulation in the reactions. (b) The pH values for precipitation increase from the extreme right beaker to the extreme left (i.e. pH 3 to 9). (c) Vacuum system used to filter the samples.

The environmental parameters measured in the field for AMD sample include hydrogen ion activity (pH), temperature (T), electrical conductivity (EC), redox potential (Eh), salinity (salt), total dissolved solids (TDS) and dissolved oxygen (DO) (Table 3.2). Table 3.3 indicates the chemistry of raw AMD collected in abandoned gold mines, generated from the tailing dumps.

Table 3.2. Field parameters for AMD sample

pH	T (ºC)	EC (µS/cm)	Eh (mV)	Salt (ppt)	TDS (ppt)	DO (ppm)
2.53	26.8	23.1	231	8.72	11.5	13.5

Table 3.3. Composition of AMD used in Experiments 3

Al	Ca	Cd	Co	Cr	Cu	Fe	Mg	Mn	Ni	S	Pb	Zn
Concentration mg ℓ^{-1}												
350	179	2.9	13.8	6.80	8.75	1276	225	62.9	17.2	4002	3.5	17.6

*Sulphate reported as sulphur

3.2.3.1 Using NaOH and $MgCO_3$ as a neutralising agent

The similar experimental setup applied in Figures 3.5 and 3.6 were used in these experiments (Figure 3.9)

Figure 3.9. pH adjustment with (a) NaOH (b) $MgCO_3$ (c) $CaCO_3$ with precipitates formed in AMD after stirring for 48 h at 25 °C.

3.2.3.2 Retreatment of filtrates with NaOH, $MgCO_3$ and $CaCO_3$

The similar experimental setup applied in Figure 3.5-3.8 were used in these experiments (Figure 3.10)

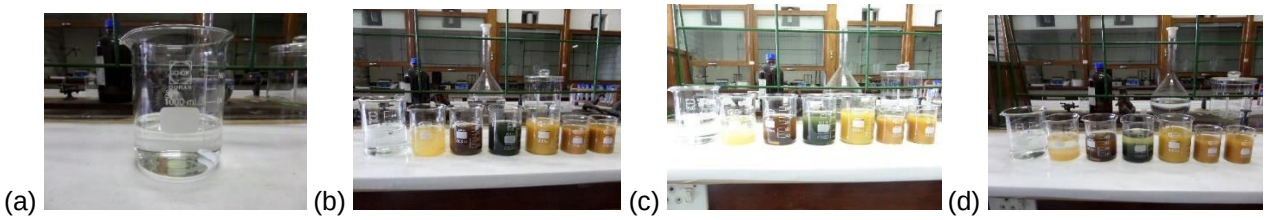

Figure 3.10. (a) Filtrates after AMD treatment (b) retreatment of filtrates with NaOH (c) retreatment of filtrates with $MgCO_3$ (d) retreatment of filtrates $CaCO_3$. pH adjusted from the extreme right beaker to the extreme left (i.e. pH 4 to 9).

3.3 CHARACTERISATION OF HIGH DENSITY SLUDGE

In this part of the study, both fresh and aged (3 months) HDS were characterised to assess their physical properties as well as their chemical properties (through microwave digestion and leaching tests). The main aim was to set a benchmark for determining if either sludge is usable for further adsorption of elements from AMD (e.g. when pumped into mine voids) and to adsorb phosphates in agricultural- and sewage-type water. The dry solids in HDS ranged from 2.5% to 37.2% and an increase from 20% to 25% was observed from fresh to aged HDS. Metal and sulphate concentrations in aged sludge were found to be higher than in fresh sludge.

3.3.1 Physical characterisation of HDS

HDS samples were collected in 1 ℓ polypropylene bottles from the Central Basin AMD treatment plant (Johannesburg, South Africa) and they were characterised to determine mineralogy and other parameters. Fresh sludge was collected which was then divided into portions with some being aged through air-drying in the laboratory. Mineralogical composition was determined using powder X-ray diffraction (PXRD) D2 Phaser (Bruker, Germany). Elemental composition was determined using X-ray fluorescence (XRF) (PAnalytical, Netherlands). Scanning electron microscopy (SEM) (Bruker, Germany) was used to determine surface morphology before and after adsorption. Samples were attached to the sample stub and coated with palladium and gold for SEM analysis. Fourier-transform infrared spectroscopy (FTIR) (Bruker Corporation, USA) was used to determine the functional groups of the HDS. The surface area, pore size, and pore volume were determined using the TriStar 3000 V6.05 A Brunauer-Emmett-Teller (BET) technique (Micro metrics, USA).

3.3.2 Chemical characterisation of HDS

To determine the release of trace metals from the dried HDS, leaching and microwave digestion were done followed by analysis using inductively coupled plasma optical emission spectroscopy (ICP-OES) (Spectro Genesis, Germany) for metals and ion chromatography (IC) for anions, mainly sulphate. For the metals, microwave digestion of the HDS was conducted using aqua regia (a 1:3 mixture of nitric and hydrochloric acids) using a ratio of 0.1 g of HDS to 10 mℓ the aqua regia mixture followed by analysis using ICP-OES. For the sulphate content, 1 g of HDS:20 mℓ of deionized water was used over a shaker for 24 h followed by filtration with a 0.45 µm cellulose nitrate filter paper and analysis using IC. Filtrates from microwave digestion were analysed for the targeted trace metals (i.e., Pb, Cu, Zn, Ni, and Co) using ICP-OES. Standard solutions used for instrumental calibration were from Ultra Spec (in 5% HNO_3 + HF). A solution of 5% HNO_3 was utilised as a blank sample for calibration purposes. All analytical tests were conducted in triplicate with analytical results of relative standard deviation (RSD) <10% used.

3.4 COMPUTATIONAL SIMULATIONS FOR SLUDGE-MINE WATER INTERACTION

Water pollution from gold mines is mainly associated with the leaching of trace metals from tailings dumps and other mine wastes. This has a bearing on the composition of water in abandoned mine shafts and voids. As part of the intention to repurpose HDS, it was necessary to assess the capability of hydrous ferric oxide (Hfo, represented chemically as ≡FeOH) to adsorb trace elements from AMD that is found in such mine shafts and voids. For this purpose, the PHREEQC geochemical modeling code was used for experimental design and to build a platform to understand the interaction between AMD and HDS. The approach involved using surface complexation models based on the Dzombak and Morel assumption of two surface sites (strong and weak sites) having densities of 0.005 and 0.2 $(mol\ Fe)^{-1}$. Trace metal adsorption onto pure Hfo was described by the Donnan diffuse layer in both strong (Hfo_sOH) and weak (Hfo_wOH) sites. The Hfo_wOH sites gave the best adsorption fit to the Hfo for Ni and Co, where they occupied 0.0022 mol $(mol\ Fe)^{-1}$. This was based on an Hfo surface area of 600 m^2/g and mass of 0.5 g. When the surface area and mass were reduced (to 200 m^2/g and 0.2 g, respectively) for Ni and Co, the site moles were also reduced to 0.001124 mol $(mol\ Fe)^{-1}$. The Hfo_sOH showed the best fit for the Hfo adsorption of Pb, Cu, and Zn giving a site density of 0.00055 mol $(mol\ Fe)^{-1}$ for a surface area of 600 m^2/g and Hfo mass of 1 g. This site density for Pb, Cu, and Zn was reduced to 0.00028 mol $(mol\ Fe)^{-1}$ for a surface area of 200 m^2/g and Hfo mass of 0.5 g. The Hfo_sOH showed an elevated adsorption of Pb, Cu and Zn, accounting for 0.00055 mol $(mol\ Fe)^{-1}$. Adsorption of metals onto the Hfo is important in the monitoring of trace metal attenuation and for understanding saturation capacities that will be important in determining the potential of adsorption for the Hfo, that is, if the HDS has further capacity of metal adsorption.

3.4.1 Generalised surface complexation simulations studies

The chemical composition of AMD collected at the treatment plant and the simulation of its interaction with Hfo (in PHREEQC) is shown in Figure 3.11. The Minteq.v4.dat database was used in all simulations. Different pH values, a varying mass of Hfo and different Hfo surface areas (strong and weak sites) were considered to assess the optimal conditions of adsorption of metals (Figure 3.11-3.14). In Figure 3.14, generalised surface complexation with calculated log k value of individual potentially toxic trace metals were assessed to look at the effect of pH to find out if adsorption of potentially toxic trace metals onto Hfo is through physisorption (adsorption) or surface complexation (chemisorption). The simulations were conducted for: Hfo surface areas of 600, 200 and 60 m^2/g; Hfo_sOH concentrations of 2.2 x 10^{-3}, 1.12 x 10^{-6}, 2.80 x 10^{-5} and 5.62 x 10^{-5} moles; and Hfo_wOH concentrations of 2.2 x 10^{-3}, 1.12 x 10^{-4}, 5.5 x 10^{-4}, 4.49 x 10^{-5}.

```
TITLE RAW AMD
SOLUTION 1
    temp      25
    pH        5.02
    pe        4
    redox     pe
    units     mg/l
    density   1
    Al        23.7
    Alkalinity 0
    Ca        509
    Co        5.1
    Cu        7.6
    Fe        1888
    K         2.1
    Li        1.1
    Mg        301
    Mn        67.8
    Na        186
    Ni        19.7
    Pb        6.9
    S(6)      7434
    Zn        8.8
    -water    1 # kg

SURFACE 1 #HFO surface
    -equilibrate with solution 1
    Hfo_s     2.2e-03    600       1
    Hfo_w     5.5e-04

SURFACE 2 #HFO surface
    -equilibrate with solution 1
    Hfo_w     2.2e-03    200       1
    Hfo_s     5.5e-04

SURFACE 3 #HFO surface
    -equilibrate with solution 1
    Hfo_w     2.2e-03    60        1
    Hfo_s     5.5e-04

END
```

Figure 3.11. Input PHREEQC script for the effect of pH

```
TITLE RAW AMD
SOLUTION 1
    temp      25
    pH        5.02
    pe        4
    redox     pe
    units     mg/l
    density   1
    Al        23.7
    Alkalinity 0
    Ca        509
    Co        5.1
    Cu        7.6
    Fe        1888
    K         2.1
    Li        1.1
    Mg        301
    Mn        67.8
    Na        186
    Ni        19.7
    Pb        6.9
    S(6)      7434
    Zn        8.8
    -water    1 # kg

SURFACE 1 #HFO surface
    -equilibrate with solution 1
    Hfo_w     2.25e-04    600       0.1
    Hfo_s     5.62e-05

SURFACE 2 #HFO surface
    -equilibrate with solution 1
    Hfo_w     1.12e-04    200       0.05
    Hfo_s     2.80e-05

SURFACE 3 # HFO surface
    -equilibrate with solution 1
    Hfo_s     1.12e-06    60        0.02
    Hfo_w     4.49e-05

END
```

Figure 3.12. Input PHREEQC script for the effect of mass

```
TITLE RAW AMD
SOLUTION 1
    temp      25
    pH        5.02
    pe        4
    redox     pe
    units     mg/l
    density   1
    Alkalinity 0
    Co        5
    Cu        5
    Ni        5
    Pb        5
    Zn        5
    -water    1 # kg

SURFACE 1 #HFO surface
    -equilibrate with solution 1
    Hfo_s      2.2e-03    600       1
    Hfo_w      5.5e-04

SURFACE 2 #HFO surface
    -equilibrate with solution 1
    Hfo_w      2.2e-03    200       1
    Hfo_s      5.5e-04

SURFACE 3 #HFO surface
    -equilibrate with solution 1
    Hfo_w      2.2e-03    60        1
    Hfo_s      5.5e-04

END
```

Figure 3.13. Input PHREEQC script for the effect of concentrations

```
TITLE RAW AMD
SOLUTION 1
    temp      25
    pH        5.03
    pe        4
    redox     pe
    units     mg/l
    density   1
    Al        23.7
    Alkalinity 0
    Ca        509
    Co        5.1
    Cu        7.6
    Fe        1888
    K         2.1
    Li        1.1
    Mg        301
    Mn        67.8
    Na        186
    Ni        19.7
    Pb        6.9
    S(6)      7434
    Zn        8.8
    -water    1 # kg

SURFACE_MASTER_SPECIES
 Hfo_s  Hfo_sOH
 Hfo_w  Hfo_wOH

SURFACE_SPECIES
Hfo_sOH + Pb+2 = Hfo_sOPb+ + H+
        log_k  4.65

Hfo_sOH + Cu+2 = Hfo_sOCu+ + H+
        log_k  2.89

Hfo_sOH + Zn+2 = Hfo_sOZn+ + H+
        log_k  0.99

Hfo_sOH + Ni+2 = Hfo_sONi+ + H+
        log_k  0.37

Hfo_sOH + Co+2 = Hfo_sOCo+ + H+
        log_k  0.41

SURFACE 1 #HFO surface
    -equilibrate with solution 1
    Hfo_s       .06114000000
    Hfo_w       .00611400000
    -no_edl

SELECTED_OUTPUT 1
    -file                  selected.xls
    -high_precision        true
    -reset                 false
    -solution              true
    -inverse_modeling      false
    -active                true
    -user_punch            true

END
```

Figure 3.14. Generalised surface complexation input script for the effect of pH 5

3.4.2 Parameter optimisation with PEST

The PHREEQC geochemical modelling code coupled with Parameter Estimation (PEST) was used to estimate generalised surface complexation (adsorption constants) and site density parameters using experimental data for AMD-HDS interactions. What has motivated the of use PHREEQC coupled with PEST in this study was that while a built-in thermodynamic database and activity coefficient in PHREEQC is useful, PEST can optimise any number or type of parameters when the number of parameters are less than or equal to the number of observations. The advantage of using PEST is that it can avoid the non-convergence problem experienced by other models while fitting multiple model parameters.

3.5 BATCH SORPTION STUDIES OF SLUDGE FOR MINE WATER TREATMENT

As indicated above, further studies are required that will help in establishing parameters such as adsorption capacities (under varying conditions) that are important in the use of HDS as a generic adsorption surface in simulations. This is usually achieved through conducting batch adsorption studies.

The idea of using this HDS in mineshafts and voids where the AMD is pumped from has been mooted for some time. This is predicated on the thinking that HDS has potential to further adsorb toxic elements contained in the AMD and to increase its pH. This increase will be useful in reducing the dosage of neutralising agents when AMD is pumped into reaction tanks. This part of the study used optimised parameters derived from above computational simulations to conduct batch studies to determine: the effect of pH; adsorbent dosage; concentration of metals (1-5 mg ℓ^{-1}) and contact time; and desorption studies. Mineralogical characterisation showed that HDS consisted of goethite, ferrihydrite and gypsum ($CaSO_4.2H_2O$). The former are iron minerals similar to those constituting Hfo while the latter is from precipitates following neutralisation of AMD with limestone ($CaCO_3$), the current neutralising agent used at the plants.

The following sections discuss sample preparation, set up of batch adsorption studies and data treatment (models) approaches used for the experimental data obtained.

3.5.1 Sample preparation

Standard solutions of the trace metal ions were prepared from AMD samples collected in the Central Rand basin of the Witwatersrand. A 10 mg ℓ^{-1} AMD stock solution was used to prepare lower concentration solutions (1, 2, 3, 4 and 5 mg ℓ^{-1}) through serial dilution. Ultra-pure water (18.2 MΩ grade water) was used for stock solution preparation and dilutions. Adjusted pH values (2.5, 3.5, 4.5, 5.5, 6.5, 7.5, 8.5, 9.5 and 10.5) were achieved using 0.1 mol ℓ^{-1} HNO_3 and 0.1 mol ℓ^{-1} NaOH solutions. The pH of the solutions was measured using a pH probe (Hanna Instruments, Johannesburg). All glassware used was cleaned with dilute HNO_3 (10% HNO_3) and dried in the oven (at 100 ºC) before use. HDS was used as an adsorbent in batch experiments conducted at room temperature (25 ºC).

3.5.2 Adsorption studies

3.5.2.1 Batch adsorption studies

Batch experiments were conducted in triplicate to determine the effect of HDS dosage on the adsorption of trace metals. Different masses (10, 20, 50, 100, 500 and 1000 mg) of HDS were contacted with 10 mℓ of synthetic AMD at room temperature. The effects of varying pH of the solution, adsorbent dosage, concentration and contact time were studied. The volume of the solution (10 mℓ) was kept constant throughout. The centrifuge tubes were shaken using an elliptical benchtop shaker (Labcon, South Africa) at a constant rate of 150 rpm, allowing enough time for adsorption and equilibrium to be reached. The filtrates were analysed using ICP-OES. The point of zero charge (pH_{pzc}) from previous studies of HDS was used in order to assess the effect of changes of surface charge on HDS adsorption during the experiments. The pH_{Pzc} value was 4.5, meaning that the surface is positive below this value and negative above it.

The capacity (q_e) and the adsorption percentage (%R) were calculated using the equations:

$$q_e = \frac{(C_o - C_e)V}{m} \quad (3.1)$$

$$\%R = \frac{(C_o - C_e)}{C_o} * 100 \quad (3.2)$$

where: C_o is initial the concentration of adsorbate (mg ℓ^{-1}), C_e is the concentration of adsorbate at equilibrium (mg ℓ^{-1}), m is the mass of adsorbent (g), V is the volume of the solution (mℓ).

3.5.2.2 Desorption studies

The HDS residue after adsorption was dried for 5 h in an oven (80 ºC) prior to conducting desorption studies. The desorption experiments were conducted for 24 h using deionized water and 0.5 mol ℓ^{-1} HCl in 50 mℓ polyethylene centrifuge tubes. The filtrates were then analysed using ICP-OES. The desorption efficiency was determined as follows:

$$\text{Desorption efficiency} = \frac{C_{des}}{C_{ads}} * 100 \quad (3.3)$$

where: C_{des} and C_{ads} are the concentrations of trace metals desorbed and adsorbed onto HDS sorbent (mg ℓ^{-1}), respectively.

3.5.3 Adsorption isotherms

The data from the adsorption studies was modelled using the Langmuir, Freundlich, Dubinin-Radushkevich and Temkin isotherms. These isotherms are described below.

3.5.3.1 Langmuir isotherm

The Langmuir isotherm makes assumptions on the finite number of both strong and weak sites, constant binding energy in surface sites (binding energy is independent on the adsorption density) and the adsorption capacity is limited to monolayer coverage in both strong and weak sites. The equation for the isotherm is presented in the following form (Langmuir, 1918; Gerard *et al.,* 2016; Xie *et al.,* 2019):

$$\frac{C_e}{q_e} = \frac{1}{K_L q_m} + \frac{C_e}{q_m} \quad (3.4)$$

where: C_e is adsorbate concentration at equilibrium (mg g^{-1}). K_L is the Langmuir equilibrium constant and it can be correlated with the variations in surface area and adsorbent porosity (this means that large surface area and pore volume on the adsorbent, influences high adsorption (more attraction of analyte from the aqueous phase to adsorbent surface) on the adsorbent (adsorption capacity). Langmuir adsorption isotherm characteristics can be defined by its dimensionless constant (separation factor, R_L).

$$R_L = \frac{1}{1+k_L C_o} \quad (3.5)$$

where: K_L is the Langmuir adsorption constant (mg g^{-1}), C_o is the adsorbent initial concentration (mg g^{-1}). R_L values gives overview on either adsorption is unfavourable when $R_L > 1$, favourable when $0 < R_L < 1$, linear when $R_L = 1$ and irreversible when $R_L = 0$.

3.5.3.2 Freundlich isotherm

The Freundlich adsorption isotherm is applied in the sorption processes that occur on heterogeneous surfaces. It helps to understand the surface heterogeneity and the exponential distribution in both strong and weak sites and their surface energies. The equation for the isotherm is presented as follows (Chen, 2015: Gu *et al.,* 2018):

$$\log q_e = \log K_F + \frac{1}{n} . \log C_e \quad (3.6)$$

where: K_f is the adsorption capacity ($\ell\ mg^{-1}$) and 1/n is the adsorption intensity, it helps in understanding the relative distribution on the surface energy and the heterogeneity of the sites in the adsorbent. The choice of presenting results in different isotherms depends on the high correlation coefficients.

3.5.3.3 Dubinin-Radushkevich isotherm

The Dubinin-Radushkevich (D-R) adsorption isotherm is applicable to adsorption mechanisms with Gaussian energy distribution (in heterogeneous surfaces). It is temperature-dependent and the adsorption data at different temperatures are plotted as the logarithm function of the analyte adsorbed versus the potential energy square root. The equation for the D-R isotherm is presented as follows (Chen and Yang, 1994; Mosai *et al.,* 2017):

$$\ln q_e = \ln q_m - \beta\varepsilon^2 \quad (3.7)$$

where: β ($mol^2\ (kJ^{2)-1}$ represent the D-R isotherm constant is defined from the lnq_e versus ε^2, q_m (mg g^{-1}) is the D-R adsorption capacity which is defined by the intercept of the plot and ε is the Polanyi constant which can be presented as:

$$\varepsilon = RT \ln\left(1 + \frac{1}{C_e}\right) \quad (3.8)$$

The adsorption energy, E_s was presented as (ε) (kJ mol^{-1}), is defined as free energy transfer of a mole of analyte from the affinity of adsorbent surface and this can be defined by using the value of β from the equation below.

$$E_S = \frac{1}{\sqrt{-2.\beta}} \quad (3.9)$$

The mechanism is defined as follows depending on the value of E_s obtained: E_s < 16 kJ mol^{-1} (Ion exchange); E_s < 8 kJ mol^{-1} (Physisorption) and Es > 40 kJ mol^{-1} (chemisorption).

3.5.3.4 Temkin Isotherm

The Temkin isotherm has factor that considers the interaction between the sorbates. It assumes that the heat of adsorption of analytes in the adsorbents will decrease linearly than logarithmically with coverage and concentration averages. The heat of adsorption is determined by the uniform distribution in active sites (binding energies) that may influence maximum removal of contaminants (metals maximum binding energy). The Temkin model is expressed in the equation below:

$$q_e = \frac{R_T}{b} \ln[A_T\ C_e] \quad (3.10)$$

$$q_e = \frac{R_T}{b_T} \ln A_T + \left[\frac{R_T}{b}\right] \ln C_e \quad (3.11)$$

$$B = \frac{R_T}{b_T} \quad (3.12)$$

$$q_e = B \ln A_T + B \ln C_e \quad (3.13)$$

Where A_T is the Temkin isotherm equilibrium binding constant (L g^{-1}), B_T is the Temkin isotherm constant, B is the constant related to heat of adsorption. A_T and b_T were determined from the intercept and slope (the plot of qt against ln t).

3.5.4 Kinetic models

The time-dependence of adsorption was studied and the data were fitted using the pseudo first-order, pseudo second-order, Elovich, Intraparticle diffusion and Film diffusion models. The goodness of the models was determined using the correlation coefficient (R^2 value).

3.5.4.1 Pseudo first-order model

The pseudo first-order model is represented by the equation below (Huang *et al.,* 2014; Pan *et al.,* 2017):

$$\log (q_e - q_t) = \log q_e - \frac{k_1}{2.303} t \quad (3.14)$$

where: qt (mg g^{-1}) is the amount of adsorbate adsorbed at a time (t) per unit mass, t was presented in minutes (min) and k_1 (min^{-1}) is the pseudo first-order rate constant.

3.5.4.2 Pseudo second-order model

The pseudo second-order model is defined by the following equation (Qiu *et al.,* 2009; Etale *et al.,* 2015):

$$\frac{t}{q_t} = \frac{1}{k_2 q_{e^2}} + \frac{t}{q_e} \quad (3.15)$$

where: k_2 in the above equation represents the pseudo second-order rate constant.

3.5.4.3 Elovich kinetic

The Elovich model is generally expressed as follows:

$$qt = \frac{1}{\beta}\ln[\alpha\beta t] = \frac{1}{\beta}\ln[\alpha\beta t] + \frac{1}{\beta}\ln t \quad (3.16)$$

Where α (mg g^{-1} min^{-1}) is the initial adsorption rate and the parameter β (g mg^{-1}) is related to the extent of maximum (saturation) surface coverage of adsorbate and activation energy for chemical adsorption (chemisorption). The kinetic results will be linear on a qt against ln(t) plot, if the results best fit in an Elovich model. This model suggests that diffusion in the Elovich kinetics trend; pattern (form) to this equation might be taken as evidence that the rate-determining step is diffusion in nature and that this kinetic model should apply in conditions where desorption rate can be ignored. The kinetic curve of adsorption demonstrated good fitting with the model ($R^2 > 0.99$) which may indicate that the diffusional rate-limiting is more particularly noticeable in potentially toxic trace metals adsorption by HDS.

3.5.4.4 Intraparticle diffusion

The mechanism of adsorption is either particle diffusion or film diffusion controlled. Before the adsorption occurs on adsorbent surface, many diffusion processes affect the adsorption process. The adsorbate diffuses through the bulk of the solution around the adsorbent (this involves the micro pores and macro pores of the HDS (adsorbent). The bulk diffusion resistance is reduced when sufficient agitation reduces the concentration gradient, the external mass transfer resistance and intraparticle mass transfer resistance. The rate of adsorption was assessed to analyse the rate controlling step and the intraparticle diffusion was explored which is represented by the Weber and Morris equation below:

$$q_t = k_{ip} t^{1/2} + C \quad (3.17)$$

where C is the intercept related to the thickness of layer boundary, k_{ip} is the intraparticle diffusion rate constant. According to intraparticle diffusion model, if sorption of adsorbate is controlled by the intraparticle diffusion process, a plot of q_t against $t^{1/2}$, the R^2 value is 0.99 (this gives a straight line).

3.5.4.5 Film diffusion

The kinetics of adsorption of contaminants on different adsorbents is controlled by several processes like bulk diffusion, external mass transfer, chemical reaction, film diffusion and intraparticle diffusion. The equation below indicates a linear driving force principle which develops a simple relationship:

$$\ln\left[1-\alpha_e\right] = -k_p t + D_F \quad (3.18)$$

where $\alpha_e = q_t/q_e$ is the fractional attainment of equilibrium constant and k_p is the rate constant.

A plot of ln $(1-\alpha_e)$ against time (t) yields the rate constant as the slope of the graph and the D_F is the dimensionless constant (as intercept).

3.5.5 Thermodynamic Parameters

Thermodynamic parameters including Gibbs free energy (ΔG^o), enthalpy (ΔH^o) and entropy (ΔS^o) were considered to look at the effects of temperature during the adsorption of potentially toxic trace metals onto HDS. The above parameters can be determined from the variation in the equilibrium constant (K). The equations below indicate a change in Gibbs free energy:

$$\ln K = \frac{q_e}{C_e} \quad (3.19)$$

$$\Delta G^o = -RT \ln K_d \quad (3.20)$$

$$\ln K_d = \left[\frac{\Delta S^0}{R}\right] - \left[\frac{\Delta H^0}{RT}\right] \quad (3.21)$$

$$\Delta G^o = \Delta H^o - T\Delta S^o \quad (3.22)$$

ΔG^o is the Gibbs free energy, T is the temperature, R is the gas constant, K_d is the distribution coefficient, ΔH is the enthalpy and ΔS entropy.

The activation energy was derived from Arrhenius equation:

$$\ln K_d = \ln A - \frac{E_a}{RT} \quad (3.23)$$

Where A is the Arrhenius constant, E_a is the activation energy

3.6 COLUMN SORPTION SIMULATION STUDIES OF HFO FOR MINE WATER TREATMENT

Simulation studies were conducted for optimisation of parameters in the column adsorption studies. The PHREEQC geochemical modelling code was used for the simulations due to the availability of hydrous ferric oxide (Hfo) as a surface in its databases. Different parameters including the effect of pH, concentration of trace metals in the inlet, bed height and flow rates were considered. Parameters established from simulation studies were then used in the actual column experimental studies (simulation studies were providing a foundation for experimental design in this regard, much the same way as was observed for batch studies).

3.6.1 Reactive transport model construction

A sample of a reactive transport simulation script is presented (Figure 3.15). Simulations were conducted using the PHREEQC geochemical modelling code and based on the llnl.dat database for the Hfo surface and reactions.

```
SOLUTION 0 #Raw AMD
    temp      25
    pH        5.02 charge
    pe        10.59
    redox     pe
    units     mg/l
    density   1
    Co        5
    Cu        5
    Ni        5
    Pb        5
    Zn        5
    -water    1 # kg

SOLUTION 1-50 Initial solution for column
    temp      25
    pH        7.0 charge
    pe        8
    redox     pe
    units     mg/l
    density   1
    K         1.8
    N(5)      45
    Na        30
    -water    1 # kg

EXCHANGE 1-50
    X       0.0011
    -equilibrate with solution 1
    -pitzer_exchange_gammas false

SURFACE 1
    -equilibrate with solution 1-50
    Hfo_w      0.00055    600       1
    Hfo_s      0.0022

USE solution none
TRANSPORT 1-50
-cells 50
-shifts 50


PRINT
        -reset  false
       -totals true
       -status true

SELECTED_OUTPUT
        -file answer.xls
        -totals Pb Cu Zn Ni Co
       -solution true
END
```

Figure 3.15. PHREEQC input script for transport model

The script can be explained as follows:

a) The solution to be contacted with the Hfo surface is defined as “Solution 0”. In this case, it is the simulated acid mine drainage (AMD).

b) The solution labelled “Solution 1-50” is the initial solution in the column. As indicated previously, the “column” in this case is imaginary as this is only computational simulations. The range of numbers “1-50” are cells, from the first cell to the 50th cell. Thus, all cells have the same solution initially. It should be noted here that the solution is in contact with Hfo in each cell.

c) The Hfo is defined as both an “exchange” as well as a “surface”. An exchange defines the clayey nature of the Hfo and accounts for ordinary cationic exchange reactions (represented as “X”) while a surface accounts for the unidirectional surface complexation reactions (on strong (Hfo_s) and weak (Hfo_w) adsorption sites). As pointed out earlier, the exchange and surface cover all the 50 cells with Solution 1-50 being the pore water in them.

d) The next block has important instructions to effect a reactive transport simulation. The “Use Solution none” instructs the code to ignore any reactions that will mix the initial solution “Solution 1-50” in the cells with the new incoming solution “Solution 0”. This sounds a bit simplistic, but that mix, if allowed to occur, could complicate the simulation and result in clumsy results. To avoid that, the new solution is allowed to push the existing one out and new reactions between the surface and the new solution established.

The instruction “Transport 1-50” introduces the new solution into the 1st cell of the column and flushes it through the 50 cells. This is repeated 50 times as indicated by the number of “shifts”.

e) The length of each cell is only arbitrary here. In the actual column experiments, it is determined by the flow rate and bed height of the adsorbent.

f) Other factors such as dispersivity of the fluid in the cells have been ignored, making this a 1 dimensional (1-D) reactive transport model. These factors are important in other models such as 2-D and 3-D models.

g) The rest are just output options that the user defines e.g. if the interest is in knowing the extent of adsorption in any cell after any number of shifts or knowing the resulting solution in any of those cells after the adsorption reactions have occurred.

The reactive transport models were used for the optimisation of parameters that were used in the actual column of experimental studies.

3.6.2 Column sorption studies

Adsorption studies of elements in a fixed-bed column as a setup for large scale operation is applicable in real mine water treatment. In this second part of the study, the application potential of HDS for the adsorption of Pb, Cu, Zn, Ni, and Co from mine water in a fixed-bed adsorption column was investigated. The effect of breakthrough parameters including: initial elemental concentration, bed height, and the flow rate was investigated. Column adsorption experimental data were fitted to Thomas, Yoon-Nelson, Adam-Bohart, and Bed Depth Service Time (BDST) models under the column adsorption process.

The following sections discuss sample preparation, set up of column adsorption studies and data treatment (models) approaches used for the experimental data obtained.

3.6.2.1 Sample preparation

Standard solutions of elements were prepared from an efflorescent crust (obtained from an abandoned mine site in the Central Rand Basin, Johannesburg). Efflorescent crusts are repositories of constituents of evaporated AMD and as such their dissolution in deionised water yields solutions that resemble the original AMD. A 10 mg ℓ^{-1} stock solution was prepared (0.5 g of efflorescent salt was dissolved in 100 mℓ beakers) from which lower concentration solutions (1, 3, and 5 mg ℓ^{-1}) were prepared through serial dilution. Ultra-pure water (18.2 MΩ grade water) was used for stock solution preparation and dilutions. An adjusted pH value of 5.02 was achieved using 0.1 mol ℓ^{-1} HNO_3 and 0.1 mol ℓ^{-1} NaOH solutions. The pH of the solutions was measured using a pH probe (Hanna Instruments, Johannesburg). All glassware used was cleaned with dilute HNO_3 (10% HNO_3) and dried in the oven (at 100 ºC) before use. HDS was used as an adsorbent in column experiments and all experimental studies were conducted at room temperature (25 ºC).

3.6.2.2 Column adsorption studies

Column adsorption studies were conducted in triplicate to determine the effect of HDS dosage on the adsorption of trace metals. Different masses (1, 5, and 10 g) of HDS were used at flow rates 3, 5, and 7 mℓ min^{-1} of AMD at 25 ºC. The effects of varying pH of the solution, initial trace metal concentration, bed height, and flow rates were studied. The filtrates were analysed using ICP-OES. The pH_{pzc} of HDS was determined through the steps described below. A 40 mℓ of potassium nitrate (KNO_3) solution of known concentration was transferred into a series of volumetric flasks. The initial pH of the solution was adjusted from pH 2.03 to 6.01 by adding drops of 0.1 mol ℓ^{-1} HCl and 0.1 mol ℓ^{-1} NaOH. The volume of the total solution was made up to 30 mℓ by adding KNO_3 solution of the same ionic strength. The initial pH of each solution was taken into consideration and 0.5 g of HDS was added to each volumetric flask. The heterogeneous mixtures that contain solid particles were shaken and allowed to equilibrate, with occasional stopping (through manual shaking). The pH regimes of the clear liquid that lies above the solid residue after settling were noted. The change (ΔpH) between the initial pH (pH_o) and final pH (pH_i) was calculated using equation 3.24 (Gulicovski *et al.,* 2008).

$$(\Delta pH = pH_o - pH_i) \quad (3.24)$$

The change between the initial and final pH was plotted against the pH and the point of the intersection of the resulting curve was used to determine the point of zero charges (the point where the ΔpH is equal to zero gave the pH_{pzc}).

The continuous fixed-bed adsorption experiment was conducted in an acrylic cylinder glass column with an internal diameter of 3 cm and a height of 10 cm. Filters were placed at both ends of the column to keep the HDS inside the column. HDS was packed into the adsorption column to obtain the required bed height. The initial solution concentrations were pumped downward through the adsorption column using a peristaltic pump. All experiments were performed at 25 ºC, each sample was collected after 30 min (time intervals) and analysis was done using ICP-OES. The breakthrough point was considered as the time at which collected filtrates (effluent concentration) has reached 5% of the initial trace metal concentration and the exhaustion of bed was considered as the time when the filtrates reach 95% of the initial trace metal concentration. The adsorption capacity of trace metals was estimated (equation 3.25) (Alslaibi *et al.,* 2013; Lim and Aris, 2014).

$$q_{e=} \frac{Q_{fr}\, t_{br}\, C_{in}}{m} \quad (3.25)$$

where Q_{fr} is the effluent flow rate (mℓ min^{-1}), t_{br} is the breakthrough time, C_{in} is the influent concentration (mg $ℓ^{-1}$) and m is the mass (g) of HDS. The removal efficiency of trace metals was estimated (equation 3.26) (Abdulrazak *et al.,* 2015).

$$\%R = \frac{C_{in}-C_{ef}}{C_{in}} * 100 \quad (3.26)$$

where C_{in} and C_{ef} are influent and effluent trace metal concentration, respectively. The critical bed height is also described as the height of mass transfer zone (Z_m) is related to bed height (Z), breakthrough time (t_{br}), and exhaustion time (t_{ex}) and are calculated (equation 3.27) (Guo *et al.,* 2014).

$$Z_m = Z\left[1 - \frac{t_{br}}{t_{ex}}\right] \quad (3.27)$$

The volume of the outlet (effluent), V_{ef} in mℓ was calculated (equation 3.28) (Karunarathne and Amarasinghe, 2013).

$$V_{ef} = Q_{fr} t_{ex} \quad (3.28)$$

where Q_{fr} is the flow rate in mℓ min^{-1} and t_{ex} is the exhaustion time (min).

Effect of inlet trace metals concentration

The inlet trace metal ions concentration was observed at different trace metal concentrations at 1, 3, 5 mg $ℓ^{-1}$. The feed solution (inlet concentration) was pumped in a downward flow direction, at a constant flow rate of 3 mℓ min^{-1} (the pH of the solution was fixed at 5.02). The filtrates were collected after 30 min (time interval) and analysed with ICP-OES.

Effect of bed height

AMD was pumped in a downward direction through the adsorption column which contained a separate bed height of 3, 6, 8 cm which has close similarity (corresponds) to 1, 5, 10 g of HDS. The inlet trace metal concentration and hydrogen ion activity of the solution were made constant (concentration at 1 mg $ℓ^{-1}$ and pH at 5.02, respectively). The filtrates were collected at an interval of half an hour (30 min) and analysis of trace metals was done using ICP-OES.

Effect of flow rate

The inlet solution was pumped in a downward flow direction at flow rates of 3, 5, and 7 mℓ min^{-1} separately through the adsorption columns. The bed height and hydrogen ion activity were fixed (maintained) at 10 g and

pH 5.02, respectively. The filtrates were collected after every 30 min (time interval) and trace metal analysis was done using ICP-OES.

3.6.2.3 Column desorption studies

To conduct the desorption studies, the HDS was washed by pumping 1 ℓ of Ultra-pure water (18.2 MΩ grade water) through the column at 10 mℓ min^{-1} and after flushing some trace metals remaining on the outer sphere on HDS surface, the column was dried in a vacuum to remove water from the HDS surface. Desorption with 0.1 mol $ℓ^{-1}$ NaOH, 0.1 mol $ℓ^{-1}$ H_2SO_4, 0.1 mol $ℓ^{-1}$ HCl and deionised water was conducted. After desorption studies were done, the HDS was rinsed once more to remove excess acid. The desorption efficiency was determined (equation 3.29).

$$\%R = \frac{C_{des}}{C_{ads}} * 100 \quad (3.29)$$

where: C_{des} and C_{ads} are the concentrations of trace metals desorbed and adsorbed onto HDS sorbent (mg $ℓ^{-1}$), respectively.

3.6.2.4 Sorption isotherms

In the continuous fixed-bed column, the breakthrough time and the shape of the breakthrough curve are key parameters in determining the operational performance of the column. The breakthrough curve is achieved by plotting the ratio of C_{in} to C_{ef} against t. Several models (Thomas, Yoon-Nelson, Adam-Bohart, Bed Depth Service Time models, etc.) were developed for use in the design of continuous fixed-bed adsorption columns. These models were applied in this study to identify the best model for predicting the behaviour of adsorption data (prediction of dynamic behaviour) from experimental data.

Thomas model

The Thomas model was applied to describe the breakthrough curve of a continuous fixed-bed column and the influence of adsorption parameters in a column. This model was represented through the second-order law of kinetic reaction (with no axial dispersion) when the bed height was at a minimum and the breakthrough curve formed immediately after flow stated. The Thomas model in a linearized form is expressed in equation 3.30 (Lee *et al.,* 2015).

$$\ln\left[\frac{C_o}{C_t} - 1\right] = \frac{k_{Th}q_o m}{Q} - k_{Th}c_o t \quad (3.30)$$

In the Thomas model, C_o - is the inlet potentially toxic trace metals concentration, C_t - represent the outlet potentially toxic trace metals concentration, *m* - a mass of adsorbent in the fixed bed column (g), k_{Th} – represent the Thomas kinetic coefficient (mℓ min^{-1} mg), q_o – is the maximum solid phase concentration (mg g^{-1}) and *t* – is the total flow rate (time, min). The k_{Th} and q_o values can be determined from the linear plot of ln [(C_o/C_t) – 1] versus t.

Adam-Bohart model

The Adam-Bohart model is applied in the delineation of the continuous fixed-bed column (breakthrough curve) for the initial state of the column system. This model states that reaction does not automatically be model (it is based on the theory of the surface chemistry or reaction). When making assumptions that adsorption equilibrium occurs instantly, the relationship between C_t/C_o and t (in the breakthrough curve) best describes a continuous flow adsorption mechanism. The Adam-Bohart model was presented in equation 3.31 (Lakshmipathy and Sarada, 2016).

$$\ln\left[\frac{C_t}{C_o}\right] = k_{AB}C_o t - \frac{k_{AB}N_o Z}{U_o} \quad (3.31)$$

The k_{AB} – represents the Adam-Bohart kinetic constant (L/mg min), N_o – saturation concentration (mg ℓ^{-1}), Z – the bed height of column (cm), U_o – linear velocity (cm min^{-1}) determined from the calculation of flow rate over the fixed bed section area (the area between the breakthrough and exhaustion point). The k_{AB} and N_o can be determined from the plot of ln (C_t/C_o) vs t.

Yoon-Nelson model

The Yoon-Nelson model was established based on the theory of adsorption and the breakthrough of analyte (adsorbate) probability. The rate of decrease in probability for each analyte molecule is proportional to the probability of analyte adsorption (also proportional to the probability of the analyte breakthrough on the adsorbent). This model is simple (involves less fixed-bed column parameters and this also include the data). The Yoon-Nelson model is mostly applicable in the single component system and linearized model equation described in equation 3.32 (Lim and Aris, 2014).

$$ln\left[\frac{C_t}{C_o - C_t}\right] = k_{YN}t - \tau k_{YN} \quad (3.32)$$

k_{YN} – represent the rate constant (min^{-1}) and τ – is the time needed for 50% adsorbate breakthrough (min). The k_{YN} and τ can be determined from the linear plot of ln[$C_t/(C_o - C_t)$] versus t.

Bed depth service time model

The bed depth service time (BDST) model is applicable when investigating the relationship between the bed depth (Z) and the breakthrough time (t_{br}) for effluent concentration provided. The BDST model is used in the evaluation of the capacity of the bed column at various breakthrough values percentage. It assumes that the rate of adsorption is proportional to both the residual capacity of adsorbent and the concentration of adsorbate. The BDST model was formed by Hudchins from partial or minor changes made from the Adam-Bohart model and this derivation made some assumptions that forces like intra-particle diffusion and external mass transfer are not important, considering that the trace metals are directly adsorbed on the adsorbent surface. BDST is simple and utilised to predict the effect of the different influent concentrations, bed depth, and flow rates in the performance of the fixed-bed column. It also assumes that the service time, breakthrough concentration, and the bed height are correlated with the adsorption process parameters including adsorption capacity and the adsorption rate constant (it is important in the determination of the adsorption process for the flow rates and the adsorbate concentrations). The BDST was calculated using equation 3.33 (Rangabhashiyam *et al.,* 2016).

$$t = \frac{N_o Z}{C_o v} - \frac{1}{K_a C_o}\ln\left[\frac{C_o}{C} - 1\right] \quad (3.33)$$

where: t is the BDST model which assumes service time, C is the breakthrough concentration of trace metal (mg ℓ^{-1}), N_o is the adsorption capacity of the bed column (mg ℓ^{-1}), *v* is the linear velocity (cm min^{-1}), and K_a is the rate constant (L/mg min).

3.7 INTERACTION OF SLUDGE AND PHOSPHATE CONTAINING WATER

Untreated sewage, agricultural and industrial wastewater contains an elevated concentration of phosphates. Such water is discharged into receiving water bodies, resulting in eutrophication which adversely affects aquatic life. Hydrous ferric oxide (Hfo, represented chemically as ≡FeOH) tends to have a strong adsorption capacity and affinity for phosphate ions. The purpose of this study was to use the PHREEQC geochemical modeling code for experimental design in building a platform to understand adsorption of phosphates onto HDS which is enriched in Hfo. The approach involved using surface complexation models based on the Dzombak and Morel assumption of two surface sites (strong and weak sites) having densities of 0.005 and 0.2 mol Fe^{-1}, respectively. The Donnan diffuse layer in both strong (Hfo_sOH) and weak (Hfo_wOH) sites described phosphate adsorption onto pure Hfo. The Hfo_wOH sites gave the best adsorption fit to the Hfo for phosphate species ($H_2PO_4^-$), where they occupied 0.0018 mol (mol Fe)$^{-1}$. This was based on an Hfo surface

area of 600 m^2/g and a mass of 0.5 g. When the surface area and mass were reduced (to 200 m^2/g and 0.1 g, respectively) for $H_2PO_4^-$, the site moles were also reduced to 0.0011 mol (mol Fe)$^{-1}$. The Hfo_wOH showed the best fit for the Hfo adsorption of $H_2PO_4^-$ species giving a site density of 0.00055 mol (mol Fe)$^{-1}$ for a surface area of 600 m^2/g and an Hfo mass of 0.1 g. This site density for $H_2PO_4^-$ was reduced to 0.00028 mol (mol Fe)$^{-1}$ for a surface area of 200 m^2/g and Hfo mass of 0.5 g. Adsorption of phosphates onto Hfo is important in monitoring of phosphates in water and for understanding saturation capacities that are important in determining potential of adsorption for the Hfo. This is important in assessing the potential of repurposing HDS for removal of phosphate from contaminated water.

3.7.1 Computational simulation studies for batch mode

Interaction of cations and anions (mainly phosphates) was studied using simulation with the PHREEQC geochemical modelling code (sample input script in Figure 3.16).

```
SOLUTION 1 #Sample chemical composition
    temp        value
    pH          value
    pe          value
    redox       pe
    units       mg/l
    density     1
    Br          concentration value
    Cl          concentration value
    F           concentration value
    N(5)        concentration value
    P           concentration value
    S(6)        concentration value
    Ca          concentration value
    K           concentration value
    mg          concentration value
    Na          concentration value

SURFACE_MASTER_SPECIES
    Hfo_s       Hfo_sOH
    Hfo_w       Hfo_wOH

SURFACE_SPECIES
 Hfo_surface species = Hfo_surface species
    log_k     value

PHASES
fix_pH
    H+ = H+
    log_k    0
fix_pe
    e- = e-
    log_k    0

SURFACE 1
 Hfo_s #no. of moles# #Surface area (m2 g-1)# #mass of adsorbent (g)#
 Hfo_w   #no. of moles#

SELECTED_OUTPUT 1
-file                 selected.xls
-high_precision       true
-reset                false
-solution             true
-inverse modelling    false
-active               true
-user_punch           true
-totals          P

END
```

Figure 3.16. PHREEQC input script format for phosphates adsorption onto Hfo

To predict elemental speciation, the code creates a first run of “SOLUTION 1” to achieve the speciation calculation (in this case, phosphate species were considered). For the experimental design, the number of moles of both weak and strong surface sites, surface area, a mass of adsorbent, hydrogen ion activity, and temperature could be established. Experimental conditions used in batch studies were similar to those in the simulation input script. Thermodynamic parameters were obtained from the Wateq4f.dat database as it contains phosphorous ($P\text{-}PO_4^{3-}$) and other analytes of interest. The chemical composition of the initial wastewater and the generalised surface complexation simulation of the interaction with Hfo is shown in Figure 3.17. Different pH values, varying masses of Hfo, and different Hfo surface areas (strong and weak sites) were considered to assess the optimal conditions of adsorption of $P\text{-}PO_4^{3-}$ (Figures 3.17-3.20). The simulations were conducted for: Hfo surface areas of 600, 200 and 60 m^2/g; Hfo_sOH concentrations of 4.46 x 10^{-6}, 8.93 x 10^{-7}, 4.46 x 10^{-7} and 8.93 x 10^{-8} moles; and Hfo_wOH concentrations of 1.79 x 10^{-4}, 3.57 x 10^{-5}, 1.79 x 10^{-5}, 3.57 x 10^{-6}.

The sewage water used was collected in the Klip River, Soweto (Johannesburg). It was filtered using 0.45 µm cellulose nitrate filter paper and analysed for phosphate using ion chromatography (IC) (Metrohm, Switzerland). The sample had a concentration of 196.05 mg ℓ^{-1} phosphate among other anions such as NO_3^-, Cl^- and SO_4^{2-}. Serial dilution with deionised water was conducted to obtain concentrations of 10, 50 and 100

mg ℓ^{-1} of phosphate. An adjusted pH value of 4.03 was achieved using 0.1 mol ℓ^{-1} HNO_3 and 0.1 mol ℓ^{-1} NaOH solutions. The pH of the solutions was measured using a pH probe (Hanna Instruments, Johannesburg). All glassware used was cleaned with dilute HNO_3 (10% HNO_3), rinsed with deionised water and dried in the oven (at 100 ºC) before use. HDS was used as an adsorbent in column experiments and all experimental studies were conducted at room temperature (25 ºC).

```
TITLE #Generalised Surface complexation of phosphates

SOLUTION 1 #Sewage wastewater
    temp      25
    pH        4.03
    pe        4
    redox     pe
    units     mg/l
    density   1
    Br        0.049
    Cl        20.5
    F         0.02
    N(5)      10.65
    P         196.05
    S(6)      143.03
    Ca        5.64
    K         2.62
    Mg        3.95
    Na        6.02
    -water    1 # kg

SURFACE_MASTER_SPECIES
 Hfo_s  Hfo_sOH
 Hfo_w  Hfo_wOH

SURFACE_SPECIES

 Hfo_wOH + PO4-3 + 3H+ = Hfo_wH2PO4 + H2O
        log_k   31.29

 Hfo_wOH + PO4-3 + 2H+ = Hfo_wHPO4- + H2O
        log_k   25.39

 Hfo_wOH + PO4-3 + H+ = Hfo_wPO4-2 + H2O
        log_k   17.72


SURFACE 1 #HFO Surface
    -equilibrate with solution 1
    Hfo_s      4.46e-06    600       0.5
    Hfo_w      1.79e-04

SELECTED_OUTPUT 1
    -file                  selected.xls
    -high_precision        true
    -reset                 false
    -solution              true
    -inverse_modeling      false
    -active                true
    -user_punch            true
    -totals                P
END
```

Figure 3.17. Input PHREEQC script for the effect of pH on phosphates adsorption onto Hfo

```
SOLUTION 1 #Sewage wastewater
    temp      25
    pH        4.03
    pe        4
    redox     pe
    units     mg/l
    density   1
    Br        0.049
    Cl        20.5
    F         0.02
    N(5)      10.65
    P         196.05
    S(6)      143.03
    Ca        5.64
    K         2.62
    Mg        3.95
    Na        6.02
    -water    1 # kg


 SURFACE_MASTER_SPECIES
  Hfo_s  Hfo_sOH
  Hfo_w  Hfo_wOH

SURFACE_SPECIES

 Hfo_wOH + PO4-3 + 3H+ = Hfo_wH2PO4 + H2O
        log_k   31.29

 Hfo_wOH + PO4-3 + 2H+ = Hfo_wHPO4- + H2O
        log_k   25.39

 Hfo_wOH + PO4-3 + H+ = Hfo_wPO4-2 + H2O
        log_k   17.72

SURFACE 1 #HFO Surface
    -equilibrate with solution 1
    Hfo_s      8.93e-08    600       0.01
    Hfo_w      3.57e-06

SURFACE 2 #HFO Surface
    -equilibrate with solution 1
    Hfo_s      1.79e-07    600       0.02
    Hfo_w      7.14e-06

SURFACE 3 #HFO Surface
    -equilibrate with solution 1
    Hfo_s      4.46e-07    600       0.05
    Hfo_w      1.79e-05

SELECTED_OUTPUT 1
    -file                  answer.xls
    -solution              true
    -totals                P
END
```

Figure 3.18. Input PHREEQC script for the effect of mass on phosphates adsorption onto Hfo

```
SOLUTION 1 #Sewage wastewater
    temp      25
    pH        4.03
    pe        4
    redox     pe
    units     mg/l
    density   1
    Br        0.049
    Cl        20.5
    F         0.02
    N(5)      10.65
    P         2.05
    S(6)      143.03
    Ca        5.64
    K         2.62
    Mg        3.95
    Na        6.02
    -water    1 # kg

SURFACE_MASTER_SPECIES
 Hfo_s  Hfo_sOH
 Hfo_w  Hfo_wOH
```

```
SOLUTION 2 #Sewage wastewater
    temp      25
    pH        4.03
    pe        4
    redox     pe
    units     mg/l
    density   1
    Br        0.049
    Cl        20.5
    F         0.02
    N(5)      10.65
    P         10.05
    S(6)      143.03
    Ca        5.64
    K         2.62
    Mg        3.95
    Na        6.02
    -water    1 # kg

SURFACE_SPECIES

 Hfo_wOH + PO4-3 + 3H+ = Hfo_wH2PO4 + H2O
        log_k   31.29

 Hfo_wOH + PO4-3 + 2H+ = Hfo_wHPO4- + H2O
        log_k   25.39

 Hfo_wOH + PO4-3 + H+ = Hfo_wPO4-2 + H2O
        log_k   17.72
```

```
SOLUTION 3 #Sewage wastewater
    temp      25
    pH        4.03
    pe        4
    redox     pe
    units     mg/l
    density   1
    Br        0.049
    Cl        20.5
    F         0.02
    N(5)      10.65
    P         100.05
    S(6)      143.03
    Ca        5.64
    K         2.62
    Mg        3.95
    Na        6.02
    -water    1 # kg

SURFACE 1 #HFO Surface
    -equilibrate with solution 1
    Hfo_s       4.46e-06    600    0.5
    Hfo_w       1.79e-04


SELECTED_OUTPUT 1
    -file                   answer.xls
    -solution               true
    -totals                 P
END
```

Figure 3.19. Input PHREEQC script for the effect of concentration on phosphates adsorption onto Hfo

```
SOLUTION 1 #Sewage wastewater
    temp      25
    pH        4.03
    pe        4
    redox     pe
    units     mg/l
    density   1
    Br        0.049
    Cl        20.5
    F         0.02
    N(5)      10.65
    P         196.05
    S(6)      143.03
    Ca        5.64
    K         2.62
    Mg        3.95
    Na        6.02
    -water    1 # kg

SURFACE_MASTER_SPECIES
 Hfo_s  Hfo_sOH
 Hfo_w  Hfo_wOH
```

```
SOLUTION 2 #Sewage wastewater
    temp      30
    pH        4.03
    pe        4
    redox     pe
    units     mg/l
    density   1
    Br        0.049
    Cl        20.5
    F         0.02
    N(5)      10.65
    P         196.05
    S(6)      143.03
    Ca        5.64
    K         2.62
    Mg        3.95
    Na        6.02
    -water    1 # kg

SURFACE_SPECIES

 Hfo_wOH + PO4-3 + 3H+ = Hfo_wH2PO4 + H2O
        log_k   31.29

 Hfo_wOH + PO4-3 + 2H+ = Hfo_wHPO4- + H2O
        log_k   25.39

 Hfo_wOH + PO4-3 + H+ = Hfo_wPO4-2 + H2O
        log_k   17.72
```

```
SOLUTION 3 #Sewage wastewater
    temp      40
    pH        4.03
    pe        4
    redox     pe
    units     mg/l
    density   1
    Br        0.049
    Cl        20.5
    F         0.02
    N(5)      10.65
    P         196.05
    S(6)      143.03
    Ca        5.64
    K         2.62
    Mg        3.95
    Na        6.02
    -water    1 # kg

SURFACE 1 #HFO Surface
    -equilibrate with solution 1
    Hfo_s       4.46e-06    600    0.5
    Hfo_w       1.79e-04


SELECTED_OUTPUT 1
    -file                   answer.xls
    -solution               true
    -totals                 P
END
```

Figure 3.20. Input PHREEQC script for the effect of temperature on phosphates adsorption onto Hfo

3.7.2 Experimental batch studies

Batch adsorption studies were carried out under different conditions to evaluate the effects of pH (4.03, 5.02, and 6.03), adsorbent dosage (10, 20, 50, 100, and 500 mg), initial P-PO_4^{3-} concentration (2, 10, 100, 300 and 500 mg ℓ^{-1}), and contact time (1 – 1080 min) on the adsorption of P-PO_4^{3-} ions onto HDS. To evaluate the effect of the presence of coexisting ions (effects of competing ions) in HDS, batch experiments with sulphates, chlorides, nitrates, and phosphates were performed at optimal conditions. Solution pH was adjusted using 0.1 mol ℓ^{-1} HNO_3 and 0.1 mol ℓ^{-1} NaOH, with their volume contribution kept at <10% of the total solution volume. Centrifuge tubes were shaken using an elliptical benchtop shaker (Labcon, South Africa) at a constant rate of

150 rpm, allowing for sufficient time for adsorption capacity to reach equilibrium. The filtrates were analysed using IC for anions (SO_4^{2-}, NO_3^-, Cl^-, PO_4^{3-}, etc.) and ICP-OES for cations (Na^+, Mg^{2+}, K^+, Ca^{2+}, etc.).

Adsorption capacity (q_e) and removal efficiency (%R) were calculated using the equations:

$$q_e = \frac{(C_o - C_e)V}{m} \quad (3.34)$$

$$\%R = \frac{(C_o - C_e)}{C_o} * 100 \quad (3.35)$$

where: C_o is initial the concentration of P-PO_4^{3-} (mg ℓ^{-1}); C_e is the concentration of P-PO_4^{3-} at equilibrium (mg ℓ^{-1}); m is the mass of HDS (g); V is the volume of the solution (mℓ).

3.7.3 Experimental desorption studies of phosphates from HDS

Batch adsorption experiments (loading) were carried out using 10 mℓ of 100 mg ℓ^{-1} of P-PO_4^{3-} solution. This was contacted with 50 mg of HDS in 50 mℓ polyethylene centrifuge tubes for 24 h, followed by drying of the residue in an oven (100 ºC) for 5 h. Desorption was then conducted using 0.1 mol ℓ^{-1} NaOH and 0.1 mol ℓ^{-1} $NaHCO_3$ solutions (Chitrakar *et al.,* 2006) followed by analysis of the filtrates with IC for P-PO_4^{3-} ions. Removal efficiency of P-PO_4^{3-} was calculated using the following equation:

$$\%R = \frac{C_{des}}{C_{ads}} * 100 \quad (3.36)$$

where: C_{des} and C_{ads} are the concentrations of P-PO_4^{3-} ions desorbed and adsorbed onto HDS sorbent (mg ℓ^{-1}), respectively

Data from adsorption studies were modelled using the Langmuir, Freundlich, Dubinin-Radushkevich and Temkin isotherms (refer to 3.3.4). The Kinetic models to evaluate the time-dependence of adsorption was studied, and the data were fitted using the pseudo first-order, pseudo second-order, Elovich, intraparticle diffusion and film diffusion model. The goodness of fit of the models was determined using the correlation coefficient (R^2 value) (refer to 3.3.5). Thermodynamic parameters including Gibbs free energy (ΔG^o), enthalpy (ΔH^o), and entropy (ΔS^o) were considered to evaluate the effects of temperature during adsorption. The equations below indicate a change in Gibbs free energy (refer to 3.3.6)

3.7.4 Reactive transport model construction for column studies

The PHREEQC geochemical modelling code (Parkhurst and Appelo, 2013) was used for reactive transport simulation (input script is presented in Figure 3.21) based on the Wateq4f database. The models produced provided parameters that were later used to design actual column experimental studies.

```
SOLUTION 0 #Sewage wastewater
    temp      25
    pH        4.03
    pe        4
    redox     pe
    units     mg/l
    density   1
    Br        0.049
    Cl        20.5
    F         0.02
    N(5)      10.65
    P         196.05
    S(6)      143.03
    Ca        5.64
    K         2.62
    Mg        3.95
    Na        6.02
    -water    1 # kg

SOLUTION 1-50 #Column initial solution
    temp      25
    pH        7 charge
    pe        4
    redox     pe
    units     mg/l
    density   1
    Mg        0.074
    N(5)      1.23
    Na        1.05
    -water    1 # kg

EXCHANGE 1-50
    X       0.0011
    -equilibrate with solution 1
    -pitzer_exchange_gammas false

SURFACE 1 #HFO Surface
    -equilibrate with solution 1-50
    Hfo_w      2.86e-03    600       8
    Hfo_s      7.14e-05


USE solution none
TRANSPORT 1-50
-cells 50
-shifts 50

PRINT
        -reset  false
       -totals true
       -status true

SELECTED_OUTPUT
        -file answer.xls
        -totals P
       -solution true
END
```

Figure 3.21. PHREEQC input script for reactive transport model

The script can be explained as follows:

a) The solution to be contacted with the Hfo surface is defined as “Solution 0”. In this case, it is sewage wastewater.

b) The solution labelled “Solution 1-50” is the initial solution in the column. As indicated previously, the “column” in this case is arbitrary as it is only for computational simulations. The range of numbers “1-50” are cells, from the first cell to the 50th cell. All cells have the same solution initially and the solution is in contact with Hfo in each cell.

c) The Hfo is defined as both an “exchange” as well as a “surface”. An exchange (represented as “X”) defines the clayey nature of the Hfo and accounts for ordinary anionic exchange reactions while a surface accounts for the unidirectional surface complexation reactions (on strong (Hfo_s) and weak (Hfo_w) adsorption sites). As pointed out earlier, the exchange and surface cover all the 50 cells with Solution 1-50 being the pore water in them.

d) The next block has important instructions to effect a reactive transport simulation. The “Use Solution none” instructs the code to ignore any reactions that will mix the initial solution “Solution 1-50” in the cells with the new incoming solution “Solution 0”. This sounds a bit simplistic, but that mix, if allowed to occur, could complicate the simulation and result in clumsy results. To avoid that, the new solution is allowed to push the existing one out and new reactions between the surface and the new solution established.

The instruction “Transport 1-50” introduces the new solution into the 1st cell of the column and flushes it through the 50 cells. This is repeated 50 times as indicated by the number of “shifts”. A shift can be thought of as a complete pore volume or total fluid volume to saturate a cell each time.

e) The length of each cell is only arbitrary here. In the actual column experiments, it is determined by the flow rate and bed height of the adsorbent.

f) Other factors such as dispersivity of the fluid in the cells have been ignored, making this a 1 dimensional (1-D) reactive transport model. These factors are important in other models such as 2-D and 3-D models.

g) The rest are just output options that the user defines. For instance, if the interest is in knowing the extent of adsorption in any cell after any number of shifts or knowing the resulting solution in any of those cells after the adsorption reactions have occurred, the output options can be manipulated to reflect this information.

The reactive transport models were used for the optimisation of parameters that were used in the actual column of experimental studies.

3.7.5 Column adsorption studies

Column adsorption studies were conducted in triplicate to determine the effect of HDS dosage on the adsorption of P-PO_4^{3-}. Different masses (1, 4, and 8 g) of HDS were determined at flow rates 1, 3, and 5 mℓ min^{-1} of sewage wastewater at room temperature. The effects of initial P-PO_4^{3-} concentration, bed height, and flow rates were studied. Filtrates were analysed using ion chromatography for anions (PO_4^{3-}, NO_3^-, etc.) and ICP-OES for cations (Ca^{2+}, Mg^{2+}, K^+, Na^+, etc.) The point of zero charge (pH_{PZC}) of HDS was determined through the steps described below. A 40 mℓ solution of potassium nitrate (KNO_3) of known concentration was transferred into a series of volumetric flasks. The initial pH of the solution was adjusted from pH 6.88 to 4.03 by adding drops of 0.1 mol $ℓ^{-1}$ HCl and 0.1 mol $ℓ^{-1}$ NaOH. The volume of the total solution was made up to 30 mℓ by filling up to the meniscus by adding KNO_3 solution of the same ionic strength. The initial pH of each solution was taken into consideration and 0.5 g of HDS was added to each volumetric flask. The heterogeneous mixtures containing solid particles were shaken and allowed to equilibrate with stopping or ceasing for a time (through manual shaking). The pH regimes of the clear liquid that lies above the solid residue after settling were noted. The change (ΔpH) between the initial pH (pH_i) and final pH (pH_f) was calculated using equation 3.37.

$$(\Delta pH = pH_i - pH_f) \quad (3.37)$$

The change between initial and final pH was plotted against the pH and the point of the intersection of the resulting curve was used to determine pH_{PZC} (i.e. where ΔpH = 0).

The continuous fixed-bed adsorption experiment was conducted in a glass column with an internal diameter of 2 cm and a height of 15 cm. A filter was placed at the end of the column to keep the HDS inside. HDS was packed into the adsorption column to obtain the required bed height. The phosphate solutions were pumped upward through the column using the peristaltic pump. All experiments were performed at room temperature, with filtrates collected at 30 min intervals followed by analysis. The breakthrough point was considered as the time at which collected filtrates had reached 5% of the initial P-PO_4^{3-} concentration and the exhaustion of the bed was considered as the time when filtrates reached 95% of the initial P-PO_4^{3-} concentration. The adsorption capacity of P-PO_4^{3-} was computed from equation 3.38.

$$q_{e=} \frac{Q_{fr}\, t_{br}\, C_{in}}{m} \quad (3.38)$$

where: Q_{fr} is the effluent flow rate (mℓ min^{-1}), t_{br} is the breakthrough time, C_{in} is the influent concentration (mg $ℓ^{-1}$) and m is the mass (g) of HDS. The removal efficiency of P-PO_4^{3-} was computed from equation 3.39.

$$\%R = \frac{C_{in} - C_{ef}}{C_{in}} * 100 \quad (3.39)$$

where: C_{in} and C_{ef} are influent and effluent concentrations of $P\text{-}PO_4^{3-}$, respectively. The critical bed height is described as the height of mass transfer zone (Z_m) and is related to bed height (Z), breakthrough time (t_{br}), and exhaustion time (t_{ex}) based on equation 3.40.

$$Z_m = Z\left[1 - \frac{t_{br}}{t_{ex}}\right] \quad (3.40)$$

The volume of the outlet (effluent), V_{ef} in mℓ was calculated using the given in equation 3.41.

$$V_{ef} = Q_{fr} t_{ex} \quad (3.41)$$

where: Q_{fr} is flow rate in mℓ min^{-1} and t_{ex} is exhaustion time (min).

Effect of inlet phosphate concentration

Solutions of $P\text{-}PO_4^{3-}$ at concentrations of 10, 50, 100 mg ℓ^{-1} were fed into the column in an upward flow direction at a constant flow rate of 1 mℓ min^{-1} (the pH of the solution was fixed at 4.03). Filtrates were collected at 30 min and analysed with using ion chromatography.

Effect of bed height

Bed heights of 1, 3, 6 cm which closely corresponded to 1, 4, 8 g of HDS, respectively were used. As predicted from computational simulations, a $P\text{-}PO_4^{3-}$ of concentration of 10 mg ℓ^{-1} at a pH of 4.03 was fed into the column in an upward flow direction. Filtrates were collected at 30 min intervals followed by analysis using ion chromatography.

Effect of flow rate

Previous conditions (concentration of 10 mg ℓ^{-1}, pH of 4.03 and bed height of 6 cm) were maintained with flow rates of 1, 3, and 5 mℓ min^{-1} being used followed by analysis of filtrates.

3.7.6 Column desorption studies

To conduct desorption studies, 1 ℓ of deionised was flushed through the column at 5 mℓ min^{-1} to remove any phosphate that was not adsorbed. This was followed by flushing with 0.1 mol ℓ^{-1} NaOH 0.1 $NaHCO_3$ as desorbing agents. Rinsing with deionised was then done to remove any excess desorbed phosphate remaining in the pore spaces. Desorption efficiency was determined using equation 3.42.

$$\%R = \frac{C_{des}}{C_{ads}} * 100 \quad (3.42)$$

Where: C_{des} and C_{ads} are the concentrations of $P\text{-}PO_4^{3-}$ desorbed and adsorbed onto HDS sorbent (mg ℓ^{-1}), respectively.

CHAPTER 4: RESULTS AND DISCUSSION

This chapter presents the findings of the study according to the methodology discussed above. Discussions are incorporated alongside the findings, supported by relevant literature where appropriate. Brief conclusions have been included at the end of each section whose findings are reported.

4.1 COMPUTATIONAL PREDICTION OF PRECIPITATES

The results from the simulations of selective formation of precipitates of the previously mentioned parameters are discussed below. They include individual neutralising agents, their combinations/mixtures, varying temperature, equilibration with gases and varying concentrations (or dosage amounts) of the neutralising agents.

4.1.1 Individual neutralising agents

Different neutralising agents gave different pH values and varying amounts of iron minerals that precipitated (Table 4.1). The magnesium-based neutralising agents provided satisfactory results in terms of treatment of AMD, pH and the iron precipitates produced. In particular $MgCO_3$, MgO and $Mg(OH)_2$ proved to be the best neutralising agents as they raised the pH to above 9 which is in agreement with what the industries are currently allowing for waste disposal after treatment (Masindi *et al*., 2017). The advantage of using the $MgCO_3$ is that gypsum ($CaSO_4.2H_2O$) does not precipitate with the iron minerals, allowing its easy separation. This is a challenge with the current HDS process (using $CaCO_3$) in treatment plants where co-precipitation with iron minerals is unavoidable, resulting in a heterogeneous and complex sludge as indicated previously. $CaCO_3$ and Na_2O also produced acceptable treated AMD and iron precipitates at pH>9.

Using $Ca(OH)_2$, NaOH, CaO, $CaHCO_3$ and Na_2CO_3 as individual neutralising agents yielded acceptable pH and iron minerals, but poor overall water treatment results (e.g. ineffective removal of toxic elements and sulphates). Other neutralising agents such as NH_3, NH_4OH, and $NaHCO_3$ gave poor results with respect to the precipitated minerals and the treated water. The maximum pH after the addition of these agents was less than 7, resulting in ineffectively treated AMD. The iron precipitates were very few and had low SI, implying that they may not be precipitating effectively. Therefore, these neutralising agents were not used for subsequent simulations for the AMD treatment.

At lower concentrations (0.2 - 1.0 moles) of the neutralising agents, goethite (FeOOH), hematite (Fe_2O_3) and siderite ($FeCO_3$) could be separated at acidic pH (5 - 6.9) for all the neutralising agents that were used. Hematite was observed to be a derivative of goethite as in the treated water a small amount of hematite was observed. Essentially, a loss of water by goethite will result in the formation of hematite. At higher concentrations (1.2 - 2.0 moles), the following iron precipitates were observed: $Fe(OH)_3$, FeS, goethite (FeOOH), hematite (Fe_2O_3), mackinawite (FeS), pyrite (FeS_2), siderite ($FeCO_3$) at varying pH for the effective neutralising agents as shown in Table 4.1. The neutralising agents were chosen based on the acceptable pH reached and the better quality of the water treated.

Table 4.1. Neutralising agents for AMD treatment

Neutralising agents	**$MgCO_3$**	**MgO**	**$Mg(OH)_2$**	**Na_2O**	**$CaCO_3$**	**NaOH**
pH	9.44	12.15	11.34	12.77	9.43	9.65

4.1.2 Combined neutralising agents

The main aim of combining the neutralising agents was to check the changes in pH, treated water composition and iron precipitates produced. This was done by combining the individual neutralising agents that were considered effective for AMD treatment and those that were deemed to be poor as individual neutralising agents. It should be noted here that the reasoning was premised on that a mixture of good and bad neutralising agents would produce acceptable effects. The pH range that was of interest was from 7 - 9 which is an acceptable pH range for discharging waste to the streams. At this pH range, the concentration of trace metals in the water is low, reducing their environmental threat. The iron minerals that precipitated were observed to be more compared to those produced by the individual neutralising agents.

The combinations that yielded good precipitates, pH and treated water were: $MgCO_3$+NH_3, MgO+NaOH, and $Mg(OH)_2$+NH_4OH. The minerals $Fe(OH)_3$, FeS, goethite (FeOOH), hematite (Fe_2O_3), mackinawite (FeS), pyrite (FeS_2) and siderite ($FeCO_3$) were the iron minerals that precipitated at higher concentrations of the combinations. Table 4.2 shows that the combined neutralising agents used still yielded a pH that is desirable (7 - 9). The benefit of using $MgCO_3$, MgO, $Mg(OH)_2$, $CaCO_3$ and Na_2O as neutralising agents is that the obtained minerals are not precipitated simultaneously with gypsum (Bologo *et al.*, 2009; Mulopo *et al.,* 2012).

In other instances, depending on the individual and combined neutralising agents used, the iron minerals precipitated were observed to decrease. For instance, the combination of $CaCO_3$ and Na_2CO_3 decreased the iron precipitates by 30% compared to $CaCO_3$ individually. The $Mg(OH)_2$/NH_4OH combination decreased the iron precipitates by 40% compared to $Mg(OH)_2$ individually. Likewise, the $MgCO_3$/NH_4 combination decreased the iron precipitates by 25% compared to the $MgCO_3$ individually. The MgO had similar observations as $MgCO_3$. When the Na_2O/NH_3 combination was used, the iron precipitates were found to be 30% less compared to Na_2O individually. The improvement when the neutralising agents were combined in the iron mineral precipitates yielded good pH and better water quality.

Table 4.2. Effect of the combined neutralising agents on pH of the treated AMD

Combined neutralising agents	pH
Na_2O + NH_3	9.17
CaO + $CaHCO_3$	9.47
MgO + NaOH	9.84
$Mg(OH)_2$ + NH_4OH	9.19
$MgCO_3$ + NH_3	8.04
$MgCO_3$ + NaOH	7.23
NH_3 + NH_4OH	6.50

4.1.3 Equilibrating with CO_2

To assess the effect of carbon dioxide (CO_2) in the AMD, the degassing of CO_2 was conducted with individual and combined neutralising agents and the results are shown in Table 4.3. The highest pH reached was 9. Most individual neutralising agents gave satisfactory results when CO_2 was introduced. Gypsum was observed to precipitate before the introduction of CO_2, meaning that it would be possible to separate gypsum from other minerals by controlling equilibration with CO_2. The treated water quality showed greater improvement and more iron precipitates were produced. The most common iron precipitate is siderite which varies with the type of neutralising agent used. Comparing individual $MgCO_3$ which had a molality of 0.1091 and the combined

$MgCO_3$/NaOH which had a molality of 0.1041, the concentration does not vary much as it changes by only 0.44%. This implies that $MgCO_3$ is a good neutralising agent when equilibrated with CO_2 as both individual and combined neutralising agent.

Table 4.3. Final pH-values in AMD for individual neutralising agents equilibrated with CO_2

Neutralising agent	**$MgCO_3$**	**MgO**	**$Mg(OH)_2$**	**Na_2O**	**$CaCO_3$**	**NaOH**
pH	9.58	9.58	9.58	9.76	9.51	9.64

4.1.4 Equilibrating with O_2

The AMD was then equilibrated with atmospheric oxygen, where the highest pH of 8 was reached with most neutralisation agents as shown in Table 4.4. The iron precipitates and the resulting treated were not satisfactory for these neutralising agents even though Jarosite-K ($KFe_3(SO_4)_2(OH)_6$) was observed to precipitate. Jarosite-K was predicted to precipitate for both the individual and the combined neutralising agents when the system was equilibrated with oxygen. A less complex sludge would likely be obtained as the predictions showed that fewer precipitates would be produced.

Table 4.4. Final pH-values in AMD for individual neutralising agents equilibrated with O_2

Neutralising agent	**$MgCO_3$**	**MgO**	**$Mg(OH)_2$**	**Na_2O**	**$CaCO_3$**	**NaOH**
pH	8.73	8.80	8.71	8.37	8.73	8.43

4.1.5 Fixed pH

The pH was fixed to assess the changes in iron precipitates and the treated water and the results are shown in Table 4.5. At acidic conditions, nitric acid was used to fix the pH at 3.0 and what was observed is that few iron minerals precipitated, which included Fe_2O_3, $Fe(OH)_3$ and FeOOH which were common in the treated water of most of the neutralising agents. The composition of the treated water did not change much and this was expected since the pH was acidic. However, the precipitation of these minerals means that if the interest is in precipitating them, the pH must be fixed at 3.0 with nitric acid. Whereas for alkalinity, the neutralising agents were used to fix the pH at 9.5 which was observed to be the maximum pH where the treated water was satisfactory and the iron mineral precipitates were significant (judging from the molal yields predicted). The fixing of pH at 9.5 proved to work better than fixing the pH at values higher than 10. This, of course, depends on the mineral of interest for a study. Although most iron minerals precipitated at pH ≥ 9, using $MgCO_3$, MgO and Na_2O improved water treatment. This then led to the conclusion that these neutralising agents can be used in the treatment of AMD.

4.1.6 Varying temperature

The temperature was varied from 25 - 100 °C to assess the effect of heating the water before treatment. A temperature of 33 °C, with other factors, held constant, was found to yield satisfactory. This was ideal as this temperature is quite ambient and easily attainable.

4.1.7 Varying concentration (or dosage) of neutralising agent

Varying the dosage amounts of neutralising agents resulted in non-convergence of the simulation iterations as the highest pH reached was 14 at higher moles (10 moles). Calcite was observed to precipitate gypsum at higher amounts and pH. At higher concentrations, there were fewer precipitates predicted and the treated water quality was poor as most metals dissolved in the solution.

To be certain that the model works, a different AMD was used with the same neutralising agents at a different temperature. It was observed that the identified effective neutralising agents worked best (Table 4.5). The precipitated iron minerals are as follows: $Fe(OH)_3$, FeS, goethite (FeOOH), hematite (Fe_2O_3), mackinawite (FeS), pyrite (FeS_2), siderite ($FeCO_3$) which were common in all the identified effective neutralising agents.

Table 4.5. pH values produced by the effective individual neutralising agents

Neutralising agent	**$MgCO_3$**	**MgO**	**$Mg(OH)_2$**	**Na_2O**	**$CaCO_3$**	**NaOH**
pH	9.02	9.51	12.21	9.57	8.89	9.05

4.1.8 Indicative cost analysis

An indicative cost analysis was performed for effective neutralising agents. According to Sigma-Aldrich/Merck (for the month of December 2018), the following prices were obtained (per 500 g): $MgCO_3$ - R 3160, $Mg(OH)_2$ – R583.54, $CaCO_3$ – R1447.64, MgO – R713.97 and Na_2O – R1078. The actual experiments would determine how much exactly the respective neutralising agents are required for instance to treat 1 ℓ of AMD. These neutralising agents were identified to result in the precipitation of the following iron precipitates: $Fe(OH)_3$ has a white to greenish colour; FeS has a brown colour; goethite (FeOOH) has a yellowish colour; hematite (Fe_2O_3) has a brown to reddish colour; mackinawite (FeS) has a bronze to white grey colour; pyrite (FeS_2) has a pale yellow colour, and siderite ($FeCO_3$) has light brown to yellow colour. A few grams (25 g) of an artist's paint pigment can cost anywhere above R1500. Thus, precipitation of such ochres may provide an economically promising way of producing them.

4.2 EXPERIMENTAL FORMATION OF PRECIPITATES

In this section, the formation of precipitates experimentally is presented and described. This includes the initial formation of the precipitates from the initial AMD solutions whose pH was adjusted with NaOH and $MgCO_3$. From those, some filtrates were selected for further treatment with each neutralising agent to precipitate more ochres. The characterisation of the ochres is also presented as well as some illustrations of the applications of the ochres to paint and artwork. Lastly, the changes in water chemistry are presented, that is, the composition of the initial AMD and the composition after treatment with NaOH

4.2.1 Using NaOH as a neutralising agent

The precipitates obtained at the seven pH values of precipitation (pH 3, 4, 5, 6, 7, 8 and 9) ranged from yellowish to brown (Figures 4.1 to 4.14).

(a)  (b) 

Figure 4.1. (a) Seven beakers stirred for 48 h to allow oxygen circulation in the reactions. The pH values for precipitation increase from the extreme left beaker to the extreme right (i.e. pH 3 to 9) (b) Vacuum system used to filter the samples.

The precipitates for the individual beakers in Fig. 4.1a are shown below (Figures 4.2-4.8, starting from the extreme left beaker to the extreme right beaker). The precipitates were dried at 180 ^{o}C in the oven for an hour followed by pulverising with a mortar and pestle to yield a powder. It should be pointed out here that no difference in colouration and mineralogy was observed between these precipitates and those that had been air dried over 5 days. Thus, oven drying was chosen as it was a quicker method.

(a)  (b)  (c) 

Figure 4.2. Yellow precipitates (pH 3): (a) Filtered (25 °C) (b) Dried (180 °C for 1 h) (c) Ground with pestle and mortar after drying

(a)  (b)  (c) 

Figure 4.3. Yellow-brown precipitates (pH 4): (a) Filtered (25 °C) (b) Dried (180 °C for 1 h) (c) Ground with pestle and mortar after drying

(a)  (b)  (c) 

Figure 4.4. Yellow-brown precipitate (pH 5): (a) Filtered (25 °C) (b) Dried (180 °C for 1 h) (c) Ground with pestle and mortar after drying

(a)  (b)  (c) 

Figure 4.5. Brown precipitate (pH 6): (a) Filtered (25 °C) (b) Dried (180 °C for 1 h) (c) Ground with pestle and mortar after drying

(a)  (b)  (c) 

Figure 4.6. Light brown precipitate (pH 7): (a) Filtered (25 °C) (b) Dried (180 °C for 1 h) (c) Ground with pestle and mortar after drying

(a)  (b)  (c) 

Figure 4.7. Reddish-brown precipitate (pH 8): (a) Filtered (25 °C) (b) Dried (180 °C for 1 h) (c) Ground with pestle and mortar after drying

(a)  (b)  (c) 

Figure 4.8. Brown precipitate (pH 9): (a) Filtered (25 °C) (b) Dried (180 °C for 1 h) (c) Ground with pestle and mortar after drying

Grinding with a mortar and pestle produced ochres that can be workable for art paintings as will be discussed later. The brown to reddish colour was due to hematite (Fe_2O_3) and the yellowish colour was due to goethite (FeOOH) as confirmed by PXRD analysis. Further details are provided in the characterisation section (4.2.6). The recovered precipitates ranged from 22.22 to 27.82 g per litre of treated AMD solution (Table 4.6).

Table 4.6. Mass (g ℓ^{-1}) of precipitates recovered at different pH values using NaOH

pH	Colour of Precipitate	*m* Precipitate
3	Yellow	22.22
4	Yellow-brown	22.00
5	Yellow-brown	26.16
6	Brown	27.82
7	Brown	24.14
8	Reddish-brown	27.36
9	Brown	26.46

4.2.2 Retreatment of filtrates with NaOH

After filtering the Fe precipitates above, three selected filtrates (i.e. those from pH of precipitation of 3, 5 and 7) were retreated (or further neutralised) with NaOH followed by stirring for 48 h at 2 rpm and filtration. They produced new precipitates shown in Figures 4.9-4.11, respectively. This was done to assess if further precipitates could be recovered following the initial precipitation. Reddish-brown to black iron precipitates were obtained, implying that the filtrates had the potential to yield more precipitates.

(a)  (b)  (c) 

Figure 4.9. Reddish-brown precipitate (pH 5): (a) Filtered (25 °C) (b) Dried (180 °C for 1 h) (c) Ground with pestle and mortar after drying

(a)  (b)  (c) 

Figure 4.10. Brown precipitate (pH 7): (a) Filtered (25 °C) (b) Dried (180 °C for 1 h) (c) Ground with pestle and mortar after

(a)  (b)  (c) 

Figure 4.11. Black precipitate (pH 9): (a) Filtered precipitates (25 °C) (b) Dried (180 °C for 1 h) (c) Ground with pestle and mortar after drying

The yields of the precipitates following retreatment with NaOH at different pH regimes are presented in Table 4.7. As mentioned before, the filtrate of pH 3 was neutralised to a new pH of 5; the filtrate of pH 5 to pH 7; and that of pH 7 to pH of 9). Thus, close to 10%, more yield was observed in the retreatment.

Table 4.7. Mass (g ℓ^{-1}) of precipitates recovered at different pH regimes following retreatment of selected initial filtrates with NaOH

pH	Colour of Precipitate	*m* Precipitate
5	Reddish-brown	2.672
7	Brown	2.242
9	Black	1.896

4.2.3 Addition of ferrocyanide and precipitation with NaOH

Bluish, greenish and brownish Fe precipitates were obtained (Figures 4.12-4.16) following the addition of ferrocyanide to the initial AMD solution. Only 4 pH values of precipitation were assessed i.e. pH 3, 5, 7 and 9 (beakers A, B, C and D in Figure 4.12, respectively).

(a)  (b) 

Figure 4.12. (a) Bluish, green and brown precipitates forming at various pH regimes during neutralisation (b) Sample filtration with a vacuum system

(a)  (b)  (c) 

Figure 4.13. Light blue precipitates (pH 3): (a) Filtered (25 °C) (b) Dried (180 °C for 1 h) (c) Ground with pestle and mortar after drying

(a)  (b)  (c) 

Figure 4.14. Dark blue precipitates (pH 5): (a) Filtered (25 °C) (b) Dried (180 °C for 1 h) (c) Ground with pestle and mortar after drying

(a)  (b)  (c) 

Figure 4.15. Green precipitate (pH 7): (a) Filtered (25 °C) (b) Dried (180 °C for 1 h) (c) Ground with pestle and mortar after drying

(a)  (b)  (c) 

Figure 4.16. Brown precipitate (pH 9): (a) Filtered (25 °C) (b) Dried (180 °C for 1 h) (c) Ground with pestle and mortar after drying

To recap, the precipitates formed were as follows: at pH 3 (light blue precipitate), at pH 5 (dark blue precipitate), at pH 7 (green precipitate) and at pH 9 (dark brown precipitate). The yield for the recovered precipitates ranged from 1.644 to 3.514 g per litre of the initial synthetic AMD solution as presented in Table 4.8.

Table 4.8. Mass (g ℓ^{-1}) of the recovered precipitates at different pH values (of ferrocyanide containing solutions) using NaOH

pH	Colour of Precipitate	*m* Precipitate
3	Light blue	1.644
5	Dark blue	2.194
7	Green	3.030
9	Dark brown	3.514

The precipitates involving ferrocyanide largely consist of Prussian blue ($Fe^{III}[Fe^{III}Fe^{II}(CN)_6]_3$) and have been observed in previous studies (Bakatula and Tutu, 2016) in the vicinity of active gold tailings dumps (slimes dams) (Figure 4.17).

(a)  (b) 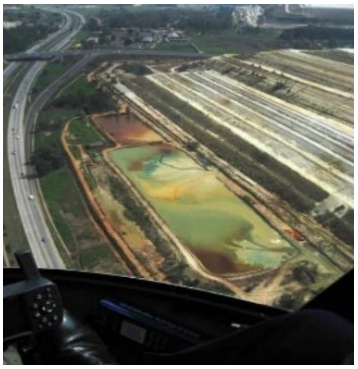 (c) 

Figure 4.17. Prussian blue colouration: (a) in the foreground at an AMD affected stream (b) in a water retain dam of a slimes dam (photo courtesy Prof T.S. McCarthy) and (c) in a solution trench of a slimes dam (the pipe was discharging ferrocyanide containing water at pH 9 that mixed with AMD in the trench at pH 3, resulting in the formation of Prussian blue).

The Prussian blue precipitates are formed *via* the following reaction:

$$4Fe^{3+} + 3[Fe(CN)_6]^{4-} \rightarrow Fe^{III}[Fe^{III}Fe^{II}(CN)_6]_3 \qquad (4.1)$$

The precipitates obtained experimentally (Figures 4.13-4.15) show that they are quite persistent and tend to overshadow the other precipitates e.g. the yellow and brown ones. The distribution of the colourations observed in the field (Figure 4.17) substantiates this persistence as the bluish colouration is quite elaborate.

4.2.4 Using $MgCO_3$ as a neutralising agent

The precipitates obtained following neutralisation with $MgCO_3$ are shown in Figure 4.18. There are some similarities in colours to those obtained when using NaOH (Figures 4.2, 4.5 and 4.8). The similarities of colours were due to the same experimental conditions for both alkaline materials. The same salts were dissolved at room temperature and had similar fixed neutralisation pH values. Yellowish to brown Fe precipitates were obtained. The precipitates obtained are shown in Figures 4.19-4.25. Only precipitates obtained at pH of neutralisation 3, 6 and 9 are shown.

(a)  (b) 

Figure 4.18. (a) Beakers stirred for 48 h to allow oxygen circulation in the reactions (b) Vacuum system used to filter the samples

(a)  (b)  (c) 

Figure 4.19. Yellow precipitates (pH 3): (a) Filtered (25 °C) (b) Dried in oven (180 °C) (c) Sample grinded with pestle and mortar after it was dried

(a)  (b)  (c) 

Figure 4.20. Yellow-brown precipitates (pH 4): (a) Filtered (25 °C) (b) Dried (180 °C for 1 h) (c) Ground with pestle and mortar after drying

(a)  (b)  (c) 

Figure 4.21. Yellow-brown precipitate (pH 5): (a) Filtered (25 °C) (b) Dried (180 °C for 1 h) (c) Ground with pestle and mortar after drying

(a)  (b)  (c) 

Figure 4.22. Yellow-brown precipitate (pH 6): (a) Filtered (25 °C) (b)Dried (180 °C for 1 h) (c) Ground with pestle and mortar after drying

(a)  (b)  (c) 

Figure 4.23. Light brown precipitate (pH 7): (a) Filtered (25 °C) (b) Dried (180 °C for 1 h) (c) Ground with pestle and mortar after drying

(a)  (b)  (c) 

Figure 4.24. Reddish-brown precipitate (pH 8): (a) Filtered (25 °C) (b) Dried (180 °C for 1 h) (c) Ground with pestle and mortar after drying

(a)  (b)  (c) 

Figure 4.25. Brown precipitate (pH 9): (a) Filtered (25 °C) (b) Dried (180 °C for 1 h) (c) Ground with pestle and mortar after drying

The yields of the recovered precipitates are presented in Table 4.9. The yields are generally comparable to those obtained using NaOH.

Table 4.9. Mass (g ℓ^{-1}) of precipitates recovered at different pH values using $MgCO_3$

pH	Colour of Precipitate	*m* precipitate
3	Yellow	17.0
4	Yellow-brown	19.1
5	Yellow-brown	27.1
6	Yellow-brown	28.5
7	Brown	25.0
8	Reddish-brown	29.4
9	Brown	31.6

Some of the filtrates from the initial neutralisation experiments were used for further treatment with $MgCO_3$ so as to assess any potential precipitates that could be obtained. The filtrates that were retreated were from beakers A, B, and C (i.e. they had an initial neutralisation pH of 3, 4 and 5, respectively). The targeted new pH values were 5 (for the filtrate that was at pH 3); 7 for the filtrate at pH 4; and 9 for the filtrate at pH 9. The precipitates formed from the retreatment are shown in Figures 4.26-4.28.

(a)  (b)  (c) 

Figure 4.26. Reddish-brown precipitate (pH 5): (a) Filtered (25 °C) (b) Dried (180 °C for 1 h) (c) Ground with pestle and mortar after drying

(a) 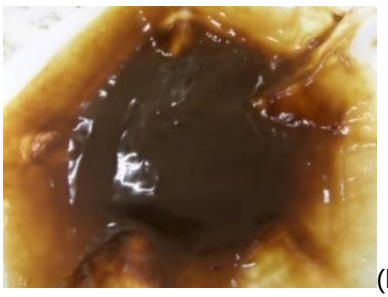 (b)  (c) 

Figure 4.27. Brown precipitate (pH 7): (a) Filtered (25 °C) (b) Dried (180 °C for 1 h) (c) Ground with pestle and mortar after drying

(a)  (b)  (c) 

Figure 4.28. Brown-black precipitate (pH 9): (a) Filtered precipitates (25 °C) (b) Dried (180 °C for 1 h) (c) Ground with pestle and mortar after drying.

The yields for precipitates obtained from the retreatment of filtrates with $MgCO_3$ are presented in Table 4.10.

Table 4.10. Mass (g ℓ^{-1}) recovered from retreatment of selected filtrates with $MgCO_3$ at different pH values

pH	Colour of Precipitate	*m* Precipitate
5	Reddish-brown	1.82
7	Brown	2.04
9	Black	1.96

4.2.5 Formation of precipitates from AMD

4.2.5.1 Using NaOH, $MgCO_3$ and $CaCO_3$ as a neutralising agent

Figure 4.29. Precipitates using NaOH (pH 3-9): (a) to (i) Dried (180 °C for 1 h), ground with pestle and mortar after drying.

Figure 4.30. Precipitates using $MgCO_3$ (pH 3-9): (a) to (i) Dried (180 °C for 1 h), ground with pestle and mortar after drying.

(g)  (h)  (i) 

Figure 4.31. Precipitates using $CaCO_3$ (pH 3-9): (a) to (i) Dried (180 °C for 1 h), ground with pestle and mortar after drying.

4.2.5.2 Using NaOH, $MgCO_3$ and $CaCO_3$ as a neutralising agent

Similar precipitates were observed using NaOH, $MgCO_3$ and $CaCO_3$ in the pre-treatment of filtrates. The pre-treatment using $CaCO_3$ was only presented in Figure 4.32.

(a)  (b)  (c) 

(d)  (e)  (f) 

Figure 4.32. Precipitates using $CaCO_3$ (pH 3-9): (a) to (i) Dried (180 °C for 1 h), ground with pestle and mortar after drying.

4.2.6 Characterisation of Fe precipitates

The iron precipitates were characterised using PXRD to determine their mineralogy. The results showed that the dominant Fe minerals were: goethite, hematite, and magnetite. The mineralogy of Fe precipitates analysed showed elevated concentrations of Fe in the form of oxides and oxyhydroxides and this was confirmed by PXRD analysis (Figures 4.33).

The precipitates for Prussian blue have not been included here, but as pointed out earlier, their characterisation has been conducted in separate studies. The pH in the experiments was found to be more influential in determining the colours of the precipitates produced than the temperature of the reaction. This was proven during experimental work in that even at room temperature, it was possible to produce the desired Fe precipitates. This implies that less energy (electricity) is required as no heating had to be done to enhance the production of the precipitates. The potential lower costs for recovering Fe precipitates from AMD make it an attractive alternative to replace Fe oxides (ochre minerals) found in weathered natural iron ores (Lottermoser, 2011).

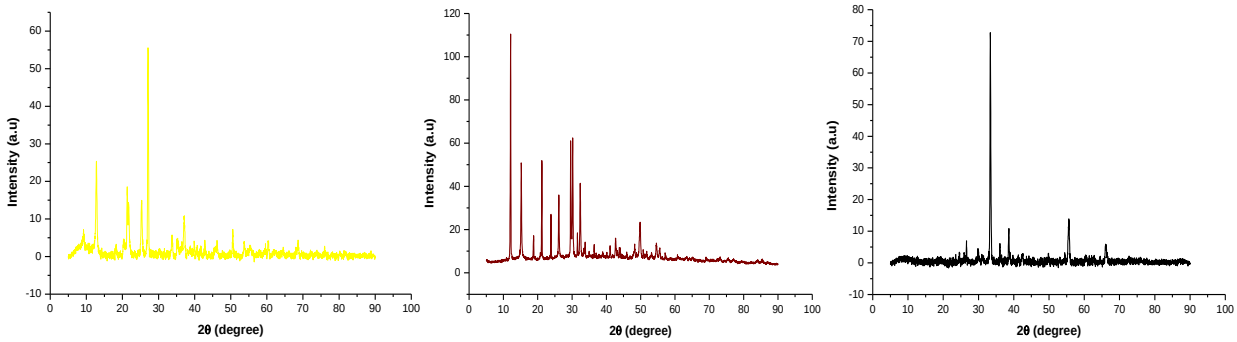

Figure 4.33. X-ray diffractograms (from left to right) of the yellow (goethite), reddish-brown (hematite) and black precipitate (magnetite).

The compositions of the dominant Fe precipitates are presented in Table 4.11.

Table 4.11. Major Fe precipitates and their composition

Fe precipitate	Chemical formula	Chemical composition (wt %)	Density (g cm^{-3})
Goethite	FeOOH	Fe: 62.85; O: 36.01; H: 1.13	3.8
Hematite	Fe_2O_3	Fe: 69.94; O: 30.06	5.3
Magnetite	Fe_3O_4	Fe: 72.36; O: 27.64	5.15

4.2.7 Application in paintings and artwork

The potential of the produced precipitates for use in paintings and artwork was assessed (Figure 4.40). As pointed out earlier, the precipitates maintained their colours following the addition of water to make painting pastes.

(a)  (b)  (c)  (d) 

Figure 4.34. Art paintings from Fe precipitates recovered from synthetic AMD: (a) environmental terrains (b) shepherd and flock (c) painted tree (d) soccer field (paintings by Khathutshelo Netshiongolwe).

The potential precipitation of Fe precipitates from AMD and their subsequent use for painting and artwork may offer a potential affordable source of these precipitates while cleaning up the contaminated water.

4.2.8 Water chemistry

The nature of the synthesised AMD was influenced by the combination of chemicals dissolved in the solutions. The measured pH in the AMD solutions ranged from 2 to 3, with high electrical conductivity (EC) and elevated concentrations of Fe and sulphate. The addition of NaOH to one of the chosen solutions (of pH 2.76), for instance, increased the pH and precipitated some metals out of the solution as observed by significant decreases in the concentrations of metals in the solution (Table 4.12).

Table 4.12. Analytical results for synthetic AMD and treated water (mg ℓ^{-1}) for one of the solutions that was neutralised using NaOH; EC in µS/cm

	pH	EC	Fe	Al	Ca	Cu	Zn	Mn	Cd	Ni	S
Synthetic AMD	2.04	4680	369	1.06	15.6	0.05	0.10	0.28	0.05	0.36	188
Treated AMD	6.34	363	7.57	0.06	0.29	<0.02	0.01	0.03	<0.02	0.01	92

*sulphate reported as sulphur

More than 95% of Fe was precipitated in this case. The sulphate concentration also decreased by about 50%, suggesting that sulphate salts are formed in the precipitates. These were not observed in the PXRD diffractograms, most likely due to the dominance of Fe minerals that tend to shield other minerals. The equation for neutralisation by NaOH can be simplified as:

$$NaOH(aq) + FeSO_4(aq) \rightarrow Fe(OH)_2(s) + Na_2SO_4(aq) \quad (4.2)$$

The oxidation of Fe^{2+} to Fe^{3+} results in the formation of $Fe(OH)_3$. The Fe^{2+} precipitates are yellowish in colour while those for Fe^{3+} are reddish to brownish. The drying process results in the loss of the water component of the precipitated and formation of minerals such as FeOOH and Fe_2O_3. Magnetite (Fe_3O_4) forms as a result of the combination of oxides of Fe^{2+} and Fe^{3+}.

For neutralisation with $MgCO_3$, the reaction can be simplified as:

$$MgCO_3(s) + FeSO_4(aq) \rightarrow FeCO_3(s) + MgSO_4(aq) \quad (4.3)$$

It should be noted here that the stability and existence of the carbonate depend largely on the pH. At low pH, it is easily destroyed.

While not shown in the results above, elevated concentrations of Na were recorded (as well as Mg in instances where $MgCO_3$ was used). It is possible to recover salts such as epsom ($MgSO_4$) from these additional ions, but that can be subject to further studies.

4.2.9 Conclusion

This study explored the possibility of deriving value from the AMD treatment process by forming Fe precipitates or ochres that can be useful for paint and artwork applications. Using conditions established in computational simulations, NaOH and $MgCO_3$ were found to be the best choices for the neutralisation of AMD with the aim of precipitating desired ochres. Precipitates ranging in colour from yellow, brown to black were obtained by varying the pH of neutralisation from 3 to 9 at room temperature. This meant that recoveries could be done without any extra energy applied to the reactions. Sufficient yields of the precipitates were obtained e.g. above 30 g per litre of AMD in some instances and further neutralisation of some of the filtrates showed that more precipitates could be obtained. The different ochres produced were used for some artwork and proved viable, suggesting that this route of their production may offer some potential. The water after treatment with the neutralising agents showed an elevated pH and a significant decrease in elemental concentrations. Thus, the study has demonstrated that the treatment of AMD can enable more value to be derived in the form of treated water and precipitation of useful ochres. The study underscored the importance of computational simulations as an experimental design tool that can be used to save on time and experimental costs.

4.3 CHARACTERISATION OF HDS

4.3.1 Powder X-ray diffraction (PXRD)

The mineralogy of HDS was determined using PXRD and the results are presented in Figure 4.35. The dominant minerals included: magnetite, hematite, goethite, maghemite, pyrophyllite, chloritoid, mica, chlorite, jarosite, pyrite, gypsum, copiapite and clay minerals, mostly kaolinite and montmorillonite. The observation of elevated concentrations of iron oxides in HDS was also confirmed by XRF analysis. The presence of iron minerals is apparent from the reddish-brown colouration of the sludge. The dominant iron oxide mineral in HDS was goethite.

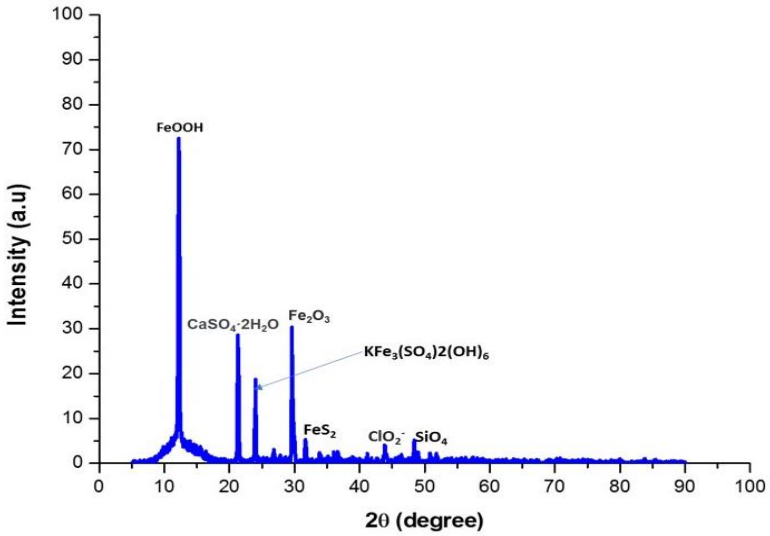

Figure 4.35. PXRD diffractogram of HDS

4.3.2 X-ray fluorescence (XRF)

XRF analysis was conducted to determine the elemental composition of HDS. The observation of elevated concentrations of iron oxides in HDS was also confirmed by XRF analysis (Figure 4.36). The presence of the iron minerals is apparent from the reddish-brown colouration of the sludge. As indicated earlier, an elevated amount of Fe was observed (over 20%).

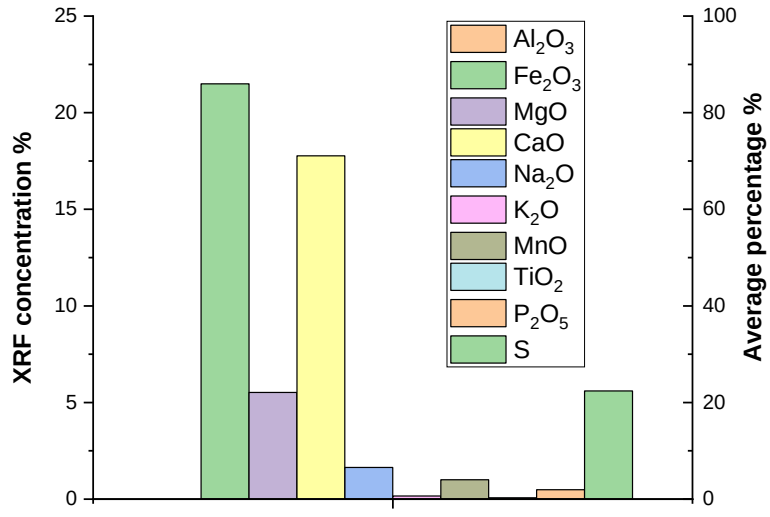

Figure 4.36. X-ray fluorescence analysis of HDS

The chemical composition of the fresh HDS after leaching with deionised water is shown in Figure 4.37.

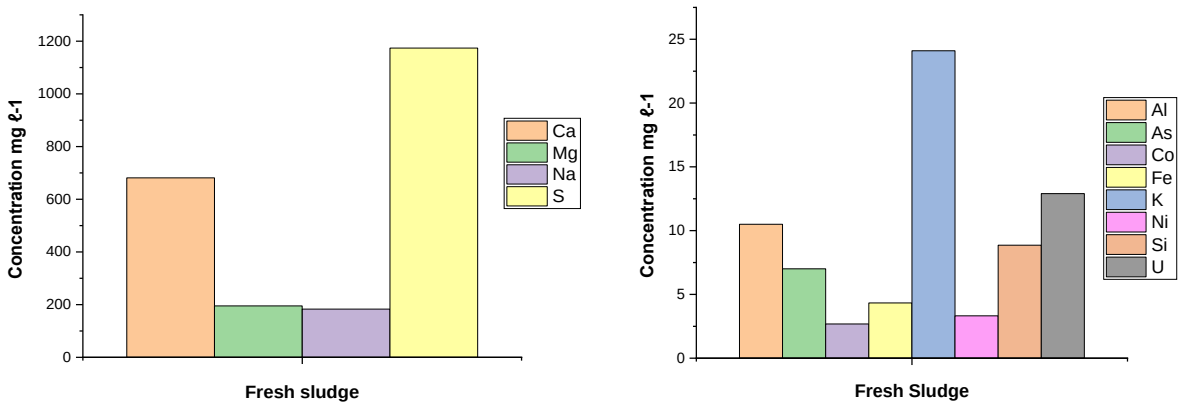

Figure 4.37. Major (left) and minor (right) elements in fresh HDS (sulphate reported as sulphur)

The results point to the presence of elevated concentrations of sulphur and trace metals such as U. These represent accumulated concentrations following precipitation and co-precipitation with iron precipitates during the neutralisation process. The sulphur results here are from ICP-OES and the equivalent sulphate concentration would be about three times that. The use of limestone and lime for neutralisation in these plants is shown by the elevated concentration of Ca. A combination of this and sulphates results in large amounts of gypsum being precipitated (as substantiated by the PXRD results).

The results for the chemical composition of aged sludge are shown in Figure 4.38. The results show elevated concentrations of elements compared to the fresh sludge. The reason mainly lies in that in the fresh sludge most of the minerals are likely to be in the soluble phase while in aged sludge these have been allowed to precipitate onto the bulk sludge, resulting in the observed increased concentrations.

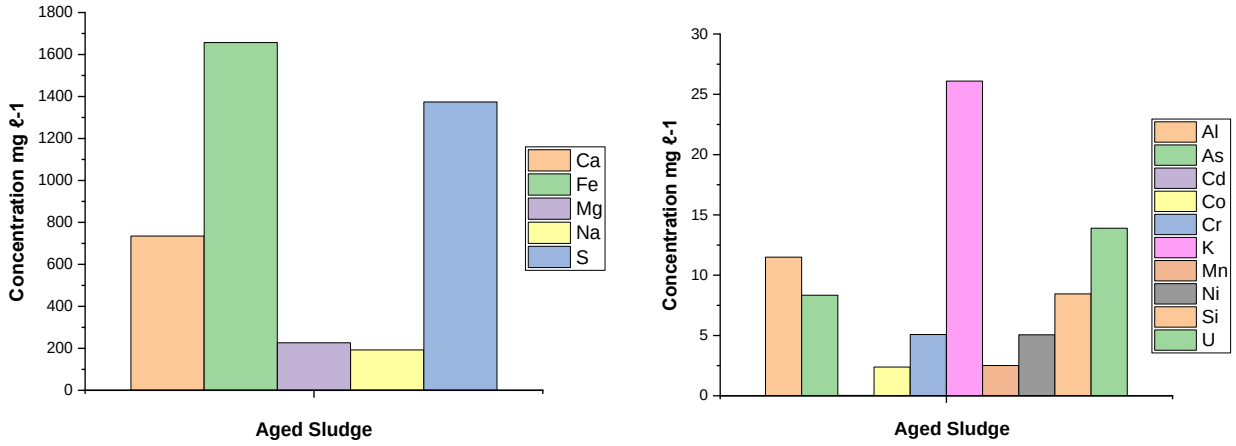

Figure 4.38. Major (left) and minor (right) elements in the aged HDS

The sulphate concentration and other anions in the aged sludge is presented in Figure 4.39. The high sulphate concentrations corroborate the observations for the fresh sludge. Higher concentrations were observed here (three times those for fresh sludge). Low concentrations of nitrites, bromides and nitrates were recorded, meaning that these ions did not play a significant role in the chemistry of the sludge.

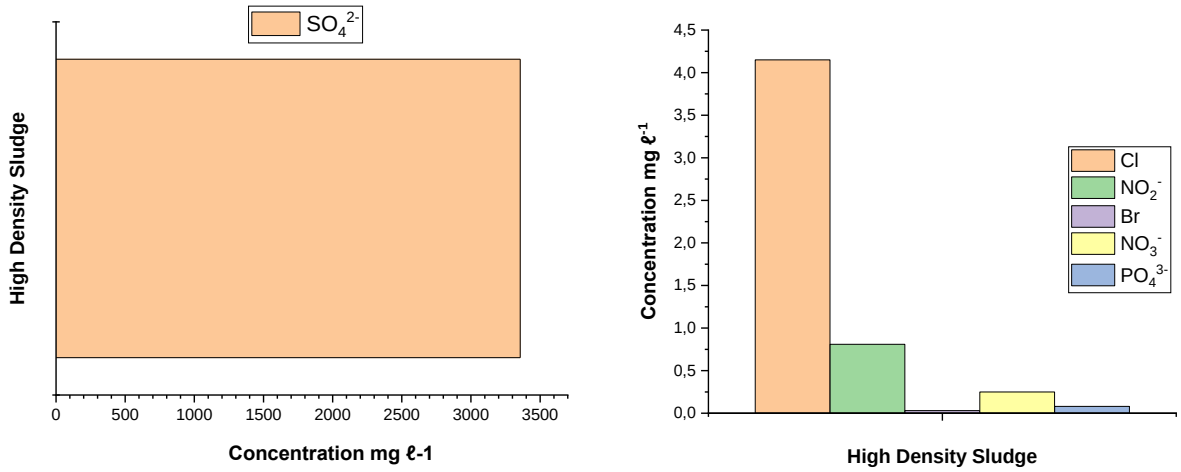

Figure 4.39. Major (left) and minor (right) anions in High Density Sludge

4.3.3 Scanning electron microscopy (SEM)

SEM analysis was done to determine the surface morphology before and after adsorption (Figure 4.40). The dominant mineral on the crystals was gypsum ($CaSO_4 . 2H_2O$). After adsorption, the surface morphology was changed (more fine particles were formed) and the alteration of particle sizes creates more electrostatic forces (and has implications on adsorption).

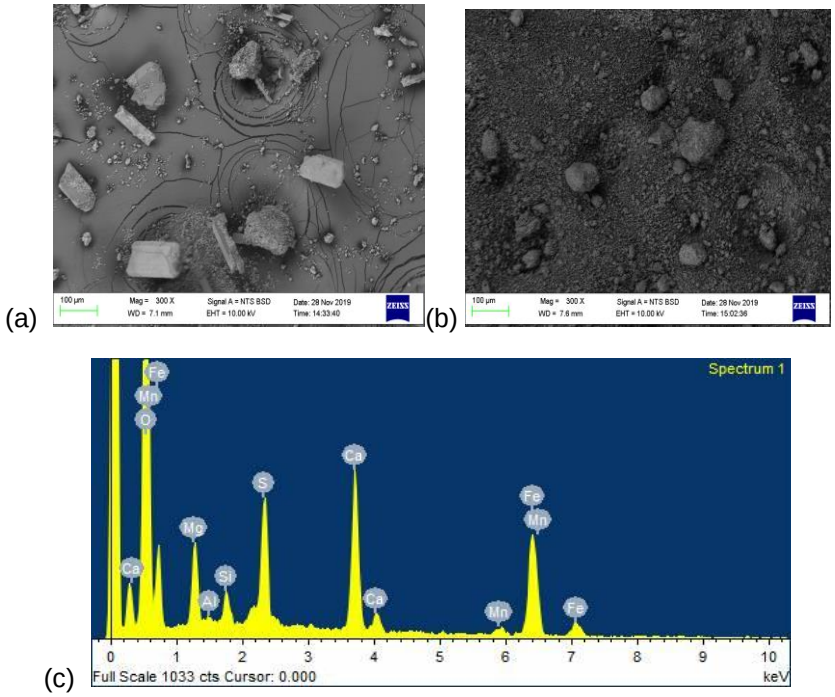

Figure 4.40. (a) HDS before adsorption (b) HDS after adsorption (c) SEM-EDX to characterize the elemental composition of HDS

4.3.4 Fourier-transform infrared spectroscopy (FTIR)

FTIR analysis was also done to check the functional groups of the HDS (Figure 4.41). It was observed that the sludge contains an OH^- group possibly from ferrihydrite ($Fe(OH)_3$), which is attributed to the broad peak at around 3349.2 cm^{-1} (Yan *et al.,* 2010). The medium broad stretch at around 1458.1 cm^{-1} corresponds to the carbonyl functional group. The weakness of this stretch is because the carbonyl functional group is not well defined (i.e. distorted bond order) from the resonance nature of the ester group in polyacrylate polymer that is used to densify the sludge or possibly from free carbonate ions precipitated on HDS. The weak bend at around 1083.9 cm^{-1} can be attributed to Me-O-M^{2+} in the metal complex (Parikh *et al.,* 2014).

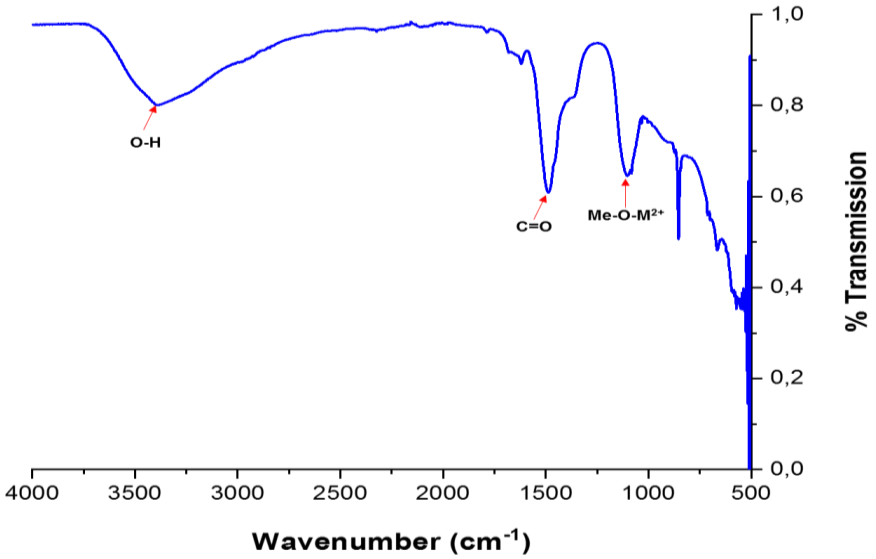

Figure 4.41. FTIR analysis to determine the functional groups of HDS

4.3.5 Brunauer-Emmett-Teller (BET) surface area analysis

The volume of HDS and its matrix (structure of pore spaces) may change with moisture (water) content and this may be through shrinking and swelling processes. At a point of shrinkage, when mine water enters the macropores between the HDS matrix, mostly the part of macropores may be filled and the shrinkage volume will be nonlinear. When mine water enters the HDS macropores in all dimensions in its matrix (saturation point), the shrinkage volume forms linear functional of water content. The surface area of HDS has sufficient space for interaction of the analyte with the adsorbent on its active sites (improves the adsorption capacity). The adsorption capacity of the HDS is based on its specific surface area and the pore volume. The textural parameters in BET surface analysis show that the HDS surface area and total pore volume were higher (Table 4.13). The results pointed out that the contribution of mesopores in HDS was dominant and the porous structure was well developed. Based on the BET surface analysis, HDS has adequate active sites for adsorption and has surface functional groups for electrostatic attraction and strong surface complexation with trace metals.

Table 4.13. Textural properties of HDS before adsorption

Sample	Surface area (m^2 g^{-1})	Pore size (nm)	Pore volume (cm^3 g^{-1})
HDS	80.98	13.24	0.272

4.3.6 Conclusion

The physical and chemical properties of HDS sampled showed some differences between fresh and aged sludge. Aged sludge showed an increase in stability compared to fresh sludge. Low concentrations of metals and high alkalinity in fresh sludge may reduce metals leachability. Aged HDS properties may transform based on its mineral composition into carbonate rock enriched with iron oxide and toxic metals may be accumulated in the matrix of solid sludge and be a secondary source of pollution. Further characterisation of both the fresh and aged sludge would shed some light as to the possibility of further adsorption that can occur on their surfaces. This will make it possible to deduce if use in conditioning AMD or adsorption of phosphate is feasible.

4.4 BATCH SIMULATION STUDIES FOR HFO INTERACTION WITH MINE WATER

4.4.1 Effect of pH

The pH of the AMD solution is a very important parameter in the sorption process. Its effect on the adsorption of trace metals into Hfo was studied at pH ranging from 2.5-10.5. The maximum adsorption capacity of Hfo was found to occur at pH 5.5. It should be noted here that the example presented in Figure 3.7 only shows the simulation at pH 5.02. When pH increased and adsorption capacity reached, a decrease in the recovery efficiency percentage was observed. A decrease in the surface area implied a few adsorption sites and a general decrease in adsorption capacity (Figure 4.42). The percentage efficiency has to be read in the context of the two active sites, namely the weak and strong sites that have a higher and lower concentration per mole of Hfo, respectively.

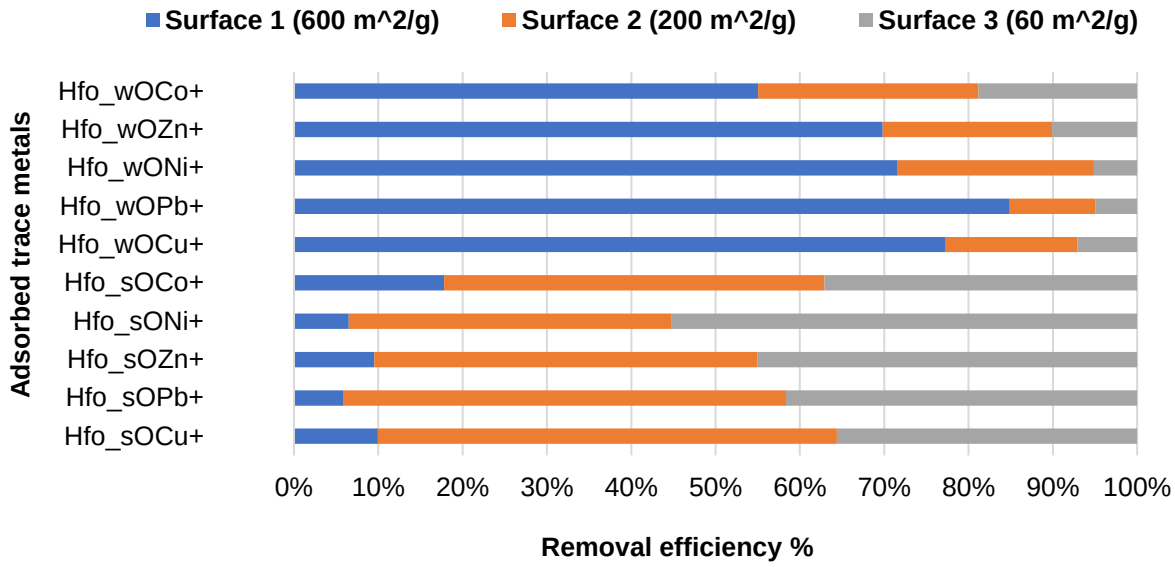

Figure 4.42. Effect of pH on removal efficiency

4.4.2 Effect of Hfo dosage

The effect of adsorbent dosage on the adsorption of the trace metals onto Hfo was studied. The concentration of trace metals in AMD solution was reduced by 78% (Pb), 73% (Cu), 66% (Zn), 58% (Ni) and 54% (Co) after adsorption following an increase in dosage. This could be attributed to an increase in active sites (Figure 4.43). The surface chemistry of Hfo on the adsorption of trace metals is through surface complexation and the reactions below indicate how surface complexation occurs on the Hfo surface:

$$SOH + Pb^{2+} \leftrightarrow SOHPb^{+} \quad (4.4)$$

$SOH + Cu^{2+} \leftrightarrow SOHCu^{+}$ (4.5)

$SOH + Zn^{2+} \leftrightarrow SOHZn^{+}$ (4.6)

$SOH + Ni^{2+} \leftrightarrow SOHNi^{+}$ (4.7)

$SOH + Co^{2+} \leftrightarrow SOHCo^{+}$ (4.8)

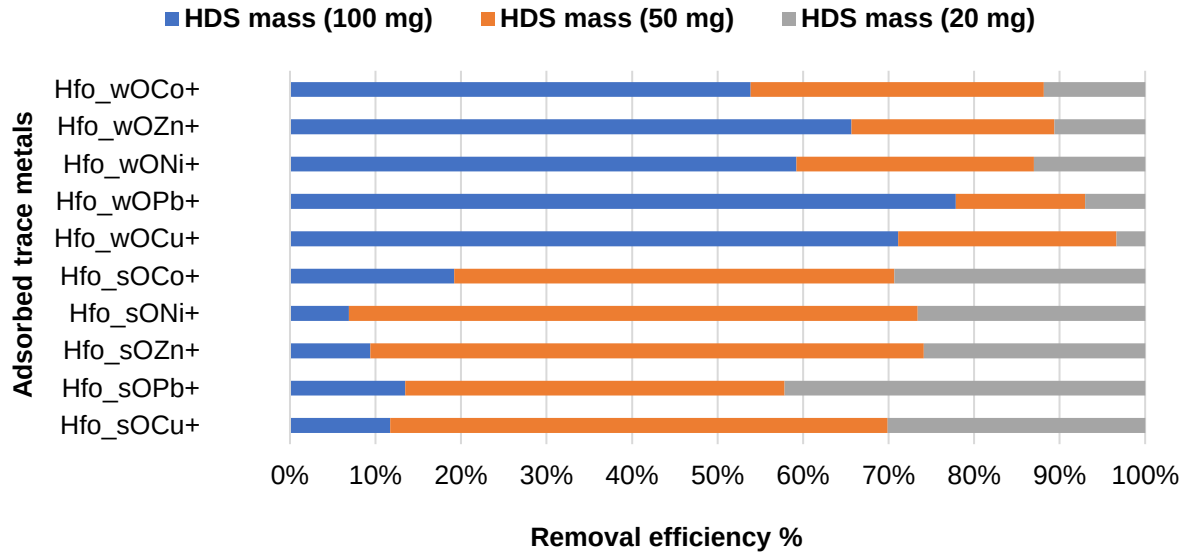

Figure 4.43. Effect of HDS mass on removal efficiency

4.4.3 Effect of concentration

The effect of concentration of the metals on their adsorption onto Hfo was investigated. Varying concentrations of trace metals (1, 2, 3, 4 and 5 mg ℓ^{-1}) were contacted with Hfo surfaces (both strong and weak sites). The results showed an increase in uptake of metals with concentration. Only 1, 3 and 5 mg ℓ^{-1} were chosen and shown in the figure. The metal ions (Pb, Cu, Zn, Ni and Co) concentration were reduced by 55-85% (in 5 mg ℓ^{-1}), 15-25% (3 mg ℓ^{-1}), and 5-19% (1 mg ℓ^{-1}) after adsorption (Figure 4.44).

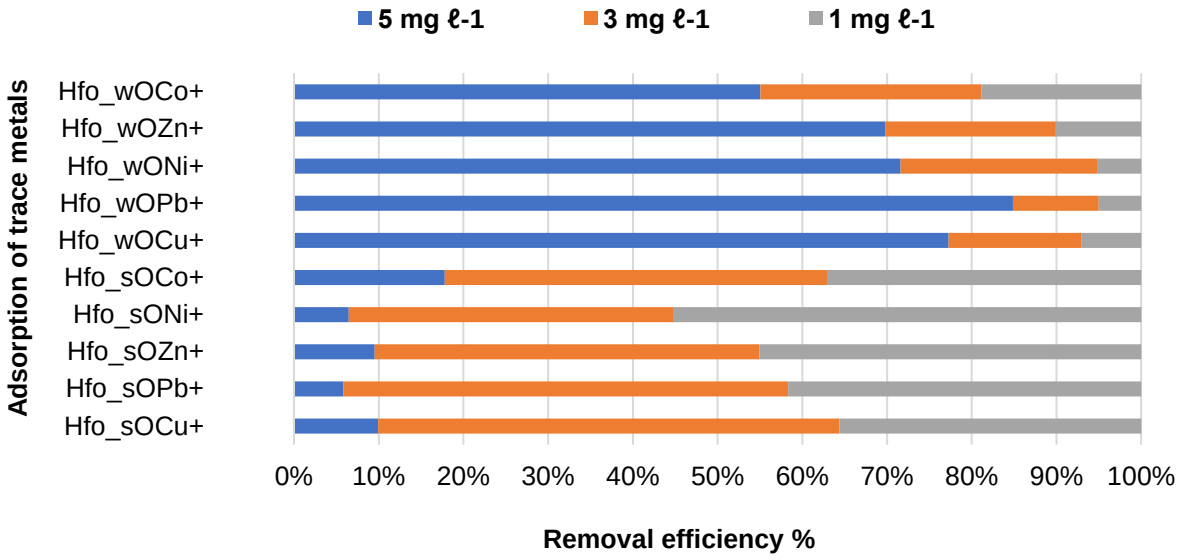

Figure 4.44. Effect of concentration on removal efficiency

4.4.4 Conclusion

Simulations of the adsorption of trace metals (Pb, Cu, Zn, Ni and Co) in mine water onto Hfo showed the potential of HDS for removal of these elements. Varying of different factors showed the dependence of adsorption capacity on them. As expected, a high surface area and dosage of Hfo resulted in increased adsorption. A pH of 5.5 was found to give optimum adsorption for the metals. The adsorption capacities followed the order: Pb>Cu>Zn>Ni>Co for both strong sites (Hfo_sOH) and weak sites (Hfo_wOH). Owing to the complexity of HDS, it cannot be concluded at this stage how accurate it is to use Hfo as a surrogate adsorption surface. Further studies involving actual adsorption of HDS to that lead to the determine the parameters used in a generalised surface complexation model were done below. This way, it was possible to conduct different simulations of adsorption onto HDS. PHREEQC coupled with Parameter Estimation (PEST) were used to estimate generalised surface complexation (adsorption constants) and the site density parameters in HDS from the experimental data.

4.5 BATCH STUDIES FOR HDS INTERACTION WITH MINE WATER

The findings of this study were presented and discussed following adsorption experiments (isotherms and kinetics), and the desorption study.

4.5.1 Effects of pH on adsorption

The results for the effect of pH on adsorption are presented in Figure 4.45-5.11. To optimise the pH for maximum removal efficiency and to avoid the precipitation of divalent cations (trace metals), the adsorption experiment was conducted from pH 2.5 to pH 5.5. When H_+ ions dominate in the solution (low pH), the surface of HDS was surrounded by hydronium ions that compete with trace metal ions for binding sites on the HDS. The effect of pH on the removal of metals onto HDS was studied from pH 2.5-10.5, and the maximum removal efficiency of HDS was found to be 5.5. The adsorption percentage increased rapidly as hydrogen ions (H^+) were replaced by hydroxide ions (OH^-) in the solution, reaching an optimal pH of 5.5.

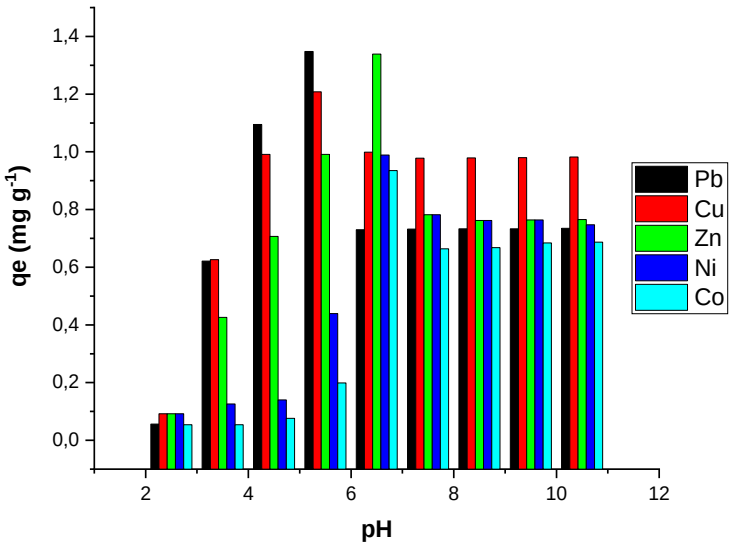

Figure 4.45. Effect of pH on the adsorption of trace metals onto HDS for a metal concentration of 5 mg ℓ^{-1} (solid;liquid ratio of 1 g:10 mℓ) (n = 3; RSD <10%).

PHREEQC coupled with Parameter Estimation (PEST) was be used to estimate generalised surface complexation (adsorption constants) and site density parameters in HDS from experimental data (Figure 4.46).

Further studies involving actual adsorption of HDS were done and that led to the determination of parameters that were used in a generalised surface complexation model.

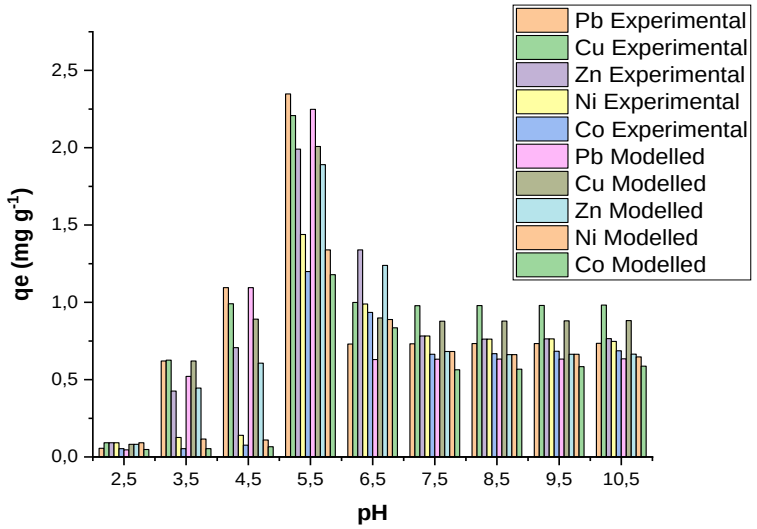

Figure 4.46. Generalised surface complexation for metals sorption with PHREEQC coupled with PEST

4.5.2 Effect of adsorbent mass on adsorption

Results for the effect of adsorbent mass on adsorption are presented in Figure 4.47. The effect of adsorbent dosage (10, 20, 50, 100 and 500 mg) on the adsorption of the trace metals onto HDS was investigated. The metal concentrations were reduced by 92.20% (Pb), 87.45% (Cu), 80.98% (Zn), 78.32% (Ni) and 73.34% (Co). The removal efficiency increased with an increase in adsorbent dose. This pointed to the increase of active adsorption sites. The surface complexation reactions were envisaged to proceed as follows:

$FeOH + Pb^{2+} \leftrightarrow FeOHPb^{+}$ (4.9)

$FeOH + Cu^{2+} \leftrightarrow FeOHCu^{+}$ (4.10)

$FeOH + Zn^{2+} \leftrightarrow FeOHZn^{+}$ (4.11)

$FeOH + Ni^{2+} \leftrightarrow FeOHNi^{+}$ (4.12)

$FeOH + Co^{2+} \leftrightarrow FeOHCo^{+}$ (4.13)

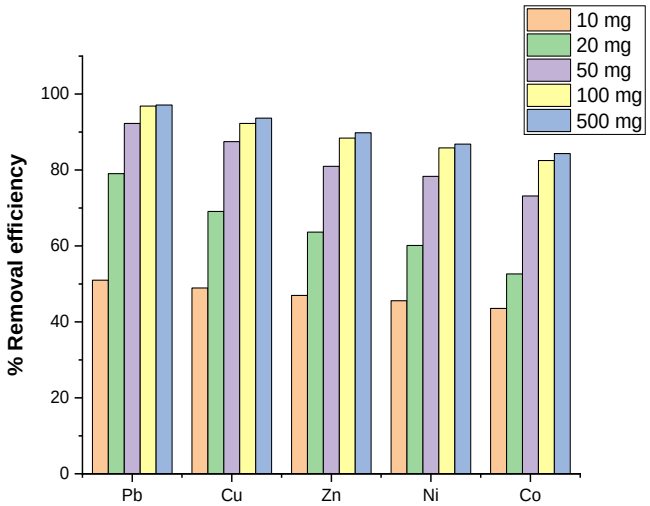

Figure 4.47. Effect of mass on the adsorption of trace metals onto HDS for a pH = 5.5; metal concentration of 5 mg ℓ^{-1} (constant liquid volume of 10 mℓ) (n = 3; RSD <10%).

4.5.3 Effect of contact time on adsorption

The effect of contact time on the adsorption of trace metals was studied and the results are presented in Figure 4.48. The rate of adsorption initially increased rapidly, and the optimal adsorption efficiency was achieved after 1 h. Further increase in contact time did not result in any improvement in adsorption as equilibrium had been reached.

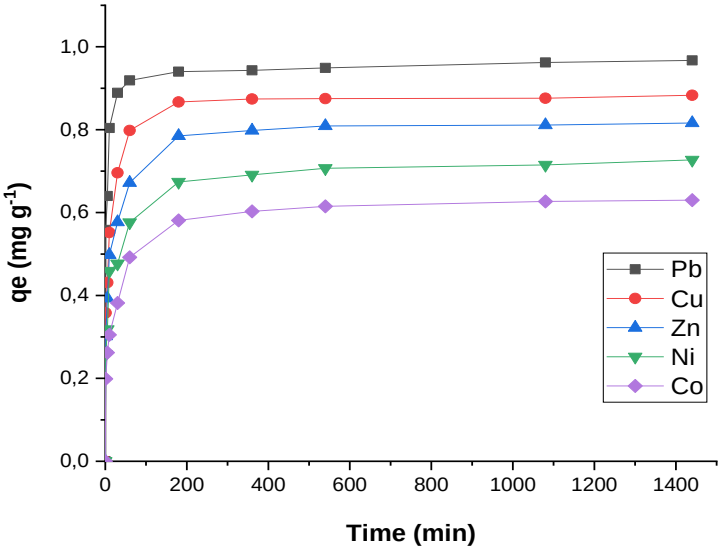

Figure 4.48. Effect of contact time on the adsorption of trace metals onto HDS for a pH = 5.5; metal concentration of 5 mg ℓ^{-1} (solid:liquid ratio of 1 g:10 mℓ) (n = 3; RSD <10%).

4.5.4 Effect of concentration on adsorption

The effect of concentration on adsorption was studied and the results are presented in Figure 4.49. The results point to an increase in adsorption with an increase in concentration. This implies that there is likely to be more uptake of the metals before saturation is reached.

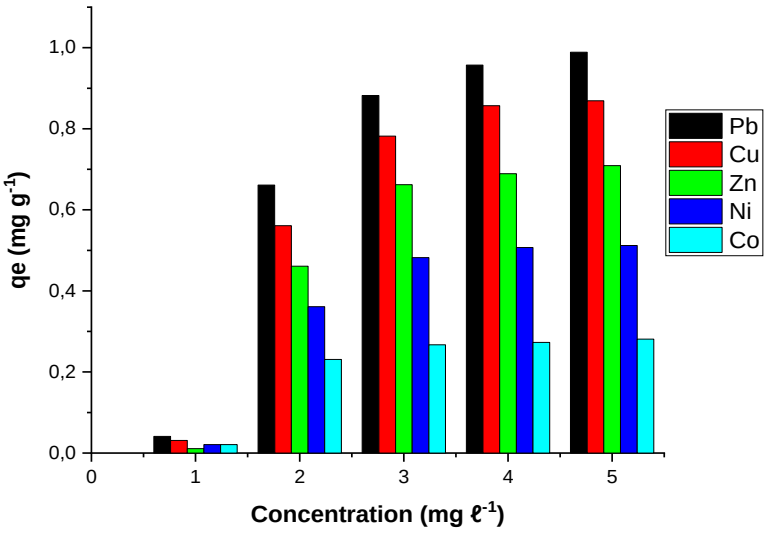

Figure 4.49. Effect of concentration on adsorption of trace metals onto HDS for a pH = 5.5; (solid:liquid ratio of 1 g:10 mℓ); for 24 h (n = 3; RSD <10%).

4.5.5 Adsorption isotherm models

The Langmuir, Freundlich, Dubinin-Radushkevich and Temkin isotherms were applied for data fitting on the models (this has included the initial concentration and results from data). The results for these are presented in Table 4.14. The Langmuir isotherm best fitted the adsorption data for Pb, Cu, Zn, Ni, and Co. The maximum monolayer adsorption capacity (q_{max}) value that was calculated from the Langmuir isotherm model ranged from 0.144 to 0.555 mg g^{-1} and these values were similar to those found in the experimental data. The adsorption mechanism may be proceeding through physical adsorption and the monolayer coverage chemical complexation in the inner sphere and outer sphere (this may be due to the heterogeneous surface of the HDS). The surface energy on the HDS was determined in the D-R isotherm model. The adsorption energy was between 8 and 16 kJ mol^{-1} for most metals and this may be due to strong chemical ion-exchange on the HDS. The adsorption intensity onto HDS was greater than 1 and this confirms the chemical adsorption. The R_L values of HDS ranged from 0-1 for all trace metals, implying favourable adsorption.

Table 4.14. Isotherms parameters of adsorption of trace metals onto HDS (pH = 5.5; solid:liquid ratio of 1 g:10 mℓ; shaking for 24 h; temp = 25 ^{o}C) (n = 3; RSD <10%)

Isotherms	Metal ion	Estimated isotherms parameters		
		q_{max} (mg g^{-1})	K_L (ℓ mg^{-1})	R^2
	Pb	0.555	0.0624	0.997
	Cu	0.347	0.0613	0.998
Langmuir	Zn	0.278	0.0312	0.996
	Ni	0.205	0.0210	0.999
	Co	0.144	0.0123	0.997
	Metal ion	n	K_f (mg g^{-1})/ (mol $ℓ^{-1}$)$^{1/n}$	R^2
	Pb	2.340	3.457	0.991
	Cu	2.234	1.016	0.995
Freundlich	Zn	1.931	2.706	0.995
	Ni	1.750	1.231	0.997
	Co	1.567	0.838	0.953
	Metal ion	X_m (mol g^{-1})	E_s (kJ.mol^{-1})	R^2
	Pb	4.89	22.36	0.988
	Cu	3.92	11.18	0.993
Dubinin-	Zn	3.64	10.00	0.994
Radushkevich	Ni	3.45	7.905	0.996
	Co	3.36	6.742	0.934
	Metal ion	a_T (L kg^{-1})	b_T (kJ mol^{-1})	R^2
	Pb	4.39	21.36	0.968
	Cu	3.52	12.13	0.943
Temkin	Zn	3.25	11.55	0.894
	Ni	3.35	8.815	0.796
	Co	3.41	7.344	0.934

4.5.6 Kinetic models

The results for kinetic models are presented in Table 4.15. The maximum adsorption of Pb, Cu, Zn, Ni, and Co was reached after 60 min of contact with HDS. The adsorption rate was observed to be much faster within 5 min and after 1 h the adsorption capacity remains constant throughout. The results have pointed out that the sorption of metals onto HDS followed this order: Pb>Cu>Zn>Ni>Co. The pseudo first-order and pseudo second-order kinetic models were utilised to find out the mechanism that influences the attraction of trace metals onto the HDS surface (Table 4.15). The pseudo second-order model better fitted the kinetic data compared to the pseudo first-order (this was based on the R_2 values that were greater than 0.999 for all trace

metals). The experimental adsorption capacity was compared with the calculated adsorption capacity and for the pseudo second-order, the values were very close.

Table 4.15. Kinetic parameters of trace metals removal onto HDS (pH = 5.5; concentration = 5 mg ℓ^{-1}; solid:liquid ratio of 1 g:10 mℓ; temp = 25 ^{o}C) (n = 3; RSD <10%)

Kinetics	Metal ion	Estimated kinetic parameters			
		$q_{e(exp)}$ (mg g^{-1})	K_1 (min^{-1})	q_{cal} (mg g^{-1})	R^2
Pseudo first-order	Pb	0.919	0.003	0.802	0.951
	Cu	0.798	0.004	0.695	0.923
	Zn	0.672	0.004	0.564	0.972
	Ni	0.576	0.003	0.373	0.958
	Co	0.492	0.005	0.387	0.973
	Metal ion	q_{cal} (mg g^{-1})	K_2 (mg g^{-1} min)		R^2
Pseudo second-order	Pb	0.902	0.102		0.999
	Cu	0.795	0.302		0.999
	Zn	0.667	0.345		0.999
	Ni	0.573	0.321		0.999
	Co	0.487	0.301		0.999
	Metal ion	*a*/(kg.mol^{-1}.min^{-1})	*b*/(kg.mol^{-1}.min^{-1})		R^2
Elovich	Pb	0.003	0.802		0.851
	Cu	0.004	0.695		0.823
	Zn	0.004	0.564		0.872
	Ni	0.003	0.373		0.858
	Co	0.005	0.387		0.873
	Metal ion	Ip	Kp		R^2
Intraparticle Diffusion model	Pb	0.003	0.802		0.951
	Cu	0.004	0.695		0.723
	Zn	0.004	0.564		0.872
	Ni	0.003	0.373		0.658
	Co	0.005	0.387		0.873
	Metal ion	I_f	K_f		R^2
Film diffusion model	Pb	0.003	0.802		0.751
	Cu	0.004	0.695		0.823
	Zn	0.004	0.564		0.972
	Ni	0.003	0.373		0.858
	Co	0.005	0.387		0.873

4.5.7 Thermodynamic studies

Due to electrostatic attraction, the removal of cations (positively charged metals) could be possible when the surface is negatively charged (FeO^{-} is the predominant on the HDS surface). The PXRD results also showed that the HDS mainly consisted of goethite (69.87%) and 30.13% of calcite (calcite in HDS may be from lime and limestone used in AMD treatment). Therefore, due to relatively complexed composition of HDS, it was very important to explain the removal mechanism of potentially toxic trace metals by HDS in sorption studies. Batch sorption studies was conducted to assess the potential of HDS in the removal of potentially toxic trace metals in AMD. The adsorption capacity decreases with an increase in temperature. Physical adsorption seems to be the dominant adsorption mechanism as E_a of metals ranged from 1.73-3.79 kJ mol^{-1}. Change in ΔH^o, ΔS^o and ΔG^o in the adsorption Pb, Cu, Zn, Ni and Co onto HDS can be related to K_d of the analyte between the HDS and AMD interactions (Equation 3.19-3.23). The adsorption of Pb (34.12 mg ℓ^{-1}), Cu (29.45

mg ℓ^{-1}), Zn (38.78 mg ℓ^{-1}), Ni (19.33 mg ℓ^{-1}), Co (14.67 mg ℓ^{-1}) onto HDS decreased slightly with an increase in temperature from 288-333 K (Figure 4.50). The negative charge in ΔH^o of -3.14, -4.47, -5.89, -7.15 and -7.88 kJ mol^{-1} for Pb, Cu, Zn, Ni and Co respectively, shows that the adsorption of potential toxic trace metals by HDS is exothermic, in which the adsorption of potential toxic metals decreases with an increase in temperature. The negative charge in adsorption Gibbs free energy show that the adsorption mechanism is through spontaneous reaction process. The positive charge in ΔS^o confirms that the decreased randomness between the HDS and AMD interface during adsorption (Table 4.16).

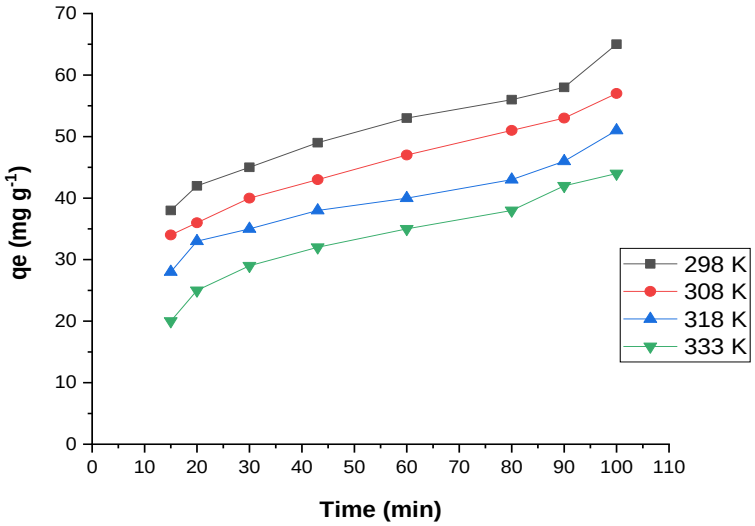

Figure 4.50. Effect of temperature on the adsorption of trace metals onto HDS

Table 4.16. Thermodynamic parameters of potentially toxic trace metals

Metal ion	Temperature (K)	ΔG^o (kJ mol^{-1})	ΔH^o (kJ mol^{-1})	ΔS^o (J mol^{-1} K^{-1})	K (L g^{-1})
Pb	298	-3.89	3.14	11.38	4.21
	308	-4.59		11.42	4.53
	318	-5.62		16.13	6.95
	333	-6.34		17.25	7.63
Cu	298	-2.79	4.47	10.38	3.51
	308	-3.13		10.50	3.48
	318	-4.65		14.98	6.67
	333	-5.33		16.32	6.88
Zn	298	-2.72	5.89	9.22	3.12
	308	-3.04		10.14	3.28
	318	-4.43		11.78	4.41
	333	-5.11		12.46	5.14
Ni	298	-1.65	7.15	8.23	2.74
	308	-2.98		9.33	2.55
	318	-3.77		10.34	3.43
	333	-4.09		11.02	4.67
Co	298	-1.25	7.88	7.15	2.48
	308	-2.45		8.44	2.51
	318	-4.31		9.01	3.01
	333	-4.69		10.34	3.57

4.5.8 Desorption of trace metals

The desorption study was done to assess the likelihood of release of metals already contained in the HDS. These are the metals that would have been precipitated out from the AMD treatment plant and disposed with the HDS. The results are presented in Figures 4.51 and 4.52.

The results indicate that desorption capacity of the HDS increased in some trace metals (e.g. Pb, Cu, and Zn) with an increase in H^+ in the solution and for Ni it was opposite (desorption decreased with HCl concentration). Deionised water leached out more Ni. It is not clear at this stage why this trend was observed and as such further studies have to be conducted to confirm this.

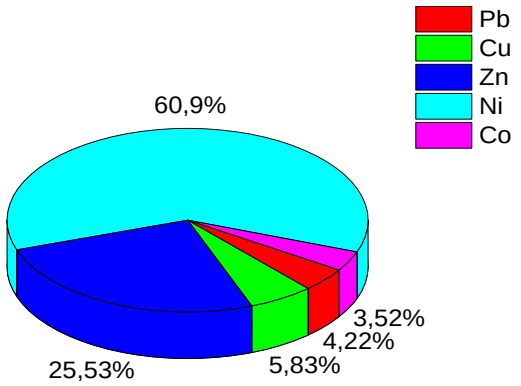

Figure 4.51. Desorption percentage of metals using deionised water as a desorbing agent.

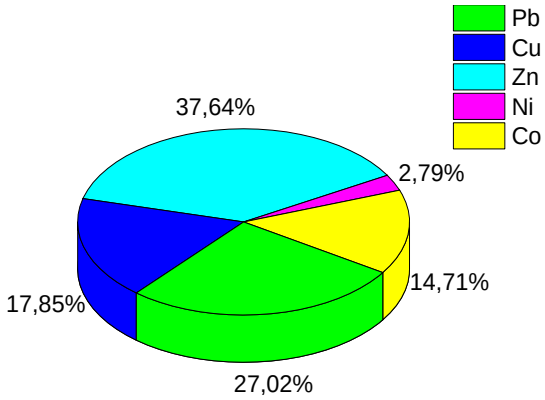

Figure 4.52. Desorption percentage of metals using HCl as a desorbing agent.

4.5.9 Conclusion

The adsorption and desorption of Pb, Cu, Zn, Ni, and Co ions onto HDS were investigated. The selectivity sequence for adsorption followed the order: Pb>Cu>Zn>Ni>Co. The adsorption capacity of Pb and Cu were observed to be higher. An increase in adsorbent amount and concentration of metals resulted in increased adsorption. pH was found to result in the peaking of adsorption at 5.5. The Langmuir isotherm best fitted the adsorption data while the pseudo second-order model, implying that the mechanism was chemisorptive, best described the kinetics of adsorption. While desorption showed that it was possible to dislodge metals from HDS, this did not seem to affect metal adsorption. Thus, it would be expected that on contact with AMD, the net migration of metals will be to the HDS than from it *via* dislodging from its surface. Overall, the trend in adsorption onto HDS resembles that observed for Hfo. However, the effect of components such as the polyacrylate polymer within the HDS structure was studied. To achieve this, generalised surface complexation

model was useful in achieving this based on the results obtained. The findings showed that simulations could be successfully used where limited experimental data was available.

4.6 COLUMN STUDIES OF HFO FOR MINE WATER TREATMENT

The reactive transport models for continuous adsorption of Pb, Cu, Zn, Ni, and Co in the fixed-bed column were established using the Hfo surface (e.g. FeOOH) and only selected results are presented in this study. The breakthrough curves were predicted for the design of fixed-bed adsorption experimental studies. A breakthrough curve is influenced by the transport of analytes in the column, as well as the adsorbent, reflecting the uptake behaviour of elements being recovered. To examine the fixed-bed column parameters (initial element concentration, bed height, pH of adsorbate, flow rate, and particle size) and its interdependence on the column performance, adsorption transport simulations (for column studies) was applied for the experimental setup. Transport models were developed to evaluate the effect of process variables on the efficiency of the adsorption process in the fixed-bed column and the flow rate (in actual experimental work) was evaluated by keeping relevant parameters constant throughout.

4.6.1 Effects of initial concentration of elements

The results presented were only for the 1 mg ℓ^{-1} (Figure 4.53). Breakthrough curves for different initial concentrations of elements (1, 3, and 5 mg ℓ^{-1}) at a constant flow rate (3 mℓ min^{-1}) and a bed height of 8 cm (10 g of Hfo) were predicted in these simulation studies. Adsorption of divalent ions (Pb, Cu, Zn, Ni, and Co) onto Hfo was performed at a similar pH of 5.02 in the column simulation studies, and this includes other optimised parameters. For the adsorption of divalent ions onto Hfo, increasing initial concentration from 1 to 5 mg ℓ^{-1} has gave less removal efficiency of analytes from the initial solution and at lower concentrations removal efficiency was much better (as observed in the improvement of water quality).

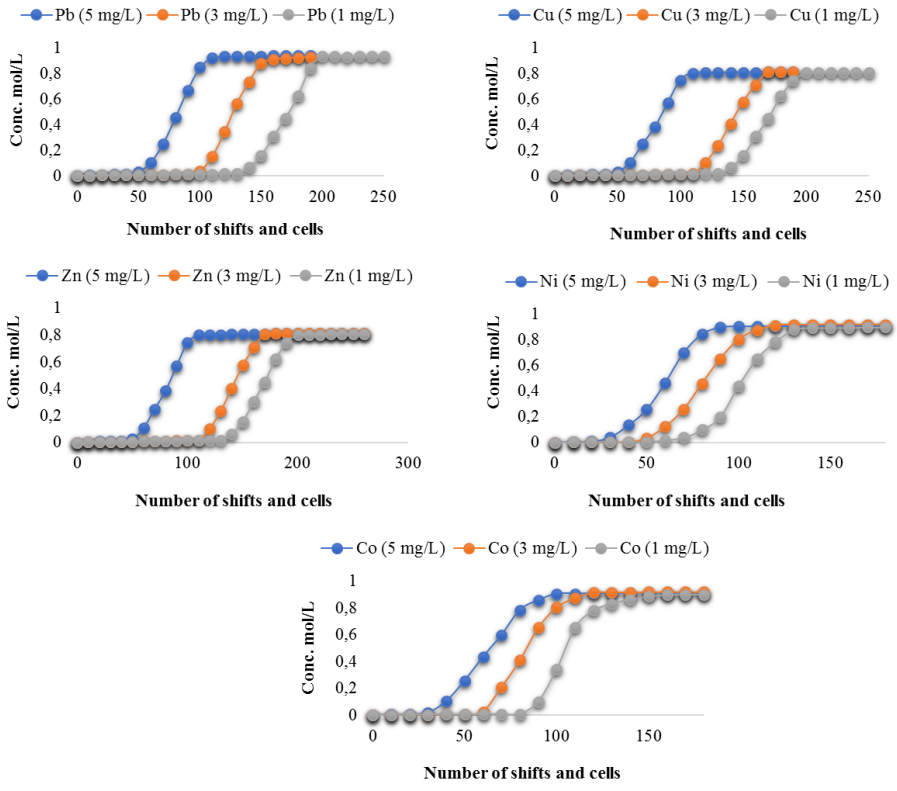

Figure 4.53. Effects of initial concentration of elements (pH = 5.02, bed height = 8 cm (10 g of Hfo), concentration = 1 mg ℓ^{-1}, flow rate = 3 mℓ min^{-1})

4.6.2 Effect of bed height

The effect of bed height (3, 6 and 8 cm) was studied (Figure 4.54). Only the 8cm bed height (i.e. 10 g of Hfo) results are presented. The initial solution pH of 5 and elemental concentrations of 1, 3, and 5 mg ℓ^{-1} were used (flow rate was assumed to be 3 mℓ min^{-1}) with the 1 mg ℓ^{-1} presented. An increase in the bed height from 5 to 8 cm resulted in a slight increase in breakthrough values (presented by the number of shifts and cells), increase for divalent ions adsorption by Hfo, whereas the exhaust point (time to reach this point) was increased when analytes contacted with Hfo surface area. Breakthrough time increased while the exhaust point was nearly unchanged for the adsorption of Pb, Cu, and Zn by Hfo when the bed height was changed from 5 to 8 cm.

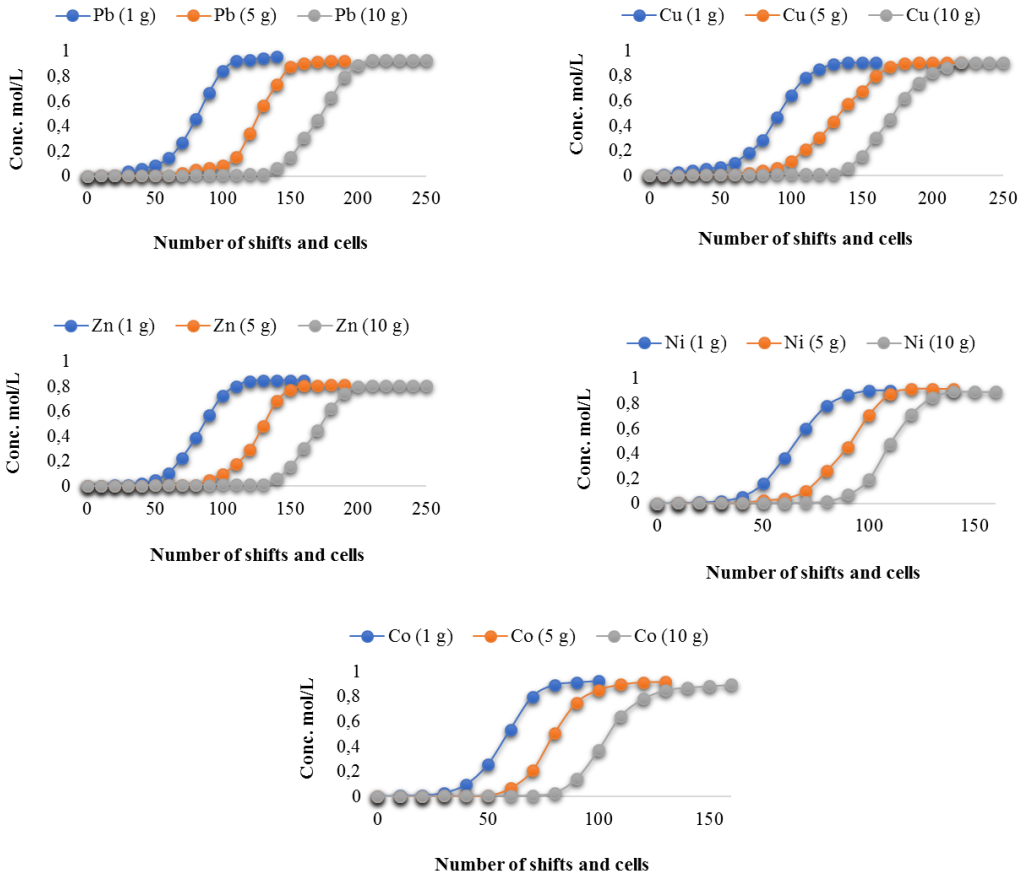

Figure 4. 54. Effect of bed height (bed height = 8 cm, pH = 5.02, concentration = 1 mg ℓ^{-1}, flow rate = 3 mℓ min^{-1}).

4.6.3 Effects of flow rate

The adsorption of Pb, Cu, Zn, Ni, and Co at flow rates (3, 5, and 7 mℓ min^{-1}) was investigated and the results at a lower flow rate (3 mℓ min^{-1}) were only presented (Figure 4.55). The simulations for flow rate estimation were interpreted by looking at breakthrough curves. The initial solution pH of 5.02 with a bed height of 8 cm and an average particle size of 10 µm was used, whereas initial elemental concentrations (1, 3, and 5 mg ℓ^{-1}) were used for Pb, Cu, Zn, Ni, and Co. The breakthrough curve and exhaust point for these divalent ions adsorption onto Hfo were decreased slightly by increasing the flow rate from 5 to 8 mℓ min^{-1}. This result has pointed out that in the column (transport model cells), it is more difficult to exhaust at low flow rates (e.g. 1 mg ℓ^{-1}) due to the higher removal efficiency of elements in the fixed-bed column. The lower removal efficiency at high flow rates may be due to low contact time between Hfo and elements. At higher flow rates, adsorption efficiency in the fixed-bed column was reduced.

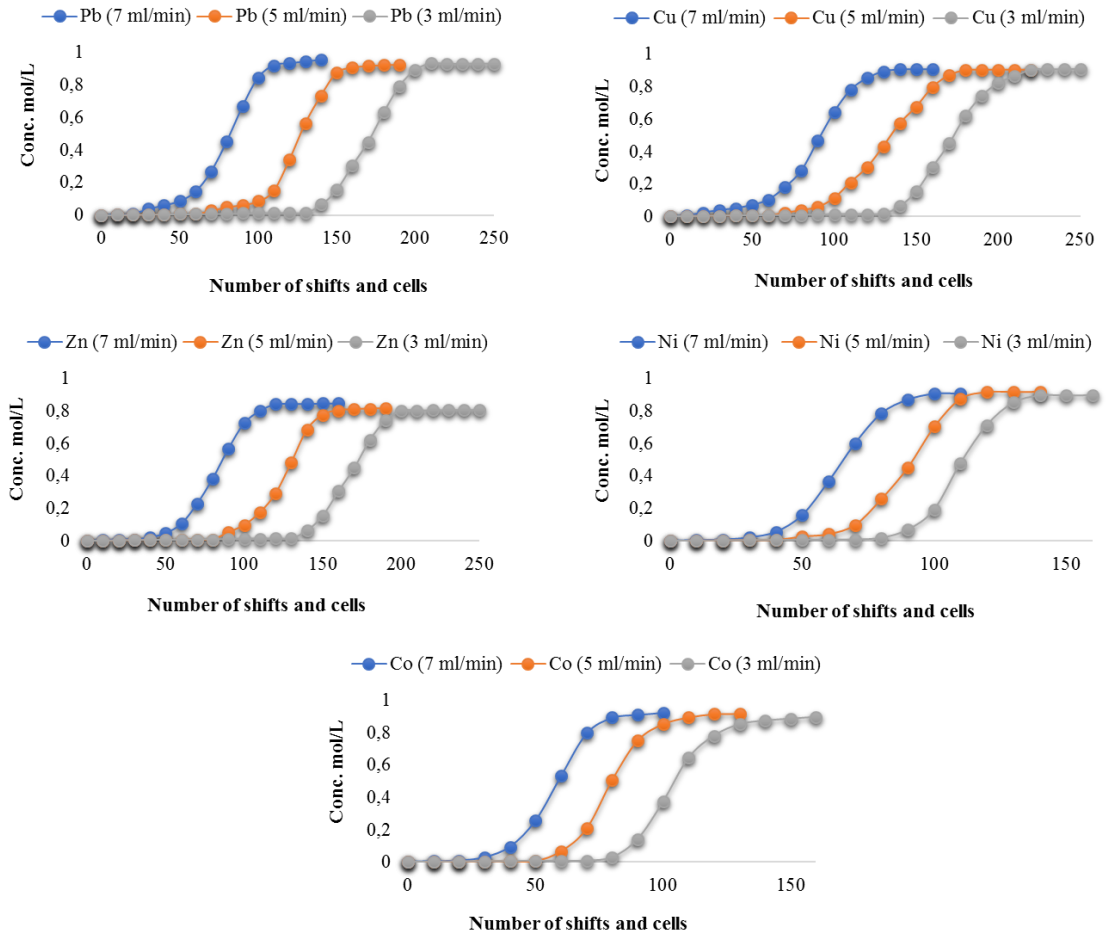

Figure 4.55. Effects of flow rate (flow rate = 3 mℓ min^{-1}, concentration = 1 mg $ℓ^{-1}$, pH = 5.02, bed height = 8 cm)

4.6.4 Conclusion

Fixed-bed column adsorption studies to remove Pb, Cu, Zn, Ni, and Co from contaminated mine water onto the Hfo surface (e.g. FeOOH) were conducted using computational simulations. The findings have shown the importance of simulations for situations in which experimental studies may be difficult to conduct. Several possible scenarios assessing the effects of elemental concentrations, flow rates and bed heights were studied. The well-known effect of increased adsorption with longer residence times (or bed heights) and lower flow rates and concentration was observed. This yielded delayed breakthroughs, giving valuable insight into how columns can be designed within this context. However, it should be noted here that the success of reactive transport modelling for Hfo does not necessarily that this can be substituted for any iron oxyhydroxide surfaces. Further studies will be necessary to determine the amount of Hfo and the existence of other unknown surfaces on which adsorption could be more pronounced.

4.7 COLUMN SORPTION STUDIES OF SLUDGE FOR MINE WATER TREATMENT

Adsorption studies of elements in a fixed-bed column as a setup for large scale operation is applicable in real mine water treatment. In this second part of the study, the application potential of HDS for the adsorption of Pb, Cu, Zn, Ni, and Co from mine water in a fixed-bed adsorption column was investigated, deriving some parameters from the simulations conducted above. The effect of breakthrough parameters including initial elemental concentration, bed height and flow rate was investigated. The column adsorption experimental data were fitted to Thomas, Yoon-Nelson, Adam-Bohart and Bed Depth Service Time (BDST) models. The adsorption efficiency, breakthrough and exhaustion point in a fixed-bed column increased with an increase in

bed height, and a decrease in adsorption efficiency was observed with an increase in flow rate and initial elemental concentration.

4.7.1 Effect of inlet (trace metals) concentration

Breakthrough curves for Pb, Cu, Zn, Ni, and Co adsorption onto HDS at various inlet concentrations (1, 3 and 5 mg ℓ^{-1}) at a constant flow rate and a bed height of 3 mℓ min^{-1} and 8 cm, were determined (Figure 4.56). Adsorption efficiency, breakthrough, and exhaustion time decreased with increasing inlet elemental concentration as observed from the computational simulations. The adsorption parameters in a fixed-bed column at different concentrations are presented in Table 4.17. The t_{br} (min) at the inlet concentrations (1, 3, and 5 mg ℓ^{-1}) are from 160-60 min, 150-50 min, 150-55 min, 120-50 min, and 120-40 min for Pb, Cu, Zn, Ni, and Co, respectively. The exhaustion time followed the trend: Pb (250-100 min), Cu (250-100 min), Zn (280-90 min), Ni (190-80 min), and Co (200-90 min). When inlet trace metals concentration is very low, retention time becomes longer for the active site available for adsorption in the HDS to be exhausted due to the slow transport of trace metals. When inlet concentration increases, the slopes of the breakthrough curves become steeper and the breakthrough time becomes shorter as result of the HDS reaching saturation faster.

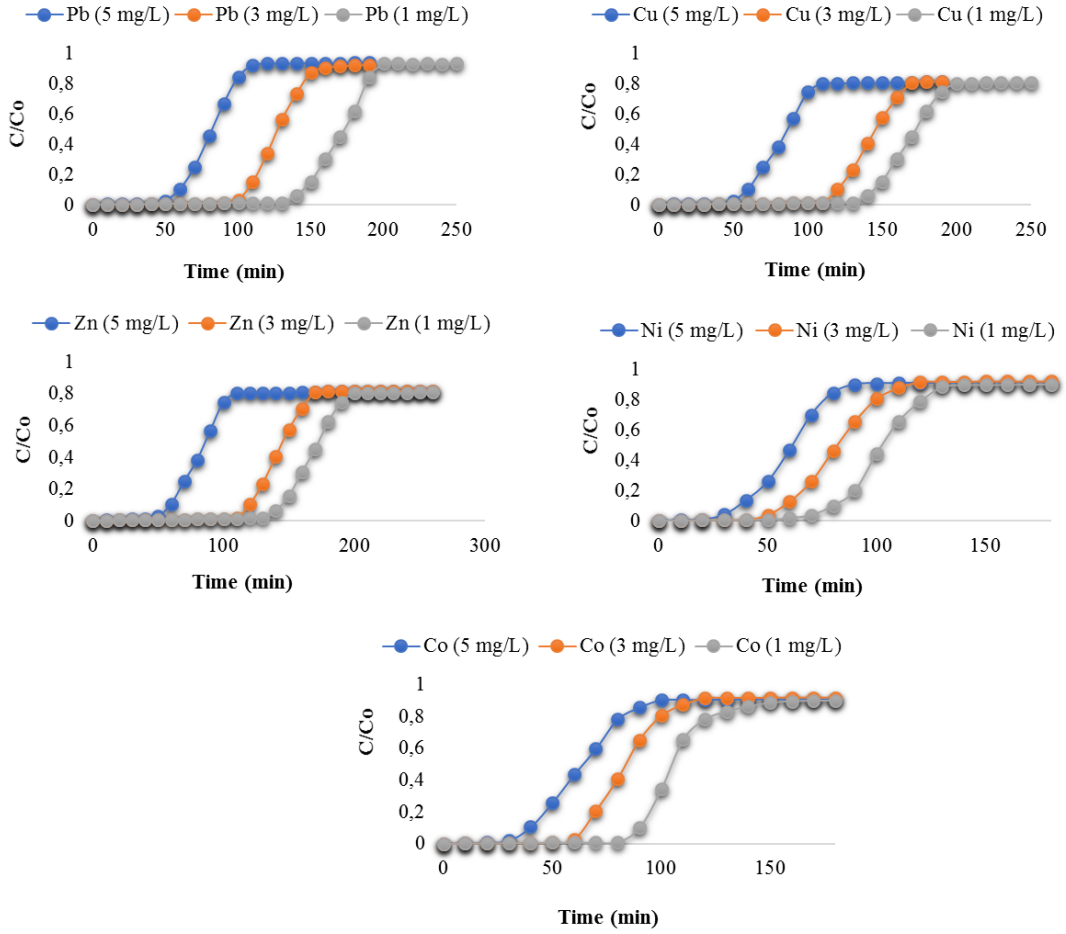

Figure 4.56. Effects of initial potentially toxic trace metal concentration (pH = 5.02, HDS particle size = 10 µm, bed height = 8 cm, concentration = 1 mg ℓ^{-1}, flow rate = 3 mℓ min^{-1})

Table 4.17. Fixed bed column parameters for adsorption of trace metals onto HDS at inlet concentrations of 1, 3 and 5 mg ℓ^{-1} (flow rate = 3 mℓ min^{-1}, bed height = 8 cm, temp = 25 ºC)

Inlet conc. (mg ℓ^{-1})	Metal ions	t_{br} (min)	t_{ex} (min)	V_{ef} (mℓ)	Z_m (cm)	Removal efficiency (%)
1	Pb	100	150	1500	4.56	99.52
	Cu	150	250	2500	2.03	99.03
	Zn	150	280	2800	8.03	97.87
	Ni	120	190	1900	3.50	95.12
	Co	120	200	2000	4.43	90.84
3	Pb	160	310	3100	2.29	97.78
	Cu	150	280	2800	4.14	96.35
	Zn	170	220	2200	2.52	95.67
	Ni	110	240	2400	2.54	94.03
	Co	140	200	2000	5.50	90.58
5	Pb	170	240	2400	3.04	96.14
	Cu	110	250	2500	4.58	94.44
	Zn	120	200	2000	2.75	94.10
	Ni	180	220	2200	4.02	93.86
	Co	120	240	2400	5.42	88.57

4.7.2 Effect of bed height

Adsorption in a fixed bed column is highly affected by the adsorbent dosage used (higher bed height may increase surface area or mass transfer zone). The breakthrough curves for trace metals (Pb, Cu, Zn, Ni, and Co) adsorbed at different bed heights (3, 6, 8 cm) corresponding to 1, 5, 10 g of HDS, respectively (3 mℓ min^{-1} constant flow rate and at an inlet concentration of 1 mg ℓ^{-1}) were determined (Figure 4.57). The breakthrough time, exhaustion time, and recovery efficiency depend on the bed height (an increase in adsorption capacity with an increase in bed height was observed). The column adsorption parameters on the effect of bed height (8 cm), an increase in breakthrough time from Pb (90-240 min), Cu (70-230 min), Zn (60-200 min), Ni (80-160 min) and Co (50-130 min) were observed (Table 4.18). An increase in bed height (increase in adsorbent dosage) has made an exhaustion time to be later from 100-210 min (Pb), 130-210 min (Cu), 110-200 min (Zn), 100-140 min (Ni) and 80-140 min (Co). When bed height is lower (axial dispersion predominated the mass transfer), this reduces the trace metal diffusion like insufficient time for diffusion of trace metals onto HDS. Therefore, an increase in bed height makes more intense adsorption efficiency, breakthrough, and exhaustion time (this is due to the availability of active sites on the HDS, as bed height increases with adsorbent dosage).

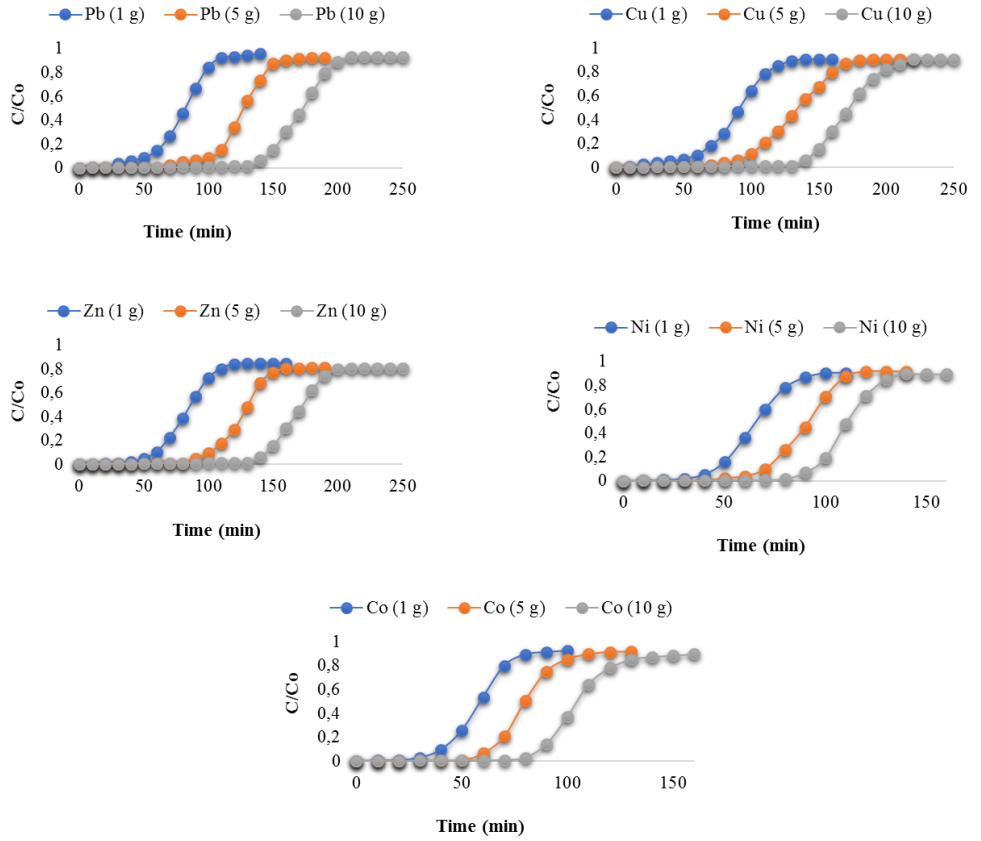

Figure 4.57. Effect of bed height (HDS particle size = 10 µm, bed height = 8 cm, pH = 5.02, concentration = 1 mg ℓ^{-1}, flow rate = 3 mℓ min^{-1}).

Table 4.18. Fixed bed column parameters for adsorption of trace metals onto HDS at varying bed height of 3, 6 and 8 cm (concentration = 1 mg ℓ^{-1}, flow rate = 3 mℓ min^{-1}, temp = 25 ºC)

Bed height (cm)	Metal ions	t_{br} (min)	t_{ex} (min)	V_{ef} (mℓ)	Z_m (cm)	Removal efficiency (%)
3	Pb	100	140	1400	5.46	93.73
	Cu	170	120	1200	4.50	91.69
	Zn	150	130	1300	3.55	90.08
	Ni	150	200	2000	2.50	85.05
	Co	90	220	2200	5.13	83.18
6	Pb	140	210	2100	5.22	97.44
	Cu	130	190	1900	4.24	95.85
	Zn	160	130	1300	4.75	93.87
	Ni	110	220	2200	5.86	91.56
	Co	110	200	2000	6.03	90.82
8	Pb	160	230	2300	4.66	99.43
	Cu	100	230	2300	2.67	99.33
	Zn	120	200	2000	5.21	99.28
	Ni	80	110	1100	3.29	98.85
	Co	110	240	2400	5.35	98.56

4.7.3 Effect of flow rate

The flow rate in a continuous fixed-bed column controls the retention time when trace metals contact the HDS surface. In wastewater treatment plants (large-scale application), the removal of trace metals from mine water was achieved in continuous fixed-bed columns. The breakthrough curves of trace metals (Pb, Cu, Zn, Ni, and Co) adsorbed onto HDS at various flow rates (3, 5, 7 mℓ min^{-1}) at constant inlet concentration (1 mg $ℓ^{-1}$) and a bed height of 8 cm were determined (Figure 4.58). The assessment of the effect of flow rate was conducted and the results indicated that breakthrough time, exhaustion time, and adsorption percentage decreased as the flow rate increased from 3 to 7 mℓ min^{-1} (Table 4.19). The breakthrough time of each trace metal was observed as follows: Pb (60-200 min), Cu (70-190 min), Zn (60-190 min), Ni (50-140 min), and Co (50-130 min). The exhaustion time also follows a similar selectivity sequence (this may be due to insufficient retention time of trace metals to interact with HDS) from 100-200 min, 100-220 min, 100-210 min, 90-140 min and 390-240 min for Pb, Cu, Zn, Ni, and Co, respectively. As expected, at low flow rates retention time increased leading to increased contact with HDS (due to accessibility of active sites). The best performance of bed column was observed at a flow rate of 3 mℓ min^{-1} and this means that when flow rate increases, the distribution of trace metals in the bed column becomes weaker (due to insufficient time of trace metals to diffuse into active sites in HDS responsible for adsorption).

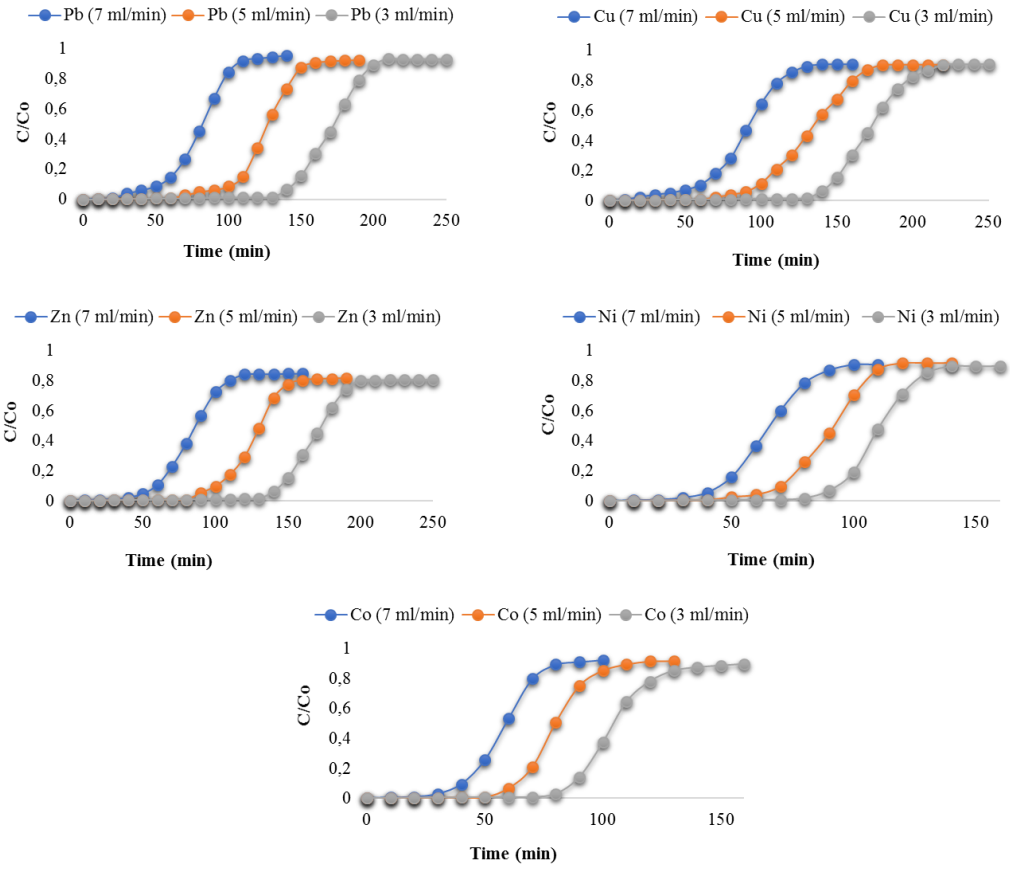

Figure 4.58. Effects of flow rate (HDS particle size = 10 µm, flow rate = 3 mℓ min^{-1}, concentration = 1 mg $ℓ^{-1}$, pH = 5.02, bed height = 8 cm)

Table 4.19. Fixed bed column parameters for adsorption of trace metals onto HDS at varying flow rate of 3, 5 and 7 mℓ min^{-1} (concentration = 1 mg $ℓ^{-1}$, bed height = 8 cm, temp = 25 ºC)

Flow rate (mℓ min^{-1})	Metal ions	t_{br} (min)	t_{ex} (min)	V_{ef} (mℓ)	Z_m (cm)	Removal efficiency (%)
3	Pb	90	170	1700	5.21	99.12
	Cu	80	150	1500	4.29	99.04

	Zn	100	200	4800	3.94	98.98
	Ni	100	180	4200	4.89	98.38
	Co	110	190	3600	5.05	97.41
5	Pb	60	110	1100	4.29	96.31
	Cu	70	180	1800	4.94	94.08
	Zn	90	220	2200	6.09	93.31
	Ni	90	180	1800	5.50	93.07
	Co	100	200	2000	5.50	91.25
7	Pb	350	440	4400	3.75	89.78
	Cu	180	360	3600	6.50	83.46
	Zn	330	300	3000	5.50	82.58
	Ni	120	270	2700	6.44	77.18
	Co	90	240	2400	5.88	75.39

4.7.4 Parameters of the sorption models

Thomas, Yoon–Nelson, Adams-Bohart, and bed depth service time (BDST) models were fitted with acquired column experimental data (inlet trace metal concentration, bed height, and flow rate). The best results for breakthrough and adsorption percentages were obtained at a bed height of 8 cm, the flow rate of 3 mℓ min^{-1}, and the inlet concentration of 1 mg $ℓ^{-1}$. The fitting of the best experimental data on the models was interpreted based on the correlation coefficient (R^2) value. The R^2 value (greater or equal to 0.998) was the best reference for assessing the best fit of column experimental data on the models applied in this study (Table 4.20).

Table 4.20. Thomas, Yoon–Nelson, Adams-Bohart models and Bed depth service time model parameters for the adsorption of Pb, Cu, Zn, Ni, and Co onto HDS at varying bed heights (3, 6 and 8 cm), flow rates (3, 5 and 7 mℓ min^{-1}) and inlet concentration (1, 3, 5 mg $ℓ^{-1}$).

		Thomas model		
Parameters	Metal ion	$k_{Th} * 10^{-5}$ (mℓ min^{-1} mg)	q_o (mg g^{-1})	R^2
Bed height (cm)				
3	Pb	0.0038	240	0.987
	Cu	0.0028	300	0.975
	Zn	0.0058	210	0.974
	Ni	0.0018	155	0.945
	Co	0.0078	100	0.929
6	Pb	0.0013	324	0.986
	Cu	0.0027	250	0.958
	Zn	0.0031	212	0.957
	Ni	0.0038	337	0.951
	Co	0.0045	125	0.943
8	Pb	0.0014	430	0.995
	Cu	0.0035	410	0.994
	Zn	0.0033	320	0.993
	Ni	0.0037	260	0.985
	Co	0.0046	170	0.981
Initial conc. (mg $ℓ^{-1}$)				
1	Pb	0.0096	120	0.998
	Cu	0.0094	260	0.995

	Zn	0.0086	230	0.975
	Ni	0.0085	170	0.964
	Co	0.0073	110	0.954
3	Pb	0.0096	320	0.989
	Cu	0.0089	200	0.987
	Zn	0.0086	140	0.967
	Ni	0.0082	220	0.965
	Co	0.0068	142	0.923
5	Pb	0.0089	510	0.997
	Cu	0.0078	330	0.965
	Zn	0.0071	240	0.964
	Ni	0.0039	137	0.943
	Co	0.0054	170	0.934
Flow rate (mℓ min^{-1})				
3	Pb	0.0013	420	0.998
	Cu	0.0022	360	0.997
	Zn	0.0029	330	0.985
	Ni	0.0040	270	0.976
	Co	0.0046	150	0.954
5	Pb	0.0044	540	0.989
	Cu	0.0024	495	0.987
	Zn	0.0075	360	0.956
	Ni	0.0098	225	0.945
	Co	0.0033	180	0.942
7	Pb	0.0047	660	0.988
	Cu	0.0021	360	0.963
	Zn	0.0078	300	0.945
	Ni	0.0012	240	0.944
	Co	0.0035	180	0.926

Adams-Bohart model

Parameters	Metal ion	k_{AB} (L/mg min)	N_o (mg ℓ^{-1})	R^2
Bed height (cm)				
3	Pb	0.0042	350	0.985
	Cu	0.0027	300	0.964
	Zn	0.0065	200	0.963
	Ni	0.0020	150	0.946
	Co	0.0086	100	0.936
6	Pb	0.0014	425	0.987
	Cu	0.0032	350	0.976
	Zn	0.0031	312	0.965
	Ni	0.0035	237	0.945
	Co	0.0047	125	0.932
8	Pb	0.0011	530	0.996
	Cu	0.0022	410	0.995
	Zn	0.0031	320	0.994
	Ni	0.0041	260	0.987
	Co	0.0046	270	0.980

Initial conc. (mg ℓ$^{-1}$)				
1	Pb	0.0098	320	0.998
	Cu	0.0092	260	0.997
	Zn	0.0088	230	0.975
	Ni	0.0085	170	0.967
	Co	0.0073	110	0.955
3	Pb	0.0095	520	0.989
	Cu	0.0088	300	0.987
	Zn	0.0085	440	0.967
	Ni	0.0081	320	0.965
	Co	0.0070	140	0.922
5	Pb	0.0091	610	0.996
	Cu	0.0080	530	0.962
	Zn	0.0072	440	0.956
	Ni	0.0038	335	0.944
	Co	0.0053	230	0.921
Flow rate (mℓ min^{-1})				
3	Pb	0.0012	320	0.998
	Cu	0.0032	260	0.997
	Zn	0.0030	230	0.985
	Ni	0.0038	170	0.984
	Co	0.0045	100	0.955
5	Pb	0.0045	440	0.989
	Cu	0.0023	395	0.987
	Zn	0.0076	260	0.945
	Ni	0.0097	125	0.937
	Co	0.0032	100	0.925
7	Pb	0.0045	560	0.987
	Cu	0.0023	260	0.962
	Zn	0.0076	200	0.944
	Ni	0.0013	140	0.943
	Co	0.0032	100	0.935
		Yoon-Nelson model		
Parameters	Metal ion	k_{YN} * 10^{-3} (L/mg min)	τ (min^{-1})	R^2
Bed height (cm)				
3	Pb	0.023	145	0.991
	Cu	0.043	240	0.998
	Zn	0.047	155	0.996
	Ni	0.037	154	0.998
	Co	0.012	115	0.979
6	Pb	0.076	265	0.996
	Cu	0.068	235	0.995
	Zn	0.065	305	0.989
	Ni	0.053	245	0.992
	Co	0.062	125	0.988
8	Pb	0.083	475	0.996
	Cu	0.085	455	0.994

	Zn	0.089	390	0.987
	Ni	0.074	335	0.999
	Co	0.052	305	0.987
Initial conc. (mg ℓ^{-1})				
1	Pb	0.093	395	0.963
	Cu	0.098	337	0.997
	Zn	0.097	305	0.985
	Ni	0.089	245	0.998
	Co	0.093	185	0.987
3	Pb	0.091	335	0.924
	Cu	0.087	305	0.965
	Zn	0.088	245	0.988
	Ni	0.081	185	0.997
	Co	**0.083**	100	0.960
5	Pb	0.082	245	0.934
	Cu	0.081	185	0.967
	Zn	0.074	125	0.987
	Ni	0.069	120	0.945
	Co	0.074	155	0.989
Flow rate (mℓ min^{-1})				
3	Pb	0.098	350	0.946
	Cu	0.089	320	0.997
	Zn	0.096	284	0.982
	Ni	0.088	179	0.993
	Co	0.085	240	0.988
5	Pb	0.087	120	0.996
	Cu	0.082	260	0.995
	Zn	0.085	189	0.984
	Ni	0.074	140	0.997
	Co	0.086	105	0.977
7	Pb	0.082	450.56	0.999
	Cu	0.076	240.65	0.997
	Zn	0.072	205.55	0.967
	Ni	0.069	325.44	0.998
	Co	0.078	144.99	0.967

Bed depth service time (BDST) model

Trace metal ion	k_a (L/mg min)	N_o (mg ℓ^{-1})	R^2
Pb	0.0045	157.56	0.991
Cu	0.0022	140.43	0.996
Zn	0.0075	134.32	0.980
Ni	0.0012	120.34	0.993
Co	0.0031	115.45	0.987

Based on all models fitted with experimental data, the Yoon-Nelson and Bed depth service time models were the best. The R^2 value was used in the assessment of experimental data fitting (in Yoon-Nelson and bed depth service time models, the R^2 was greater than 0.98). The indication was that these models are applicable, and constants obtained can be used is a large-scale process of the continuous fixed-bed column. The Yoon-Nelson

model indicates that the rate of adsorption decreases in the probability of sorption of each analyte in the inlet solution. The adsorption of each analyte is proportional to the probability of the sorbate adsorption and the sorbate breakthrough on the HDS. The BDST assumed the relationship between bed depth and service time. Therefore, this assumes that experimental data follows the linear relationship that exists between the bed height and service time on the column adsorption models. The hydroxyl group in the HDS matrix bonds with trace metals as the surface becomes negatively charged (OH^-) with a variation in pH. The effect of pH can also be revealed in terms of pH_{Pzc} (point where the surface positively or negatively charged functional group no longer affect the hydrogen ion activity of the solution). The surface of the HDS is negatively charged when hydrogen ion activity is greater than the point of zero charge and positively charged when hydrogen ion activity is less than the point of zero charge. The point of zero charge was found to be 4.5, which has favoured adsorption as surface is negatively charged. The surface reaction in HDS has pointed out that adsorption is through metal surface complexation.

4.7.5 Desorption studies

The desorption study was done to assess the likelihood of release of trace metals already contained in the HDS. Re-use of HDS was evaluated by its adsorption performance through adsorption and desorption studies. The desorption data with 0.1 mol ℓ^{-1} HCl desorbing agent was only presented as best results obtained in desorption studies. The desorption data indicate that desorption capacity of metals from HDS increased when more H^+ ions are introduced from the solution (Table 4.21).

Table 4.21. Desorption efficiency of trace metals from HDS

Metal ion	t_b (min)	t_e (min)	% Removal efficiency
Pb	130	220	99.38
Cu	110	200	99.16
Zn	100	200	99.44
Ni	90	180	98.65
Co	90	180	97.23

4.7.6 Conclusion

Adsorption studies in a fixed bed column for adsorption of Pb, Cu, Zn, Ni, and Co from AMD by HDS was assessed. It was considered that the HDS has a potential (ability) to bind potentially toxic trace metals due to its high adsorption capacity and affinity. This was observed by its better performance in a fixed bed column (bed height of 8 cm, adsorbent dosage = 10 g of HDS), inlet concentration of 1 mg ℓ^{-1}, and flow rate of 3 mℓ min^{-1}. Breakthrough curves achieved during the experimental run indicated that the breakthrough point was achieved earlier when flow rate and elemental concentrations were increased. Increasing the bed height resulted in increased removal of elements and delayed breakthroughs owing to increased contact between the HDS and solution. The Yoon-Nelson and BDST models have described the column experimental data better. This has important implications if a column configuration is used in the conditioning of AMD prior to actual treatment. Generally, the success of the set-up suggests that HDS can potentially be used more extensively in the conditioning of AMD than in the limited scale currently used.

4.8 BATCH SIMULATION STUDIES OF THE TREATMENT OF PHOSPHATE CONTAINING WATER USING HFO

4.8.1 Effect of pH

The pH of the sewage wastewater solution is an important parameter in the adsorption process. The effect of pH on the adsorption of P-PO_4^{3-} into Hfo was studied at pH ranging from 4.03-7.02 (Figure 4.59). The maximum adsorption capacity of Hfo was found to occur at pH 4.03. The presence of Na^+, K^+ and Mg^{2+} cations in sewage wastewater may also influence the adsorption of P-PO_4^{3-} by making the Hfo surface more positive, and thus leading to the adsorption of P-PO_4^{3-} by the formation of Na_2HPO_4, NaH_2PO_4, $MgHPO_4$, and KH_2PO_4 species. It was observed that the P-PO_4^{3-} adsorption pattern in sewage water containing Ca^{2+} differed significantly from that containing Na^+, K^+, and Mg^{2+}. This is mostly due to the formation of hydroxyapatite ($(Ca_5(PO_4)_3(OH))$ precipitates. The co-precipitation of P-PO_4^{3-} in the solution started at pH 7.02. The co-precipitates observed in saturation indices from pH 7.02 to 13.03 were fluorapatite ($Ca_5(PO_4)_3F$) and $Ca_5(PO_4)_3(OH)$ (Table 4.22). $Ca_5(PO_4)_3(OH)$ can be a good source of P-PO_4^{3-} for plant growth (slow release of P-PO_4^{3-} from $Ca_5(PO_4)_3(OH)$), but this would need to be investigated further. When pH increases, a decline in the removal efficiency was observed from pH 4.03 to 6.01 (this was due to adsorption reaching equilibrium). A decline in adsorption capacity occurred when active adsorption sites decrease in the Hfo surface area. A high removal efficiency of P-PO_4^{3-} was observed at weak sites compared to strong sites in terms of concentration per mole of Hfo.

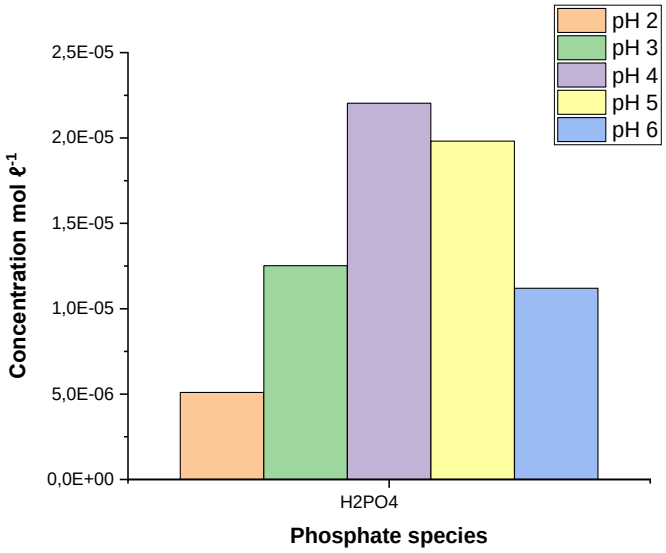

Figure 4.59. Effect of pH on phosphates adsorption onto Hfo

Table 4.22. Saturation indices (SI) of mineral phases at different hydrogen ion activity

Phase (at pH 2.01-4.03)	**SI**	**log IAP**	**log K (298 K, 1 atm)**	
Fluorapatite	-13.1	-30.7	-17.6	Ca5(PO_4)3F
Hydroxylapatite	-20.3	-23.5	-3.22	$Ca_5(OH)(PO_4)_3$
Epsomite	-4.91	-7.05	-2.14	$MgSO_4$:7H2O
Phase (at pH 7.02-13.03)	**SI**	**log IAP**	**log K (298 K, 1 atm)**	
Fluorapatite	6.16	-11.4	-17.6	Ca5(PO_4)3F
Hydroxyapatite	8.04	4.62	-3.42	$Ca_5(PO_4)_3OH$

4.8.2 Effect of Hfo dosage

The effect of adsorbent dosage on the adsorption of P-PO_4^{3-} onto Hfo was studied. The concentration of P-PO_4^{3-} ion in sewage wastewater was reduced by 99.66% following an increase in Hfo dosage (Figure 4.60). This could be due to sufficient active adsorption sites onto the Hfo surface area. The surface chemistry of Hfo on the adsorption of P-PO_4^{3-} is through surface complexation (the OH^- functional group play a role in surface complexation) and the reactions below indicate how surface complexation occurs on the Hfo surface:

$$SOH + PO_4^{3-} + 3H^+ \leftrightarrow SO\text{-}H_2PO_4 + H_2O \quad (4.14)$$

$$SOH + PO_4^{3-} + 2H^+ \leftrightarrow SO\text{-}HPO_4 + H_2O \quad (4.15)$$

$$SOH + PO_4^{3-} + H^+ \leftrightarrow SO\text{-}PO_4^{2-} + H_2O \quad (4.16)$$

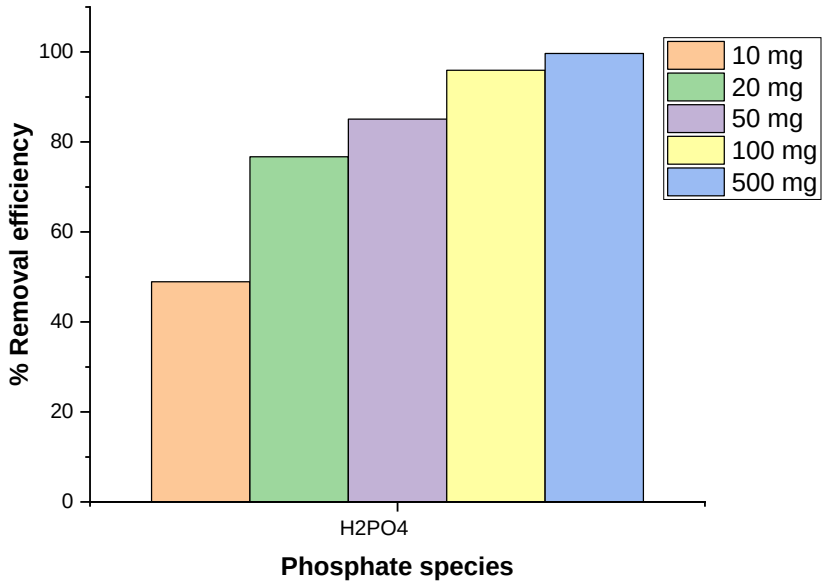

Figure 4.60. Effect of Hfo dosage on phosphates adsorption

4.8.3 Effect of initial P-PO_4^{3-} concentration

The effect of concentration of P-PO_4^{3-} on adsorption onto Hfo was simulated. Varying concentrations of P-PO_4^{3-} ion (2, 10, 100, 300, and 500 mg ℓ^{-1}) were contacted with Hfo surfaces (both strong and weak sites). The results showed an increase in adsorption of P-PO_4^{3-} with concentration. The concentration of P-PO_4^{3-} was reduced by 75.6% (in 2 mg ℓ^{-1}), 86.7% (10 mg ℓ^{-1}), 90.4% (100 mg ℓ^{-1}), 97.8% (300 mg ℓ^{-1}) and 99.79% (500 mg ℓ^{-1}) after adsorption (Figure 4.61).

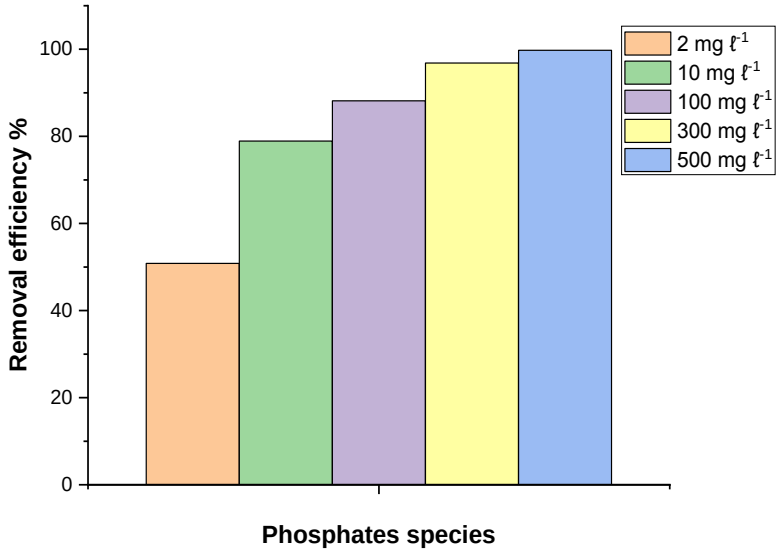

Figure 4.61. Effect of initial P-PO_4^{3-} concentration on phosphates adsorption onto Hfo

4.8.4 Effect of temperature

The effect of temperature on P-PO_4^{3-} adsorption was simulated at various temperatures (Figure 4.62). The adsorption capacity of P-PO_4^{3-} increased as the temperature increased and favoured the diffusion of unabsorbed P-PO_4^{3-} ions onto the Hfo surfaces. Overall Gibbs energy (ΔG^o) values were negative, indicating the spontaneity of the adsorption of P-PO_4^{3-} (Table 4.23). The increased ratio of the equilibrium concentration (Kc) values as a function of increased temperature and positive enthalpy change ($\Delta H°$) indicate that the adsorption of P-PO_4^{3-} onto Hfo are an endothermic reaction. The positive entropy change (ΔS^o) value further indicates the spontaneity of the adsorption.

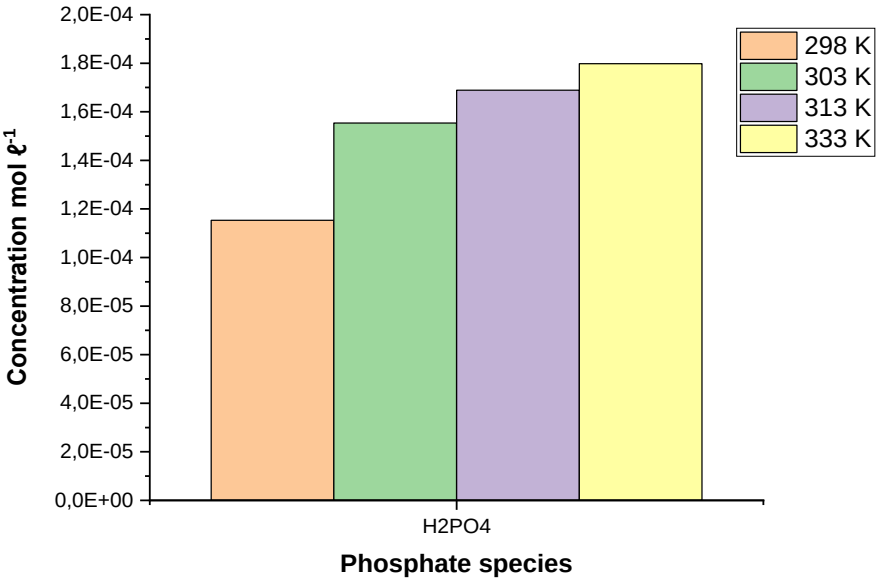

Figure 4.62. Effect of temperature on phosphates adsorption onto Hfo

Table 4.23. Thermodynamic parameters for $P\text{-}PO_4^{3-}$ adsorption onto Hfo

Anion	Temperature (K)	ΔG^o (kJ mol^{-1})	ΔH^o (kJ mol^{-1})	ΔS^o (J mol^{-1} K^{-1})	K (L g^{-1})
$P\text{-}PO_4^{3-}$	298	-2.85	2.14	10.42	3.18
	303	-3.64		10.36	3.46
	313	-4.58		15.09	5.85
	333	-5.34		16.31	6.58

4.8.5 Conclusion

The simulations of the adsorption of $P\text{-}PO_4^{3-}$ in sewage wastewater onto Hfo showed the potential, by extension, of HDS for the removal of $P\text{-}PO_4^{3-}$. As expected, due to the availability of active sites, a high surface area and dosage of Hfo resulted in increased adsorption. A pH of 4.03 was found to give optimum adsorption. The adsorption process was found to be endothermic and spontaneous. Adsorption of $P\text{-}PO_4^{3-}$ onto Hfo was observed to occur in two distinct phases: through surface complexation caused by electrostatic interactions, followed by a slower process of adsorption of $P\text{-}PO_4^{3-}$ due to inner-sphere complexation. The presence of cations like Na^+ and Mg^{2+} promotes $P\text{-}PO_4^{3-}$ adsorption and the adsorption process is electrostatic. In the presence of Ca^{2+}, the formation and precipitation of $Ca_5(PO_4)_3(OH)$ plays an essential role in the removal of $P\text{-}PO_4^{3-}$ from the solution at pH 7.02. Electrostatic attraction and surface complexation interactions between $P\text{-}PO_4^{3-}$ and Hfo were the key mechanism for $P\text{-}PO_4^{3-}$ removal from sewage wastewater rather than intraparticle diffusion (this will be confirmed on the experimental data using HDS in a similar experimental setup). The adsorption capacities followed the order: $H_2PO_4 > HPO_4^{2-} > PO_4^{3-}$ for weak sites (Hfo_wOH) and none was observed for strong sites (Hfo_sOH).

4.9 BATCH SORPTION STUDIES OF THE TREATMENT OF PHOSPHATE CONTAINING WATER USING SLUDGE

In this study, high density sludge (HDS) rich in iron (Fe), generated from acid mine drainage (AMD) treatment was used as an adsorbent in the removal of $P\text{-}PO_4^{3-}$ in contaminated water bodies (sewage wastewater). The potential use of the loaded HDS as a virtual fertiliser was also assessed. Batch studies were conducted to check the effect of HDS dosage, hydrogen ion activity (pH), ionic strength, concentration, contact time, and competing ions on adsorption. The adsorption of $P\text{-}PO_4^{3-}$ was strongly dependent on pH and initial concentration of the solution. The adsorption process was via the chemisorptive (chemical ion exchange) mechanism in the rate-determining step. Batch adsorption results agreed with those of computational simulation studies conducted to optimize the experimental parameters (pH, adsorbent dosage, initial concentration, etc.). To assess the slow release of $P\text{-}PO_4^{3-}$ adsorbed onto HDS, desorption studies were conducted using deionised water, sodium hydroxide (NaOH), and sodium bicarbonate ($NaHCO_3$) as desorbing agents. The desorption results showed that 0.1 mol ℓ^{-1} NaOH gave superior desorption compared to 0.1 mol ℓ^{-1} $NaHCO_3$.

The following sections present the materials and methods that were employed for batch studies. Experimental design for these studies was informed by the findings from computational simulations described in the previous section. The findings of this study were presented and discussed following the characterisation of the HDS, adsorption experiments (including isotherm and kinetic models), and the desorption study.

4.9.1 Effects of pH on adsorption

Aqueous solution pH determines the relevant $P\text{-}PO_4^{3-}$ species dominating in the sewage water and it influences the strength of electrostatic attraction. The results for the effect of pH on $P\text{-}PO_4^{3-}$ adsorption are presented in Figure 4.63. To optimise the pH for maximum removal efficiency and to avoid the precipitation of $P\text{-}PO_4^{3-}$,

adsorption was conducted at pH 2.01 to 4.03. When H^+ ions dominated in the solution (low pH), the surface of HDS was surrounded by hydronium (H_3O^+) ions that create a high adsorption affinity for binding sites on HDS. Maximum removal efficiency of HDS was found to occur at pH 4.03. Higher pH values (e.g. pH 7.02-13.03) were omitted to prevent precipitation that may occur in chemical reactions as was observed in simulation studies (Table 7.3). When pH increases, strong competition occurs between P-PO_4^{3-} species ($H_2PO_4^-$, HPO_4^{2-}, and PO_4^{3-}) and hydroxyl (OH^-) ions as H^+ are reduced or replaced by OH^- ions, creating strong repulsions between P-PO_4^{3-} and OH^- that reduces P-PO_4^{3-} adsorption. However, P-PO_4^{3-} adsorption can also be stimulated and enhanced by the presence of free OH^-, which could be replaced by P-PO_4^{3-} ions on the HDS surface. The adsorption percentage increased rapidly as H^+ ions were replaced by OH^- ions in the solution, reaching an optimal pH of 4.03. The pH of the initial solution plays an important role in adsorption as many anions exist in different species at different pH values. The P-PO_4^{3-} species adsorbed at pH 4.03 was $H_2PO_4^-$ and this was confirmed by the speciation distribution at different pH regimes (Figure 7.12). After maximum adsorption capacity was reached at pH 4.03, a decline in adsorption capacity was observed at pH 6.02 (this was due to a change in H^+ ions in the solution that lowered the H_2PO_4- and a new HPO_4^{2-} species in solution started to dominate). This may be due to the variation in operating pH, which also changes the HDS surface charge and P-PO_4^{3-} degree of ionisation and dissociation of surface functional groups. Thus, the decrease in P-PO_4^{3-} adsorption with an increase in OH^- ions replacing H^+ ions, may be due to electrostatic attraction (this may be due to reduction in electrostatic interaction and reduced inner-sphere complexation between the P-PO_4^{3-} and HDS surface functional groups). The surface of the HDS can either be positively charged, negatively charged, or even neutral (based on the pH of the initial solution used). The point of zero charge (pHpzc) on the HDS surface was pH 4.5. In this study, pH 4.03 (the surface of the HDS was positively charged) was the main target for maximum adsorption capacity of P-PO_4^{3-} (pH < pHpzc) and surface complexation was via an inner-sphere mechanism. The proposed surface complexation reaction was assumed to occur as presented below:

$$\equiv FeOH + PO_4^{3-} + 3H^+ \leftrightarrow \equiv FeO\text{-}H_2PO_4 + H_2O \qquad (4.17)$$

This agreed with simulation results observed in Figure 4.65, where the pH of the P-PO_4^{3-} after adsorption was observed to drastically increase. A decline in pH could be attributed to the formation of OH^- ions after adsorption occurred (H^+ ions reduced in the solution).

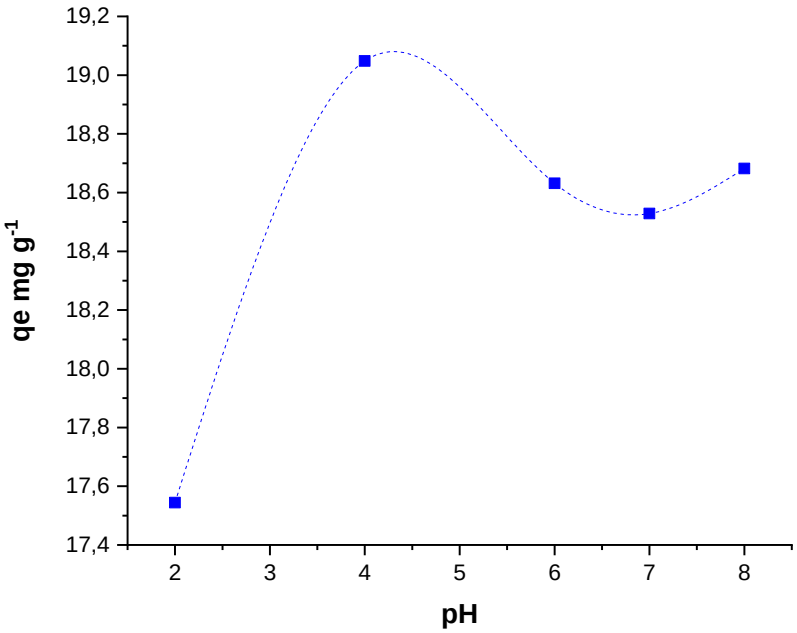

Figure 4.63. Effect of pH on the adsorption of P-PO_4^{3-} onto HDS for a concentration of 50 mg ℓ^{-1} (solid:liquid ratio of 500 mg:10 mℓ) (n = 3; RSD <10%).

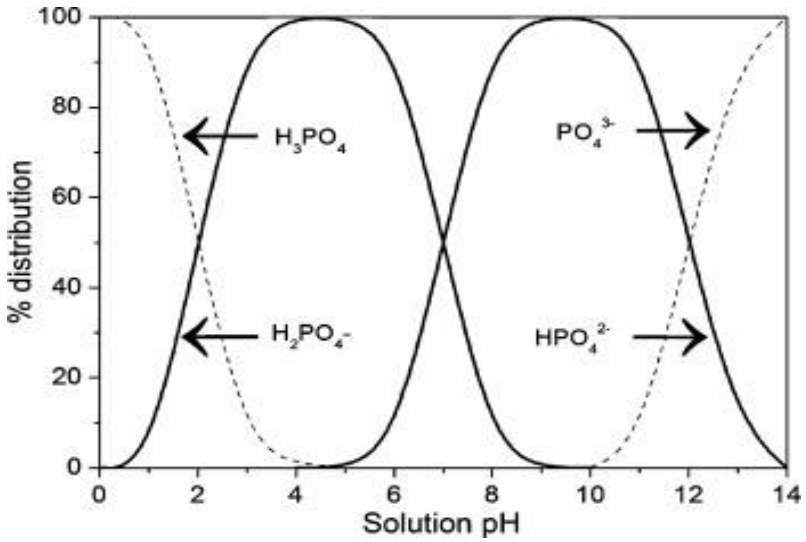

Figure 4.64. The speciation distribution of P-PO_4^{3-} at different pH regimes (Chubar *et al.,* 2005)

Estimation of generalised surface complexation (adsorption constants) and site density parameters in HDS from experimental data (Figure 4.65) was conducted using PHREEQC coupled with parameter estimation (PEST). This made it possible to conduct different simulations of P-PO_4^{3-} adsorption onto HDS and the fit with experimental data gave confidence that in cases of limited experimental data or where experimentation is expensive, simulations can be used. This has proven useful at the time of conducting this work as most of the experimental work has been negatively impacted by the pandemic.

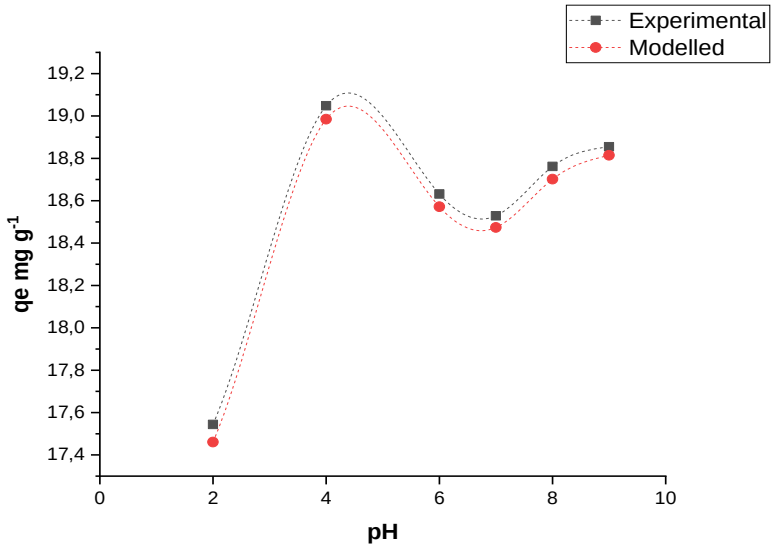

Figure 4.65. Generalised surface complexation for P-PO_4^{3-} adsorption with PHREEQC coupled with PEST

4.9.2 Effect of HDS dosage on adsorption

Results for the effect of adsorbent mass on adsorption are presented in Figure 4.66. The effect of HDS dosage (10, 20, 50, 100, 300, and 500 mg) on the adsorption of the P-PO_4^{3-} onto HDS was investigated. The P-PO_4^{3-} ions in aqueous solution were reduced by 48.92% (10 mg), 76.70% (20 mg), 85.08% (50 mg), 95.95% (100 mg), 99,33% (300 mg) and 99.67% (500 mg). Adsorption efficiency increased with an increase in HDS dosage. This is due to an increase of active adsorption sites on the HDS surface (attributed to the fact that as the mass increases, more of the active sites for adsorption of P-PO_4^{3-} on the HDS become available). HDS particle aggregation and repulsive forces between active adsorption sites may also cause incremental improvement in

P-PO_4^{3-} adsorption. However, P-PO_4^{3-} sorption was maintained at high HDS dosages, possibly due to resistance in the P-PO_4^{3-} mass transfer from the sewage water to HDS surface sites at high HDS dosage. A maximum adsorption capacity was observed at 100 mg of HDS as there were no significant changes observed after that, signifying that equilibrium had been established.

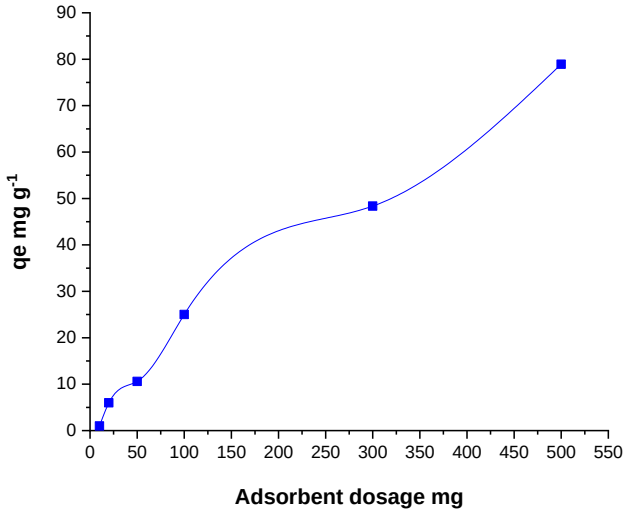

Figure 4.66. Effect of mass on the adsorption of P-PO_4^{3-} onto HDS for a pH = 4.03; concentration of 50 mg ℓ^{-1} (constant liquid volume of 10 mℓ) (n = 3; RSD <10%).

4.9.3 Effect of contact time on adsorption

Contact time plays an essential role in the adsorption process. It defines the adsorption equilibrium between P-PO_4^{3-} ions and HDS, as well as a description of P-PO_4^{3-} kinetics in adsorption. The effect of contact time on adsorption of P-PO_4^{3-} was studied and the results are presented in Figure 4.67. The rate of adsorption initially increased rapidly and optimal adsorption efficiency was achieved after 1 h. Further increase in contact time did not result in any improvement in adsorption as equilibrium had been reached.

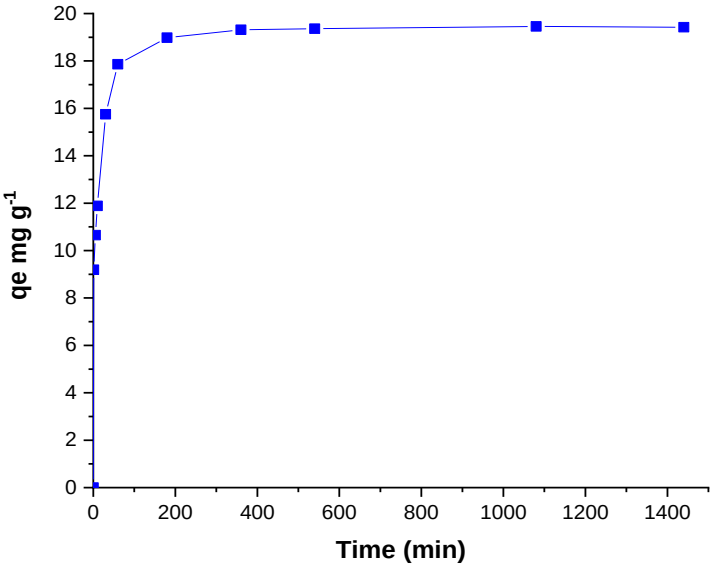

Figure 4.67. Effect of contact time on the adsorption of P-PO_4^{3-} onto HDS for a pH = 4.03; metal concentration of 50 mg ℓ^{-1} (solid:liquid ratio of 500 mg:10 mℓ) (n = 3; RSD <10%)

4.9.4 Effect of concentration on adsorption

The effect of concentration on adsorption was studied and the results are presented in Figure 4.68. The results pointed to an increase in adsorption with an increase in P-PO_4^{3-} concentration. This implies that there is likely to be more uptake of P-PO_4^{3-} before adsorption capacity reaches an equilibrium point.

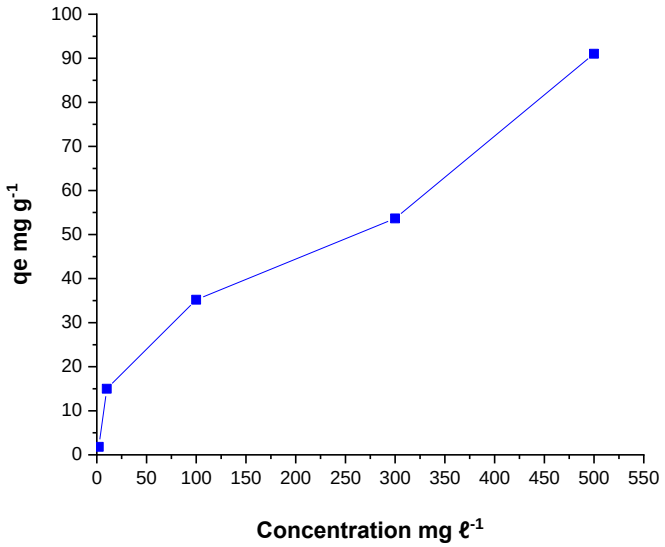

Figure 4.68. Effect of concentration on adsorption of P-PO_4^{3-} onto HDS for a pH = 4.03; (solid:liquid ratio of 500 mg:10 mℓ); for 24 h (n = 3; RSD <10%).

4.9.5 Effect of competing ions

Chemical composition of sewage wastewater does not only contain P-PO_4^{3-} ions, but there are also co-existing ions such as nitrates (NO_3^-), sulphates (SO_4^{2-}), chlorides (Cl^-), etc. The coexistence of these ions in sewage wastewater may either have effects on the adsorption process or have no effect on the adsorption of P-PO_4^{3-} on HDS. In this study, the effect of these co-existing anions was evaluated with different adsorbent dosages (50, 100, and 500 mg) at a constant concentration of 50 mg ℓ^{-1} for each anion. Experimental results showed that co-existing anions affect the uptake of P-PO_4^{3-} ions on the HDS surface, and this was observed by the high removal efficiency of P-PO_4^{3-} as presented in Table 4.24. Anions of higher valence showed a more significant interfering effect than the monovalent anions in P-PO_4^{3-} adsorption on HDS (SO_4^{2-}, Cl^-, NO_3^- etc.). Divalent anions such as SO_4^{2-} contributed notably in retarding adsorption of P-PO_4^{3-} by HDS. This was also observed in weak sites of Hfo in simulation studies. The decrease in the adsorption capacity may be due to the ion-exchange mechanism, in which SO_4^{2-} has high affinity for the HDS and compete most effectively with P-PO_4^{3-} adsorption.

Table 4.24. Adsorption percentage of P-PO_4^{3-} on the HDS with the mixture of the co-existing anions in solution at different HDS dose

Mass (mg)	C_e (mg ℓ^{-1})	q_e (mg g^{-1})	% Removal efficiency
50	0.176	19.96	85.8
100	0.481	59.95	90.5
500	0.927	85.98	98.9

4.9.6 Adsorption isotherm models

The Langmuir, Freundlich, Dubinin-Radushkevich, and Temkin isotherms were applied for data fitting on the models (this has included the initial $P\text{-}PO_4^{3-}$ concentration and results from data). The results for these are presented in Table 4.25. The Freundlich isotherm best fitted the adsorption data for $P\text{-}PO_4^{3-}$. This may be due to heterogeneous surfaces. Heterogeneous surface areas may exhibit the homogeneous adsorption site (at a constant enthalpy of adsorption). Sometimes the heterogeneous adsorption has a variable (enthalpy of adsorption) depending on the active sites occupied in HDS. When the $P\text{-}PO_4^{3-}$ concentration (pressure) is low, the high energy sites may be occupied and as the concentration of $P\text{-}PO_4^{3-}$ increases, few active sites (energy sites) result in a lower enthalpy of adsorption. The adsorption mechanism may be proceeding through physical adsorption and the heterogeneous coverage chemical complexation in the inner sphere and outer sphere (this may be due to the heterogeneous surface of the HDS). The surface energy on the HDS was determined in the D-R isotherm model. The adsorption energy was between 8 and 16 kJ mol^{-1} for $P\text{-}PO_4^{3-}$ and this may be due to strong chemical ion-exchange on the HDS. The adsorption intensity onto HDS was greater than 1 and this confirms the chemical adsorption. The R_L values of HDS ranged from 0-1 for $P\text{-}PO_4^{3-}$ ions, implying favourable adsorption.

Table 4.25. Isotherms parameters of adsorption of $P\text{-}PO_4^{3-}$ onto HDS (pH = 4.03; solid:liquid ratio of 500 mg:10 mℓ; shaking for 24 h; temp = 25 ^oC) (n = 3; RSD <10%)

Isotherms	$P\text{-}PO_4^{3-}$ ion	Estimated isotherms parameters		
		q_{max} (mg g^{-1})	K_L (ℓ mg^{-1})	R^2
Langmuir	H_2PO_4	85.9	3.47E+06	0.930
	$P\text{-}PO_4^{3-}$ ion	n	K_f (mg g^{-1})/ (mol $ℓ^{-1})^{1/n}$	R^2
Freundlich	H_2PO_4	2.7	60.1	0.995
	$P\text{-}PO_4^{3-}$ ion	X_m (mol g^{-1})	E_s (kJ.mol^{-1})	R^2
Dubinin-Radushkevich	H_2PO_4	0.00133	15.3	0.941
	$P\text{-}PO_4^{3-}$ ion	a_T (L kg^{-1})	b_T (kJ mol^{-1})	R^2
Temkin	H_2PO_4	6.85	0.031	0.956

4.9.7 Kinetic models

The results for kinetic models are presented in Table 4.26. The maximum adsorption of $P\text{-}PO_4^{3-}$ was reached after 1 h of contact with HDS. The adsorption rate was observed to be much faster within 5 min and after 60 min the adsorption capacity remains constant throughout. The results have pointed out that the adsorption of $P\text{-}PO_4^{3-}$ onto HDS followed this order: $H_2PO_4^- > HPO_4^{2-} > PO_4^{3-}$. The pseudo first-order and pseudo second-order kinetic models were utilised to find out the mechanism that influences the attraction of $P\text{-}PO_4^{3-}$ onto the HDS surface (Table 4.26). The pseudo second-order model best fitted the kinetic data compared to the pseudo first-order (this was based on the R^2 values that were greater than 0.998 for $H_2PO_4^-$). The experimental adsorption capacity was compared with the calculated adsorption capacity and for the pseudo second-order, the values were very close.

Table 4.26. Kinetic parameters of P-PO_4^{3-} removal onto HDS (pH = 4.03; concentration = 50 mg ℓ^{-1}; solid:liquid ratio of 500 mg:10 mℓ; temp = 25 ^oC) (n = 3; RSD <10%)

Kinetics	P-PO_4^{3-} ion	Estimated kinetic parameters			
		$Q_{e(exp)}$ (mg g^{-1})	K_1 (min^{-1})	Q_{cal} (mg g^{-1})	R^2
Pseudo first-order	H_2PO_4	0.017	0.035	0.010	0.959
		$Q_{cal\ (}$mg g^{-1})	K_2 (mg g^{-1} min)		R^2
Pseudo second-order	H_2PO_4	0.017	2.786		0.998
		a/(kg.mol^{-1}.min^{-1})	*b*/(kg.mol^{-1}.min^{-1})		R^2
Elovich	H_2PO_4	0.0035	247.34		0.937
		Ip	Kp	R^2	
Intraparticle diffusion model	H_2PO_4	0.003	0.001		0.891
		I_f	K_f		R^2
Film diffusion model	H_2PO_4	-0.197	0.035		0.958

4.9.8 Thermodynamic studies of phosphate adsorption

Figure 4.69 shows the rate of increase of P-PO_4^{3-} adsorption with an increase in temperature and this was observed in sewage wastewater with high initial P-PO_4^{3-} concentration. Thermodynamic studies were conducted to have a better understanding of the nature of the adsorption process (Table 4.27). The parameters including Gibbs free energy, ΔG^o (kJ/mol), enthalpy change, ΔH^o (kJ/mol), and entropy change ΔS^o (J/ mol/K) were calculated. The change of ΔH^o and ΔS^o is determined by slope and intercept of the distribution coefficient (ln K_d) plotted against temperature (1/T). The positive values of ΔH^o confirm that the adsorption reaction of P-PO_4^{3-} is endothermic, and the positive value of ΔS^o shows the good affinity of the HDS toward P-PO_4^{3-} species. The ΔG^o for P-PO_4^{3-} adsorption declined from -4.85 to -8.36 kJ mol^{-1} as the temperature rises from 25-60 ºC (298, 303, 313 and 333 K). Therefore, the negative values of ΔG^o at the conducted thermodynamic studies (effect of temperature) indicates that the adsorption of P-PO_4^{3-} onto the HDS is highly favourable and spontaneous. Based on the thermodynamic studies conducted, the adsorption improved with an increase in temperature. The removal efficiency at different temperatures is as follows: 298 K (96%), 303 K (97%), 313 K (98%), 333 K (99%). The overall results indicate that HDS has the potential of P-PO_4^{3-} removal in large scale application in wastewater treatment.

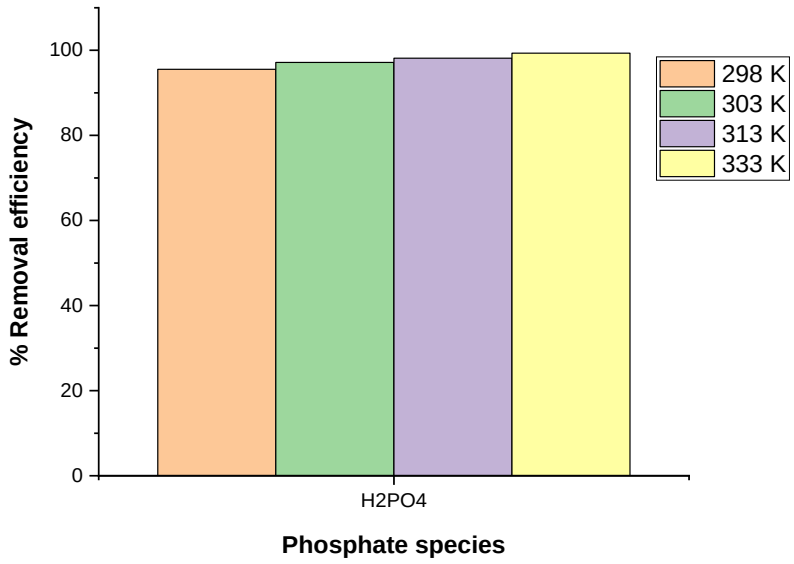

Figure 4.69. Effect of temperature on the adsorption of P-PO_4^{3-} onto HDS

Table 4.27. Thermodynamic parameters for the adsorption of P-PO_4^{3-} onto HDS

Anion	Temperature (K)	ΔG^o (kJ mol^{-1})	ΔH^o (kJ mol^{-1})	ΔS^o (J mol^{-1} K^{-1})	K (L g^{-1})
P-PO_4^{3-}	298	-4.85	3.23	9.42	4.07
	303	-6.64		9.36	4.39
	313	-7.21		14.09	6.65
	333	-8.36		15.31	7.53

4.9.9 Desorption of P-PO_4^{3-}

The desorption study was done to assess the slow release of P-PO_4^{3-} adsorbed on the HDS. To evaluate the slow release of the adsorbed P-PO_4^{3-} ions were conducted after adsorption studies. The desorption of P-PO_4^{3-} ions was to investigate the potential use of adsorbed P-PO_4^{3-} on HDS (as a carrier of P-PO_4^{3-}) as a fertilizer to support plant growth (in plants species used for phytoremediation) in woodlots in the tailings. 10 mℓ of deionised water, 0.1 mol $ℓ^{-1}$ NaOH and 0.1 mol $ℓ^{-1}$ $NaHCO_3$ were used as the desorbing agents. The ionic strength of NaOH (0.01, 0.05, and 0.1 mol $ℓ^{-1}$) was assessed, and 0.1 mol $ℓ^{-1}$ NaOH showed to be the best desorbing agent with high desorbing efficiency of P-PO_4^{3-} and the results are presented in Figures 4.70-4.71.

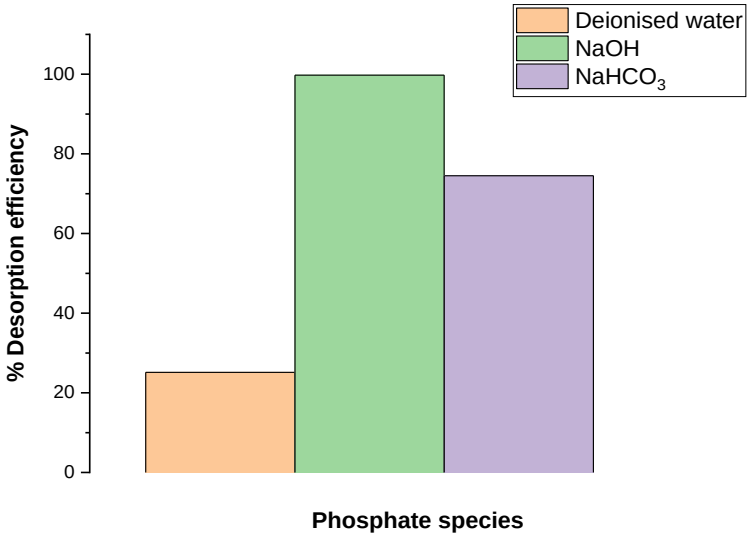

Figure 4.70. Desorption percentage of P-PO_4^{3-} using different desorbing agents.

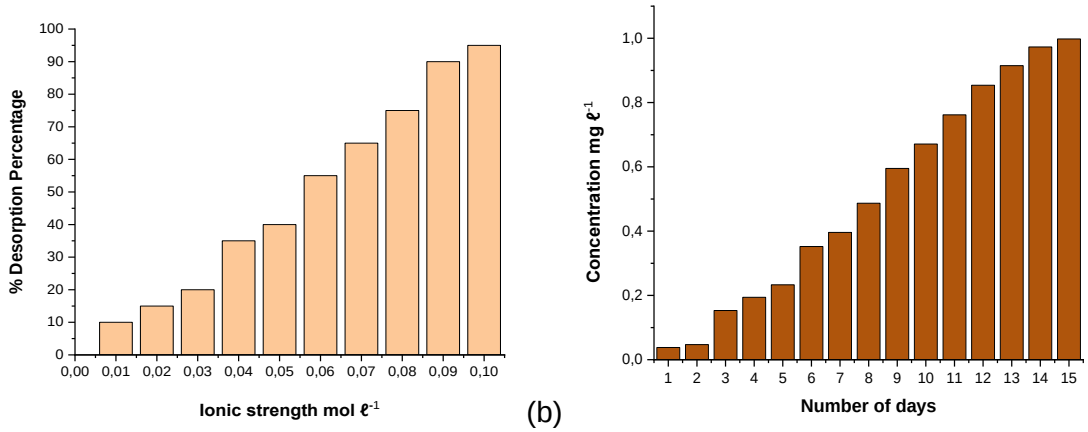

Figure 4.71. (a) Effect of NaOH ionic strength during desorption of P-PO_4^{3-} (b) Slow release of P-PO_4^{3-} phosphates from HDS with deionised water

The slow release of P-PO_4^{3-} from HDS shows that HDS can be used as carrier of P in a form of fertilizer to assist growth of plants that are mostly used for phytoremediation around the contaminated sites.

4.9.10 Conclusion

Simulations of adsorption of P-PO_4^{3-} in sewage wastewater onto Hfo showed the potential of HDS for the removal of these ions. As expected, a high surface area and dosage of Hfo resulted in increased adsorption. A pH of 4.03 was found to give optimum adsorption for P-PO_4^{3-}. Due to the complexity of HDS, it could not be concluded at that stage how accurate it would be to use Hfo as a surrogate adsorption surface. Thus, further studies involving actual P-PO_4^{3-} adsorption onto HDS were done that led to the determination of parameters that were used in a generalised surface complexation model. Therefore, based on surface complexation results, it may be possible to conduct different simulations of P-PO_4^{3-} adsorption onto HDS. Both adsorption and desorption of P-PO_4^{3-} onto HDS were investigated. The selectivity sequence for adsorption followed the order: $H_2PO_4^-$ > HPO_4^{2-} > PO_4^{3-}. The adsorption capacity of $H_2PO_4^-$ was observed to be higher. An increase in HDS dose and concentration of P-PO_4^{3-} resulted in increased adsorption. Hydrogen ion activity was found to result in the peaking of adsorption at 4.03. The Freundlich isotherm and pseudo second-order kinetic model fitted the experimental data (R^2 value equal to 0.99) best, with the latter model showing that the mechanism

was chemisorptive (chemical ion exchange). The high influent P-PO_4^{3-} concentration affects P-PO_4^{3-} removal as the adsorption process is through mass transfer (P-PO_4^{3-}adsorption was inversely proportional to HDS dosage and temperature) and a high adsorption capacity of P-PO_4^{3-} was observed as temperature increases. Thermodynamic studies have shown that the adsorption of P-PO_4^{3-} onto the HDS surface was endothermic and the reaction was spontaneous. Desorption studies showed that it was possible for slow release of P-PO_4^{3-} from HDS. Thus, it would be expected that in contact with sewage wastewater, the net migration of P-PO_4^{3-} will be to the HDS than from its release from its surface. Overall, the trend in adsorption onto HDS resembled that observed for Hfo. The effect of components such as the polyacrylate polymer within the HDS structure was studied further using a generalised surface complexation model. The findings showed that simulations could be successfully used where limited experimental data was available.

4.10 REACTIVE TRANSPORT SIMULATIONS FOR HFO-PHOSPHATE CONTAINING WATER INTERACTION

Adsorption of P-PO_4^{3-} in a fixed-bed column was investigated using the Hfo surface and only selected results are presented here. Breakthrough curves were predicted that were important for the design of fixed-bed adsorption experimental studies. To examine fixed-bed column parameters (e.g. initial P-PO_4^{3-} concentration, bed height and flow rate) and their interdependence on column performance, adsorption transport simulations (for column studies) were applied for the experimental setup. Reactive transport models were helpful in assessing the effect of process variables on the efficiency of adsorption of P-PO_4^{3-} in the fixed-bed column and the flow rate (in actual experimental work) was evaluated by keeping relevant parameters constant throughout.

4.10.1 Effects of initial P-PO_4^{3-} concentration

Breakthrough curves for different P-PO_4^{3-} concentrations (10, 50, and 100 mg ℓ^{-1}) at a constant flow rate (1 mℓ min^{-1}) and a bed height of 6 cm (8 g of Hfo) were observed for simulation studies (Figure 4.72). A pH of 4.03 was used for the simulations. Increasing initial P-PO_4^{3-} concentration from 10 to 100 mg ℓ^{-1} showed a decrease in removal efficiency and thus quicker breakthroughs (Figure 4.72).

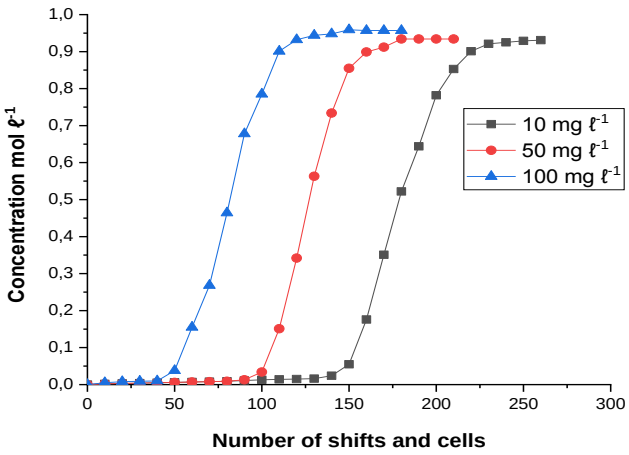

Figure 4.72. Effects of initial P-PO_4^{3-} concentration (pH = 4.03, bed height = 6 cm (8 g of Hfo), flow rate = 1 mℓ min^{-1}).

4.10.2 Effect of bed height

The effects of bed height (1, 3, and 6 cm) on adsorption were studied at pH 4.03, concentration of 10 mg ℓ^{-1}, a flow rate assumed to be 1 mℓ min^{-1} and 8 g of Hfo (Figure 4.73). An increase in bed height from 3 to 6 cm

resulted in an increase in breakthrough times (i.e. delayed) as a result of increased residence time and adsorption

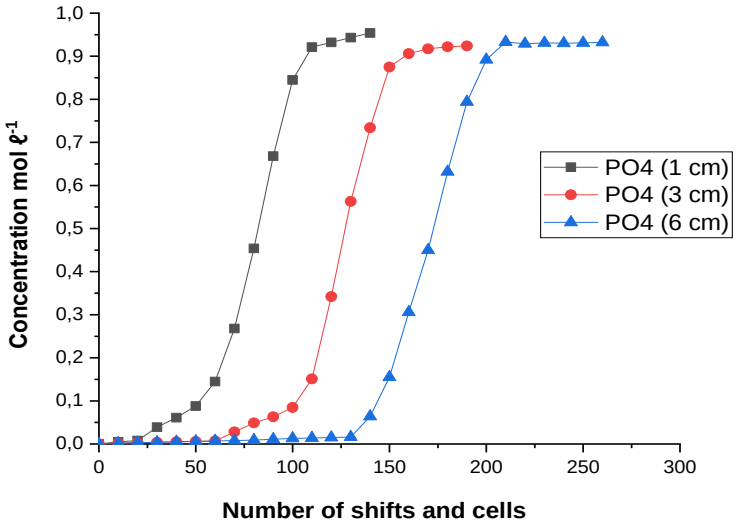

Figure 4.73. Effect of bed height (pH = 4.03, concentration = 10 mg ℓ^{-1}, flow rate = 1 mℓ min^{-1})

4.10.3 Effects of flow rate

Adsorption of P-PO_4^{3-} at different flow rates (1, 3, and 5 mℓ min^{-1}) was investigated (Figure 4.74). Breakthrough times decreased with increasing flow rate due to less contact time between phosphate and Hfo.

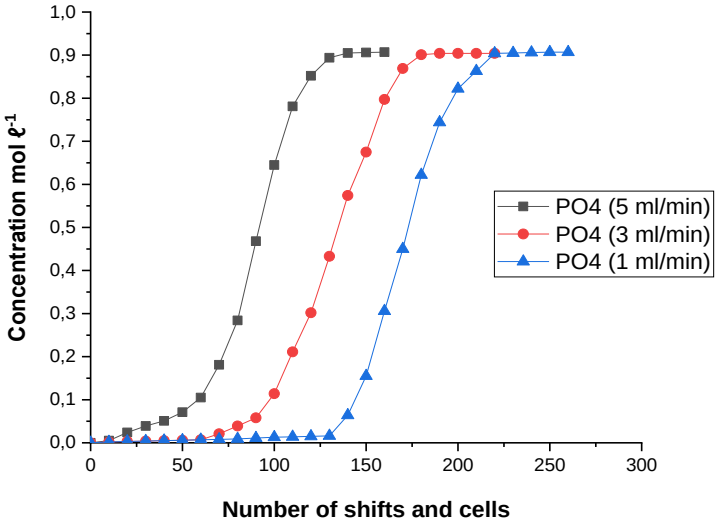

Figure 4.74. Effects of flow rate (concentration = 10 mg ℓ^{-1}, pH = 4.03, bed height = 6 cm (8 g of Hfo)).

4.10.4 Conclusion

Simulated fixed-bed column adsorption studies to remove P-PO_4^{3-} from P-PO_4^{3-} containing water onto the Hfo surface (e.g. FeOOH) were investigated. Based on the simulation results, a low-cost adsorbent highly rich in Fe (e.g. HDS) can potentially be used in the removal of P-PO_4^{3-} in wastewaters. Simulations have helped in establishing and optimising parameters for use in designing actual experimental studies, thus giving the advantage of reducing time and costs that would be incurred if these were to be established by trial-and-error

as is normally the case. The Hfo surface has shown good adsorption capacity, but it still remains to be seen how closely this represents the performance of HDS of which it is a predominant constituent.

4.11 COLUMN SORPTION STUDIES OF SLUDGE FOR PHOSPHATE CONTAINING WATER TREATMENT

4.11.1 Effect of inlet P-PO_4^{3-} concentrations

Breakthrough curves for P-PO_4^{3-} adsorption onto HDS were determined (Figure 4.75). Adsorption efficiency, breakthrough, and exhaustion time decreased with increasing inlet concentration. Adsorption parameters for different concentrations were also assessed (Table 4.28). The t_{br} (min) at the inlet P-PO_4^{3-} concentrations (10, 50, and 100 mg ℓ^{-1}) is from 150-50 min and the exhaustion time is from 250-100 min. When inlet P-PO_4^{3-} concentration is very low, retention time becomes longer for the active sites available for adsorption in the HDS to be exhausted. This trend is similar to that observed in computational simulation studies. When inlet P-PO_4^{3-} concentration increases, the slopes of the breakthrough curves become steeper and the breakthrough time becomes shorter. This may be since the active adsorption sites are covered by phosphate as the HDS reaches the saturation point faster.

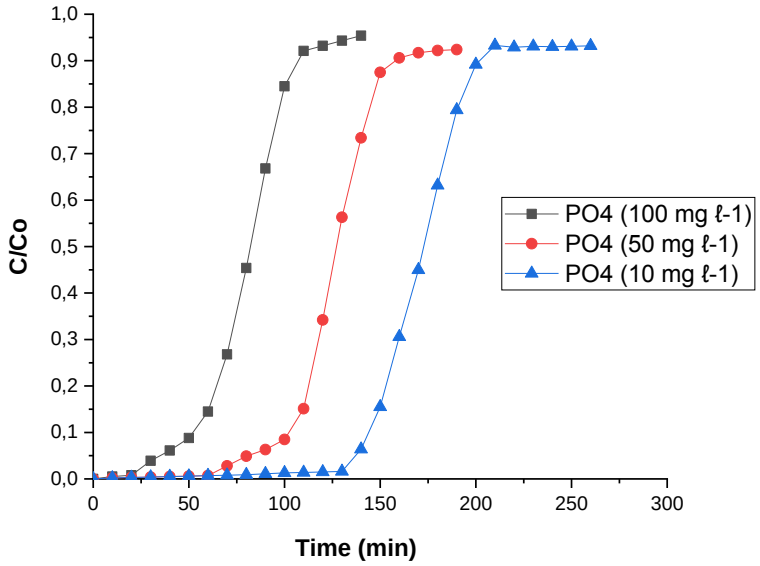

Figure 4.75. Effects of initial P-PO_4^{3-} concentration (pH = 4.03, HDS particle size = 10 µm, bed height = 6 cm, flow rate = 1 mℓ min^{-1})

Table 4.28. Fixed-bed column parameters for adsorption of P-PO_4^{3-} ions onto HDS at varying inlet concentration of 10, 50 and 100 mg ℓ^{-1} (flow rate = 1 mℓ min^{-1}, bed height = 6 cm, temp = 25 ºC)

Inlet conc. (mg ℓ^{-1})	Anions	t_{br} (min)	t_{ex} (min)	V_{ef} (mℓ)	Z_m (cm)	Removal efficiency (%)
10	PO_4^{3-}	100	150	1500	4.56	99.75
50	PO_4^{3-}	160	310	3100	2.29	97.78
100	PO_4^{3-}	170	240	2400	3.04	88.57

4.11.2 Effect of bed height

Breakthrough curves for P-PO_4^{3-} adsorbed at different bed heights (1, 3, 6 cm) corresponding to 1, 4, 8 g of HDS, respectively (1 mℓ min^{-1} constant flow rate and at an inlet concentration of 10 mg $ℓ^{-1}$) were determined (Figure 4.76). The breakthrough time, exhaustion time, and recovery efficiency depend on the bed height (an increase in adsorption capacity with an increase in bed height was observed). An increase in breakthrough time from 60-150 min was observed. An increase in bed height (increase in HDS dosage) delayed exhaustion time from 100-200 min. When bed height is lower (axial dispersion predominated the mass transfer), which reduced diffusion of phosphate resulting in insufficient time for diffusion to occur. Therefore, an increase in bed height makes more intense adsorption efficiency, breakthrough, and exhaustion time (this is due to the availability of active sites on the HDS, as bed height increases with adsorbent dosage) (Table 4.29).

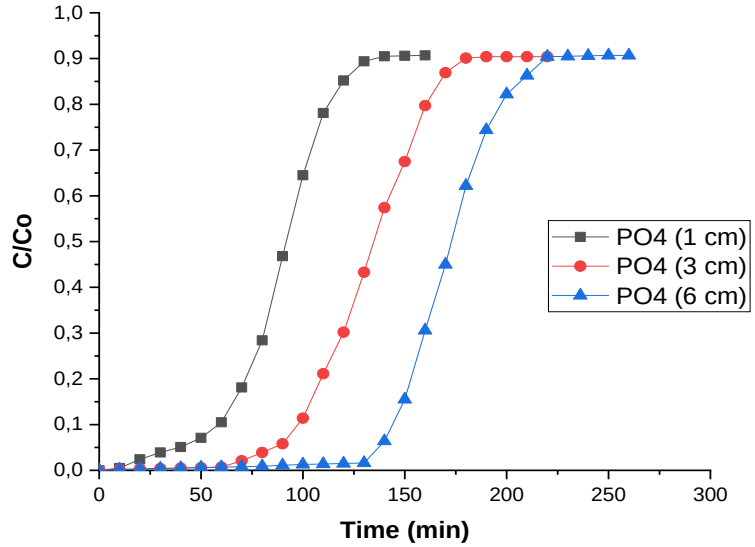

Figure 4.76. Effect of bed height (HDS particle size = 10 µm, pH = 4.03, concentration = 10 mg $ℓ^{-1}$, flow rate = 1 mℓ min^{-1}).

Table 4.29. Fixed bed column parameters for adsorption of P-PO_4^{3-} onto HDS at varying bed height of 1, 3 and 6 cm (concentration = 10 mg $ℓ^{-1}$, flow rate = 1 mℓ min^{-1}, temp = 25 ºC)

Bed height (cm)	Anions	t_{br} (min)	t_{ex} (min)	V_{ef} (mℓ)	Z_m (cm)	Removal efficiency (%)
1	PO_4^{3-}	100	140	1400	5.46	93.73
3	PO_4^{3-}	140	210	2100	5.22	97.44
6	PO_4^{3-}	160	230	2300	4.46	99.88

4.11.3 Effect of flow rate

The flow rate in a continuous fixed-bed column controls retention time and the adsorbate-adsorbent interaction. Breakthrough curves at various flow rates (1, 3, 5 mℓ min^{-1}) at constant inlet concentration (10 mg $ℓ^{-1}$) and a bed height of 6 cm were determined (Figure 4.77). Assessment of the effect of flow rate was conducted and the results showed that breakthrough time, exhaustion time, and adsorption percentage declined as the flow rate increased from 1 to 5 mℓ min^{-1}. The breakthrough time of P-PO_4^{3-} was observed from 50-100 min and exhaustion time also followed a similar selectivity sequence (this may be due to insufficient retention time), from 80-150 min for phosphates. It was observed that at low flow rate, retention time increased due to increased adsorbate-adsorbent interaction. The best performance of the bed column was observed at a flow rate of 1 mℓ min^{-1} and this means that when the flow rate increases, diffusion of phosphate decreases (Table 4.30).

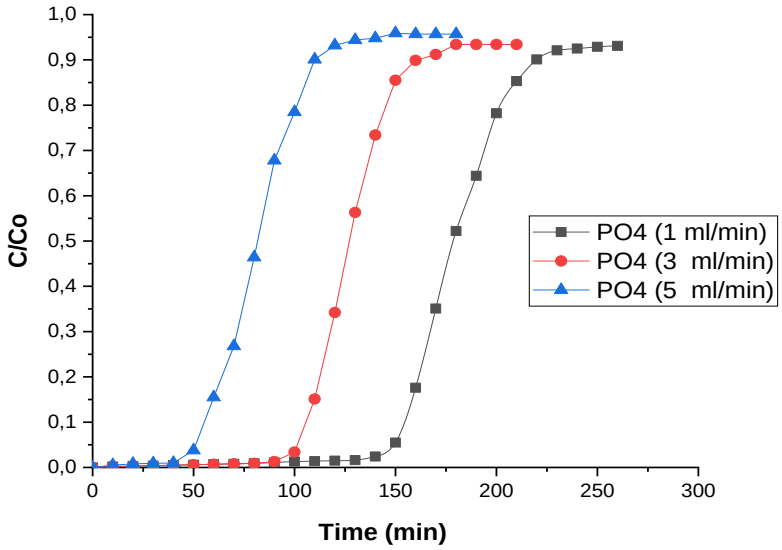

Figure 4.77. Effects of flow rate (HDS particle size = 10 µm, concentration = 10 mg ℓ^{-1}, pH = 4.03, bed height = 6 cm)

Table 4.30. Fixed-bed column parameters for adsorption of P-PO_4^{3-} onto HDS at varying flow rate of 1, 3 and 5 mℓ min^{-1} (concentration = 10 mg ℓ^{-1}, bed height = 6 cm, temp = 25 ºC)

Flow rate (mℓ min^{-1})	**Anions**	**t_{br} (min)**	**t_{ex} (min)**	**V_{ef} (mℓ)**	**Z_m (cm)**	**Removal efficiency (%)**
1	PO_4^{3-}	90	170	1700	5.21	99.52
3	PO_4^{3-}	60	110	1100	4.29	96.31
5	PO_4^{3-}	180	360	3600	6.50	83.46

4.11.4 Parameters of the sorption models

The Thomas, Yoon–Nelson, Adams-Bohart, and Bed depth service time (BDST) models were fitted with acquired column experimental data (inlet P-PO_4^{3-} concentration, bed height, and flow rate). The best results for breakthrough and adsorption percentages were obtained at a bed height of 6 cm, flow rate of 1 mℓ min^{-1}, and the inlet concentration of 10 mg ℓ^{-1}. The fitting of the best experimental data on the models was interpreted based on the correlation coefficient (R^2) value. An R^2 value (greater or equal to 0.997) was the best reference for assessing the best fit of column experimental data on the models applied in this study (Table 4.31).

Table 4.31. Thomas, Yoon–Nelson, Adams-Bohart models and Bed depth service time model parameters for the adsorption of P-PO_4^{3-} onto HDS at varying bed heights (1, 3 and 6 cm), flow rates (1, 3 and 5 mℓ min^{-1}), and inlet concentration (10, 50, 100 mg ℓ^{-1}).

		Thomas model		
Parameters	Anion	k_{Th} * 10^{-5} (mℓ min^{-1} mg)	q_o (mg g^{-1})	R^2
Bed height (cm)				
1	PO_4^{3-}	0.0038	240	0.978
3	PO_4^{3-}	0.0013	324	0.986
6	PO_4^{3-}	0.0014	430	0.995
Initial conc. (mg ℓ^{-1})				
10	PO_4^{3-}	0.0096	120	0.998
50	PO_4^{3-}	0.0096	320	0.989
100	PO_4^{3-}	0.0089	510	0.967

Flow rate (mℓ min^{-1})				
1	PO_4^{3-}	0.0013	420	0.998
3	PO_4^{3-}	0.0044	540	0.972
5	PO_4^{3-}	0.0047	660	0.958
		Adams-Bohart model		
Parameters	Anion	k_{AB} (L/mg min)	N_o (mg ℓ$^{-1}$)	R^2
Bed height (cm)				
1	PO_4^{3-}	0.0042	350	0.985
3	PO_4^{3-}	0.0014	425	0.987
6	PO_4^{3-}	0.0011	530	0.995
Initial conc. (mg ℓ$^{-1}$)				
10	PO_4^{3-}	0.0098	320	0.998
50	PO_4^{3-}	0.0095	520	0.939
100	PO_4^{3-}	0.0091	610	0.876
Flow rate (mℓ min^{-1})				
1	PO_4^{3-}	0.0012	320	0.996
3	PO_4^{3-}	0.0045	440	0.951
5	PO_4^{3-}	0.0045	560	0.902
		Yoon-Nelson model		
Parameters	Anion	k_{YN} * 10^{-3} (L/mg min)	τ (min^{-1})	R^2
Bed height (cm)				
1	PO_4^{3-}	0.023	145	0.896
3	PO_4^{3-}	0.076	265	0.954
6	PO_4^{3-}	0.083	475	0.991
Initial conc. (mg ℓ$^{-1}$)				
10	PO_4^{3-}	0.093	395	0.987
50	PO_4^{3-}	0.091	335	0.942
100	PO_4^{3-}	0.082	245	0.914
Flow rate (mℓ min^{-1})				
1	PO_4^{3-}	0.089	320	0.997
3	PO_4^{3-}	0.082	260	0.975
5	PO_4^{3-}	0.072	205	0.868

Bed depth service time (BDST) model

Anion	k_a (L/mg min)	N_o (mg ℓ$^{-1}$)	R^2
PO_4^{3-}	0.0022	140.43	0.998

Based on R^2 values for the models, the Adams-Bohart, Yoon-Nelson and bed depth service time models fitted experimental data better. The Yoon-Nelson model indicates that the rate of adsorption decreases in the probability of sorption of each P-PO_4^{3-} ion in the inlet solution. The adsorption of each P-PO_4^{3-} ion is proportional to the probability of the sorbate adsorption and sorbate breakthrough on HDS. The BDST assumes that experimental data follows a linear relationship between bed height and service time on column adsorption models (adsorption of P-PO_4^{3-} onto HDS was assumed to be controlled by surface chemistry between the P-PO_4^{3-} and availability of adsorption active sites). Based on computational simulations, a strong dependency (influenced by pH) of P-PO_4^{3-} adsorption on the HDS surface was observed. Adsorption efficiency of P-PO_4^{3-} was based on the surface charge of the HDS and the different types of P-PO_4^{3-} species at different pH as found in different forms based on the pH of the solution ($H_2PO_4^-$ = 4.03, HPO_4^{2-} = 7.02 and PO_4^{3-} = 12.43). When hydrogen ion activity increases, P-PO_4^{3-} adsorption decreases because the hydroxyl ion (OH^-) competes with divalent anions for the active sites. A high adsorption capacity occurs at pH levels ranging from 3-4 (as was confirmed by simulation studies previously). The hydroxyl group in the HDS matrix bond with P-

PO_4^{3-} ion as the surface becomes positively charged (H^+ ion is introduced to HDS surface) and this since P-PO_4^{3-} ion complexation varies with the type of adsorbent (sorbents have different functional groups) and pH of the solution. The effect of pH can also be explained in terms of pH_{Pzc} (a point where the surface positively or negatively charged functional groups no longer affect the pH of the solution). The pH_{Pzc} in HDS is 4.5 and this means that surface charge below 4.5 is positive and above 4.5 is negative.

4.11.5 Desorption studies

Potential release of phosphate from HDS was assessed through desorption studies. Desorption with 0.1 mol ℓ^{-1} NaOH gave better results, just above 99% removal efficiency for a breakthrough time of 130 min and exhaustion time of 220 min. Desorption data indicate that desorption capacity of P-PO_4^{3-} from HDS increased as OH^- ions are introduced into the solution. The reaction is likely an anion exchange, with OH^- replacing phosphate on the adsorbent surface.

4.11.6 Conclusion

Adsorption studies in a fixed-bed column for adsorption of P-PO_4^{3-} from sewage water by HDS was assessed. The HDS is positively charged at lower pH and this favours adsorption of phosphate. This was observed to occur best at optimised parameters of solution pH of 4.03, bed height = 6 cm, inlet phosphate concentration = 10 mg ℓ^{-1}, and flow rate of 1 mℓ min^{-1}. These parameters were established from computational simulations, thus underpinning the importance of this approach in experimental design. Breakthrough curves indicated that breakthrough points were achieved at later times for reduced flow rates, lower inlet concentration and increased bed height. The Yoon-Nelson, Adams-Bohart, and BDST models better described the desorption process. The BDST gives better insight as it relates service time to the exhaustion of the adsorbent.

Desorption studies showed that high removal efficiency of phosphate can be achieved by using 0.1 mol ℓ^{-1} NaOH. Further studies would be required to explore other desorbing agents that would closely simulate conditions under which phosphate laden HDS would be used.

CHAPTER 5: CONCLUSIONS & RECOMMENDATIONS

5.1 CONCLUSIONS

High density sludge (HDS) remains after treatment of acid mine drainage (AMD) with no end use. Disposal of this HDS is quite a challenge, as it may be a secondary source of pollution and to prevent this, one of the key questions the study sought to address was the possibility of repurposing of sludge generated and discharged from AMD treatment. Thus, part of the study focused on understanding the characteristics of HDS generated at an AMD treatment plant and its potential for use as an adsorbent (in both batch and column experimental modes) for contaminants in mine water as well as in phosphate containing wastewater. The other key question was on whether more value could be derived from AMD treatment beyond just repurposing the bulk HDS currently generated. Thus, an innovative idea was considered that aimed at exploring the possibility of having a separate stream in the flow process for treatment of AMD in which selective precipitation of valuable ochres could be done.

In both cases above, another question was addressed that aimed at assessing capabilities of computational simulations (based on the PHREEQC geochemical modelling code) for establishing experimental parameters as well as giving insights into the solution chemistry.

This study came up with the following general conclusions:

- Optimisation of parameters for use in small- and large-scale applications can be achieved using computational simulations. This was found to be an attractive approach as it has potential to reduce time-consuming and expensive experimental trials. Further, more insights about the chemistry of processes under study can be obtained that are usually not possible from conventional experimental work.
- Simulations helped in exploring the possibility of deriving value from the current AMD treatment process by selectively precipitating ochreous minerals. Experimental trials based on these simulations yielded ochres with varying colours e.g. yellow, brown, red and turquoise that matched their commercial counterparts when applied to artwork. Application of these ochres as pigments in paint still remains a subject of study. This will be important in driving production of high volumes, which will in turn make the treatment process viable.
- Simulations also helped in understanding the chemistry of AMD and processes governing interactions of AMD and high density sludge (HDS). This provided informed platforms for designing batch and column experimental studies.
- Both batch and column studies indicated the potential of repurposing HDS as an adsorbent for removal of trace elements from AMD as a way to condition and pretreat it before introduction to the main neutralisation process. This is important in that it provides the possibility of applying HDS in abandoned mine voids and shafts from where AMD is pumped and allow for *in situ* treatment.
- Repurposing of HDS was extended to removal of inorganic phosphate in contaminated water with the intention to use the phosphate laden HDS as an amendment in woodlots on mine tailings. The results were very promising, but further studies would be required to obtain slow release of phosphate when it is applied in this context and also this will have to be considered in conjunction with potassium and nitrogen if its fertiliser value has to be realised.

5.2 RECOMMENDATIONS

The following recommendations would be important to consider:

- Use of computational simulations would be important to consider as they also provide extended use in understanding processes e.g. exploring the efficiency of mixtures of neutralising agents beyond just their uses as individual entities. Different mixing ratios can be simulated to assess the quality of treated water and precipitates that would likely form. Many scenarios can be modelled from which important information about the AMD treatment process can be gleaned and used for process improvement or other innovation.
- Apart from deriving further value from the neutralisation process of AMD, attention should also be focused on deriving more value from the treated water. The very elevated sulphate concentrations can be treated with appropriate biological methods such as those involving sulphate-reducing bacteria to produce valuable elemental sulphur. This would likely be of better quality than that produced from AMD because of reduced concentrations of cations and trace elements.

- Evidence of natural production of sulphur following discharge of treated water into streams is apparent, particularly in wetland areas where patches of yellowish sulphur solids tend to form. This is, in part, as a result of the presence of sulphate-reducing bacteria in these areas. Thus, it would be more appropriate to explore the possibility of adding a unit for this process to occur in the plant before the water is finally discharged.

REFERENCES

ABDULRAZAK S, SULYMAN YI, BELLO HI, AKANNI AS, ONIWAPELE YA., and MUKTARI M (2015). Tannery wastewater treatment using activated carbon from Moringa oleifera pods. *J Environ Sci Toxicol Food Technol*, 12, 96-99. DOI: 10.9790/2402-091219699.

ABEL-DENEE M, ABBOTT T, and ESKICIOGLU C (2018). Using mass struvite precipitation to remove recalcitrant nutrients and micropollutants from anaerobic digestion dewatering centrate. *Water Res*. 132, 292–300. http://dx.doi.org/10.1016/j.watres.2018.01.004.

ABREU MM, SANTOS ES, MAGALHÃES MC, and BATISTA MJ (2012). São Domingos mine wastes phytostabilization using spontaneous plant species. In: Batista, M.J , Matos JX, Oliveira D, Abreu MM, Figueiredo MO, Quental L, Africano F, Branquinho C, Pena T, Santana H, Pereira Z, Silva TP, Santana H, Matielli N (editors), Field Guide-book: Multidisciplinary Contribution for Environmental Characterization and Improvement at the S. Domingos Mining Site. 9th ISEG–International Symposium of Environmental Geochemistry, Aveiro , 42–49.

ADAMSON RJ (1972). The Chemistry of the Extraction of Gold from its Ores, Gold Metallurgy in South Africa, Cape and Transvaal Printers, Ltd., Cape Town, South Africa.

AGUIAR AO, ANDRADE LH, RICCI BC, PIRES WL, MIRANDA GA, AND AMARAL MC (2016). Gold acid mine drainage treatment by membrane separation processes: an evaluation of the main operational conditions. *Sep. Purif. Technol*. 170, 360-369. DOI: 10.1016/j.seppur.2016.07.003.

AGUIAR A, ANDRADE L, GROSSI L, PIRES W, and AMARAL M (2018). Acid mine drainage treatment by nanofiltration: a study of membrane fouling, chemical cleaning, and membrane ageing. *Sep. Purif. Technol*. 192, 185-195. DOI: 10.1016/j.seppur.2017.09.043.

AHAMED MI, and LICHTFOUSE E (2020). Water Pollution and Remediation: Heavy Metals. In: Inamuddin, Mohd Imran Ahamed, Eric Lichtfouse (editors) *Springer*. ISBN: 978-3-030-52421-0, Netherlands, 20-35.

AHMED SF, MOFIJUR M, NUZHAT S, CHOWDHURY AT, RAFA N, UDDIN MA, INAYAT A, MAHLIA TMI, ONG HC, CHIA WY, and SHOW PL (2021). Recent developments in physical, biological, chemical, and hybrid treatment techniques for removing emerging contaminants from wastewater. J*. Hazard Mater*. 416, 125912. https://doi.org/10.1016/j.jhazmat.2021.125912.

AKCIL A, and KOLDAS S (2006). Acid Mine Drainage (AMD): causes, treatment and case studies. *J. Clean. Prod*. 14, 1139-1145. https://doi.org/10.1016/j.jclepro.2004.09.006.

AKINWEKOMI V, (2017). Formation of magnetite during desalination of Acid Mine Drainage. D. Tech thesis, Tshwane University of Technology.

AKINWEKOMI V, MAREE JP, ZVINOWANDA CM, and MASINDI V (2017). Synthesis of magnetite from iron-rich mine water using sodium carbonate. *J. Environ. Chem. Eng.* 5, 2699-2707. http://dx.doi.org/10.1016/j.jece.2017.05.025.

AKINWEKOMI V, MAREE JP, MASINDI V, ZVINOWANDA C, OSMAN MS, FOTEINIS S, MPENYANA-MONYATSI L, and CHATZISYMEON E (2020). Beneficiation of acid mine drainage (AMD): a viable option for the synthesis of goethite, hematite, magnetite, and gypsum – Gearing towards a circular economy concept. *Miner. Eng*. 148, 106204. https://doi.org/10.1016/j.mineng.2020.106204.

ALAM MS, GORMAN-LEWIS D, CHEN N, FLYNN SL, OK YS, and KONHAUSER KO (2018).Thermodynamic analysis of nickel(II) and zinc(II) adsorption to biochar. *Environ. Sci. Technol*. 52 (11), 6246–6255. DOI: 10.1021/acs.est.7b06261.

ALBANESE S, DE VIVO B, LIMA A, FRATTASIO G, KRÍBEK B, NYAMBE I, AND MAJER V (2014). Prioritising environmental risk at the regional scale by a GIS aided technique: the Zambian Copperbelt Province case study*. J. Geochem. Explor.* 144, 433-442. https://doi.org/10.1016/j.gexplo.2014.03.014.

ALI H, and KHAN E (2018). Assessment of potentially toxic heavy metals and health risks in water, sediments, and different fish species of River Kabul, Pakistan. *Hum. Ecol. Risk Assess*. 24(3):1-18. DOI: 10.1080/10807039.2018.1438175.

ALI H, KHAN E, and ILAHI I, (2019). Environmental chemistry and ecotoxicology of hazardous heavy metals: environmental persistence, toxicity, and bioaccumulation. *J. Chem*. 67, 30-35. DOI: 10.1155/2019/6730305.

ALLISON LM, and MARGARET EW (2015). Investigation into the use of cement kiln dust in high density sludge (HDS) treatment of acid mine water. *Water Res*, 85, 443-450. DOI: 10.1016/j.watres.2015.08.056.

ALLOWAY BJ (2013). Sources of heavy metals and metalloids in soils. In: Alloway, B.J. (editors), Heavy Metals in Soils: Trace Metals and Metalloids in Soils and Their Bioavailability, Environmental Pollution. Springer Netherlands, Dordrecht, 11–50. DOI: 10.1007/978-94-007-4470-72.

ALSLAIBI TM, ABUSTAN I, AHMAD MA, and FOUL AA (2013). Cadmium removal from aqueous solution using microwaved olive stone activated carbon. *J. Environ. Chem. Eng*. 1 (3), 589–599. DOI: 10.1016/j.jece.2013.06.028.

AMANN A, ZOBOLI O, KRAMPE J, RECHBERGER H, ZESSNER M, and EGLE L (2018). Environmental impacts of phosphorus recovery from municipal wastewater. *Resour. Conserv. Recycl*. 130, 127-139. https://doi.org/10.1016/j.resconrec.2017.11.002.

AMBIADO K, BUSTOS C, SCHWARZ A., and BÓRQUEZ R, (2017). Membrane technology applied to acid mine drainage from copper mining. *Water Sci. Technol*. 75, 705–715. DOI: 10.2166/wst.2016.556.

ANAWAR HM, (2015). Sustainable rehabilitation of mining waste and acid mine drainage using geochemistry, mine type, mineralogy, texture, ore extraction and climate knowledge. *J. Environ. Manag*. 158, 111-121. https://doi.org/10.1016/j.jenvman.2015.04.045.

ANDALAF J, SCHWARZ A, PINO L, FUENTES P, BORQUEZ R, and AYBAR, M (2018). Assessment and modelling of nanofiltration of acid mine drainage. *Ind. Eng. Chem. Res*. 57, 14727-14739. https://doi.org/10.1021/acs.iecr.8b03576.

ANDERSSON K, ROSEMARIN A, LAMIZANA B, KVARNSTROM E, MCCONVILLE J, SEIDU R, DICKIN S, and TRIMMER C (2016). Sanitation, Wastewater Management, and Sustainability: from Waste Disposal to Resource Recovery. United Nations Environment Programme and Stockholm Environment Institute, Caspar Trimmer (editor) Nairobi, and Stockholm. ISBN: 978-92-807-3488-1.

AGANGI, A., HOFMANN, A., ROLLION-BARD, C., MARIN-CARBONNE, J., CAVALAZZI, B., LARGE, R., and MEFFRE, S. (2015). Gold accumulation in the Archaean Witwatersrand Basin, South Africa - Evidence from concentrically laminated pyrite. Earth Sci. Rev., 140, 27-53.

ANNA B, KLEOPAS M, CONSTANTINE S, ANESTIS F, and MARIA B (2014). Adsorption of Cd(II), Cu(II), Ni(II) and Pb(II) onto natural bentonite: study in mono- and multi-metal systems. *Environ. Earth. Sci*. 73, 5435-5444. DOI 10.1007/s12665-014-3798-0.

ANTELO J, AVENA M, FIOL S, LOPEZ R, and ARCE F (2005). Effects of pH and ionic strength on the adsorption of phosphate and arsenate at the goethite-water interface. *J. Colloid Interface Sci*. 285, 476-486. DOI: 10.1016/j.jcis.2004.12.032.

ANTWI-AGYEI P, HOGARH JN, and FOLI G (2009). Trace elements contamination of soils around gold mine tailings dams at Obuasi, Ghana*. Afri. J. Environ. Sci. Technol*. 3(11), 353-359. http://www.academicjournals.org/ajest.

ARROYAVE JM, PUCCIA V, ZANINI GP, and AVENA MJ (2018). Surface speciation of phosphate on goethite as seen by InfraRed Surface Titrations (IRST). Spectrochim. Acta. A: *Mol. Biomol. Spectrosc*. 199, 57-64. Doi: 10.1016/j.saa.2018.03.043.

ASCOTT MJ, GOODDY DC, LAPWORTH DJ, and STUART M.E (2016). Estimating the leakage contribution of phosphate dosed drinking water to environmental phosphorus pollution at the national-scale. *Sci. Total Environ*. 572, 1534–1542. Doi: 10.1016/j.scitotenv.2015.12.121.

ATIBU EK, DEVARAJAN N, LAFFITE A, GIULIANI G, SALUMU JA, MUTEB RC, MULAJI CK, OTAMONGA JP, ELONGO V, MPIANA PT, and POTÉ J (2016). Assessment of trace metal and rare earth elements contamination in rivers around abandoned and active mine areas. Chemie der Erde Geochemistry. 76, 353–362. https://doi.org/10.1016/j.chemer.2016.08.004.

AUBERTIN, M, BRUNO B, PABST T, JAMES M, and MBONIMPA M (2016). Review of the Reclamation Techniques for Acid-Generating Mine Wastes upon Closure of Disposal Sites. Geo-Chicago 2016, Chicago, Illinois. DOI: 10.1061/9780784480137.034.

AYANGBENRO AS, and BABALOLA OO (2017). A new strategy for heavy metal polluted environments: A review of microbial biosorbents. *Int. J. Environ. Res*. Public Health 14 (1), 94. DOI: 10.3390/ijerph14010094.

AYDIN H, BULUT Y, and YERLIKAYA C (2008). Removal of copper (II) from aqueous solution by adsorption onto low-cost adsorbents, *J. Environ. Manag*. 87, 37–45. DOI: 10.1016/j.jenvman.2007.01.005.

AYORA C, MACÍAS F, TORRES E, LOZANO A, CARRERO S, NIETO JM, PEREZ-LOPEZ R, FERNANDEZ-MARTÍNEZ A, and CASTILLO-MICHEL H (2016). Recovery of rare earth elements and yttrium from passive-remediation systems of acid mine drainage. *Environ. Sci. Technol*. 50, 8255-8262. DOI: 10.1021/acs.est.6b02084.

BABEL S, and KURNIAWAN TA (2003). Low-cost adsorbents for heavy metals uptake from contaminated water: a review, *J. Hazard. Mater.* 97 (1-3), 219-243. https://doi.org/10.1016/S0304-3894(02)00263-7.

BADHURAHMAN A, GAUTAMA RS, and KUSUMA GJ (2020). REE Enrichment Pattern in Acid Mine Drainage and Overburden from Coal Mine in Indonesia, Pope, J.; Wolkersdorfer, Ch.; Weber, A.; Sartz, A.; Wolkersdorfer, K. (editors). – In: Proceedings of International Mine Water Association Congress, New Zealand. 1-7. http://nsi.psu.ru/labs/gtp/stat/2020/570.

BAI H, KANG Y, QUAN H, HAN Y, SUN J, AND FENG Y (2013). Treatment of acid mine drainage by sulfate reducing bacteria with iron in bench scale runs. *Bioresour. Technol*. 128, 818-822. DOI: 10.1016/j.biortech.2012.10.070.

BAI J, YE X, JIA J, ZHANG G, ZHAO Q, CUI B, and LIU X (2017). Phosphorus sorption-desorption and effects of temperature, pH, and salinity on phosphorus sorption in marsh soils from coastal wetlands with different flooding conditions. *Chemosphere* 188, 677-688. https://doi.org/10.1016/j.chemosphere.2017.08.117.

BAKATULA E, and TUTU H (2016). Characterization and speciation modelling of cyanide in effluent from an active slimes dam. *S. Afr. J. Chem*., 69: 140–147. DOI: 10.17159/0379-4350/2016/v69a00.

BAKATULA EN, CUKROWSKA EM, CHIMUKA L, and TUTU H (2012). Characterization of cyanide in a natural stream impacted by gold mining activities in the Witwatersrand Basin, South Africa. *Toxicolological and Environmental Chemistry*, 94(1), 7-19. DOI: 10.1080/02772248.2011.638637.

BÁLINTOVÁ M, and SINGOVSZKÁ E (2011). Acid mine drainage as environmental risk for surface water. 11th International Multidisciplinary Scientific Geoconference and EXPO – Modern Management of Mine Producing, Geology and Environmental Protection, SGEM, 3, 175-182. DOI: 10.5593/SGEM2011/S20.104.

BARNICOAT, A., HENDERSON, I.H.C., KNIPE, R.J., YARDLEY, B.W.D., NAPIER, R.W., FOX, N.P.C., KENYON, A.K., MUNTINGH, D.J., STRYDOM, D., WINKLER, K.S., LAWRENCE, S.R. and CORNFORD, C., (1997). Hydrothermal gold mineralization in the Witwatersrand Basin. Nature V.386, 820-823.

BEUCHER A, ADHIKARI K, BREUNING-MADSEN H, GREVE MB, ¨OSTERHOLM P, FROJDO S, JENSEN NH, GREVE, MH (2017). Mapping potential acid sulfate soils in Denmark using legacy data and LiDAR-based derivatives. Geoderma 308, 363–372. https://doi.org/10.1016/j.geoderma.2016.06.001.

BEJAN D, AND BUNCE NJ (2015). Acid mine drainage: electrochemical approaches to prevention and remediation of acidity and toxic metals*. J Appl Electrochem* 45, 1239-1254. https://doi.org/10.1007/s10800-015-0884-2.

BENAVENTE M, MORENO L, and MARTINEZ J (2011). Sorption of potentially toxic trace metals from gold mining wastewater using chitosan. *J Taiwan Inst Chem Eng*., 42(6): 976-988. DOI: 10.1016/j.jtice.2011.05.003.

BENNER SG, BLOWES DW, PTACEK CJ, and MAYER KU (2002). Rates of sulfide reduction and metal sulfide precipitation in a permeable reactive barrier. *Appl Geochem*. 17, 301–320. DOI: 10.1016/S0883-2927(01)00084-1.

BHARGAVA A, CARMONA FF, BHARGAVA M, and SRIVASTAVA S (2012). Approaches for enhanced phytoextraction of heavy metals. *J. Environ. Manag*. 105, 103–120. DOI: 10.1016/j.jenvman.2012.04.002.

BINNEMANS K, JONES, PT, BLANPAIN B, VAN GERVEN T, YANG Y, WALTON A, and BUCHERT M (2013). Recycling of rare earths: a critical review. *J. Clean. Prod*. 51,1-22. https://doi.org/10.1016/j.jclepro.2012.12.037.

BLOWES DW, PTACEK CJ, JAMBOR JL, WEISENER CG, PAKTUNC D, GOULD WD and JOHNSON DB (2014). The Geochemistry of acid mine drainage. In: Holland, HD. and Turekian, KK. (editors). Treatise on Geochemistry (Second Edition). Oxford: Elsevier, 11, 131−190. https://doi.org/10.1016/B978-0-08-095975-7.00905-0.

BOLOGO V, MAREE JP, and ZVINOWANDA, CM, (2009). Treatment of acid mine drainage using magnesium hydroxide. In Proceedings of the International Mine Water Conference, Pretoria, South Africa, 19-23. ISBN Number: 978-0-9802623-5-3.

BONNAIL E, CUNHA LIMA R, BAUTISTAECHAMIZO, E, SALAMANCA MJ, and CRUZ-HERNANDEZ P (2018). Biomarker responses of the freshwater clam Corbicula fluminea in acid mine drainage polluted systems*. Environ. Pollut*. 242, 1659-1668. Doi: 10.1016/j.envpol.2018.07.111.

BONNAIL E, PEREZ-LOPEZ R, SARMIENTO AM, NIETO JM, and DELVALLS TA (2017). A novel approach for acid mine drainage pollution biomonitoring using rare earth elements bioaccumulated in the freshwater clam Corbicula fluminea. *J. Hazard Mater*. 338, 466-471. DOI: 10.1016/j.jhazmat.2017.05.052.

BONNELYE V (2015). Acid Mine Drainage: Case Study of One of the Largest Copper Mine Sites in the World. SUEZ Environment Australia, Sydney, NSW, OZ Water. https://scholar.google.com/scholar.

BOUKHALFA C, and CHAGUER M (2012). Characterisation of sediments polluted by acid mine drainage in the northeast of Algeria*. Int. J. Sediment Res*. 27, 402-407. DOI: 10.1016/S1001-6279(12)60045-6.

BRAHAITA ID, POP IC, BACIU C, MIHAIESCU R, MODOI C, POPITA G, and TRUTA RM (2017). The efficiency of limestone in neutralizing acid mine drainage - A laboratory study. Caprath. *J. Earth. Env*. 12 (2), 347–356. https://www.researchgate.net/publication/309209993.

BRINDHA K, PAVELIC P, and SOTOUKEE T (2017). Geochemical characteristics and groundwater quality in the vientiane plain. Laos Expo Health 9, 89–104. https://doi.org/10.1007/s12403-016-0224-8.

BUNCE JT, NDAM E, OFITERU ID, MOORE A, and GRAHAM DW (2018). A review of phosphorus removal technologies and their applicability to small-scale domestic wastewater treatment systems. Front. *Environ. Sci*. 6, 1–15. https://doi.org/10.3389/fenvs.2018.00008.

BUSSIERE B, (2009). Acid mine drainage from abandoned mine sites: problematic and reclamation approaches. In: Proc. of Int. Symp. on Geoenvironmental Eng. ISGE 2009 September 8-10. Hangzhou. 111-125. DOI:10.1007/978-3-642-04460-16.

BUZZI DC, VIEGAS LS, RODRIGUES MAS, BERNARDES AM, AND TENORIO JAS (2013). Water recovery from acid mine drainage by electrodialysis. *Min. Eng*. 40, 82-89. https://doi.org/10.1016/j.mineng.2012.08.005.

CAMDEN-SMITH B, PRETORIUS N, TURTON A, CAMDEN-SMITH P, and TUTU, H (2015). Chemical Transformations of Metals Leachings from Gold Tailings. Paper presented at the Agreeing on solutions for more sustainable mine water management-Proceedings of the 10th ICARD and IMWA Annual Conference, Santiago, Chile. https://www.researchgate.net/publication/302592866.

CARRERO S, PEREZ-LOPEZ R, FERNANDEZ-MARTINEZ A., CRUZ-HERNANDEZ P, AYORA C, AND POULAIN A (2015). The potential role of aluminium hydroxysulphates in the removal of contaminants in acid mine drainage. *Chem. Geol*. 417, 414-423. https://doi.org/10.1016/j.chemgeo.2015.10.020.

CAROLIN CF, KUMAR PS, SARAVANAN A, and JOSHIBA GJ (2017). Efficient techniques for the removal of toxic heavy metals from an aquatic environment: *J. Environ. Chem. Eng*. 5, 2782–2799. https://doi.org/10.1016/j.jece.2017.05.029.

CHEN H, ZHANG J, TANG L, SU M, TIAN D, and ZHANG L (2019). Enhanced Pb immobilization via the combination of biochar and phosphate solubilizing bacteria. *Environ. Int*. 127, 395–401. https://doi.org/10.1016/j.envint.2019.03.068.

CHEN HY, TENG YG, LU SJ, WANG YY, and WANG JS, (2015). Contamination features and health risk of soil heavy metals in China. *Sci. Total Environ*. 513, 143-153. https://doi.org/10.1016/j.scitotenv.2015.01.025.

CHEN X (2015). Modeling of experimental adsorption isotherm data. Information, 6(1), 14–22. https://doi.org/10.3390/info6010014.

CHEN T, YAN B, LEI C, and XIAO X (2014). Pollution control and metal resource recovery for acid mine drainage. *Hydrometallurgy* 12, 147-148. DOI: 10.1016/j.hydromet.2014.04.024.

CHEN SG, and YANG RT (1994). The theoretical basis for the potential theory adsorption isotherms. The Dubinin-Radushkevich and Dubinin-Astakhov equations. Langmuir, 10(11), 4244–4249. https://doi.org/10.1021/la00023a054.

CHENG H, HU Y, LUO J, XU B, and ZHAO J (2009). Geochemical processes controlling fate and transport of As in acid mine drainage (AMD) and natural systems. *J. Hazard. Mater*, 165, 13-26. DOI: 10.1016/j.jhazmat.2008.10.070.

CHEN M, SHAFER-PELTIER K, RANDTKE SJ, and PELTIER E (2018). Competitive association of cations with poly(sodium 4-styrenesulfonate) (PSS) and heavy metal removal from water by PSS-assisted ultrafiltration*. J. Chem. Eng*. 344, 155–164. https://doi.org/10.1016/j.cej.2018.03.054.

CHEONG Y, HUR W, YIM G, JI S, and SEO E (2016). Evaluation of neutralization precipitation process of acid mine drainage using a process simulator. *J. Kor. Soc. Min. Energy Resour. Eng.* 53 (1), 1-9. https://www.jksmer.or.kr/articles/article/0POj/.

CHESTERS S, MORTON P, and FAZEL M (2016). Membranes and Mine Water-Waste or Revenue Stream, Mining Meets Water-Conflicts and Solutions. IMWA, Freiberg, Germany, 1310-1322.

CHITRAKAR R, TEZUKA S, SONODA A, SAKANE K, OOI K, and HIROTSU T, (2006). Phosphate adsorption on synthetic goethite and akaganeite. *J. Colloid Interface Sci*. 298, 602-608. https://doi.org/10.1016/j.jcis.2005.12.054.

CHOPARD A, BENZAAZOUA M, BOUZAHZAH H, PLANTE B, and MARION P (2017). A contribution to improve the calculation of the acid generating potential of mining wastes*. Chemosphere* 175, 97-107. https://doi.org/10.1016/j.chemosphere.2017.02.036.

CHUBAR NI, KANIBOLOTSKYY VA, STRELKO VV, GALLIOS GG, SAMANIDOU VF, SHAPOSHNIKOVA TO, MILGRANDT VG, and ZHURAVLEV IZ (2005). Adsorption of phosphate ions on novel inorganic ion exchangers. Colloids and Surfaces A: *Physicochem. Eng. Aspects*, 255, 55-53. https://doi.org/10.1016/j.colsurfa.2004.12.015.

CIFUENTES L, GARCÍA I, ORTIZ, R, and CASAS, JM (2006). The use of electrohydrolysis for the recovery of sulphuric acid from copper-containing solutions*. Sep. Purif. Technol*. 50, 167-174. https://doi.org/10.1016/j.seppur.2005.11.021.

CLYDE EJ, CHAMPAGNE P, JAMIESON HE, GORMAN C, and SOURIAL J (2016). The use of a passive treatment system for the mitigation of acid mine drainage at the Williams Brothers Mine (California): pilot-scale study. *J. Clean. Prod*. 130, 116-125. https://doi.org/10.1016/j.jclepro.2016.03.145.

COETZEE H, HOBBS PJ, and BURGESS JE (2010). Mine water management in the Witwatersrand Gold fields with special emphasis on acid mine drainage. Study to the Inter-ministerial Committee on Acid Mine Drainage, 1-128. https://www.researchgate.net/publication/263067382.

COZZOLINO D, CHANDRA S, ROBERTS J, POWER A, RAJAPAKSHA P, BALL N, and GORDON R, CHAPMAN J (2018). There is gold in them hills: predicting potential acid mine drainage events through the use of chemometrics. *Sci. Total Environ*. 619-620, 1464-1472. DOI: 10.1016/j.scitotenv.2017.11.063.

CRANE RA and SAPSFORD DJ (2018). Selective formation of copper nanoparticles from acid mine drainage using nanoscale zerovalent iron particles. *J. Hazard Mater*. 347, 252-265. https://doi.org/10.1016/j.jhazmat.2017.12.014.

CREED I, LANE CR, SERRAN JN, ALEXANDER LC, BASU NB, CALHOUN AJK, CHRISTENSEN JR, COHEN M, CRAFT C, D'AMICO E, DEKEYSER E, FOWLER L, GOLDEN H, JAWITZ J, KALLA P, KIRKMAN L, LANG M, LEIBOWITZ SG, LEWIS D, SMITH L (2017). Enhancing protection for vulnerable waters. *Nat. Geosc*i. 10, 809–815. DOI: 10.1038/ngeo3041.

CRINI G, and LICHTFOUSE E (2018). Advantages and disadvantages of techniques used for wastewater treatment. *Environ Chem Lett* 17:145–155. DOI: 10.1007/s10311-018-0785-9.

CROWN GOLD RECOVERY (2003). Crown Mines. Crown Gold Recovery, Unpublished internal study, 13.

DANKERT, B., and HEIN, K. (2010). Evaluating the structural character and tectonic history of the Witwatersrand Basin. Precambrian Research, 1-22.

DAVIS JR, CHEN Y, BAYGENTS JC, and FARRELL J (2015). Production of acids and bases for ion exchange regeneration from dilute salt solutions using bipolar membrane electrodialysis. *ACS Sustain. Chem. Eng*. 3 (9), 2337-2342. DOI: 10.1021/acssuschemeng.5b00654.

DEMERS I, BUSSIÈRE B, ROUSSELLE M, AUBERTIN M, PABST T, and LACROIX R (2013). Laboratory evaluation of reclamation scenarios for the spillage areas of the abandoned Manitou site using Goldex tailings. In Proceedings of the 23rd World Mining Congress, Montréal, Que., 11–15 August 2013. https://www.researchgate.net/publication/319916247.

DEMERS I, MBONIMPA M, BENZAAZOUA M, BOUDA M, AWOH S, LORTIE S, and GAGNON M (2017). Use of acid mine drainage treatment sludge by combination with a natural soil as an oxygen barrier cover for mine waste reclamation: laboratory column tests and intermediate scale field tests. *Miner. Eng*. 107, 43-52. https://doi.org/10.1016/j.mineng.2016.11.017.

DEMERS I, BOUDA M, MBONIMPA M, BENZAAZOUA M, BOIS D, and GAGNON M (2015). Valorization of acid mine drainage treatment sludge as remediation component to control acid generation from mine wastes, part 2: Field experimentation*. Miner Eng*. 76, 117-125. https://doi.org/10.1016/j.mineng.2014.10.015.

DENG D, and LIN LS (2013). Two-stage combined treatment of acid mine drainage and municipal wastewater. *Water Sci. Technol*. 67, 1000–1007. DOI: 10.2166/wst.2013.653.

DICKINSON AW, POWER A, HANSEN MG, BRANDT KK, PILIPOSIAN G, APPLEBY P, O'NEILL PA, JONES RT, SIEROCINSKI P, KOSKELLA B, and VOS M (2019). Heavy metal pollution and co-selection for antibiotic resistance: a microbial paleontology approach. *Int. J. Environ. Sci*. 132, 105117. DOI: 10.1016/j.envint.2019.105117.

DIIS (2016). Australian Energy Update 2016. Department of Industry, Innovation and Science (DIIS). 1-32.

DOLD B (2014). Evolution of Acid Mine Drainage Formation in Sulphidic Mine Tailings. *Minerals*, 4, 621–641. DOI: 10.3390/min4030621.

DOLD B (2017). Acid rock drainage prediction: A critical review. *J. Geochem. Explor*. 172,120–132. https://doi.org/10.1016/j.gexplo.2016.09.014.

DUTTA M, ISLAM N, RABHA S, NARZARY B, BORDOLOI M, SAIKIA D, SILVA LFO, and SAIKIA BK (2020). Acid mine drainage in an Indian high-sulfur coal mining area: cytotoxicity assay and remediation study*. J. Hazard. Mater*. 389, 121851. https://doi.org/10.1016/j.jhazmat.2019.121851.

DWIKI S, SHIMADA H, GAUTAMA RS, KUSUMA GJ, SASAOKA T, KOTEN F, and MATSUMOTO S (2015). Evaluation of Acid Mine Drainage Characterization for Predicting Post Drainage Water Quality in Coal Mines, *Miner Eng*. R.16-Nr.2, 23-28. https://www.researchgate.net/publication/319093747.

DZOMBAK DA, and MOREL FMM (1990). Surface Complexation Modeling: Hydrous Ferric Oxide. Wiley-Interscience, New York. 30-56. ISBN: 978-0-471-63731-8.

ELIZABETH RANI C, BALAJI AYYADURAI V, and KAVITHA KK (2021). Bioremediation of heavy metals and toxic chemicals from muttukadu lake, Chennai by biosurfactant and biomass treatment strategies. Bioremediation and Green Technologies. Springer, Cham, 67–85. DOI: 10.1007/978-3-030-64122-16.

ETALE A, TUTU H, and DRAKE DC (2015). Mesoporous silica nanoparticles for the adsorptive removal of Cu(II), Mn(II), and U(VI) from acid mine drainage, *Mine Water Environ*. 34 (2), 231–240. https://doi.org/10.1007/s10230-014-0311-7.

ETTER K, and LANGILL PD (2016). Acid Recycling-Process and Design Notes on Hot-Dip Galvanizing. http://www.galvanizeit.org/images/uploads.

FAN J, CAI C, CHI H, REID BJ, COULON F, and ZHANG Y (2020). Remediation of cadmium and lead polluted soil using thiol-modified biochar. *J. Hazard. Mater*. 388, 122037. DOI: 10.1016/j.jhazmat.2020.122037.

FEATHER CE, and KOEN GM (1975). The mineralogy of the Witwatersrand Reefs. *Minerals Science Engineering*, 7, 189-224. http://sp.lyellcollection.org/.

FERREIRA AR, COUTO N, GUEDES P, PINTO J, MATEUS EP, and RIBEIRO AB (2018). Electrodialytic 2-compartment cells for emerging organic contaminants removal from effluent. *J. Hazard. Mater*. 358, 467–474. DOI: 10.1016/j.jhazmat.2018.04.066.

FILIPEK L, HATTON G, GUSEK J, and TSUKAMOTO T (2003). Passive treatment of acid rock drainage (ARD): state of the practice. Tailings and mine waste'03. Balkeman Publishers, Netherlands, 293. https://semspub.epa.gov/work/01/43547.

FUCHS, S., WILLIAMS-JONES, A., and PRZYBYLOWICZ, W. (2016). The origin of the gold and uranium ores of the Black Reef Formation, Transvaal Supergroup, South Africa. Ore Geol. Rev. v.72, 149-164.

GAIKWARD RW, and GUPTA DV (2008). Review on removal of heavy metals from acid mine drainage. *Appl. Ecol. Environ. Res*. 6, 81-98. DOI: 10.15666/aeer/0603_081098.

GARLAND R (2012). Acid mine drainage: the chemistry. Study, Senior Researcher, CSIR Pretoria. http://researchspace.csir.co.za/dspace/bitstream/handle/10204/5391.

GAUTAM RK, SHARMA SK, MAHIYA S, AND CHATTOPADHYAYA MC (2014). Contamination of heavy metals in aquatic media: transport, toxicity, and technologies for remediation. In: Heavy Metals in Water: Presence. removal, and safety, 1–24. DOI: 10.1039/9781782620174-00001.

GAUTAMA RS and KUSUMA GJ (2016). Characterization Of Acid Producing Potential of Spent Ore From Heap Leach Plant, Drebenstedt, Carsten, Paul, Michael (editors.).-In: Proceedings of 2016 International Mine Water Association, Leipzig, Germany, 11-15. https://www.imwa.info/docs/imwa2016.

GERARD N, KRISHNAN RS, PONNUSAMY SK, CABANA H, and VAIDYANATHAN VK (2016). The adsorptive potential of dispersible chitosan-coated iron-oxide nanocomposites toward the elimination of arsenic from aqueous solution. *Process Saf. Environ. Prot*, 104, 185–195. https://doi.org/10.1016/j.psep.2016.09.006.

GITARI, W., PETRIK, L., ETCHEBERS, O., KEY, D., and OKUJENI, C. (2008). Utilization of fly ash for treatment of coal mines wastewater: solubility controls on major inorganic contaminants, Fuel. 87, 2450–2462.

GOLDER ASSOCIATES, INC. (2009). Literature Review of Treatment Technologies to Remove Selenium from Mining Influenced Water. https://www.namc.org/docs/00057713.

GRANDE JA, SANTISTEBAN M, DE LA TORRE ML, DAVILA JM, and PEREZ-OSTALE E (2018). Map of impact by acid mine drainage in the river network of The Iberian Pyrite Belt (Sw Spain). *Chemosphere* , 199, 269–277. https://doi.org/10.1016/j.chemosphere.2018.02.047.

GROVER BPC, JOHNSON RH, BILLING DG, WEIERSBYE IM and TUTU H (2015). Mineralogy and geochemistry of efflorescent minerals on mine tailings and their potential impact on water chemistry. *Environ. Sci. Pollut. Res*. 111. DOI: 10.1007/s11356-015-5870-z.

GROVER BPC (2016). Geochemical modelling of the speciation, transport, dispersal and fate of metal contaminants in water systems in the vicinity of tailings storage facilities. PhD thesis, University of the Witwatersrand.

GU S, KANG X, and WANG L (2018). Clay mineral adsorbents for heavy metal removal from wastewater: a review. *Environ Chem Lett* 8:8–9. DOI: 10.1007/s10311-018-0813-9.

GULICOVSKI JJ, ČEROVIĆ LS, and MILONJIĆ SK, (2008). Point of zero charge and isoelectric point of alumina, Mater. *Manuf. Processes*, 23, 615-619. DOI: 10.1080/10426910802160668.

GUO K, ZHANG ZZ, LUO HJ, DANG JX, and QIAN Z (2014). An innovative approach of the effective mass transfer area in the rotating packed bed, *Ind. Eng. Chem. Res*., 53, 4052-4058. DOI: 10.1021/ie4029285.

HAN YS, YOUM SJ, OH C, CHO YC, and AHN JS (2015). Geochemical and ecotoxicological characteristics of stream water and its sediments affected by acid mine drainage. Catena 148 (1), 52-59. 10.1016/j.catena.2015.11.015.

HANSEN RN (2020). Process network modelling of the geochemical reactions responsible for acid mine drainage emanating from the Witwatersrand tailings facilities. *S. Afr. J. Geol*. 123, 357-368. DOI: 10.25131/sajg.123.0024.

HANSEN RN (2018). An assessment of the geochemical impacts of greenfields mining projects in South Africa on both sides of the mine drainage pH divide – A geochemical modelling approach. *S. Afr. J. Geol*. 121, 487-494. https://doi.org/10.25131/sajg.121.0022.

HANSEN RN (2015). Contaminant leaching from gold mining tailings dams in the Witwatersrand Basin, South Africa: A new geochemical modelling approach. *Appl Geochem*. 61, 217-223. https://doi.org/10.1016/j.apgeochem.2015.06.001.

HAQUE N, HUGHES A, LIM S, and VERNON C (2014). Rare earth elements: overview of mining, mineralogy, uses, sustainability and environmental impact. Resources 3, 614. https://doi.org/10.3390/resources3040614.

HOANG MT, PHAM TD, NGUYEN VT, NGUYEN MK, PHAM TT, and VAN DER BRUGGEN B (2019). Removal and recovery of lead from wastewater using an integrated system of adsorption and crystallization. *J. Clean. Prod*. 213, 1204–1216. https://doi.org/10.1016/j.jclepro.2018.12.275.

HAZOTTE C, LAUBIE B, REES F, MOREL JL, and SIMONNOT MO (2017). A novel process to recover cadmium and zinc from the hyperaccumulator plant Noccaea caerulescens. *Hydrometallurgy* 174, 56–65. https://doi.org/10.1016/j.hydromet.2017.09.012.

HERNANDEZ-SANTIN L, ERSKINE PD, and BARTOLO RE (2020). A review of revegetation at mine sites in the Alligator Rivers Region, Northern Territory, and the development of a state and transition model for ecological restoration at Ranger uranium mine. *J. Clean. Prod.* 246, 119079. https://doi.org/10.1016/j.jclepro.2019.119079.

HOU R, ZHANG Y, FENG H, CHEN Y, and CHEN H (2020). Effects of sulfonated peat on Cr chemical fraction in soil and Cr uptake in Pak-choi. *J. Environ. Chem. Eng*. 8, 104278. DOI: 10.1016/j.jece.2020.104278.

HUANG YW, LI D, LIU ZQ, TAO Q, ZHU Y, YANG J, and ZHANG YM (2014). Kinetics, isotherm, thermodynamic, and adsorption mechanism studies of $La(OH)_3$-modified exfoliated vermiculites as highly efficient phosphate adsorbents, *Chem. Eng. J*. 236-191-201. DOI: 10.1016/j.cej.2013.09.077.

HUMPHRIES, MS., MCCARTHY, TS., and PILLAY, L. (2017). Attenuation of pollution arising from acid mine drainage by a natural wetland on the Witwatersrand. S Afr. J Sci. 113(1/2).

IGALAVITHANA AD, LEE S, LEE YH, TSANG DCW, RINKLEBE J, KWON EE, and OK YS (2017). Heavy metal immobilization and microbial community abundance by vegetable waste and pine cone biochar of agricultural soils. *Chemosphere* 174, 593–603. DOI: 10.1016/j.chemosphere.2017.01.148.

IGARASHI T, HERRERA PS, UCHIYAMA H, MIYAMAE H, IYATOMI N, HASHIMOTO K, and TABELIN CB (2020). The two-step neutralization ferrite-formation process for sustainable acid mine drainage treatment: Removal of copper, zinc and arsenic, and the influence of coexisting ions on ferritization. *Sci. Total Environ*, 715, 136877. https://doi.org/10.1016/j.scitotenv.2020.136877.

JADHAV DA, GHOSH RAY S, and GHANGREKAR MM (2017). Third generation in bio-electrochemical system research – A systematic review on mechanisms for recovery of valuable by-products from wastewater. *Renew. Sustain. Energy Rev*. 76, 1022–1031. https://doi.org/10.1016/j.rser.2017.03.096.

JOHNSON DB and HALLBERG KB (2005). Acid mine drainage remediation options: a review. *Sci. Total Environ*. 338: 3-14. https://doi.org/10.1016/j.scitotenv.2004.09.002.

JOHN, R., SINGLAR, V., GOYAL, M., KUMAR, P., and SINGLA, A. (2017). Acid Mine Drainage: Sources, Impacts and Prevention. Environmental Biotechnology.

KARUNARATHNE HD, and AMARASINGHE BM, (2013). Fixed bed adsorption column studies for the removal of aqueous phenol from activated carbon prepared from sugarcane bagasse. *Energy Procedia*, 34: 83-90. https://doi.org/10.1016/j.egypro.2013.06.736.

KASAINI H, KEKANA PT, SAGHTI AA, and BOLTON K (2013). Adsorption characteristics of cobalt and nickel on oxalate treated activated carbons in sulphate media. World Academy of Science, Engineering and Technology. 76, 707–721. https://www.researchgate.net/publication/285731790.

KAUR H, GIRDHAR M, and MOHAN A (2018). Acid mine drainage: an introduction and treatment strategies. *Pollut. Res*. 37, 82–90. https://www.researchgate.net/publication/334657525.

KHAZAAL SH, AL-AZAWI KF, EASSA HA, KHASRAGHI AH, ALFATLAWI WR, and Al-Gebori, AM (2019). Study the level of some heavy metals in water of Lake Habbaniyah in Al-Anbar-Iraq. *Energy Procedi*a.157, 68-74. https://doi.org/10.1016/j.egypro.2018.11.165.

KIRKELUND GM, JENSEN PE, OTTOSEN LM, and PEDERSEN KB (2019). Comparison of two-and three-compartment cells for electrodialytic removal of heavy metals from contaminated material suspensions. *J. Hazard. Mater*. 367, 68–76. DOI: 10.1016/j.jhazmat.2018.12.063.

KEFENI K, MSAGATI, T and MAMBA B (2015). Metals and sulphate removal from acid mine drainage in two steps via ferrite sludge and barium sulphate formation. *Min Eng*, 81: 79-87. DOI: 10.1016/j.mineng.2015.07.016.

KEFENI KK, MSAGATI TA and MAMBA BB (2017). Acid mine drainage: prevention, treatment options, and resource recovery: a review. *J. Clean. Prod*, 151, 475-493. https://doi.org/10.1016/j.jclepro.2017.03.082.

KHAN A, KHAN S, KHAN MA, QAMAR Z, and WAQAS M, (2015). The uptake and bioaccumulation of heavy metals by food plants, their effects on plants nutrients, and associated health risk: a review. *Environ. Sci. Pollut. Res*. 22, 13772–13799. DOI: 10.1007/s11356-015-4881-0.

KOJO IV, REUTER MA, and HEISKANEN K (2013). Some examples of reuse, repurposing and recycling of minerals to improve the resource efficiency in mining. https://www.researchgate.net/publication/270340719

LAKSHMIPATHY R, and SARADA NC (2016). Methylene blue adsorption onto native watermelon rind: batch and fixed-bed column studies. *Desalin. Water Treat*. 57(23), 10632–10645. DOI: 10.1080/19443994.2015.1040462.

LANGMUIR I (1918). The adsorption of gases on plane surfaces of glass, mica, and platinum. Journal of the American Chemical Society, 40(9), 1361–1403. DOI: 10.1021/ja02242a004.

LEBRE E, CORDER GD, and GOLEV A (2017). Sustainable practices in the management of mining waste: A focus on the mineral resource. *Miner. Eng*, 107, 34–42. https://doi.org/10.1016/j.mineng.2016.12.004.

LEE C, KIM J, KANG J, KIM S, PARK S, LEE S, and CHOI J (2015). Comparative analysis of fixed-bed sorption models using phosphate breakthrough curves in slag filter media. *Desalin. Water Treat*. 55(7), 1795–1805. DOI: 10.1080/19443994.2014.930698

LECOMTE KL, MAZA SN, COLLO G, SAR.MIENTO AM, and DEPETRIS PJ (2017). Geochemical behavior of an acid drainage system: the case of the Amarillo River, Famatina (La Rioja, Argentina). *Environ. Sci. Pollut. Res*. 24, 1630-1647. DOI: 10.1007/s11356-016-7940-2.

LI L, WEI S, LOLLAR BS, WING B, BUI TH, ONO S, LAU VETTER MCY, ONSTOTT TC, KIEFT TL, BORGONIE G, LINAGE-ALVAREZ B, KULOYO O, and VAN HEERDEN, E (2022). In situ oxidation of sulfide minerals supports widespread sulfate reducing bacteria in the deep subsurface of the Witwatersrand Basin (South Africa): Insights from multiple sulfur and oxygen isotopes. *Earth Planet. Sci. Lett*. 577,117-247. https://doi.org/10.1016/j.epsl.2021.117247.

LI X, DAI HX, and YANG XL (2013). The generation and treatment of acid mine drainage. *Adv Mat Res*. 55-71. https://doi.org/10.4028/www.scientific.net/AMR.726-731.1985.

LI ZY, MA ZW, KUIJP TJ, YUAN ZW, and HUANG L (2014). A review of soil heavy metal pollution from mines in China: pollution and health risk assessment. *Sci. Total Environ*. 468, 843-853. https://doi.org/10.1016/j.scitotenv.2013.08.090.

LI C, ZHOU K, QIN W, TIAN C, QI M, YAN X, and HAN W (2019). A review on heavy metals contamination in soil: effects, sources, and remediation techniques. *Soil Sediment Contam*. 28, 380–394. DOI: 10.1080/15320383.2019.1592108.

LIAN F, and XING B (2017). Black carbon (biochar) in water/soil environments: molecular structure, sorption, stability, and potential risk. *Environ. Sci. Technol*. 51, 13517–13532. DOI: 10.1021/acs.est.7b02528

LIANG J, LI X, YU Z, ZENG G, LUO Y, and JIANG L (2017). Amorphous MnO_2 modified biochar derived from aerobically composted swine manure for adsorption of Pb(II) and Cd(II). *ACS Sustain. Chem. Eng*. 5, 5049–5058. DOI: 10.1021/acssuschemeng.7b00434.

LIM AP, and ARIS AZ (2014). Continuous fixed-bed column study and adsorption modelling: removal of cadmium(II) and lead(II) ions in aqueous solution by dead calcareous skeletons. *J Biochem Eng*. 87, 50–61. https://doi.org/10.1016/j.bej.2014.03.019.

LIU J, ZHU R, MA L, FU H, LIN X, PARKER SC, and MOLINARI M (2021). Adsorption of phosphate and cadmium on iron (oxyhydr)oxides: a comparative study on ferrihydrite, goethite, and hematite. *Geoderma* 383, 114799. https://doi.org/10.1016/j.geoderma.2020.114799.

LIU J, ZHU R, XU T, XU Y, GE F, and XI Y (2016). Co-adsorption of phosphate and zinc (II) on the surface of ferrihydrite. *Chemosphere* 144, 1148–1155. https://doi.org/10.1016/j.chemosphere.2015.09.083.

LIU L, LI W, SONG W, and GUO M (2018). Remediation techniques for heavy metal-contaminated soils: principles and applicability. *Sci. Total Environ*. 633, 206–219. https://doi.org/10.1016/j.scitotenv.2018.03.161.

LIU X, HICHER P, MURESAN B, SAIYOURI N, and HICHER PY (2016). Heavy metal retention properties of kaolin and bentonite in a wide range of concentration and different pH conditions. *Appl. Clay Sci*. 119, 365–374. https://doi.org/10.1016/j.clay.2015.09.021.

LJUNGBERG J, and ÖHLANDER B (2001) The geochemical dynamics of oxidizing mine tailings at Laver, northern Sweden. *J. Geochem. Explor*. 2001, 74, 57–72. DOI: 10.1016/S0375-6742(01)00175-3.

LÓPEZ J, REIG M, GIBERT O, and CORTINA JL (2019). Recovery of sulphuric acid and added value metals (Zn, Cu and rare earths) from acidic mine waters using nanofiltration membranes. *Sep Purif Technol* 212:180–190. https://doi.org/10.1016/j.seppur.2018.11.022.

LOTTERMOSER BG (2010). Mine Wastes: Characterization, Treatment and Environmental Impacts, 3rd ed.; *Springer*: Berlin/Heidelberg, Germany, 2010. ISBN: 978-3-540-48630-5.

LOTTERMOSER B (2011), Recycling, reuse and rehabilitation of mine wastes., Elements,7.,405-410. DOI: 10.2113/gselements.7.6.405.

LUIZ A, SPENCER E, MCCLURE, DD, COSTER HGL, BARTON GW, and KAVANAGH JM (2018). Membrane selection for the desalination of bio-refinery effluents using electrodialysis. *Desalination* 428, 1-11. DOI: 10.1016/j.desal.2017.11.006.

LU XW, ZHANG XL, LI YL, and CHEN H, (2014). Assessment of metals pollution and health risk in dust from nursery schools in Xi'an China. *Environ.Res*.128, 27–34. https://doi.org/10.1016/j.envres.2013.11.007.

MACINGOVA E, AND LUPTAKOVA A (2012). Recovery of metals from acid mine drainage. *Chem. Eng. Trans*. 28:109-114. DOI: 10.3303/CET1228019.

MANDZHIEVA SS, MINKINA TM, CHAPLYGIN VA, MOTUZOVA GV, SUSHKOVA, SN, BAUER TV, and NEVIDOMSKAYA, DG (2016). Plant contamination by heavy metals in the impact zone of Novocherkassk Power Station in the south of Russia. *J. Soils Sediments* 16, 1383–1391. DOI: 10.1007/s11368-015-1098-2.

MAREE J, ZVINOWANDA C, and VAN DER WALT B (2010). Temporary neutralisation plant (No. Progress Study: 1-4). Pretoria: Sibanye gold.

MARTÍ-CALATAYUD MC, BUZZI DC, GARCÍA-GABALDON M, ORTEGA E, BERNARDES AM, TENORIO JAS, AND PEREZ-HERRANZ V (2014). Sulfuric acid recovery from acid mine drainage by means of electrodialysis. *Desalination* 343, 120-127. DOI: 10.1016/j.desal.2013.11.031.

MASINDI V, CHATZISYMEON E, KORTIDIS I, and FOTEINIS S (2018). Assessing the sustainability of acid mine drainage (AMD) treatment in South Africa. *Sci Total Environ* 635:793–802. https://doi.org/10.1016/j.scitotenv.2018.04.108.

MASINDI V, AKINWEKOMI V, MAREE JP and MUEDI KL (2017). Comparison of mine water neutralisation efficiencies of different alkaline generating agents. *J. Environ. Chem. Eng*. 5(4), 3903-3913. https://doi.org/10.1016/j.jece.2017.07.062.

MASINDI V, GITARI MW, TUTU H, and DE BEER M (2015). Passive remediation of acid mine drainage using cryptocrystalline magnesite: A batch experimental and geochemical modelling approach. *Water SA*, 41(5), 677-682. http://dx.doi.org/10.4314/WSA.V41I5.10.

MASUKUME M, ONYANGO MS, and MAREE JP (2014). Sea shell derived adsorbent and its potential for treating acid mine drainage. *Int. J. Min. Process* 133, 52-59. https://doi.org/10.1016/j.minpro.2014.09.005.

MCCARTHY TS (2011). The impact of acid mine drainage in South Africa. *S. Afr. J. Sci*. 107: 5-6. http://dx.doi.org/10.4102/sajs.v107i5/6.712.

MESCHKE K, HERDEGEN V, AUBEL T, JANNECK E, and REPKE JU (2015). Treatment of opencast lignite mining induced acid mine drainage (AMD) using a rotating microfiltration system. *J. Environ. Chem. Eng*. 3, 2848-2856. DOI: 10.1016/j.jece.2015.10.013.

MICHALKOVA E, SCHWARZ M, PULISOVA P, MASAM, B, and SUDOVSKY P (2013). Metals recovery from acid mine drainage and possibilities for their utilization. *Pol. J. Environ. Stud*. 22, 1111-1118. http://www.pjoes.com/Metals-Recovery-from-Acid-Mine-Drainage-r-nand-Possibilities-for-their-Utilization,89.

MIRZAEI M, VERRELST J, BAKHTIARI AR, and MAROFI S (2021). Potential use of grapevine cv Askari for heavy metal phytoremediation purposes at greenhouse scale. *Environ. Sci. Pollut. Res*. 28, 12447–12458.

MOAMERI M, and ABBASI-KHALAKI, M (2019). Capability of Secale montanum trusted for phytoremediation of lead and cadmium in soils amended with nano-silica and municipal solid waste compost*. Environ. Sci. Pollut. Res*. 26, 24315–24322. https://doi.org/10.1007/s11356-017-0544-7.

MOODLEY I, SHERIDAN CM, KAPPELMEYER U, AND AKCIL A (2018). Environmentally sustainable acid mine drainage remediation: research developments with a focus on waste/by-products. *Miner. Eng*. 126, 207-220. https://doi.org/10.1016/j.mineng.2017.08.008.

MOSA KA, SAADOUN I, KUMAR K, HELMY M, and DHANKHER OP (2016). Potential biotechnological strategies for the clean-up of heavy metals and metalloids. Front. *Plant Sci*. 7. https://doi.org/10.3389/fpls.2016.00303.

MOSAI AK, BAKATULA EN, and TUTU H (2017). Adsorption of cadmium, copper, and chromium by an agricultural soil impacted by mining activities, *Water Air Soil Pollut*, 228, 287. https://doi.org/10.1007/s11270-017-3487-1.

MULOPO J (2015a). Continuous pilot scale assessment of the alkaline barium calcium desalination process for acid mine drainage treatment. *J. Environ. Chem. Eng*. 3, 1295–1302. DOI: 10.1016/j.jece.2014.12.001.

MULOPO J (2015b). Making sense of our mining wastes: Removal of heavy metals from AMD using sulphidation media derived from waste gypsum, *J.S. Afr. Inst. Min. Metall*. 115(12), 2015. http://dx.doi.org/10.17159/2411-9717/2015/v115n12a7.

MULOPO J, BOLOGO L, and MASHEGO, M (2012). Regeneration of Barium Carbonate from Barium Sulphide in a Pilot Scale Bubbling Column Reactor and Utilization for Acid Mine Drainage, *Water Sci. Technol*. 65 (2), 324–331. DOI: 10.2166/wst.2012.857.

NAIDU G, JEONG S, VIGNESWARAN S, HWANG TM, and CHOI YJ, KIM SH (2016). A review on fouling of membrane distillation. *Desalin. Water Treat*. 57, 10052-10076. DOI: 10.1080/19443994.2015.1040271.

NAIDU G, RYU S, THIRUVENKATACHARI R, CHOI Y, JEONG S, and VIGNESWARAN S (2019). A critical review on remediation, reuse, and resource recovery from acid mine drainage. *Environ. Pollut*. 247, 1110-1124. DOI: 10.1016/j.envpol.2019.01.085.

NAME T, and SHERIDAN C (2014). Remediation of acid mine drainage using metallurgical slags. *Miner Eng* 64:15–22. DOI: 10.1016/j.mineng.2014.03.024.

NEAMTIU IA, AL-ABED SR, MCKERNAN JL, BACIU CL, GURZAU ES, POGACEAN AO, and BESSLER SM (2017). Metal contamination in environmental media in residential areas around Romanian mining sites. *Rev. Environ*. Health 32, 215-220. DOI: 10.1515/reveh-2016-0033.

NEJESCHLEBOVA L, SRACEK O, MIHALJEVIC M, ETTLER V, KRÍBEK B, KNESL, I, VANEK, A, PENÍZEK V, DOLNÍCEK Z, and MAPANI B (2015). Geochemistry and potential environmental impact of the mine tailings at Rosh Pinah, southern Namibia. *J. Afr. Earth Sci*. 105, 17-28. DOI: 10.1016/j.jafrearsci.2015.02.005.

NETSHIONGOLWE KE (2018). Geochemical characterisation of gold tailings footprints on the Central Rand Goldfield, MSc Dissertation, University of South Africa.

NETSHIONGOLWE K, MHLANA Y, MOSAI A, RICHARDS H, CHIMUKA L, CUKROWSKA E, and TUTU H (2020). Recovery of ochers from acid mine drainage treatment: a geochemical modelling and experimental approach, Chapter 6. In: Elvis Fosso-Kankeu, Christian Wolkersdorfer and Jo Burgess (editors). *Recovery of Byproducts from Acid Mine Drainage Treatment*. Scrivener Publishing LCC. ISBN:9781119620075; Online ISBN:9781119620204. 159-185. DOI:10.1002/9781119620204.

NGURE V, DAVIES T, KINUTHIA G, SITATI N, SHISIA S, OYOO-OKOTH E (2014). Concentration levels of potentially harmful elements from gold mining in Lake Victoria Region, Kenya: environmental and health implications. *J. Geochem. Explor* 144, 511-516. https://doi.org/10.1016/j.gexplo.2014.04.004.

NIEVA NE, BORGNINO L, and GARCÍA MG (2018). Long term metal release and acid generation in abandoned mine wastes containing metal-sulphides. *Environ. Pollut*. 242, 264-276. DOI: 10.1016/j.envpol.2018.06.067.

NLEYA Y, SIMATE GS, and NDLOVU S (2016). Sustainability assessment of the recovery and utilisation of acid from acid mine drainage. *J. Clean. Prod*. 113, 17-27. https://doi.org/10.1016/j.jclepro.2015.11.005.

NORDSTROM DK, BOWELL RJ, CAMPBELL KM, and ALPERS CN (2017). Challenges in Recovering Resources from Acid Mine Drainage. Mine Water Circular Economy. In: Wolkersdorfer C, Sartz L, Sillanpää M, Häkkinen A (editors) *IMWA* Lappeenranta, Finland. 1138-1146.

NSANGANWIMANA F, AL SOUKI KS, WATERLOT C, DOUAY F, PELFRENE A, RODŐSKOVA A, LOUVEL B, and POURRUT B (2021). Potentials of Miscanthus x giganteus for phytostabilization of trace element-contaminated soils: Ex situ experiment. *Ecotoxicol. Environ. Saf*. 214, 112-125. https://doi.org/10.1016/j.ecoenv.2021.112125.

OCHIENG GM, SEANEGO ES, and NKWONTA, OI (2017). Impacts of mining on water resources in South Africa: A review. *Sci. Res*. Essays 5 (22), 3351–3357. http://www.academicjournals.org/SRE.

OJONIMI, TI., OKEME, IC., PHIRI-CHANDA, T., and AMEH, EG. (2021). Acid mine drainage (AMD) contamination in coal mines and the need for extensive prediction and remediation: a review. Journal of Degraded and Mining Lands Management 9(1): 3129-3136.

OK YS, RINKLEBE J, HOU D, TSANG DC, and TACK FM (2020). Soil and Groundwater Remediation Technologies: A Practical Guide. CRC Press. ISBN: 9780367337407.

OLDS WE, TSANG DCW, WEBER PA, and WEISENER CG (2013). Nickel and zinc removal from acid mine drainage: roles of sludge surface area and neutralising agents. *J Min*. 2013:5. DOI: 10.1155/2013/698031.

OTUNOLA BO and OLOLADE O.O (2020). A review on the application of clay minerals as heavy metal adsorbents for remediation purposes*. Environ. Technol. Innov* 18. 100692. DOI: 10.1016/j.eti.2020.100692

PADHIYAR TC and THAKORE SB (2013). Recovery of acetic acid from effluent via freeze crystallization. *Int. J. Sci. Eng. Technol*. 2, 211-215. ISSN: 2277-1581.

PAN M, LIN X, XIEB J, and HUANG X (2017). Kinetic, equilibrium, and thermodynamic studies for phosphate adsorption on aluminium hydroxide modified palygorskite nanocomposites, *RSC Adv*. 7, 4492. https://doi.org/10.1039/C6RA26802A.

PARIKH SJ, MUKOME FND, and ZHANG X (2014). ATR-FTIR spectroscopic evidence for biomolecular phosphorus and carboxyl groups facilitating bacterial adhesion to iron oxides. *Colloids Surf. B*: Biointerfaces, 119, 38–46. DOI: 10.1016/j.colsurfb.2014.04.022.

PARK I, TABELIN CB, MAGARIBUCHI K, SENO K, ITO M, and HIROYOSHI N (2018). Suppression of the release of arsenic from arsenopyrite by Carrier microencapsulation using Ti-catechol complex. *J. Hazard Mater.* 344, 322-332. https://doi.org/10.1016/j.jhazmat.2017.10.025.

PARK I, TABELIN CB, JEON S, LI X, SENO K, ITO M, AND HIROYOSHI N (2019). A review of recent strategies for acid mine drainage prevention and mine tailings recycling. *Chemosphere* 219, 588–606. https://doi.org/10.1016/j.chemosphere.2018.11.053.

PARKHURST DL, and APPELO CAJ (2013). Description of Input and Examples for PHREEQC Version 3 – A Computer Program for Speciation, Batch-Reaction, One-Dimensional Transport, and Inverse Geochemical Calculations. *U.S. Geol. Surv. Tech*. Methods, 6, 1-497. http://pubs.usgs.gov/tm/06/a43.

PYRBOT W, SHABONG L, and SINGH OP (2019). Neutralization of acid mine drainage contaminated water and ecorestoration of stream in a coal mining area of east Jaintia Hills, Meghalaya. *Mine Water Environ*, 38, 551–555. DOI: 10.1007/s10230-019-00601-9.

QIU H, LV L, PAN B, ZHANG Q, ZHANG W, and ZHANG Q (2009). Critical review in adsorption kinetic models, *J. Zhejiang Univ*. A 10-716-724. DOI: 10.1631/jzus.A0820524.

QURESHI A, MAURICE C, AND OHLANDER B (2016). Potential of coal mine waste rock for generating acid mine drainage*. J. Geochem. Explor* 160, 44-54. DOI: 10.1016/j.gexplo.2015.10.014.

RANGABHASHIYAM S, NANDAGOPAL MS, NAKKEERAN E, and SELVARAJU N, (2016). Adsorption of hexavalent chromium from synthetic and electroplating effluent on chemically modified Swietenia mahagoni shell in a packed bed column. *Environ Monit Assess* 188. 411. DOI: 10.1007/s10661-016-5415-z.

REGEL-ROSOCKA M (2010). A review on methods of regeneration of spent pickling solutions from steel processing. *J. Hazard Mater*. 177, 57-69. https://doi.org/10.1016/j.jhazmat.2009.12.043.

RODRÍGUEZ-GALÁN M, BAENA-MORENO FM, VÁZQUEZ S, ARROYO-TORRALVO F, VILCHES, LF, ZHANG Z (2019). Remediation of acid mine drainage, *Environ. Chem. Lett*. 17 (4), 1529–1538. DOI: 10.1007/s10311-019-00894-w.

ROSSINI-OLIVA S, ABREU MM, and LEIDI EO (2018). A review of hazardous elements tolerance in a metallophyte model species: Erica andevalensis. *Geoderma* 319, 43–51. https://doi.org/10.1016/j.geoderma.2017.12.035.

ROZOY E, BOUDESOCQUE L, and BAZINET L (2015). Deacidification of cranberry juice by electrodialysis with bipolar membranes. *J. Agric. Food Chem*. 65, 642-651. https://doi.org/10.1021/jf502824f.

RUSINOWSKI S, KRZYZAK J, CLIFTON-BROWN J, JENSEN E, MOS M, WEBSTER R, SITKO K, and POGRZEBA M (2019). New Miscanthus hybrids cultivated at a polish metal-contaminated site demonstrate high stomatal regulation and reduced shoot Pb and Cd concentrations*. Environ. Pollut*. 252, 1377–1387. DOI: 10.1016/j.envpol.2019.06.062.

RYU S, NAIDU G, and HASAN-JOHIR MA (2019). Acid mine drainage treatment by integrated submerged membrane distillation–sorption system. *Chemosphere* 218. 955–965. DOI: 10.1016/j.chemosphere.2018.11.153.

SADRZADEH M, and MOHAMMADI T (2008). Sea water desalination using electrodialysis. *Desalination* 221, 440-447. https://doi.org/10.1016/j.desal.2007.01.103.

SANGIORGI C, LANTIERI, TATARANNI P, GOMES JC, and GABRIEL M (2016). Reuse of mining waste into innovative alkali-activated-based materials for road pavement applications. 4th International Chinese European Workshop (CEW) on functional pavement design At: Delft (NL). DOI: 10.1201/9781315643274-191.

SANTOS JALLATH JE, ROMERO FM, ARGÜELLES RI, MACEDO, AC, and ARENAS, JG (2018). Acid drainage neutralization and trace metals removal by a two-step system with carbonated rocks, Estado de Mexico, Mexico. *Environ Earth Sci*. 77. 86. DOI: 10.1007/s12665-018-7248-2.

SDIRI A, KHAIRY M, BOUAZIZ S, and EL-SAFTY S (2016). A natural clayey adsorbent for selective removal of lead from aqueous solutions. *Appl. Clay Sci*.126, 89–97. https://doi.org/10.1016/j.clay.2016.03.003.

SHEEDY M, and PARUJEN P (2012). Acid separation for industry control and acid cycle using short bed ion exchange. In: T.T. Chen Honorary Symposium on Hydrometallurgy, Electrometallurgy and Materials Characterization. TMS.

SHEORAN V, SHEORAN AS, and POONIA P (2016). Factors affecting phytoextraction: a review*. Pedosphere* 26, 148–166. DOI: 10.1016/S1002-0160(15)60032-7.

SHIRIN, S., JAMAL, A., EMMANOUIL, C., and YADAV, AK (2021). Assessment of Characteristics of Acid Mine Drainage Treated with Fly Ash. Appl. Sci. 2021, 11, 3910.

SIEBERT HM, FLORIAN G, SAND W, VASZITA E, GRUIZ K, CSŐVARI M, AND ARGYELAN JT (2019). Leaching, bioleaching, and acid mine drainage case study. Engineering Tools for Environmental Risk Management: 4. Risk Reduction Technologies and Case Studies, 363. eBook ISBN9781315778754.

SIMATE GS, and NDLOVU S (2014). Acid mine drainage: challenges and opportunities. *J. Environ. Chem. Eng*. 2, 1785–1803. https://doi.org/10.1016/j.jece.2014.07.021.

SINGER PC, and STUMM W (1970). Acid mine drainage: rate-determining step. *Science* 167, 1121–1123. DOI:10.1126/science.167.3921.1121.

SKOUSEN JG, ZIEMKIEWICZ PF, AND MCDONALD LM (2019). Acid mine drainage formation, control and treatment: Approaches and strategies. *Extract. Ind. Soc*. 6 (1), 241–249. https://doi.org/10.1016/j.exis.2018.09.008.

SKOUSEN J, ZIPPER, CE, ROSE A, ZIEMKIEWICZ, PF, NAIRN R, MCDONALD LM, and KLEINMANN RL (2017). Review of passive systems for acid mine drainage treatment. *Mine Water Environ*. 36, 133-153. https://doi.org/10.1007/s10230-016-0417-1.

SMART RSC, MILLER SD, STEWART WS, RUSDINAR Y, SCHUMANN RE, KAWASHIMA N, and LI, J (2010). In situ calcite formation in limestone-saturated water leaching of acid rock waste. *Sci. Total Environ*. 408, 3392-3402. DOI: 10.1016/j.scitotenv.2010.04.028.

SOLTANI N, MOORE F, and KESHAVARZI B (2013). Geochemistry of trace metals and rare earth elements in stream water, stream sediments and acid mine drainage from Darrehzar copper mine, Kerman, Iran. Exposure and Health 6, 97-114. DOI: 10.1007/s12403-014-0114-x.

TABELIN CB, SASAKI A, IGARASHI T, TOMIYAMA S, VILLACORTE-TABELIN M, ITO M, and HIROYOSHI N (2018). Prediction of acid mine drainage formation and zinc migration in the tailings dam of a closed mine, and possible countermeasures. In: Proceedings of the 25th Regional Symposium on Chemical Engineering, Makati, Philippines. https://doi.org/10.1051/matecconf/201926806003.

TALEBI ATOUEI M, RAHNEMAIE R, GOLI KALANPA E, and DAVOODI MH (2016). Competitive adsorption of magnesium and calcium with phosphate at the goethite water interface: kinetics, equilibrium, and CD-MUSIC modelling. *Chem. Geol*. 437, 19-29. https://doi.org/10.1016/j.chemgeo.2016.05.004.

TCTA (2011). AMD Witwatersrand Basin Due diligence Presentations. Presentation to Portfolio Committee. 7 September. Centurion: Trans-Caledon Tunnel Authority.

TOMASZEWSKA M, GRYTA M, and MORAWSKI AW (2001). Recovery of hydrochloric acid from metal pickling solutions by membrane distillation. *Sep. Purif. Technol*. 22-23, 591-600. DOI: 10.1016/S1383-5866(00)00164-7.

TUCKER, RF., VILJOEN, RP., MORRIS, J., and VILJOEN, MJ. (2016). A Review of the Witwatersrand Basin -The World's Greatest Goldfield, journal of Episodes. 39, 105-133.

TUTU H, MCCARTHY TS, and CUKROWSKA E (2008). The chemical characteristics of acid mine drainage with particular reference to sources, distribution, and remediation: The Witwatersrand Basin, South Africa as a case study. *Appl Geochem*, 23(12), 3666-3684. https://doi.org/10.1016/j.apgeochem.2008.09.002.

UDDIN MK (2017). A review on the adsorption of heavy metals by clay minerals, with special focus on the past decade. *Chem. Eng. J*. 308, 438–462. https://doi.org/10.1016/j.cej.2016.09.029.

UNITED STATES ENVIRONMENTAL PROTECTION AGENCY (USEPA) (2000). Wastewater Treatment Technologies. Chapter 8. In: Browner CM, Fox JC, Grubbs GH, Frace SE, Forsht EH, Matuszko JS, Connor TE, Wheeler WJ, Smith MD eds. Development document for effluent limitations guidelines and standards for the centralized waste treatment industry final, Volume I. US Environmental Protection Agency, Office of Water, Washington, DC. EPA 821-R-00-020.

UNITED STATES ENVIRONMENTAL PROTECTION AGENCY (USEPA) (2004). Primer for municipal wastewater treatment systems. Office of wastewater management. United States, United States Environmental Protection Agency. EPA 832-R-04-001.

VALENTE T, GRANDE, JA, TORRE ML, SANTISTEBAN M, AND CERON JC (2013). Mineralogy and environmental relevance of AMD-precipitates from the Tharsis mines, iberian pyrite Belt (SW, Spain *). Appl. Geochem*. 39, 11-25. https://doi.org/10.1016/j.apgeochem.2013.09.014.

VASS CR, NOBLE A, and ZIEMKIEWICZ PF (2019). The occurrence and concentration of rare earth elements in acid mine drainage and treatment by-products. Part 2: Regional survey of Northern and Central Appalachian Coal Basins. *Mining. Metall. Explor*. 36, 917–929. https://doi.org/10.1007/s42461-019-00112-9.

VHAHANGWELE M, and MUGERA GW (2015). The potential of ball-milled South African bentonite clay for attenuation of heavy metals from acidic wastewaters: Simultaneous sorption of Co^{2+}, Cu^{2+}, Ni^{2+}, Pb^{2+}, and Zn^{2+} ions. J*. Environ. Chem. Eng*. 3 (4), 2416–2425. DOI: 10.1016/j.jece.2015.08.016.

VILJOEN MJ, and VILJOEN RP (2004). Sedimentary Distributory Channels and Payshoots of the Conglomerate Reefs of the Central Rand Goldfield. Unpub. Study.

VITAL B, BARTACEK J, ORTEGA-BRAVO JC, and JEISON D (2018). Treatment of acid mine drainage by forward osmosis: heavy metal rejection and reverse flux of draw solution constituents. *Chem. Eng. J*. 332, 85-91. DOI: 10.1016/j.cej.2017.09.034.

WADEKAR SS, and VIDIC RD (2018). Comparison of ceramic and polymeric nanofiltration membranes for treatment of abandoned coal mine drainage. *Desalinatio*n 440. DOI: 10.1016/j.desal.2018.01.008.

WADEKAR SS, HAYES T, LOKARE OR, MITTAL D, and VIDIC RD (2017). Laboratory and pilot-scale nanofiltration treatment of abandoned mine drainage for the recovery of products suitable for industrial reuse. *Ind. Eng. Chem. Res*. 56, 7355-7364. DOI: 10.1021/acs.iecr.7b01329.

WEI C, LI X, DENG Z, FAN G, LI M, and LI C (2010). Recovery of H_2SO_4 from an acid leach solution by diffusion dialysis. *J. Hazard Mater*. 176, 226-230. DOI: 10.1016/j.jhazmat.2009.11.017.

WEI X, WOLFE F, AND HAN YWER (2014). Mine drainage: characterization, treatment, modelling, and environmental aspect. *Water Environ. Res*. 86, 1515-153. https://www.jstor.org/stable/26662281.

WEI X, ZHANG S, HAN Y, AND WOLFE FA (2018). Characterization and treatment of mine drainage. *Water Environ. Res*. 90 (10), 1899–1922. DOI: 10.2175/106143017X15131012188042.

WORLD HEALTH ORGANIZATION (WHO) (2016). Ten chemicals of major public health concern. https://chemycal.com.

WU Y, PANG H, LIU Y, WANG X, YU S, FU D, CHEN J, and WANG X (2019). Environmental remediation of heavy metal ions by novel-nanomaterials: A review*. Environ. Pollut*. 246, 608–620. https://doi.org/10.1016/j.envpol.2018.12.076.

WUANA RA, and OKIEIMEN FE (2011). Heavy metals in Contaminated Soils: A Review of Sources, Chemistry, Risks and Best Available Strategies for Remediation, International Scholarly Research Network, ISRN Ecology, ID 402647, https://doi.org/10.5402/2011/402647.

XIE F, DAI Z, ZHU Y, LI G, LI H, and HE Z (2019). Adsorption of phosphate by sediments in a eutrophic lake: isotherms, kinetics, thermodynamics, and the influence of dissolved organic matter. *Colloids Surf. A Physicochem. Eng*. Asp. 562, 16–25. DOI:10.1016/J.COLSURFA.2018.11.009.

XU T, and HUANG C (2008). Electrodialysis-based separation technologies: a critical review. *AlChE J.* 54(12): 3147 – 3159. DOI: 10.1002/aic.11643.

XU D, LEE LY, LIM FY, LYU Z, ZHU H, ONG SL, and HU J (2020). Water treatment residual: a critical review of its applications on pollutant removal from stormwater runoff and future perspectives. *J. Environ. Manag*. 259, 109649. DOI: 10.1016/j.jenvman.2019.109649.

YOUNGER PL, BANWART SA, and HEDIN RS (2002). Mine water: hydrology, pollution, remediation. Dordrecht, Netherlands, Kluwer Academic Publishers. 442. ISBN: 1-4020-0137-1.

ZHANG D, and DING A (2018). Effects of combined passivating agents on remediation of Cd and Pb compound-contaminated soil. *J. Agric Environ Sci*. 2018, 37 (12): 2718-2726. ISSN: 1672-2043. http://www.aes.org.cn/nyhjkxxben/ch/r.

ZHANG Y, ZHAO M, CHENG Q, WANG C, LI, H, HAN X, FAN Z, SU G, DENG P, and LI Z, (2021). Research progress of adsorption and removal of heavy metals by chitosan and its derivatives: a review. *Chemosphere* 279.

ZENG H, CHEN L, ZHOU X, and ZENG Q (2019). Cadmium accumulation in winter crops and the assessment of paddy soil phytoremediation in southern China. *Environ. Sci. Pollut. Res*. 26, 17173–17182. DOI: 10.1007/s11356-019-05054-9.

ZEHRA A, SAHITO ZA, TONG W, TANG L, HAMID Y, WANG Q, CAO X, KHAN MB, HUSSAIN B, JATOI SA, and HE Z (2020). Identification of high cadmium-accumulating oilseed sunflower (Helianthus annuus) cultivars for phytoremediation of an Oxisol and an Inceptisol. *Ecotoxicol. Environ. Saf*. 187, 109857. DOI: 10.1016/j.ecoenv.2019.109857.

ZIEMKIEWICZ P, HE T, NOBLE A, and LIU X (2016). Recovery of rare earth elements (REEs) from coal mine drainage. In: Proceedings 37th West Virginia Surface Mine Drainage Task Force Symposium. 43–50. https://wvmdtaskforce.files.wordpress.com/2016/04/2016-etd30-pfz.

ZINCK J, and GRIFFITH W (2013). Review of Mine Drainage Treatment and Sludge Management Operations. The Mining Association of Canada. MEND Study 3.43.1. http://mend-nedem.org/mend-report/review-of-mine-drainage-treatment-and-sludge-management-operation.

ZOU Y, WANG X, KHAN A, WANG P, LIU Y, ALSAEDI A, HAYAT T, and WANG X (2016). Environmental remediation and application of nanoscale zero-valent iron and its composites for the removal of heavy metal ions: A review. *Environ. Sci. Technol*. 50 (14), 7290–7304. DOI: 10.1021/acs.est.6b01897.

APPENDIX A: OCHRES PRECIPITATION SIMULATION RESULTS

```
-----------------------------------------
Beginning of batch-reaction calculations.
-----------------------------------------

Reaction step 1.

Using solution 1.
Using reaction 1.

Reaction 1.

        1.000e+00 moles of the following reaction have been added:

                     Relative
      Reactant          moles

      Fe(CN)2            1.00000

                     Relative
      Element           moles

      C                  2.00000
      Fe                 1.00000
      N                  2.00000

------------------------------Solution composition--------------------------------

      Elements           Molality       Moles

      Al                1.881e-02   1.796e-02
      C                 2.095e+00   2.000e+00
      Ca                1.260e-02   1.203e-02
      Cd                9.558e-08   9.126e-08
      Fe                1.164e+00   1.111e+00
      K                 2.748e-05   2.623e-05
      Mg                1.326e-06   1.266e-06
      Mn                2.462e-03   2.351e-03
      N                 2.095e+00   2.000e+00
      S                 2.013e-01   1.922e-01
      Si                5.364e-04   5.122e-04
      Zn                3.287e-06   3.138e-06

----------------------------Description of solution----------------------------

                                    pH  =  10.522      Charge balance
                                    pe  =  -8.238      Adjusted to redox
equilibrium
                       Activity of water  =   0.941
                 Ionic strength (mol/kgw)  =   1.831e-01
```

```
                    Mass of water (kg)  =   9.548e-01
               Total alkalinity (eq/kg)  =   2.776e+00
                     Total CO2 (mol/kg)  =   1.088e+00
                       Temperature (°C)  =  25.00
                Electrical balance (eq)  =  -7.125e-02
Percent error, 100*(Cat-|An|)/(Cat+|An|)  = -31.42
                            Iterations  =  21
                               Total H  = 1.110227e+02
                               Total O  = 5.627713e+01

-----------------------------Saturation indices-------------------------------

  Phase               SI** log IAP   log K(298 K,   1 atm)

  Adularia          1.74    -18.83  -20.57  KAlSi3O8
  Al(OH)3(a)       -0.49     10.31   10.80  Al(OH)3
  AlumK           -38.56    -43.73   -5.17  KAl(SO4)2:12H2O
  Alunite         -21.39    -22.79   -1.40  KAl3(SO4)2(OH)6
  Anhydrite        -7.74    -12.10   -4.36  CaSO4
  Annite           38.23    -47.42  -85.64  KFe3AlSi3O10(OH)2
  Anorthite         4.55    -15.17  -19.71  CaAl2Si2O8
  Aragonite         3.18     -5.16   -8.34  CaCO3
  Artinite         -4.72      4.88    9.60  MgCO3:Mg(OH)2:3H2O
  Basaluminite    -11.21     11.49   22.70  Al4(OH)10SO4
  Bianchite       -20.12    -21.89   -1.76  ZnSO4:6H2O
  Birnessite      -23.72     19.88   43.60  MnO2
  Bixbyite        -15.18    -15.79   -0.61  Mn2O3
  Boehmite          1.75     10.34    8.58  AlOOH
  Brucite          -2.96     13.88   16.84  Mg(OH)2
  Calcite           3.32     -5.16   -8.48  CaCO3
  Cd(gamma)       -13.17      0.42   13.59  Cd
  Cd(OH)2          -8.72      4.93   13.65  Cd(OH)2
  Cd(OH)2(a)       -8.80      4.93   13.73  Cd(OH)2
  Cd3(OH)2(SO4)2  -51.43    -44.72    6.71  Cd3(OH)2(SO4)2
  Cd3(OH)4SO4     -37.53    -14.97   22.56  Cd3(OH)4SO4
  Cd4(OH)6SO4     -38.44    -10.04   28.40  Cd4(OH)6SO4
  CdMetal         -13.07      0.42   13.49  Cd
  CdSiO3           -8.21      0.85    9.06  CdSiO3
  CdSO4           -24.73    -24.83   -0.10  CdSO4
  CdSO4:2.7H2O    -23.02    -24.90   -1.87  CdSO4:2.67H2O
  CdSO4:H2O       -23.20    -24.85   -1.66  CdSO4:H2O
  CH4(g)            2.88      0.02   -2.86  CH4
  Chlorite14A       9.44     77.82   68.38  Mg5Al2Si3O10(OH)8
  Chlorite7A        6.06     77.82   71.75  Mg5Al2Si3O10(OH)8
  Chrysotile        1.26     33.46   32.20  Mg3Si2O5(OH)4
  Clinoenstatite   -1.54      9.80   11.34  MgSiO3
  CO2(g)           -4.69     -6.16   -1.47  CO2
  Cristobalite     -0.52     -4.11   -3.59  SiO2
  Diaspore          3.46     10.34    6.88  AlOOH
  Diopside          3.48     23.37   19.89  CaMgSi2O6
  Dolomite          3.00    -14.09  -17.09  CaMg(CO3)2
  Dolomite(d)       2.45    -14.09  -16.54  CaMg(CO3)2
  Epsomite        -13.92    -16.06   -2.14  MgSO4:7H2O
  Fe(OH)3(a)        2.80      7.69    4.89  Fe(OH)3
  Fe3(OH)8         13.61     33.83   20.22  Fe3(OH)8
```

FeS(ppt)	8.15	4.24	-3.92	FeS
Forsterite	-4.60	23.71	28.31	Mg2SiO4
Gibbsite	2.20	10.31	8.11	Al(OH)3
Goethite	8.72	7.72	-1.00	FeOOH
Goslarite	-19.95	-21.91	-1.96	ZnSO4:7H2O
Greenalite	26.36	47.17	20.81	Fe3Si2O5(OH)4
Greenockite	6.65	-9.28	-15.93	CdS
Greigite	22.02	-23.02	-45.03	Fe3S4
Gypsum	-7.58	-12.16	-4.58	CaSO4:2H2O
Halloysite	-0.06	12.43	12.50	Al2Si2O5(OH)4
Hausmannite	-10.46	50.57	61.03	Mn3O4
Hematite	19.47	15.46	-4.01	Fe2O3
Huntite	-1.98	-31.94	-29.97	CaMg3(CO3)4
Hydromagnesite	-13.17	-21.94	-8.76	Mg5(CO3)4(OH)2:4H2O
Illite	4.50	-35.77	-40.27	K0.6Mg0.25Al2.3Si3.5O10(OH)2
Jarosite-K	-21.44	-30.65	-9.21	KFe3(SO4)2(OH)6
JarositeH	-31.10	-36.49	-5.39	(H3O)Fe3(SO4)2(OH)6
Jurbanite	-16.21	-19.44	-3.23	AlOHSO4
Kaolinite	5.00	12.43	7.43	Al2Si2O5(OH)4
Kmica	11.80	24.51	12.70	KAl3Si3O10(OH)2
Laumontite	7.47	-23.49	-30.96	CaAl2Si4O12:4H2O
Leonhardite	22.81	-46.95	-69.76	Ca2Al4Si8O24:7H2O
Mackinawite	8.89	4.24	-4.65	FeS
Maghemite	9.07	15.46	6.39	Fe2O3
Magnesite	-0.90	-8.93	-8.03	MgCO3
Magnetite	30.20	33.94	3.74	Fe3O4
Manganite	-7.74	17.60	25.34	MnOOH
Melanterite	-9.28	-11.49	-2.21	FeSO4:7H2O
Mn2(SO4)3	-99.43	-105.14	-5.71	Mn2(SO4)3
MnS(Green)	-2.70	1.10	3.80	MnS
MnSO4	-17.11	-14.44	2.67	MnSO4
Monteponite	-8.81	4.96	13.77	CdO
Montmorillonite-Ca	4.15	-40.88	-45.03	Ca0.165Al2.33Si3.67O10(OH)2
N2(g)	3.23	-0.03	-3.26	N2
Nesquehonite	-3.39	-9.01	-5.62	MgCO3:3H2O
NH3(g)	-2.34	-0.57	1.77	NH3
Nsutite	-22.68	19.88	42.56	MnO2
O2(g)	-74.11	-77.00	-2.89	O2
Otavite	-5.78	-17.88	-12.10	CdCO3
Phlogopite	2.23	45.53	43.30	KMg3AlSi3O10(OH)2
Portlandite	-5.15	17.65	22.80	Ca(OH)2
Prehnite	10.07	-1.62	-11.70	Ca2Al2Si3O10(OH)2
Pyrite	13.02	-5.46	-18.48	FeS2
Pyrochroite	0.12	15.32	15.20	Mn(OH)2
Pyrolusite	-21.50	19.88	41.38	MnO2
Pyrophyllite	7.23	-41.09	-48.31	Al2Si4O10(OH)2
Quartz	-0.13	-4.11	-3.98	SiO2
Rhodochrosite	3.64	-7.49	-11.13	MnCO3
Rhodochrosite(d)	2.90	-7.49	-10.39	MnCO3
Sepiolite	-0.36	15.40	15.76	Mg2Si3O7.5OH:3H2O
Sepiolite(d)	-3.26	15.40	18.66	Mg2Si3O7.5OH:3H2O
Siderite	6.53	-4.36	-10.89	FeCO3
Siderite(d)(3)	6.09	-4.36	-10.45	FeCO3
Silicagel	-1.09	-4.11	-3.02	SiO2
SiO2(a)	-1.40	-4.11	-2.71	SiO2

Smithsonite	-4.78	-14.78	-10.00	ZnCO3
Sphalerite	5.43	-6.19	-11.62	ZnS
Sulfur	-7.59	-22.62	-15.03	S
Talc	3.87	25.27	21.40	Mg3Si4O10(OH)2
Tremolite	15.44	72.01	56.57	Ca2Mg5Si8O22(OH)2
Wairakite	3.27	-23.43	-26.71	CaAl2Si4O12:2H2O
Willemite	-3.33	12.00	15.33	Zn2SiO4
Wurtzite	3.49	-6.19	-9.68	ZnS
Zincite(c)	-3.09	8.05	11.14	ZnO
Zincosite	-24.74	-21.73	3.01	ZnSO4
Zn(NO3)2:6H2O	-179.95	-176.51	3.44	Zn(NO3)2:6H2O
ZnMetal	-22.24	3.51	25.76	Zn
ZnO(a)	-3.26	8.05	11.31	ZnO
ZnS(a)	2.86	-6.19	-9.05	ZnS
ZnSiO3	1.02	3.95	2.93	ZnSiO3
ZnSO4:H2O	-21.19	-21.76	-0.57	ZnSO4:H2O

**For a gas, SI = log10(fugacity). Fugacity = pressure * phi / 1 atm.
  For ideal gases, phi = 1.

End of simulation.

APPENDIX B: BATCH SIMULATION RESULTS FOR TRACE METALS

```
-----------------------------------------------------
Beginning of initial surface-composition calculations.
-----------------------------------------------------
```

Surface 1

Diffuse Double Layer Surface-Complexation Model

Hfo

6.521e-03	Surface charge, eq
1.178e-02	sigma, C/m²
1.213e-02	psi, V
-4.720e-01	-F*psi/RT
6.237e-01	exp(-F*psi/RT)
6.000e+02	specific area, m²/g
5.340e+04	m² for 8.900e+01 g

Hfo_s

2.500e-03 moles

Species	Moles	Mole Fraction	Molality	Log Molality
Hfo_sOPb+	2.157e-03	0.863	2.157e-03	-2.666
Hfo_sOCu+	3.236e-04	0.129	3.236e-04	-3.490
Hfo_sOHCa+2	8.261e-06	0.003	8.261e-06	-5.083
Hfo_sOH2+	4.666e-06	0.002	4.666e-06	-5.331
Hfo_sOZn+	3.089e-06	0.001	3.089e-06	-5.510
Hfo_sONi+	2.984e-06	0.001	2.984e-06	-5.525
Hfo_sSO4-	6.011e-07	0.000	6.011e-07	-6.221
Hfo_sOH	1.213e-07	0.000	1.213e-07	-6.916
Hfo_sOCo+	6.926e-08	0.000	6.926e-08	-7.159
Hfo_sOHSO4-2	3.112e-08	0.000	3.112e-08	-7.507
Hfo_sO-	7.226e-11	0.000	7.226e-11	-10.141

Hfo_w

5.000e-03 moles

Species	Moles	Mole Fraction	Molality	Log Molality
Hfo_wOH2+	3.247e-03	0.649	3.247e-03	-2.488
Hfo_wOCu+	1.155e-03	0.231	1.155e-03	-2.937
Hfo_wSO4-	4.184e-04	0.084	4.184e-04	-3.378
Hfo_wOH	8.444e-05	0.017	8.444e-05	-4.073
Hfo_wOPb+	6.705e-05	0.013	6.705e-05	-4.174
Hfo_wOHSO4-2	2.166e-05	0.004	2.166e-05	-4.664
Hfo_wONi+	2.801e-06	0.001	2.801e-06	-5.553
Hfo_wOZn+	2.252e-06	0.000	2.252e-06	-5.648
Hfo_wOMg+	8.610e-07	0.000	8.610e-07	-6.065
Hfo_wOCo+	1.359e-07	0.000	1.359e-07	-6.867

Hfo_wO-	5.030e-08	0.000	5.030e-08	-7.298
Hfo_wOCa+	4.412e-08	0.000	4.412e-08	-7.355

Surface 2

Diffuse Double Layer Surface-Complexation Model

Hfo

5.845e-03	Surface charge, eq
3.168e-02	sigma, C/m²
3.100e-02	psi, V
-1.207e+00	-F*psi/RT
2.992e-01	exp(-F*psi/RT)
2.000e+02	specific area, m²/g
1.780e+04	m² for 8.900e+01 g

Hfo_s

5.000e-03 moles

Species	Moles	Mole Fraction	Molality	Log Molality
Hfo_sOPb+	4.317e-03	0.863	4.317e-03	-2.365
Hfo_sOCu+	6.476e-04	0.130	6.476e-04	-3.189
Hfo_sOH2+	9.338e-06	0.002	9.338e-06	-5.030
Hfo_sOHCa+2	7.932e-06	0.002	7.932e-06	-5.101
Hfo_sOZn+	6.183e-06	0.001	6.183e-06	-5.209
Hfo_sONi+	5.972e-06	0.001	5.972e-06	-5.224
Hfo_sSO4-	5.228e-06	0.001	5.228e-06	-5.282
Hfo_sOHSO4-2	5.643e-07	0.000	5.643e-07	-6.249
Hfo_sOH	5.062e-07	0.000	5.062e-07	-6.296
Hfo_sOCo+	1.386e-07	0.000	1.386e-07	-6.858
Hfo_sO-	6.285e-10	0.000	6.285e-10	-9.202

Hfo_w

2.500e-03 moles

Species	Moles	Mole Fraction	Molality	Log Molality
Hfo_wOH2+	1.218e-03	0.487	1.218e-03	-2.914
Hfo_wSO4-	6.819e-04	0.273	6.819e-04	-3.166
Hfo_wOCu+	4.332e-04	0.173	4.332e-04	-3.363
Hfo_wOHSO4-2	7.359e-05	0.029	7.359e-05	-4.133
Hfo_wOH	6.601e-05	0.026	6.601e-05	-4.180
Hfo_wOPb+	2.515e-05	0.010	2.515e-05	-4.600
Hfo_wONi+	1.051e-06	0.000	1.051e-06	-5.979
Hfo_wOZn+	8.444e-07	0.000	8.444e-07	-6.073
Hfo_wOMg+	3.229e-07	0.000	3.229e-07	-6.491
Hfo_wO-	8.197e-08	0.000	8.197e-08	-7.086
Hfo_wOCo+	5.096e-08	0.000	5.096e-08	-7.293
Hfo_wOCa+	1.655e-08	0.000	1.655e-08	-7.781

Surface 3

Diffuse Double Layer Surface-Complexation Model

```
Hfo
        3.369e-03  Surface charge, eq
        6.089e-02  sigma, C/m²
        5.321e-02  psi, V
       -2.071e+00  -F*psi/RT
        1.260e-01  exp(-F*psi/RT)
        6.000e+01  specific area, m²/g
        5.340e+03  m² for   8.900e+01 g

Hfo_s
        5.000e-03  moles
                                        Mole                    Log
      Species               Moles     Fraction    Molality    Molality

      Hfo_sOPb+          4.293e-03       0.859   4.293e-03      -2.367
      Hfo_sOCu+          6.441e-04       0.129   6.441e-04      -3.191
      Hfo_sSO4-          2.931e-05       0.006   2.931e-05      -4.533
      Hfo_sOH2+          9.287e-06       0.002   9.287e-06      -5.032
      Hfo_sOHSO4-2       7.512e-06       0.002   7.512e-06      -5.124
      Hfo_sOZn+          6.150e-06       0.001   6.150e-06      -5.211
      Hfo_sONi+          5.939e-06       0.001   5.939e-06      -5.226
      Hfo_sOHCa+2        3.322e-06       0.001   3.322e-06      -5.479
      Hfo_sOH            1.195e-06       0.000   1.195e-06      -5.923
      Hfo_sOCo+          1.379e-07       0.000   1.379e-07      -6.861
      Hfo_sO-            3.524e-09       0.000   3.524e-09      -8.453

Hfo_w
        2.500e-03  moles
                                        Mole                    Log
      Species               Moles     Fraction    Molality    Molality

      Hfo_wSO4-          1.442e-03       0.577   1.442e-03      -2.841
      Hfo_wOH2+          4.568e-04       0.183   4.568e-04      -3.340
      Hfo_wOHSO4-2       3.695e-04       0.148   3.695e-04      -3.432
      Hfo_wOCu+          1.625e-04       0.065   1.625e-04      -3.789
      Hfo_wOH            5.879e-05       0.024   5.879e-05      -4.231
      Hfo_wOPb+          9.432e-06       0.004   9.432e-06      -5.025
      Hfo_wONi+          3.941e-07       0.000   3.941e-07      -6.404
      Hfo_wOZn+          3.167e-07       0.000   3.167e-07      -6.499
      Hfo_wO-            1.733e-07       0.000   1.733e-07      -6.761
      Hfo_wOMg+          1.211e-07       0.000   1.211e-07      -6.917
      Hfo_wOCo+          1.911e-08       0.000   1.911e-08      -7.719
      Hfo_wOCa+          6.207e-09       0.000   6.207e-09      -8.207

------------------
End of simulation.
------------------

-----------------------------------
Reading input data for simulation 3.
-----------------------------------

------------------------------
End of Run after 0.86 Seconds.
------------------------------
```

APPENDIX C: REACTIVE TRANSPORT SIMULATION RESULTS FOR METALS

sim	state	soln	dist_x	time	step	pH	pe	Pb	Cu	Zn	Ni	Co
1	i_soln	0	-99	-99	-99	10.3	10.6	8.20e-05	2.28e-04	1.62e-04	4.89e-04	3.33e-04
1	i_soln	1	-99	-99	-99	2.75	8	0.0e+00	0.0e+00	0.0e+00	0.0e+00	0.0e+00
1	i_exch	1	-99	-99	-99	2.75	8	0.0e+00	0.0e+00	0.0e+00	0.0e+00	0.0e+00
1	i_surf	1	-99	-99	-99	2.75	8	0.0e+00	0.0e+00	0.0e+00	0.0e+00	0.0e+00
1	transp	0	0	0	0	10.3	10.6	8.20e-05	2.28e-04	1.62e-04	4.89e-04	3.33e-04
1	transp	1	0.5	0	0	2.76	17.5	0.0e+00	0.0e+00	0.0e+00	0.0e+00	0.0e+00
1	transp	2	1.5	0	0	2.76	17.5	0.0e+00	0.0e+00	0.0e+00	0.0e+00	0.0e+00
1	transp	3	2.5	0	0	2.76	17.5	0.0e+00	0.0e+00	0.0e+00	0.0e+00	0.0e+00
1	transp	4	3.5	0	0	2.76	17.5	0.0e+00	0.0e+00	0.0e+00	0.0e+00	0.0e+00
1	transp	5	4.5	0	0	2.76	17.5	0.0e+00	0.0e+00	0.0e+00	0.0e+00	0.0e+00
1	transp	6	5.5	0	0	2.76	17.5	0.0e+00	0.0e+00	0.0e+00	0.0e+00	0.0e+00
1	transp	7	6.5	0	0	2.76	17.5	0.0e+00	0.0e+00	0.0e+00	0.0e+00	0.0e+00
1	transp	8	7.5	0	0	2.76	17.5	0.0e+00	0.0e+00	0.0e+00	0.0e+00	0.0e+00
1	transp	9	8.5	0	0	2.76	17.5	0.0e+00	0.0e+00	0.0e+00	0.0e+00	0.0e+00

1	transp	10	9.5	0	0	2.76	17.5	0.0e+00	0.0e+00	0.0e+00	0.0e+00	0.0e+00
1	transp	11	10.5	0	0	2.76	17.5	0.0e+00	0.0e+00	0.0e+00	0.0e+00	0.0e+00
1	transp	12	11.5	0	0	2.76	17.5	0.0e+00	0.0e+00	0.0e+00	0.0e+00	0.0e+00
1	transp	13	12.5	0	0	2.76	17.5	0.0e+00	0.0e+00	0.0e+00	0.0e+00	0.0e+00
1	transp	14	13.5	0	0	2.76	17.5	0.0e+00	0.0e+00	0.0e+00	0.0e+00	0.0e+00
1	transp	15	14.5	0	0	2.76	17.5	0.0e+00	0.0e+00	0.0e+00	0.0e+00	0.0e+00
1	transp	16	15.5	0	0	2.76	17.5	0.0e+00	0.0e+00	0.0e+00	0.0e+00	0.0e+00
1	transp	17	16.5	0	0	2.76	17.5	0.0e+00	0.0e+00	0.0e+00	0.0e+00	0.0e+00
1	transp	18	17.5	0	0	2.76	17.5	0.0e+00	0.0e+00	0.0e+00	0.0e+00	0.0e+00
1	transp	19	18.5	0	0	2.76	17.5	0.0e+00	0.0e+00	0.0e+00	0.0e+00	0.0e+00
1	transp	20	19.5	0	0	2.76	17.5	0.0e+00	0.0e+00	0.0e+00	0.0e+00	0.0e+00
1	transp	21	20.5	0	0	2.76	17.5	0.0e+00	0.0e+00	0.0e+00	0.0e+00	0.0e+00
1	transp	22	21.5	0	0	2.76	17.5	0.0e+00	0.0e+00	0.0e+00	0.0e+00	0.0e+00
1	transp	23	22.5	0	0	2.76	17.5	0.0e+00	0.0e+00	0.0e+00	0.0e+00	0.0e+00
1	transp	24	23.5	0	0	2.76	17.5	0.0e+00	0.0e+00	0.0e+00	0.0e+00	0.0e+00
1	transp	25	24.5	0	0	2.76	17.5	0.0e+00	0.0e+00	0.0e+00	0.0e+00	0.0e+00
1	transp	26	25.5	0	0	2.76	17.5	0.0e+00	0.0e+00	0.0e+00	0.0e+00	0.0e+00
1	transp	27	26.5	0	0	2.76	17.5	0.0e+00	0.0e+00	0.0e+00	0.0e+00	0.0e+00

1	transp	28	27.5	0	0	2.76	17.5	0.0e+00	0.0e+00	0.0e+00	0.0e+00	0.0e+00
1	transp	29	28.5	0	0	2.76	17.5	0.0e+00	0.0e+00	0.0e+00	0.0e+00	0.0e+00
1	transp	30	29.5	0	0	2.76	17.5	0.0e+00	0.0e+00	0.0e+00	0.0e+00	0.0e+00
1	transp	31	30.5	0	0	2.76	17.5	0.0e+00	0.0e+00	0.0e+00	0.0e+00	0.0e+00
1	transp	32	31.5	0	0	2.76	17.5	0.0e+00	0.0e+00	0.0e+00	0.0e+00	0.0e+00
1	transp	33	32.5	0	0	2.76	17.5	0.0e+00	0.0e+00	0.0e+00	0.0e+00	0.0e+00
1	transp	34	33.5	0	0	2.76	17.5	0.0e+00	0.0e+00	0.0e+00	0.0e+00	0.0e+00
1	transp	35	34.5	0	0	2.76	17.5	0.0e+00	0.0e+00	0.0e+00	0.0e+00	0.0e+00
1	transp	36	35.5	0	0	2.76	17.5	0.0e+00	0.0e+00	0.0e+00	0.0e+00	0.0e+00
1	transp	37	36.5	0	0	2.76	17.5	0.0e+00	0.0e+00	0.0e+00	0.0e+00	0.0e+00
1	transp	38	37.5	0	0	2.76	17.5	0.0e+00	0.0e+00	0.0e+00	0.0e+00	0.0e+00
1	transp	39	38.5	0	0	2.76	17.5	0.0e+00	0.0e+00	0.0e+00	0.0e+00	0.0e+00
1	transp	40	39.5	0	0	2.76	17.5	0.0e+00	0.0e+00	0.0e+00	0.0e+00	0.0e+00
1	transp	41	40.5	0	0	2.76	17.5	0.0e+00	0.0e+00	0.0e+00	0.0e+00	0.0e+00
1	transp	42	41.5	0	0	2.76	17.5	0.0e+00	0.0e+00	0.0e+00	0.0e+00	0.0e+00
1	transp	43	42.5	0	0	2.76	17.5	0.0e+00	0.0e+00	0.0e+00	0.0e+00	0.0e+00
1	transp	44	43.5	0	0	2.76	17.5	0.0e+00	0.0e+00	0.0e+00	0.0e+00	0.0e+00
1	transp	45	44.5	0	0	2.76	17.5	0.0e+00	0.0e+00	0.0e+00	0.0e+00	0.0e+00

1	transp	46	45.5	0	0	2.76	17.5	0.0e+00	0.0e+00	0.0e+00	0.0e+00	0.0e+00
1	transp	47	46.5	0	0	2.76	17.5	0.0e+00	0.0e+00	0.0e+00	0.0e+00	0.0e+00
1	transp	48	47.5	0	0	2.76	17.5	0.0e+00	0.0e+00	0.0e+00	0.0e+00	0.0e+00
1	transp	49	48.5	0	0	2.76	17.5	0.0e+00	0.0e+00	0.0e+00	0.0e+00	0.0e+00
1	transp	50	49.5	0	0	2.76	17.5	0.0e+00	0.0e+00	0.0e+00	0.0e+00	0.0e+00
1	transp	51	50	0	0	2.76	17.5	0.0e+00	0.0e+00	0.0e+00	0.0e+00	0.0e+00
1	transp	1	0.5	0	1	6.46	14.4	3.23e-11	5.12e-09	1.82e-08	4.89e-04	3.33e-04
1	transp	2	1.5	0	1	2.76	17.5	0.0e+00	0.0e+00	0.0e+00	0.0e+00	0.0e+00
1	transp	3	2.5	0	1	2.76	17.5	0.0e+00	0.0e+00	0.0e+00	0.0e+00	0.0e+00
1	transp	4	3.5	0	1	2.76	17.5	0.0e+00	0.0e+00	0.0e+00	0.0e+00	0.0e+00
1	transp	5	4.5	0	1	2.76	17.5	0.0e+00	0.0e+00	0.0e+00	0.0e+00	0.0e+00
1	transp	6	5.5	0	1	2.76	17.5	0.0e+00	0.0e+00	0.0e+00	0.0e+00	0.0e+00
1	transp	7	6.5	0	1	2.76	17.5	0.0e+00	0.0e+00	0.0e+00	0.0e+00	0.0e+00
1	transp	8	7.5	0	1	2.76	17.5	0.0e+00	0.0e+00	0.0e+00	0.0e+00	0.0e+00
1	transp	9	8.5	0	1	2.76	17.5	0.0e+00	0.0e+00	0.0e+00	0.0e+00	0.0e+00
1	transp	10	9.5	0	1	2.76	17.5	0.0e+00	0.0e+00	0.0e+00	0.0e+00	0.0e+00
1	transp	11	10.5	0	1	2.76	17.5	0.0e+00	0.0e+00	0.0e+00	0.0e+00	0.0e+00
1	transp	12	11.5	0	1	2.76	17.5	0.0e+00	0.0e+00	0.0e+00	0.0e+00	0.0e+00

1	transp	13	12.5	0	1	2.76	17.5	0.0e+00	0.0e+00	0.0e+00	0.0e+00	0.0e+00
1	transp	14	13.5	0	1	2.76	17.5	0.0e+00	0.0e+00	0.0e+00	0.0e+00	0.0e+00
1	transp	15	14.5	0	1	2.76	17.5	0.0e+00	0.0e+00	0.0e+00	0.0e+00	0.0e+00
1	transp	16	15.5	0	1	2.76	17.5	0.0e+00	0.0e+00	0.0e+00	0.0e+00	0.0e+00
1	transp	17	16.5	0	1	2.76	17.5	0.0e+00	0.0e+00	0.0e+00	0.0e+00	0.0e+00
1	transp	18	17.5	0	1	2.76	17.5	0.0e+00	0.0e+00	0.0e+00	0.0e+00	0.0e+00
1	transp	19	18.5	0	1	2.76	17.5	0.0e+00	0.0e+00	0.0e+00	0.0e+00	0.0e+00
1	transp	20	19.5	0	1	2.76	17.5	0.0e+00	0.0e+00	0.0e+00	0.0e+00	0.0e+00
1	transp	21	20.5	0	1	2.76	17.5	0.0e+00	0.0e+00	0.0e+00	0.0e+00	0.0e+00
1	transp	22	21.5	0	1	2.76	17.5	0.0e+00	0.0e+00	0.0e+00	0.0e+00	0.0e+00
1	transp	23	22.5	0	1	2.76	17.5	0.0e+00	0.0e+00	0.0e+00	0.0e+00	0.0e+00
1	transp	24	23.5	0	1	2.76	17.5	0.0e+00	0.0e+00	0.0e+00	0.0e+00	0.0e+00
1	transp	25	24.5	0	1	2.76	17.5	0.0e+00	0.0e+00	0.0e+00	0.0e+00	0.0e+00
1	transp	26	25.5	0	1	2.76	17.5	0.0e+00	0.0e+00	0.0e+00	0.0e+00	0.0e+00
1	transp	27	26.5	0	1	2.76	17.5	0.0e+00	0.0e+00	0.0e+00	0.0e+00	0.0e+00
1	transp	28	27.5	0	1	2.76	17.5	0.0e+00	0.0e+00	0.0e+00	0.0e+00	0.0e+00
1	transp	29	28.5	0	1	2.76	17.5	0.0e+00	0.0e+00	0.0e+00	0.0e+00	0.0e+00
1	transp	30	29.5	0	1	2.76	17.5	0.0e+00	0.0e+00	0.0e+00	0.0e+00	0.0e+00

1	transp	31	30.5	0	1	2.76	17.5	0.0e+00	0.0e+00	0.0e+00	0.0e+00	0.0e+00
1	transp	32	31.5	0	1	2.76	17.5	0.0e+00	0.0e+00	0.0e+00	0.0e+00	0.0e+00
1	transp	33	32.5	0	1	2.76	17.5	0.0e+00	0.0e+00	0.0e+00	0.0e+00	0.0e+00
1	transp	34	33.5	0	1	2.76	17.5	0.0e+00	0.0e+00	0.0e+00	0.0e+00	0.0e+00
1	transp	35	34.5	0	1	2.76	17.5	0.0e+00	0.0e+00	0.0e+00	0.0e+00	0.0e+00
1	transp	36	35.5	0	1	2.76	17.5	0.0e+00	0.0e+00	0.0e+00	0.0e+00	0.0e+00
1	transp	37	36.5	0	1	2.76	17.5	0.0e+00	0.0e+00	0.0e+00	0.0e+00	0.0e+00
1	transp	38	37.5	0	1	2.76	17.5	0.0e+00	0.0e+00	0.0e+00	0.0e+00	0.0e+00
1	transp	39	38.5	0	1	2.76	17.5	0.0e+00	0.0e+00	0.0e+00	0.0e+00	0.0e+00
1	transp	40	39.5	0	1	2.76	17.5	0.0e+00	0.0e+00	0.0e+00	0.0e+00	0.0e+00
1	transp	41	40.5	0	1	2.76	17.5	0.0e+00	0.0e+00	0.0e+00	0.0e+00	0.0e+00
1	transp	42	41.5	0	1	2.76	17.5	0.0e+00	0.0e+00	0.0e+00	0.0e+00	0.0e+00
1	transp	43	42.5	0	1	2.76	17.5	0.0e+00	0.0e+00	0.0e+00	0.0e+00	0.0e+00
1	transp	44	43.5	0	1	2.76	17.5	0.0e+00	0.0e+00	0.0e+00	0.0e+00	0.0e+00
1	transp	45	44.5	0	1	2.76	17.5	0.0e+00	0.0e+00	0.0e+00	0.0e+00	0.0e+00
1	transp	46	45.5	0	1	2.76	17.5	0.0e+00	0.0e+00	0.0e+00	0.0e+00	0.0e+00

APPENDIX D: BATCH SIMULATION RESULTS FOR PHOSPHATE IONS

```
-------------------------------------------------------
Beginning of initial surface-composition calculations.
-------------------------------------------------------

Surface 1.

Diffuse Double Layer Surface-Complexation Model

Hfo
       -3.293e-05  Surface charge, eq
       -5.297e-03  sigma, C/m²
       -1.828e-02  psi, V
        7.116e-01  -F*psi/RT
        2.037e+00  exp(-F*psi/RT)
        6.000e+02  specific area, m²/g
        6.000e+02  m² for   1.000e+00 g


Hfo_s
        5.620e-07  moles
                                        Mole                    Log
      Species                Moles    Fraction    Molality    Molality

      Hfo_sOHCa+2        5.059e-07       0.900   5.059e-07      -6.296
      Hfo_sOH            3.914e-08       0.070   3.914e-08      -7.407
      Hfo_sOH2+          1.451e-08       0.026   1.451e-08      -7.838
      Hfo_sO-            2.418e-09       0.004   2.418e-09      -8.616

Hfo_w
        2.248e-05  moles
                                        Mole                    Log
      Species                Moles    Fraction    Molality    Molality

      Hfo_wPO4-2         1.176e-05       0.523   1.176e-05      -4.929
      Hfo_wHPO4-         1.046e-05       0.465   1.046e-05      -4.980
      Hfo_wH2PO4         1.580e-07       0.007   1.580e-07      -6.801
      Hfo_wOH            6.022e-08       0.003   6.022e-08      -7.220
      Hfo_wOH2+          2.233e-08       0.001   2.233e-08      -7.651
      Hfo_wOMg+          1.055e-08       0.000   1.055e-08      -7.977
      Hfo_wO-            3.721e-09       0.000   3.721e-09      -8.429
      Hfo_wOCa+          6.197e-10       0.000   6.197e-10      -9.208
      Hfo_wOHSO4-2       8.116e-11       0.000   8.116e-11     -10.091
      Hfo_wSO4-          1.508e-11       0.000   1.508e-11     -10.822
      Hfo_wOHF-          1.088e-12       0.000   1.088e-12     -11.963
      Hfo_wF             2.605e-13       0.000   2.605e-13     -12.584

----------------------------------------
Beginning of batch-reaction calculations.
----------------------------------------
```

```
Reaction step 1.

Using solution 1.
Using surface 1.

------------------------------Surface composition------------------------------

Diffuse Double Layer Surface-Complexation Model

Hfo
       -3.293e-05  Surface charge, eq
       -5.297e-03  sigma, C/m²
       -1.828e-02  psi, V
        7.116e-01  -F*psi/RT
        2.037e+00  exp(-F*psi/RT)
        6.000e+02  specific area, m²/g
        6.000e+02  m²  for   1.000e+00 g

Hfo_s
        5.620e-07  moles
                                        Mole                    Log
      Species               Moles     Fraction    Molality    Molality

      Hfo_sOHCa+2       5.059e-07       0.900   5.059e-07      -6.296
      Hfo_sOH           3.914e-08       0.070   3.914e-08      -7.407
      Hfo_sOH2+         1.451e-08       0.026   1.451e-08      -7.838
      Hfo_sO-           2.418e-09       0.004   2.418e-09      -8.616

Hfo_w
        2.248e-05  moles
                                        Mole                    Log
      Species               Moles     Fraction    Molality    Molality

      Hfo_wPO4-2        1.176e-05       0.523   1.176e-05      -4.929
      Hfo_wHPO4-        1.046e-05       0.465   1.046e-05      -4.980
      Hfo_wH2PO4        1.580e-07       0.007   1.580e-07      -6.801
      Hfo_wOH           6.022e-08       0.003   6.022e-08      -7.220
      Hfo_wOH2+         2.233e-08       0.001   2.233e-08      -7.651
      Hfo_wOMg+         1.055e-08       0.000   1.055e-08      -7.977
      Hfo_wO-           3.721e-09       0.000   3.721e-09      -8.429
      Hfo_wOCa+         6.197e-10       0.000   6.197e-10      -9.208
      Hfo_wOHSO4-2      8.116e-11       0.000   8.116e-11     -10.091
      Hfo_wSO4-         1.508e-11       0.000   1.508e-11     -10.822
      Hfo_wOHF-         1.088e-12       0.000   1.088e-12     -11.963
      Hfo_wF            2.605e-13       0.000   2.605e-13     -12.584

----------------------------Solution composition----------------------------

      Elements           Molality       Moles

      Br                6.135e-07   6.135e-07
      Ca                1.408e-04   1.408e-04
      Cl                5.785e-04   5.785e-04
      F                 1.053e-06   1.053e-06
      K                 6.703e-05   6.703e-05
```

```
      Mg                1.625e-04   1.625e-04
      N                 7.606e-04   7.606e-04
      Na                2.620e-04   2.620e-04
      P                 6.332e-03   6.332e-03
      S                 1.490e-03   1.490e-03

----------------------------Description of solution----------------------------

                                     pH  =   8.030      Charge balance
                                     pe  =  11.338      Adjusted to redox
equilibrium
                        Activity of water  =   1.000
                Ionic strength (mol/kgw)   =   1.544e-02
                      Mass of water (kg)   =   1.000e+00
                Total alkalinity (eq/kg)   =   5.793e-03
                       Temperature (°C)    =  25.00
                 Electrical balance (eq)   =  -1.551e-02
 Percent error, 100*(Cat-|An|)/(Cat+|An|)  = -93.53
                               Iterations  =  16
                                  Total H  = 1.110193e+02
                                  Total O  = 5.553979e+01

----------------------------Distribution of species----------------------------

                                                 Log       Log       Log    mole V
   Species          Molality    Activity  Molality  Activity     Gamma   cm³/mol

   OH-             1.219e-06   1.073e-06    -5.914    -5.970    -0.055      (0)
   H+              1.038e-08   9.333e-09    -7.984    -8.030    -0.046      0.00
   H2O             5.551e+01   9.998e-01     1.744    -0.000     0.000     18.07
   Br              6.135e-07
   Br-             6.135e-07   5.417e-07    -6.212    -6.266    -0.054      (0)
   Ca              1.408e-04
   CaHPO4          6.247e-05   6.269e-05    -4.204    -4.203     0.002      (0)
   Ca+2            5.387e-05   3.337e-05    -4.269    -4.477    -0.208      (0)
   CaPO4-          1.791e-05   1.589e-05    -4.747    -4.799    -0.052      (0)
   CaSO4           6.020e-06   6.041e-06    -5.220    -5.219     0.002      (0)
   CaH2PO4+        4.956e-07   4.398e-07    -6.305    -6.357    -0.052      (0)
   CaOH+           6.672e-10   5.934e-10    -9.176    -9.227    -0.051      (0)
   CaF+            3.028e-10   2.687e-10    -9.519    -9.571    -0.052      (0)
   CaHSO4+         3.740e-13   3.303e-13   -12.427   -12.481    -0.054      (0)
   Cl              5.785e-04
   Cl-             5.785e-04   5.094e-04    -3.238    -3.293    -0.055      (0)
   F               1.053e-06
   F-              1.050e-06   9.246e-07    -5.979    -6.034    -0.055      (0)
   MgF+            2.208e-09   1.952e-09    -8.656    -8.709    -0.054      (0)
   CaF+            3.028e-10   2.687e-10    -9.519    -9.571    -0.052      (0)
   NaF             1.215e-10   1.219e-10    -9.916    -9.914     0.002      (0)
   HF              1.289e-11   1.294e-11   -10.890   -10.888     0.002      (0)
   HF2-            5.216e-17   4.591e-17   -16.283   -16.338    -0.055      (0)
   H2F2            4.349e-22   4.364e-22   -21.362   -21.360     0.002      (0)
   H(0)            0.000e+00
   H2              0.000e+00   0.000e+00   -41.887   -41.885     0.002      (0)
   K               6.703e-05
   K+              6.617e-05   5.827e-05    -4.179    -4.235    -0.055      (0)
```

KHPO4-	4.388e-07	3.893e-07	-6.358	-6.410	-0.052	(0)
KSO4-	4.186e-07	3.715e-07	-6.378	-6.430	-0.052	(0)
Mg	1.625e-04					
MgHPO4	8.089e-05	8.118e-05	-4.092	-4.091	0.002	(0)
Mg+2	5.111e-05	3.196e-05	-4.291	-4.495	-0.204	(0)
MgPO4-	2.314e-05	2.053e-05	-4.636	-4.688	-0.052	(0)
MgSO4	6.773e-06	6.797e-06	-5.169	-5.168	0.002	(0)
MgH2PO4+	6.044e-07	5.363e-07	-6.219	-6.271	-0.052	(0)
MgOH+	1.395e-08	1.243e-08	-7.855	-7.905	-0.050	(0)
MgF+	2.208e-09	1.952e-09	-8.656	-8.709	-0.054	(0)
N(-3)	0.000e+00					
NH4+	0.000e+00	0.000e+00	-55.046	-55.100	-0.054	(0)
NH3	0.000e+00	0.000e+00	-56.314	-56.314	0.000	(0)
NH4SO4-	0.000e+00	0.000e+00	-56.979	-57.032	-0.053	(0)
N(0)	1.960e-09					
N2	9.800e-10	9.835e-10	-9.009	-9.007	0.002	(0)
N(3)	5.169e-14					
NO2-	5.169e-14	4.564e-14	-13.287	-13.341	-0.054	(0)
N(5)	7.606e-04					
NO3-	7.606e-04	6.679e-04	-3.119	-3.175	-0.056	(0)
Na	2.620e-04					
Na+	2.591e-04	2.291e-04	-3.587	-3.640	-0.053	(0)
NaHPO4-	1.725e-06	1.531e-06	-5.763	-5.815	-0.052	(0)
NaSO4-	1.174e-06	1.042e-06	-5.930	-5.982	-0.052	(0)
NaF	1.215e-10	1.219e-10	-9.916	-9.914	0.002	(0)
O(0)	4.900e-09					
O2	2.450e-09	2.459e-09	-8.611	-8.609	0.002	(0)
P	6.332e-03					
HPO4-2	5.563e-03	3.426e-03	-2.255	-2.465	-0.211	(0)
H2PO4-	5.804e-04	5.150e-04	-3.236	-3.288	-0.052	(0)
MgHPO4	8.089e-05	8.118e-05	-4.092	-4.091	0.002	(0)
CaHPO4	6.247e-05	6.269e-05	-4.204	-4.203	0.002	(0)
MgPO4-	2.314e-05	2.053e-05	-4.636	-4.688	-0.052	(0)
CaPO4-	1.791e-05	1.589e-05	-4.747	-4.799	-0.052	(0)
NaHPO4-	1.725e-06	1.531e-06	-5.763	-5.815	-0.052	(0)
MgH2PO4+	6.044e-07	5.363e-07	-6.219	-6.271	-0.052	(0)
CaH2PO4+	4.956e-07	4.398e-07	-6.305	-6.357	-0.052	(0)
PO4-3	4.926e-07	1.655e-07	-6.308	-6.781	-0.474	(0)
KHPO4-	4.388e-07	3.893e-07	-6.358	-6.410	-0.052	(0)
S(-2)	0.000e+00					
HS-	0.000e+00	0.000e+00	-132.256	-132.311	-0.055	(0)
H2S	0.000e+00	0.000e+00	-133.401	-133.400	0.002	(0)
S5-2	0.000e+00	0.000e+00	-133.706	-133.876	-0.170	(0)
S4-2	0.000e+00	0.000e+00	-133.930	-134.110	-0.180	(0)
S6-2	0.000e+00	0.000e+00	-134.001	-134.162	-0.161	(0)
S-2	0.000e+00	0.000e+00	-136.989	-137.199	-0.211	(0)
S3-2	0.000e+00	0.000e+00	-137.372	-137.563	-0.191	(0)
S2-2	0.000e+00	0.000e+00	-138.609	-138.809	-0.200	(0)
S(6)	1.490e-03					
SO4-2	1.475e-03	9.072e-04	-2.831	-3.042	-0.211	(0)
MgSO4	6.773e-06	6.797e-06	-5.169	-5.168	0.002	(0)
CaSO4	6.020e-06	6.041e-06	-5.220	-5.219	0.002	(0)
NaSO4-	1.174e-06	1.042e-06	-5.930	-5.982	-0.052	(0)
KSO4-	4.186e-07	3.715e-07	-6.378	-6.430	-0.052	(0)
HSO4-	9.311e-10	8.231e-10	-9.031	-9.085	-0.054	(0)

```
   CaHSO4+          3.740e-13   3.303e-13   -12.427   -12.481    -0.054      (0)
   NH4SO4-          0.000e+00   0.000e+00   -56.979   -57.032    -0.053      (0)

------------------------------Saturation indices--------------------------------

  Phase               SI** log IAP   log K(298 K,   1 atm)

  Anhydrite         -3.16     -7.52   -4.36  CaSO4
  Brucite           -5.28     11.56   16.84  Mg(OH)2
  Epsomite          -5.40     -7.54   -2.14  MgSO4:7H2O
  Fluorapatite       5.88    -11.72  -17.60  Ca5(PO4)3F
  Fluorite          -5.95    -16.54  -10.60  CaF2
  Gypsum            -2.94     -7.52   -4.58  CaSO4:2H2O
  H2(g)            -38.74    -41.89   -3.15  H2
  H2O(g)            -1.51     -0.00    1.51  H2O
  H2S(g)          -132.40   -133.40   -1.00  H2S
  Halite            -8.51     -6.93    1.58  NaCl
  Hydroxyapatite     5.76      2.34   -3.42  Ca5(PO4)3OH
  Mirabilite        -9.21    -10.32   -1.11  Na2SO4:10H2O
  N2(g)             -5.75     -9.01   -3.26  N2
  NH3(g)           -58.08    -56.31    1.77  NH3
  O2(g)             -5.72     -8.61   -2.89  O2
  Portlandite      -11.22     11.58   22.80  Ca(OH)2
  Sulfur           -99.50   -114.52  -15.03  S
  Thenardite       -10.14    -10.32   -0.18  Na2SO4

**For a gas, SI = log10(fugacity). Fugacity = pressure * phi / 1 atm.
  For ideal gases, phi = 1.

------------------
End of simulation.
------------------
```

APPENDIX E: REACTIVE TRANSPORT RESULTS FOR ANIONS

```
------------------------------------
Beginning of transport calculations.
------------------------------------

--------------------------------
Equilibrating initial solutions
--------------------------------

Using solution 10.      Solution after simulation 1.
Using exchange 10.      Exchange assemblage after simulation 1.
Using surface 10. Equilibrate the column with sewage water
Using pure phase assemblage 10.     Pure-phase assemblage after simulation 1.

-------------------------------Phase assemblage--------------------------------

                                                        Moles in assemblage
Phase               SI  log IAP  log K(T, P)   Initial       Final       Delta

Gypsum            0.00    -4.58     -4.58    7.599e-01   7.599e-01  -1.110e-15

------------------------------Surface composition-------------------------------

Hfo
        2.303e-04  Surface charge, eq
Hfo_s
        2.250e-04  moles
                                          Mole                    Log
      Species               Moles     Fraction    Molality    Molality

      Hfo_sOH2+         2.249e-04        1.000   2.243e-04      -3.649
      Hfo_sOHCa+2       6.972e-08        0.000   6.952e-08      -7.158
      Hfo_sOH           2.007e-10        0.000   2.001e-10      -9.699
      Hfo_sO-           4.103e-18        0.000   4.091e-18     -17.388

Hfo
        2.303e-04  Surface charge, eq
Hfo_w
        2.250e-05  moles
                                          Mole                    Log
      Species               Moles     Fraction    Molality    Molality

      Hfo_wH2PO4        1.708e-05        0.759   1.703e-05      -4.769
      Hfo_wOH2+         5.300e-06        0.236   5.285e-06      -5.277
      Hfo_wSO4-         1.165e-07        0.005   1.161e-07      -6.935
      Hfo_wHPO4-        3.742e-10        0.000   3.731e-10      -9.428
      Hfo_wOH           4.730e-12        0.000   4.716e-12     -11.326
      Hfo_wOHSO4-2      2.068e-13        0.000   2.062e-13     -12.686
      Hfo_wPO4-2        1.392e-16        0.000   1.388e-16     -15.858
```

```
      Hfo_wOCa+          4.326e-19       0.000   4.314e-19     -18.365
      Hfo_wO-            9.668e-20       0.000   9.640e-20     -19.016

-----------------------------Exchange composition--------------------------------

X                2.000e+00 mol

                                        Equiv-    Equivalent      Log
      Species             Moles         alents      Fraction     Gamma

      HX                1.875e+00   1.875e+00   9.375e-01    -0.000
      CaX2              6.249e-02   1.250e-01   6.249e-02    -0.000

-----------------------------Solution composition--------------------------------

      Elements           Molality       Moles

      Ca                1.755e-02   1.760e-02
      P                 1.622e-04   1.626e-04
      S                 7.983e-02   8.006e-02

----------------------------Description of solution----------------------------

                                     pH  =   1.241      Charge balance
                                     pe  =   4.911      Adjusted to redox
equilibrium
                        Activity of water  =   0.997
                  Ionic strength (mol/kgw)  =   1.235e-01
                       Mass of water (kg)  =   1.003e+00
                  Total alkalinity (eq/kg)  =  -1.247e-01
                          Temperature (°C)  =  25.00
                   Electrical balance (eq)  =  -6.842e-05
 Percent error, 100*(Cat-|An|)/(Cat+|An|)  =  -0.04
                                Iterations  =   1 (10 overall)
                                   Total H  = 1.114580e+02
                                   Total O  = 5.598724e+01

---------------------------Distribution of species-----------------------------

                                                 Log       Log       Log    mole V
   Species          Molality    Activity  Molality  Activity     Gamma   cm³/mol

   H+               7.037e-02   5.747e-02    -1.153    -1.241    -0.088      0.00
   OH-              2.331e-13   1.737e-13   -12.633   -12.760    -0.128      (0)
   H2O              5.551e+01   9.973e-01     1.744    -0.001     0.000     18.07
   Ca               1.755e-02
   Ca+2             1.011e-02   3.722e-03    -1.995    -2.429    -0.434      (0)
   CaSO4            5.118e-03   5.266e-03    -2.291    -2.279     0.012      (0)
   CaHSO4+          2.304e-03   1.773e-03    -2.638    -2.751    -0.114      (0)
   CaH2PO4+         1.410e-05   1.094e-05    -4.851    -4.961    -0.110      (0)
   CaHPO4           2.461e-10   2.532e-10    -9.609    -9.597     0.012      (0)
   CaOH+            1.368e-14   1.072e-14   -13.864   -13.970    -0.106      (0)
   CaPO4-           1.344e-17   1.042e-17   -16.872   -16.982    -0.110      (0)
   H(0)             6.833e-16
   H2               3.417e-16   3.515e-16   -15.466   -15.454     0.012      (0)
```

```
   O(0)          0.000e+00
   O2              0.000e+00   0.000e+00   -61.487   -61.474     0.012     (0)
   P             1.622e-04
   H2PO4-          1.481e-04   1.148e-04    -3.830    -3.940    -0.110     (0)
   CaH2PO4+        1.410e-05   1.094e-05    -4.851    -4.961    -0.110     (0)
   HPO4-2          3.533e-10   1.241e-10    -9.452    -9.906    -0.455     (0)
   CaHPO4          2.461e-10   2.532e-10    -9.609    -9.597     0.012     (0)
   CaPO4-          1.344e-17   1.042e-17   -16.872   -16.982    -0.110     (0)
   PO4-3           1.025e-20   9.731e-22   -19.989   -21.012    -1.023     (0)
   S(-2)         6.163e-14
   H2S             6.163e-14   6.341e-14   -13.210   -13.198     0.012     (0)
   HS-             1.693e-19   1.262e-19   -18.771   -18.899    -0.128     (0)
   S5-2            1.115e-27   5.579e-28   -26.953   -27.253    -0.301     (0)
   S4-2            7.003e-28   3.255e-28   -27.155   -27.487    -0.333     (0)
   S6-2            5.427e-28   2.888e-28   -27.265   -27.539    -0.274     (0)
   S-2             7.552e-31   2.652e-31   -30.122   -30.576    -0.455     (0)
   S3-2            2.706e-31   1.147e-31   -30.568   -30.940    -0.373     (0)
   S2-2            1.672e-32   6.509e-33   -31.777   -32.186    -0.410     (0)
   S(6)          7.983e-02
   HSO4-           5.199e-02   3.962e-02    -1.284    -1.402    -0.118     (0)
   SO4-2           2.043e-02   7.090e-03    -1.690    -2.149    -0.459     (0)
   CaSO4           5.118e-03   5.266e-03    -2.291    -2.279     0.012     (0)
   CaHSO4+         2.304e-03   1.773e-03    -2.638    -2.751    -0.114     (0)

------------------------------Saturation indices-------------------------------

  Phase               SI** log IAP   log K(298 K,   1 atm)

  Anhydrite         -0.22     -4.58   -4.36  CaSO4
  Gypsum             0.00     -4.58   -4.58  CaSO4:2H2O
  H2(g)            -12.30    -15.45   -3.15  H2
  H2O(g)            -1.51     -0.00    1.51  H2O
  H2S(g)           -12.20    -13.20   -1.00  H2S
  Hydroxyapatite   -33.48    -36.90   -3.42  Ca5(PO4)3OH
  O2(g)            -58.58    -61.47   -2.89  O2
  Portlandite      -22.75      0.05   22.80  Ca(OH)2
  Sulfur            -5.73    -20.75  -15.03  S

**For a gas, SI = log10(fugacity). Fugacity = pressure * phi / 1 atm.
  For ideal gases, phi = 1.

Transport step   1.

Transport step   1. Mixrun   1.

Transport step   1. Mixrun   2.

Transport step   1. Mixrun   3.

Using solution 10.      Solution after simulation 2.
Using exchange 10.      Exchange assemblage after simulation 2.
Using surface 10. Equilibrate the column with sewage water
Using pure phase assemblage 10.     Pure-phase assemblage after simulation 2.

------------------------------Phase assemblage--------------------------------
```

Phase	SI	log IAP	log K(T, P)	Moles in assemblage: Initial	Final	Delta
Gypsum	0.00	-4.58	-4.58	7.599e-01	7.598e-01	-6.349e-05

----------Surface composition----------

Hfo
2.303e-04 Surface charge, eq
Hfo_s
2.250e-04 moles

Species	Moles	Mole Fraction	Molality	Log Molality
Hfo_sOH2+	2.249e-04	1.000	2.243e-04	-3.649
Hfo_sOHCa+2	6.976e-08	0.000	6.956e-08	-7.158
Hfo_sOH	2.008e-10	0.000	2.002e-10	-9.698
Hfo_sO-	4.107e-18	0.000	4.095e-18	-17.388

Hfo
2.303e-04 Surface charge, eq
Hfo_w
2.250e-05 moles

Species	Moles	Mole Fraction	Molality	Log Molality
Hfo_wH2PO4	1.708e-05	0.759	1.703e-05	-4.769
Hfo_wOH2+	5.303e-06	0.236	5.288e-06	-5.277
Hfo_wSO4-	1.165e-07	0.005	1.162e-07	-6.935
Hfo_wHPO4-	3.743e-10	0.000	3.732e-10	-9.428
Hfo_wOH	4.735e-12	0.000	4.721e-12	-11.326
Hfo_wOHSO4-2	2.070e-13	0.000	2.064e-13	-12.685
Hfo_wPO4-2	1.393e-16	0.000	1.389e-16	-15.857
Hfo_wOCa+	4.334e-19	0.000	4.321e-19	-18.364
Hfo_wO-	9.684e-20	0.000	9.656e-20	-19.015

----------Exchange composition----------

X 2.000e+00 mol

Species	Moles	Equiv-alents	Equivalent Fraction	Log Gamma
HX	1.875e+00	1.875e+00	9.375e-01	0.000
CaX2	6.255e-02	1.251e-01	6.255e-02	0.000

----------Solution composition----------

Elements	Molality	Moles
Ca	1.755e-02	1.760e-02
P	1.621e-04	1.625e-04
S	7.980e-02	8.003e-02

----------Description of solution----------

```
                                    pH  =   1.241      Charge balance
                                    pe  =   4.921      Adjusted to redox
equilibrium
                         Activity of water  =   0.997
                Ionic strength (mol/kgw)  =   1.234e-01
                      Mass of water (kg)  =   1.003e+00
                Total alkalinity (eq/kg)  =  -1.246e-01
                        Temperature (°C)  =  25.00
                 Electrical balance (eq)  =  -6.828e-05
 Percent error, 100*(Cat-|An|)/(Cat+|An|)  =  -0.04
                               Iterations  =   1
                                  Total H  = 1.114578e+02
                                  Total O  = 5.598702e+01
```

----------Distribution of species----------

Species	Molality	Activity	Log Molality	Log Activity	Log Gamma	mole V cm³/mol
H+	7.033e-02	5.744e-02	-1.153	-1.241	-0.088	0.00
OH-	2.332e-13	1.738e-13	-12.632	-12.760	-0.128	(0)
H2O	5.551e+01	9.973e-01	1.744	-0.001	0.000	18.07
Ca	1.755e-02					
Ca+2	1.011e-02	3.722e-03	-1.995	-2.429	-0.434	(0)
CaSO4	5.118e-03	5.266e-03	-2.291	-2.279	0.012	(0)
CaHSO4+	2.302e-03	1.772e-03	-2.638	-2.752	-0.114	(0)
CaH2PO4+	1.409e-05	1.093e-05	-4.851	-4.961	-0.110	(0)
CaHPO4	2.460e-10	2.531e-10	-9.609	-9.597	0.012	(0)
CaOH+	1.369e-14	1.072e-14	-13.864	-13.970	-0.106	(0)
CaPO4-	1.344e-17	1.042e-17	-16.872	-16.982	-0.110	(0)
H(0)	6.531e-16					
H2	3.265e-16	3.359e-16	-15.486	-15.474	0.012	(0)
O(0)	0.000e+00					
O2	0.000e+00	0.000e+00	-61.447	-61.435	0.012	(0)
P	1.621e-04					
H2PO4-	1.480e-04	1.148e-04	-3.830	-3.940	-0.110	(0)
CaH2PO4+	1.409e-05	1.093e-05	-4.851	-4.961	-0.110	(0)
HPO4-2	3.532e-10	1.240e-10	-9.452	-9.906	-0.455	(0)
CaHPO4	2.460e-10	2.531e-10	-9.609	-9.597	0.012	(0)
CaPO4-	1.344e-17	1.042e-17	-16.872	-16.982	-0.110	(0)
PO4-3	1.025e-20	9.733e-22	-19.989	-21.012	-1.023	(0)
S(-2)	5.136e-14					
H2S	5.136e-14	5.284e-14	-13.289	-13.277	0.012	(0)
HS-	1.411e-19	1.052e-19	-18.850	-18.978	-0.128	(0)
S5-2	9.296e-28	4.653e-28	-27.032	-27.332	-0.301	(0)
S4-2	5.841e-28	2.715e-28	-27.233	-27.566	-0.333	(0)
S6-2	4.527e-28	2.409e-28	-27.344	-27.618	-0.274	(0)
S-2	6.299e-31	2.212e-31	-30.201	-30.655	-0.455	(0)
S3-2	2.257e-31	9.567e-32	-30.647	-31.019	-0.373	(0)
S2-2	1.394e-32	5.430e-33	-31.856	-32.265	-0.410	(0)
S(6)	7.980e-02					
HSO4-	5.195e-02	3.960e-02	-1.284	-1.402	-0.118	(0)
SO4-2	2.042e-02	7.090e-03	-1.690	-2.149	-0.459	(0)

```
   CaSO4           5.118e-03   5.266e-03    -2.291    -2.279     0.012      (0)
   CaHSO4+         2.302e-03   1.772e-03    -2.638    -2.752    -0.114      (0)

------------------------------Saturation indices--------------------------------

  Phase               SI** log IAP   log K(298 K,   1 atm)

  Anhydrite        -0.22     -4.58   -4.36  CaSO4
  Gypsum            0.00     -4.58   -4.58  CaSO4:2H2O
  H2(g)           -12.32    -15.47   -3.15  H2
  H2O(g)           -1.51     -0.00    1.51  H2O
  H2S(g)          -12.28    -13.28   -1.00  H2S
  Hydroxyapatite  -33.48    -36.90   -3.42  Ca5(PO4)3OH
  O2(g)           -58.54    -61.43   -2.89  O2
  Portlandite     -22.75      0.05   22.80  Ca(OH)2
  Sulfur           -5.79    -20.81  -15.03  S

**For a gas, SI = log10(fugacity). Fugacity = pressure * phi / 1 atm.
  For ideal gases, phi = 1.

Transport step   2.

Transport step   2. Mixrun   1.

Transport step   2. Mixrun   2.

Transport step   2. Mixrun   3.

Using solution 10.      Solution after simulation 2.
Using exchange 10.      Exchange assemblage after simulation 2.
Using surface 10. Equilibrate the column with sewage water
Using pure phase assemblage 10.     Pure-phase assemblage after simulation 2.

------------------------------Phase assemblage--------------------------------

                                                        Moles in assemblage
Phase               SI  log IAP  log K(T, P)   Initial       Final       Delta

Gypsum            0.00    -4.58     -4.58    7.598e-01   7.597e-01  -1.654e-04

------------------------------Surface composition-----------------------------

Hfo
        2.303e-04  Surface charge, eq
Hfo_s
        2.250e-04  moles
                                          Mole                    Log
      Species               Moles     Fraction    Molality    Molality

      Hfo_sOH2+         2.249e-04        1.000   2.243e-04      -3.649
      Hfo_sOHCa+2       6.987e-08        0.000   6.967e-08      -7.157
      Hfo_sOH           2.011e-10        0.000   2.005e-10      -9.698
      Hfo_sO-           4.118e-18        0.000   4.107e-18     -17.387

Hfo
```

```
        2.303e-04  Surface charge, eq
Hfo_w
        2.250e-05  moles
                                          Mole                    Log
      Species               Moles     Fraction    Molality    Molality

      Hfo_wH2PO4         1.708e-05        0.759   1.703e-05      -4.769
      Hfo_wOH2+          5.307e-06        0.236   5.292e-06      -5.276
      Hfo_wSO4-          1.166e-07        0.005   1.162e-07      -6.935
      Hfo_wHPO4-         3.747e-10        0.000   3.737e-10      -9.428
      Hfo_wOH            4.744e-12        0.000   4.731e-12     -11.325
      Hfo_wOHSO4-2       2.074e-13        0.000   2.068e-13     -12.685
      Hfo_wPO4-2         1.397e-16        0.000   1.393e-16     -15.856
      Hfo_wOCa+          4.349e-19        0.000   4.337e-19     -18.363
      Hfo_wO-            9.717e-20        0.000   9.689e-20     -19.014

-----------------------------Exchange composition--------------------------------

X                2.000e+00 mol

                                      Equiv-    Equivalent      Log
      Species              Moles      alents      Fraction     Gamma

      HX                 1.875e+00   1.875e+00   9.373e-01    -0.000
      CaX2               6.271e-02   1.254e-01   6.271e-02    -0.000

-----------------------------Solution composition--------------------------------

      Elements           Molality       Moles

      Ca                 1.755e-02   1.760e-02
      P                  1.619e-04   1.624e-04
      S                  7.970e-02   7.993e-02

----------------------------Description of solution----------------------------

                                       pH  =   1.241      Charge balance
                                       pe  =   4.920      Adjusted to redox
equilibrium
                          Activity of water  =   0.997
                 Ionic strength (mol/kgw)  =   1.233e-01
                       Mass of water (kg)  =   1.003e+00
                 Total alkalinity (eq/kg)  =  -1.244e-01
                        Temperature (°C)  =  25.00
                  Electrical balance (eq)  =  -6.811e-05
 Percent error, 100*(Cat-|An|)/(Cat+|An|)  =  -0.04
                                Iterations  =   1
                                   Total H  = 1.114572e+02
                                   Total O  = 5.598644e+01

----------------------------Distribution of species----------------------------

                                                 Log       Log       Log    mole V
   Species          Molality    Activity  Molality  Activity     Gamma   cm³/mol
```

```
   H+              7.023e-02   5.737e-02    -1.153    -1.241    -0.088      0.00
   OH-             2.335e-13   1.740e-13   -12.632   -12.759    -0.128     (0)
   H2O             5.551e+01   9.973e-01     1.744    -0.001     0.000     18.07
   Ca           1.755e-02
   Ca+2            1.011e-02   3.723e-03    -1.995    -2.429    -0.434     (0)
   CaSO4           5.118e-03   5.266e-03    -2.291    -2.279     0.012     (0)
   CaHSO4+         2.299e-03   1.770e-03    -2.638    -2.752    -0.114     (0)
   CaH2PO4+        1.408e-05   1.092e-05    -4.851    -4.962    -0.110     (0)
   CaHPO4          2.462e-10   2.533e-10    -9.609    -9.596     0.012     (0)
   CaOH+           1.371e-14   1.074e-14   -13.863   -13.969    -0.106     (0)
   CaPO4-          1.347e-17   1.045e-17   -16.871   -16.981    -0.110     (0)
   H(0)         6.547e-16
   H2              3.273e-16   3.368e-16   -15.485   -15.473     0.012     (0)
   O(0)         0.000e+00
   O2              0.000e+00   0.000e+00   -61.449   -61.437     0.012     (0)
   P            1.619e-04
   H2PO4-          1.478e-04   1.146e-04    -3.830    -3.941    -0.110     (0)
   CaH2PO4+        1.408e-05   1.092e-05    -4.851    -4.962    -0.110     (0)
   HPO4-2          3.532e-10   1.241e-10    -9.452    -9.906    -0.454     (0)
   CaHPO4          2.462e-10   2.533e-10    -9.609    -9.596     0.012     (0)
   CaPO4-          1.347e-17   1.045e-17   -16.871   -16.981    -0.110     (0)
   PO4-3           1.027e-20   9.751e-22   -19.989   -21.011    -1.022     (0)
   S(-2)        5.172e-14
   H2S             5.172e-14   5.321e-14   -13.286   -13.274     0.012     (0)
   HS-             1.423e-19   1.061e-19   -18.847   -18.974    -0.128     (0)
   S5-2            9.386e-28   4.699e-28   -27.028   -27.328    -0.300     (0)
   S4-2            5.898e-28   2.742e-28   -27.229   -27.562    -0.333     (0)
   S6-2            4.571e-28   2.432e-28   -27.340   -27.614    -0.274     (0)
   S-2             6.359e-31   2.234e-31   -30.197   -30.651    -0.454     (0)
   S3-2            2.278e-31   9.660e-32   -30.642   -31.015    -0.373     (0)
   S2-2            1.407e-32   5.483e-33   -31.852   -32.261    -0.409     (0)
   S(6)         7.970e-02
   HSO4-           5.187e-02   3.954e-02    -1.285    -1.403    -0.118     (0)
   SO4-2           2.041e-02   7.089e-03    -1.690    -2.149    -0.459     (0)
   CaSO4           5.118e-03   5.266e-03    -2.291    -2.279     0.012     (0)
   CaHSO4+         2.299e-03   1.770e-03    -2.638    -2.752    -0.114     (0)

-----------------------------Saturation indices-------------------------------

  Phase               SI** log IAP   log K(298 K,   1 atm)

  Anhydrite         -0.22     -4.58   -4.36  CaSO4
  Gypsum             0.00     -4.58   -4.58  CaSO4:2H2O
  H2(g)            -12.32    -15.47   -3.15  H2
  H2O(g)            -1.51     -0.00    1.51  H2O
  H2S(g)           -12.28    -13.27   -1.00  H2S
  Hydroxyapatite   -33.48    -36.90   -3.42  Ca5(PO4)3OH
  O2(g)            -58.54    -61.44   -2.89  O2
  Portlandite      -22.75      0.05   22.80  Ca(OH)2
  Sulfur            -5.79    -20.81  -15.03  S

**For a gas, SI = log10(fugacity). Fugacity = pressure * phi / 1 atm.
  For ideal gases, phi = 1.

Transport step   3.
```

```
Transport step   3. Mixrun   1.

Transport step   3. Mixrun   2.

Transport step   3. Mixrun   3.

Using solution 10.      Solution after simulation 2.
Using exchange 10.      Exchange assemblage after simulation 2.
Using surface 10. Equilibrate the column with sewage water
Using pure phase assemblage 10.     Pure-phase assemblage after simulation 2.

-------------------------------Phase assemblage--------------------------------

                                                        Moles in assemblage
Phase               SI  log IAP  log K(T, P)   Initial       Final       Delta

Gypsum            0.00    -4.58     -4.58    7.597e-01   7.594e-01  -3.237e-04

------------------------------Surface composition------------------------------

Hfo
        2.303e-04  Surface charge, eq
Hfo_s
        2.250e-04  moles
                                          Mole                    Log
      Species               Moles     Fraction    Molality    Molality

      Hfo_sOH2+         2.249e-04        1.000   2.243e-04      -3.649
      Hfo_sOHCa+2       7.007e-08        0.000   6.987e-08      -7.156
      Hfo_sOH           2.016e-10        0.000   2.010e-10      -9.697
      Hfo_sO-           4.140e-18        0.000   4.128e-18     -17.384

Hfo
        2.303e-04  Surface charge, eq
Hfo_w
        2.250e-05  moles
                                          Mole                    Log
      Species               Moles     Fraction    Molality    Molality

      Hfo_wH2PO4        1.707e-05        0.759   1.702e-05      -4.769
      Hfo_wOH2+         5.310e-06        0.236   5.295e-06      -5.276
      Hfo_wSO4-         1.166e-07        0.005   1.163e-07      -6.935
      Hfo_wHPO4-        3.756e-10        0.000   3.746e-10      -9.426
      Hfo_wOH           4.760e-12        0.000   4.746e-12     -11.324
      Hfo_wOHSO4-2      2.080e-13        0.000   2.074e-13     -12.683
      Hfo_wPO4-2        1.404e-16        0.000   1.400e-16     -15.854
      Hfo_wOCa+         4.376e-19        0.000   4.364e-19     -18.360
      Hfo_wO-           9.774e-20        0.000   9.746e-20     -19.011

-----------------------------Exchange composition-----------------------------

X                2.000e+00 mol

                                       Equiv-    Equivalent      Log
```

Species	Moles	alents	Fraction	Gamma
HX	1.874e+00	1.874e+00	9.370e-01	0.000
CaX2	6.302e-02	1.260e-01	6.302e-02	0.000

----------Solution composition----------

Elements	Molality	Moles
Ca	1.754e-02	1.759e-02
P	1.617e-04	1.622e-04
S	7.951e-02	7.974e-02

----------Description of solution----------

pH	=	1.242	Charge balance
pe	=	4.934	Adjusted to redox equilibrium
Activity of water	=	0.997	
Ionic strength (mol/kgw)	=	1.231e-01	
Mass of water (kg)	=	1.003e+00	
Total alkalinity (eq/kg)	=	-1.240e-01	
Temperature (°C)	=	25.00	
Electrical balance (eq)	=	-6.793e-05	
Percent error, 100*(Cat-|An|)/(Cat+|An|)	=	-0.04	
Iterations	=	1	
Total H	=	1.114561e+02	
Total O	=	5.598530e+01	

----------Distribution of species----------

Species	Molality	Activity	Log Molality	Log Activity	Log Gamma	mole V cm³/mol
H+	7.004e-02	5.722e-02	-1.155	-1.242	-0.088	0.00
OH-	2.340e-13	1.745e-13	-12.631	-12.758	-0.128	(0)
H2O	5.551e+01	9.973e-01	1.744	-0.001	0.000	18.07
Ca	1.754e-02					
Ca+2	1.011e-02	3.724e-03	-1.995	-2.429	-0.434	(0)
CaSO4	5.118e-03	5.266e-03	-2.291	-2.279	0.012	(0)
CaHSO4+	2.293e-03	1.765e-03	-2.640	-2.753	-0.114	(0)
CaH2PO4+	1.407e-05	1.091e-05	-4.852	-4.962	-0.110	(0)
CaHPO4	2.467e-10	2.538e-10	-9.608	-9.596	0.012	(0)
CaOH+	1.374e-14	1.077e-14	-13.862	-13.968	-0.106	(0)
CaPO4-	1.353e-17	1.049e-17	-16.869	-16.979	-0.110	(0)
H(0)	6.098e-16					
H2	3.049e-16	3.137e-16	-15.516	-15.504	0.012	(0)
O(0)	0.000e+00					
O2	0.000e+00	0.000e+00	-61.388	-61.375	0.012	(0)
P	1.617e-04					
H2PO4-	1.477e-04	1.145e-04	-3.831	-3.941	-0.110	(0)
CaH2PO4+	1.407e-05	1.091e-05	-4.852	-4.962	-0.110	(0)
HPO4-2	3.537e-10	1.243e-10	-9.451	-9.906	-0.454	(0)
CaHPO4	2.467e-10	2.538e-10	-9.608	-9.596	0.012	(0)
CaPO4-	1.353e-17	1.049e-17	-16.869	-16.979	-0.110	(0)

```
   PO4-3          1.030e-20   9.794e-22   -19.987   -21.009    -1.022     (0)
   S(-2)        3.870e-14
   H2S            3.870e-14   3.981e-14   -13.412   -13.400     0.012     (0)
   HS-            1.067e-19   7.958e-20   -18.972   -19.099    -0.128     (0)
   S5-2           7.057e-28   3.534e-28   -27.151   -27.452    -0.300     (0)
   S4-2           4.434e-28   2.062e-28   -27.353   -27.686    -0.333     (0)
   S6-2           3.437e-28   1.829e-28   -27.464   -27.738    -0.274     (0)
   S-2            4.779e-31   1.680e-31   -30.321   -30.775    -0.454     (0)
   S3-2           1.713e-31   7.265e-32   -30.766   -31.139    -0.372     (0)
   S2-2           1.058e-32   4.123e-33   -31.976   -32.385    -0.409     (0)
   S(6)         7.951e-02
   HSO4-          5.171e-02   3.942e-02    -1.286    -1.404    -0.118     (0)
   SO4-2          2.039e-02   7.086e-03    -1.691    -2.150    -0.459     (0)
   CaSO4          5.118e-03   5.266e-03    -2.291    -2.279     0.012     (0)
   CaHSO4+        2.293e-03   1.765e-03    -2.640    -2.753    -0.114     (0)

------------------------------Saturation indices-------------------------------

  Phase               SI** log IAP   log K(298 K,   1 atm)

  Anhydrite         -0.22     -4.58   -4.36  CaSO4
  Gypsum             0.00     -4.58   -4.58  CaSO4:2H2O
  H2(g)            -12.35    -15.50   -3.15  H2
  H2O(g)            -1.51     -0.00    1.51  H2O
  H2S(g)           -12.40    -13.40   -1.00  H2S
  Hydroxyapatite   -33.47    -36.89   -3.42  Ca5(PO4)3OH
  O2(g)            -58.48    -61.38   -2.89  O2
  Portlandite      -22.75      0.05   22.80  Ca(OH)2
  Sulfur            -5.88    -20.91  -15.03  S

**For a gas, SI = log10(fugacity). Fugacity = pressure * phi / 1 atm.
  For ideal gases, phi = 1.

Transport step   4.

Transport step   4. Mixrun   1.

Transport step   4. Mixrun   2.

Transport step   4. Mixrun   3.

Using solution 10.      Solution after simulation 2.
Using exchange 10.      Exchange assemblage after simulation 2.
Using surface 10. Equilibrate the column with sewage water
Using pure phase assemblage 10.     Pure-phase assemblage after simulation 2.

-------------------------------Phase assemblage--------------------------------

                                                        Moles in assemblage
Phase               SI  log IAP  log K(T, P)   Initial       Final       Delta

Gypsum            0.00    -4.58     -4.58    7.594e-01   7.588e-01  -5.250e-04

------------------------------Surface composition-----------------------------
```

```
Hfo
        2.303e-04  Surface charge, eq
Hfo_s
        2.250e-04  moles
                                          Mole                    Log
      Species               Moles     Fraction    Molality    Molality

      Hfo_sOH2+         2.249e-04        1.000   2.243e-04      -3.649
      Hfo_sOHCa+2       7.041e-08        0.000   7.021e-08      -7.154
      Hfo_sOH           2.025e-10        0.000   2.019e-10      -9.695
      Hfo_sO-           4.175e-18        0.000   4.163e-18     -17.381

Hfo
        2.303e-04  Surface charge, eq
Hfo_w
        2.250e-05  moles
                                          Mole                    Log
      Species               Moles     Fraction    Molality    Molality

      Hfo_wH2PO4        1.707e-05        0.759   1.702e-05      -4.769
      Hfo_wOH2+         5.313e-06        0.236   5.298e-06      -5.276
      Hfo_wSO4-         1.166e-07        0.005   1.163e-07      -6.934
      Hfo_wHPO4-        3.772e-10        0.000   3.761e-10      -9.425
      Hfo_wOH           4.783e-12        0.000   4.769e-12     -11.322
      Hfo_wOHSO4-2      2.089e-13        0.000   2.083e-13     -12.681
      Hfo_wPO4-2        1.415e-16        0.000   1.411e-16     -15.850
      Hfo_wOCa+         4.419e-19        0.000   4.406e-19     -18.356
      Hfo_wO-           9.863e-20        0.000   9.835e-20     -19.007

-----------------------------Exchange composition-------------------------------

X                2.000e+00 mol

                                       Equiv-    Equivalent      Log
      Species             Moles       alents      Fraction     Gamma

      HX                1.873e+00   1.873e+00   9.365e-01     0.000
      CaX2              6.352e-02   1.270e-01   6.352e-02     0.000

-----------------------------Solution composition-------------------------------

      Elements           Molality       Moles

      Ca                1.752e-02   1.757e-02
      P                 1.616e-04   1.621e-04
      S                 7.921e-02   7.944e-02

----------------------------Description of solution----------------------------

                                    pH  =   1.244      Charge balance
                                    pe  =   4.921      Adjusted to redox
equilibrium
                        Activity of water  =   0.997
                  Ionic strength (mol/kgw)  =   1.228e-01
                       Mass of water (kg)   =   1.003e+00
```

```
                Total alkalinity (eq/kg)  =  -1.235e-01
                       Temperature (°C)  =  25.00
                 Electrical balance (eq)  =  -6.775e-05
Percent error, 100*(Cat-|An|)/(Cat+|An|)  =  -0.04
                              Iterations  =   1
                                 Total H  = 1.114543e+02
                                 Total O  = 5.598348e+01

----------------------------Distribution of species----------------------------
```

Species	Molality	Activity	Log Molality	Log Activity	Log Gamma	mole V cm³/mol
H+	6.974e-02	5.697e-02	-1.157	-1.244	-0.088	0.00
OH-	2.350e-13	1.752e-13	-12.629	-12.756	-0.127	(0)
H2O	5.551e+01	9.973e-01	1.744	-0.001	0.000	18.07
Ca	1.752e-02					
Ca+2	1.011e-02	3.726e-03	-1.995	-2.429	-0.433	(0)
CaSO4	5.119e-03	5.265e-03	-2.291	-2.279	0.012	(0)
CaHSO4+	2.283e-03	1.757e-03	-2.642	-2.755	-0.114	(0)
CaH2PO4+	1.406e-05	1.091e-05	-4.852	-4.962	-0.110	(0)
CaHPO4	2.477e-10	2.548e-10	-9.606	-9.594	0.012	(0)
CaOH+	1.381e-14	1.082e-14	-13.860	-13.966	-0.106	(0)
CaPO4-	1.364e-17	1.058e-17	-16.865	-16.975	-0.110	(0)
H(0)	6.424e-16					
H2	3.212e-16	3.304e-16	-15.493	-15.481	0.012	(0)
O(0)	0.000e+00					
O2	0.000e+00	0.000e+00	-61.433	-61.420	0.012	(0)
P	1.616e-04					
H2PO4-	1.475e-04	1.145e-04	-3.831	-3.941	-0.110	(0)
CaH2PO4+	1.406e-05	1.091e-05	-4.852	-4.962	-0.110	(0)
HPO4-2	3.546e-10	1.247e-10	-9.450	-9.904	-0.454	(0)
CaHPO4	2.477e-10	2.548e-10	-9.606	-9.594	0.012	(0)
CaPO4-	1.364e-17	1.058e-17	-16.865	-16.975	-0.110	(0)
PO4-3	1.035e-20	9.870e-22	-19.985	-21.006	-1.021	(0)
S(-2)	4.722e-14					
H2S	4.722e-14	4.857e-14	-13.326	-13.314	0.012	(0)
HS-	1.307e-19	9.750e-20	-18.884	-19.011	-0.127	(0)
S5-2	8.680e-28	4.348e-28	-27.061	-27.362	-0.300	(0)
S4-2	5.453e-28	2.537e-28	-27.263	-27.596	-0.332	(0)
S6-2	4.227e-28	2.251e-28	-27.374	-27.648	-0.274	(0)
S-2	5.875e-31	2.067e-31	-30.231	-30.685	-0.454	(0)
S3-2	2.106e-31	8.940e-32	-30.677	-31.049	-0.372	(0)
S2-2	1.301e-32	5.074e-33	-31.886	-32.295	-0.409	(0)
S(6)	7.921e-02					
HSO4-	5.145e-02	3.923e-02	-1.289	-1.406	-0.118	(0)
SO4-2	2.036e-02	7.083e-03	-1.691	-2.150	-0.459	(0)
CaSO4	5.119e-03	5.265e-03	-2.291	-2.279	0.012	(0)
CaHSO4+	2.283e-03	1.757e-03	-2.642	-2.755	-0.114	(0)

```
----------------------------Saturation indices----------------------------
```

Phase	SI**	log IAP	log K(298 K, 1 atm)	
Anhydrite	-0.22	-4.58	-4.36	CaSO4

```
  Gypsum            0.00     -4.58   -4.58  CaSO4:2H2O
  H2(g)           -12.33    -15.48   -3.15  H2
  H2O(g)           -1.51     -0.00    1.51  H2O
  H2S(g)          -12.32    -13.31   -1.00  H2S
  Hydroxyapatite  -33.46    -36.88   -3.42  Ca5(PO4)3OH
  O2(g)           -58.53    -61.42   -2.89  O2
  Portlandite     -22.74      0.06   22.80  Ca(OH)2
  Sulfur           -5.82    -20.84  -15.03  S

**For a gas, SI = log10(fugacity). Fugacity = pressure * phi / 1 atm.
  For ideal gases, phi = 1.

Transport step   5.

Transport step   5. Mixrun   1.

Transport step   5. Mixrun   2.

Transport step   5. Mixrun   3.

Using solution 10.      Solution after simulation 2.
Using exchange 10.      Exchange assemblage after simulation 2.
Using surface 10. Equilibrate the column with sewage water
Using pure phase assemblage 10.     Pure-phase assemblage after simulation 2.

-------------------------------Phase assemblage--------------------------------

                                                        Moles in assemblage
Phase               SI  log IAP  log K(T, P)   Initial       Final       Delta

Gypsum            0.00    -4.58     -4.58    7.588e-01   7.581e-01  -7.488e-04

------------------------------Surface composition------------------------------

Hfo
        2.303e-04  Surface charge, eq
Hfo_s
        2.250e-04  moles
                                          Mole                    Log
      Species               Moles     Fraction    Molality    Molality

      Hfo_sOH2+         2.249e-04        1.000   2.243e-04      -3.649
      Hfo_sOHCa+2       7.088e-08        0.000   7.068e-08      -7.151
      Hfo_sOH           2.037e-10        0.000   2.031e-10      -9.692
      Hfo_sO-           4.226e-18        0.000   4.214e-18     -17.375

Hfo
        2.303e-04  Surface charge, eq
Hfo_w
        2.250e-05  moles
                                          Mole                    Log
      Species               Moles     Fraction    Molality    Molality

      Hfo_wH2PO4        1.707e-05        0.759   1.702e-05      -4.769
      Hfo_wOH2+         5.316e-06        0.236   5.301e-06      -5.276
```

```
      Hfo_wSO4-          1.166e-07       0.005   1.162e-07      -6.935
      Hfo_wHPO4-         3.794e-10       0.000   3.783e-10      -9.422
      Hfo_wOH            4.814e-12       0.000   4.800e-12     -11.319
      Hfo_wOHSO4-2       2.101e-13       0.000   2.095e-13     -12.679
      Hfo_wPO4-2         1.432e-16       0.000   1.428e-16     -15.845
      Hfo_wOCa+          4.477e-19       0.000   4.464e-19     -18.350
      Hfo_wO-            9.987e-20       0.000   9.959e-20     -19.002

-----------------------------Exchange composition--------------------------------

X                2.000e+00 mol

                                       Equiv-    Equivalent      Log
      Species             Moles        alents      Fraction     Gamma

      HX                 1.872e+00   1.872e+00   9.358e-01     0.000
      CaX2               6.423e-02   1.285e-01   6.423e-02     0.000

-----------------------------Solution composition--------------------------------

      Elements           Molality       Moles

      Ca                 1.751e-02   1.756e-02
      P                  1.615e-04   1.619e-04
      S                  7.879e-02   7.901e-02

----------------------------Description of solution----------------------------

                                     pH  =   1.247      Charge balance
                                     pe  =   4.929      Adjusted to redox
equilibrium
                        Activity of water  =   0.997
                  Ionic strength (mol/kgw)  =   1.222e-01
                       Mass of water (kg)   =   1.003e+00
                  Total alkalinity (eq/kg)  =  -1.227e-01
                         Temperature (°C)   =  25.00
                   Electrical balance (eq)  =  -6.760e-05
 Percent error, 100*(Cat-|An|)/(Cat+|An|)   =  -0.04
                                Iterations   =   1
                                   Total H   = 1.114518e+02
                                   Total O   = 5.598092e+01

---------------------------Distribution of species-----------------------------

                                                 Log       Log       Log    mole V
   Species          Molality    Activity  Molality  Activity     Gamma   cm³/mol

   H+               6.930e-02   5.663e-02    -1.159    -1.247    -0.088      0.00
   OH-              2.363e-13   1.763e-13   -12.627   -12.754    -0.127      (0)
   H2O              5.551e+01   9.973e-01     1.744    -0.001     0.000     18.07
   Ca               1.751e-02
   Ca+2             1.010e-02   3.729e-03    -1.995    -2.428    -0.433      (0)
   CaSO4            5.119e-03   5.265e-03    -2.291    -2.279     0.012      (0)
   CaHSO4+          2.268e-03   1.747e-03    -2.644    -2.758    -0.113      (0)
   CaH2PO4+         1.406e-05   1.091e-05    -4.852    -4.962    -0.110      (0)
```

```
   CaHPO4          2.493e-10   2.564e-10    -9.603    -9.591     0.012      (0)
   CaOH+           1.390e-14   1.090e-14   -13.857   -13.963    -0.106      (0)
   CaPO4-          1.380e-17   1.071e-17   -16.860   -16.970    -0.110      (0)
   H(0)          6.113e-16
   H2              3.056e-16   3.144e-16   -15.515   -15.503     0.012      (0)
   O(0)          0.000e+00
   O2              0.000e+00   0.000e+00   -61.389   -61.377     0.012      (0)
   P             1.615e-04
   H2PO4-          1.474e-04   1.144e-04    -3.832    -3.942    -0.110      (0)
   CaH2PO4+        1.406e-05   1.091e-05    -4.852    -4.962    -0.110      (0)
   HPO4-2          3.560e-10   1.254e-10    -9.449    -9.902    -0.453      (0)
   CaHPO4          2.493e-10   2.564e-10    -9.603    -9.591     0.012      (0)
   CaPO4-          1.380e-17   1.071e-17   -16.860   -16.970    -0.110      (0)
   PO4-3           1.044e-20   9.983e-22   -19.981   -21.001    -1.019      (0)
   S(-2)         3.821e-14
   H2S             3.821e-14   3.930e-14   -13.418   -13.406     0.012      (0)
   HS-             1.064e-19   7.936e-20   -18.973   -19.100    -0.127      (0)
   S5-2            7.103e-28   3.561e-28   -27.149   -27.448    -0.300      (0)
   S4-2            4.462e-28   2.077e-28   -27.350   -27.682    -0.332      (0)
   S6-2            3.460e-28   1.843e-28   -27.461   -27.734    -0.274      (0)
   S-2             4.804e-31   1.693e-31   -30.318   -30.771    -0.453      (0)
   S3-2            1.723e-31   7.320e-32   -30.764   -31.135    -0.372      (0)
   S2-2            1.064e-32   4.155e-33   -31.973   -32.381    -0.408      (0)
   S(6)          7.879e-02
   HSO4-           5.108e-02   3.897e-02    -1.292    -1.409    -0.118      (0)
   SO4-2           2.032e-02   7.077e-03    -1.692    -2.150    -0.458      (0)
   CaSO4           5.119e-03   5.265e-03    -2.291    -2.279     0.012      (0)
   CaHSO4+         2.268e-03   1.747e-03    -2.644    -2.758    -0.113      (0)

-----------------------------Saturation indices-------------------------------

  Phase               SI** log IAP   log K(298 K,   1 atm)

  Anhydrite         -0.22     -4.58   -4.36  CaSO4
  Gypsum             0.00     -4.58   -4.58  CaSO4:2H2O
  H2(g)            -12.35    -15.50   -3.15  H2
  H2O(g)            -1.51     -0.00    1.51  H2O
  H2S(g)           -12.41    -13.41   -1.00  H2S
  Hydroxyapatite   -33.44    -36.86   -3.42  Ca5(PO4)3OH
  O2(g)            -58.48    -61.38   -2.89  O2
  Portlandite      -22.74      0.06   22.80  Ca(OH)2
  Sulfur            -5.89    -20.91  -15.03  S

**For a gas, SI = log10(fugacity). Fugacity = pressure * phi / 1 atm.
  For ideal gases, phi = 1.

------------------
End of simulation.
------------------
```

APPENDIX F: ACID MINE DRAINAGE IN THE CENTRAL RAND BASIN OF THE WITWATERSRAND GOLDFIELDS

APPENDIX G: ACID MINE DRAINAGE TREATMENT PLANT IN THE CENTRAL RAND BASIN OF THE WITWATERSRAND GOLDFIELDS

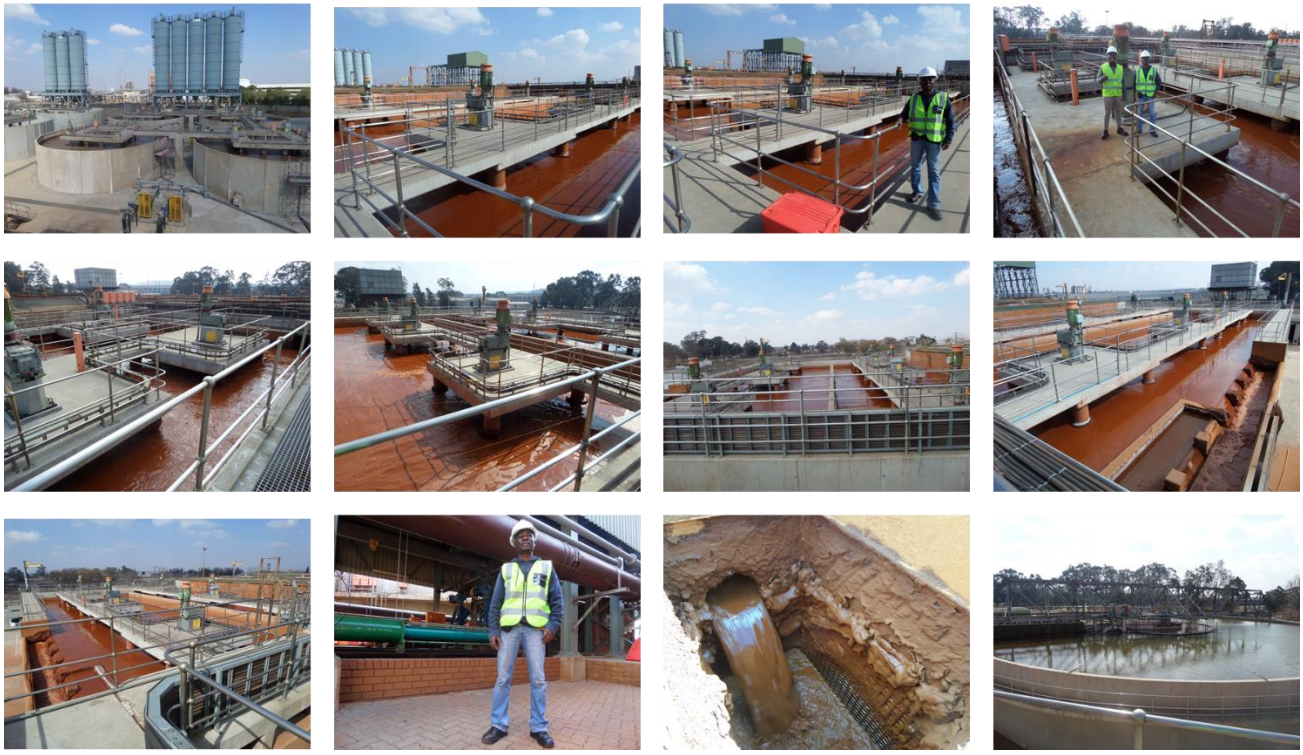

APPENDIX H: OCHRES RECOVERED FROM ACID MINE DRAINAGE

APPENDIX I: ART PAINTINGS FROM OCHRES RECOVERED FROM ACID MINE DRAINAGE

APPENDIX J: COLUMN STUDIES USING HIGH DENSITY SLUDGE AS ADSORBENT TO REMOVE TRACE METALS FROM ACID MINE DRAINAGE

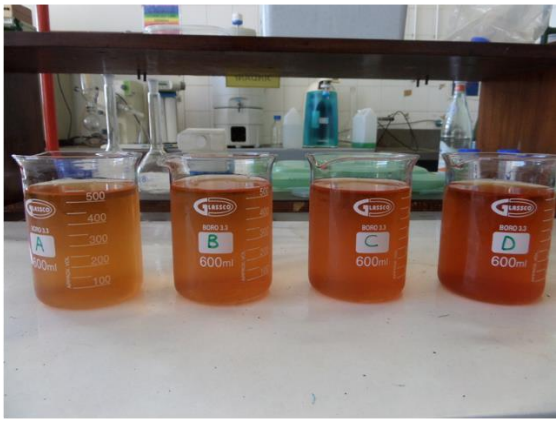

APPENDIX K: COLUMN STUDIES USING HIGH DENSITY SLUDGE AS ADSORBENT TO REMOVE PHOSPHATE IONS FROM SEWAGE WATER TYPE